HIGH ALTITUDE STUDIES OF IONIZING RADIATION

BY

P.J.EDWARDS, B.Sc. (Hons.) (Tas.)

Submitted in fulfilment of the requirements for the degree of

DOCTOR OF PHILOSOPHY

UNIVERSITY OF TASMANIA, HOBART

February, 1964.

PREFACE

This thesis is primarily concerned with investigations of ionizing radiation in the atmosphere using balloon borne instruments.

A programme of cosmic ray flights from Hobart was begun in 1959 under the direction of Dr.A.G.Fenton of the University Physics Department. I participated in the design, development, construction and successful flight of single geiger counter balloon sondes in partial fulfilment of the requirements for the degree of Bachelor of Science with honours which I received in 1960.

The balloon programme was continued during 1960 and I undertook the design and construction of a Solar Flare warning system utilizing a V.H.F. solar radiometer. This instrument was operated from the end of 1960 until early 1962 and provided early warnings of cosmic ray flare effects on a number of occasions and facilitated the recording of events during disturbed periods by both balloon borne and ground based cosmic ray monitors.

During 1961 I began an analysis of problems associated with radio-telemetry. In addition, the design and development of a balloon borne inclined cosmic ray telescope was carried out as a result of theoretical investigations suggested by Dr.K.B.Fenton. It was proposed that constant altitude flights launched from Hobart, geomagnetic latitude $52^{o}S$, of inclined geiger telescopes would, by virtue of the azimuthal dependence of cosmic ray threshold rigidities, provide information regarding the primary differential rigidity spectrum in a region of

rigidity (~ 2GV) not easily accessible to measurement. Owing to economic and technical difficulties, successful constant altitude balloon flights were not achieved at Hobart until mid 1962. First flights of the telescope equipment were therefore made at Mildura on the Australian mainland with the polyethylene balloons launched for air sampling purposes by the Department of Supply under the U.S.A.E.C., "Project Hibal" programme. As a result of damage to the recording equipment upon impact, these initial flights did not recommence until early 1963 when a successful series of flights was undertaken. I was responsible for the incorporation, by Mr.R.Francey, of a Cerenkov counter in the flight equipment. Following development of the level flight technique by Dr. K.B.Fenton, telescope flights were also launched from Hobart during 1962 and 1963.

I also participated in a series of balloon flights undertaken by the Hobart Cosmic Ray Group in the latter part of 1962 with the object of detecting effects due to high altitude nuclear detonations. A single counter balloon sonde, successfully flown on July 9th 1962, gave evidence of a time delayed radiation enhancement following the nuclear explosion, Starfish Prime, over Johnston Island. An analysis of this event and of magnetic and ionospheric measurements following the nuclear explosion was also made.

The execution of the experimental programme was dependent upon the cooperation of a number of individuals both within and without the Physics Department.

I am indebted to the Department of Supply for permission to

fly equipment at Mildura and in particular to Mr,E.Curwood,Project Leader at the Mildura Balloon Launching Station.

I wish to thank Dr.D.Parkinson of the Bureau of Mineral Resources for permission to make use of the Hobart magnetograph record. I also thank Mr.C.Bisdee for his cooperation in providing these records and in generously making his observatory available for telemetry purposes.

The assistance of Mr.H.Dwyer in the construction of electronic equipment, Mr.M.Mason who constructed the geiger counters, and Mr.R. Francey who constructed the Cerenkov counter is gratefully acknowledged. Invaluable help in computation was provided by Mrs.P.Bashford.

I wish to thank members of the Hobart Cosmic Ray Group for invaluable help and advice. In particular I am grateful to Dr.A.G. Fenton, the leader of the group, for his continued interest and to Dr. K.B.Fenton who supervised the work reported in this thesis. I also express my gratitude to Professor G.R.Ellis, Dr.K.G.McCracken, and Mr. R.M.Jacklyn for their encouragement during the course of the work.

P.J. Edwards

Publications

1. "The Existence of an Optimum Frequency for Line of Sight Telemetry", Edwards,P.J., Proc.I.R.E.(Aust.),24,8,639 (1963)

2. "Radiation Enhancement Following Johnston Island Thermonuclear Explosion", Edwards,P.J., Fenton,A.G., Fenton,K.B.,Greenhill,J., and Parsons,N.R., Nature, 196, 4852, 367 (1962)

3. "Discussion of Paper 'Interpretation of Satellite Detector Counter Rates' by A.Petschek", Edwards,P.J., to be published in J.Geophys.Res. (April, 1964)

4. "Effects of the Nuclear Explosion, 'Starfish Prime', observed at Hobart, Tasmania on July 9, 1962", Edwards,P.J. and Reid,J.R. (Submitted to J.Geophys.Res.)

CONTENTS

SUMMARY

CHAPTER 1: A general introduction to the topics treated in the thesis.

CHAPTER 2 : A review of the various treatments of the motion of charged particles in the magnetic fields with special reference to cosmic rays in a dipole field and in the geomagnetic field.

Stoermer theory and the theory of the allowed cone are shown to permit utilization of the geomagnetic effects for the purpose of rigidity spectrum analysis. It is shown that the cosmic ray flux allowed from the west but not from the east consists of particles having rigidities within a restricted number of adjacent rigidity intervals centred near the vertical Stoermer threshold rigidity.

A simple analytic approximation to the latitude dependence of the east-west Stoermer threshold rigidity difference is derived (Equation 2.7).

Alfven's theory of the adiabatic invariants of motion is reviewed, as are recent theories of the cosmic ray rigidity thresholds which make combined use of the Alfven and Stoermer theories.

The theory of magnetic trapping of charged particles in a dipole field is discussed.

CHAPTER 3 : A review of the theoretical consequences of geomagnetic control of cosmic ray particle motion and a brief account of directional cosmic ray measurements.

Analytic approximationsto the latitude dependence of the east-west asymmetry and the east-west cosmic ray flux difference are derived for a primary power law spectrum using Stoermer theory (Equations 3.4; 3.5).

The aims of the present experimental investigation of directional cosmic ray intensities are discussed.

CHAPTER 4 : A discussion of instrument design and basic experimental techniques involved in the directional measurements.

CHAPTER 5 : A discussion of the instrumental techniques and the procedures used in handling the data from the instruments described in the previous chapter.

Section 5.2 describes a device designed to automatically acquire and store directional intensity data.

Section 5.3 describes several simple and economic data modulation and multiplexing schemes, developed and used in these investigations, these being particularly suited to the telemetry of directional cosmic ray data.

Section 5.4 discusses the choice of optimum carrier frequency for line of sight radio telemetry.

CHAPTER 6 : Presentation of the results of the directional cosmic ray intensity measurements at Hobart ($52^{o}S$) and Mildura ($44^{o}S$).

Values of the east-west asymmetry, east-west intensity ratio and the east-west intensity difference obtained from the balloon flights are quoted.

Graphs of the telescope counting rates are presented in which it is possible by inspection to detect the azimuthal intensity variation.

The data from a Cerenkov-geiger counter telescope flown at a depth close to the primary particle transition depth are tabulated.

CHAPTER 7 : A discussion and interpretation of the experimental results of the previous chapter.

The data from the Hobart balloon flights in which the descent rate was unusually low, is used to derive the depth dependence of the east-west asymmetry and east-west intensity difference at zenith 45° and geomagnetic latitude $52^{\circ}S$. Both these quantities are shown to decrease with increasing atmospheric depth.

The primary differential cosmic ray flux at rigidity 1.7 GV, deduced from the Hobart data of December 1963, is shown to be not significantly different from that expected from the 1954 (solar minimum) spectrum.

The east-west asymmetry and flux differences at zenith 45° and geomagnetic latitude $44^{\circ}S$ is presented as a function of atmospheric depth. The depth dependence is shown to be more complicated than at latitude $52^{\circ}S$, the quantities initiall increasing with depth, to reach maximum values at depths below the mean transition depth.

The deduced primary differential flux in the interval 3.7 - 4.8 GV is shown to be not significantly different from that expected from the 1954 (solar minimum) spectrum.

CHAPTER 8 : A discussion of monidirectional cosmic ray intensity measurements.

The latitude and time dependence of the attenuation lengths derived from the ionization chamber balloon flights of Neher is discussed.

Hobart geiger counter balloon flight data obtained during the period 1959-63 are presented. A decrease in the attenuation length derived from the geiger counter ascents is shown to have occurred during 1959-63. The interpretation of an unusual counting rate increase observed in 1961 is discussed.

CHAPTER 9 : A summary of balloon geiger counter, riometer and magnetic observations following the high altitude nuclear explosion 'Starfish Prime' on July 9, 1962, at Hobart.

CHAPTER 10 : A discussion of the nature of the radiation burst observed over Hobart with a balloon borne geiger counter following the 'Starfish Prime' explosion.

The response of the geiger counter, riometer, and the Mt. Wellington neutron monitor to a mono-energetic flux of protons is examined. It is shown that the observations made with these instruments do not exclude protons, with an energy

spectrum intermediate between that of solar and galactic protons, as a possible source of the counting rate increase.

The energy dependence of the ionospheric absorption due to precipitation of mono-energetic electrons into the atmosphere is derived. The response of a geiger counter to a mono-energetic flux of electrons stopping in the atmosphere above the counter is also discussed. Theories of electron bremsstrahlung are reviewed. It is shown that electron dumping following the 'Starfish Prime' explosion of sufficient magnitude to account for the radiation burst, would be expected to produce ionospheric absorption well in excess of that actually observed.

Magnetic measurements at Hobart and at equatorial stations are discussed. It is suggested that these indicate the injection and trapping of positively charged particles in the magnetosphere following the explosion.

The results of statistical analyses of the counting rate data are presented. These show an association between the magnetic micropulsations and radiation intensity fluctuations following the explosion.

It is suggested that the Hobart radiation increase might be due to the gamma activity of positively charged fission products injected at altitudes of several earth radii above the explosion.

CHAPTER ONE

GENERAL INTRODUCTION

We shall outline in this chapter the general features of the cosmic ray phenomena relevant to the experimental investigations to be described. Emphasis will therefore be placed on the characteristics of cosmic radiation at balloon altitudes as determined by ionizing particle detectors. In a later chapter a separate discussion of the ionizing effects associated with nuclear detonations in the upper atmosphere will be found.

1.1 THE PASSAGE OF COSMIC RAYS THROUGH THE ATMOSPHERE

The cosmic radiation observed within the atmosphere may be genetically classified into a primary and secondary component. The primary particle flux is known to consist of protons, α-particles and heavier nuclei in the approximate proportion 86 : 13 : 1 .

These primary particles interact with nuclei of the atmosphere, and the products of the interactions, together with their progeny, constitute the secondary cosmic rays. They include photons, leptons, mesons, hyperons, nucleons and stripped nuclei.

The dependence of the composition and intensity of cosmic rays upon atmospheric depth is therefore determined by the properties of primary particles and by the various processes that occur.

The following three processes,

(a) The Nucleon Cascade

(b) Meson Decay

(c) The Electromagnetic Cascade

account for the main features of the diffusion of cosmic rays through

the terrestrial atmosphere.

In general terms, a cascade of nucleons and mesons, initiated by primary particle collisions with oxygen and nitrogen nuclei extends deep into the atmosphere. The neutral pi-mesons decay into photons which, by alternate pair production and bremsstrahlung generate the electromagnetic cascade of electrons and photons.

The principal contribution to the sea level intensity is made by mu-mesons from the decay of charged pi-mesons. Rocket and balloon flights of charged particle detectors have established the following features of the depth-dependence of the omnidirectional cosmic ray intensity at medium latitude.

(1) The intensity is independent of depth at depths less than 1 gm/cm^2 and at altitudes small compared with the radius of the earth.

(2) The intensity initially increases with atmospheric depth as the primary particle energy is shared among secondaries.

(3) Deeper in the atmosphere the intensity (principally of electrons) rises to a maximum, the PFOTZER MAXIMUM, at depths of the order of 10^2 gm/cm^2 and thereafter declines approximately exponentially with increasing depth.

(4) The sea level intensity is typically 1/50 of the intensity at the maximum, 1/25 of that at a depth of 1 gm/cm^2.

The exponential decline of the omnidirectional cosmic-ray flux with increasing depth in the lower atmosphere will be referred to in connection with the changing energy spectrum of the primary radiation. It is well known that the value of the exponent (or its reciprocal, the attenuation length) for the nucleonic component is latitude

dependent and fluctuates as a result of spectral changes. Similar behaviour of the attenuation length for the ionizing component, not hitherto published, will be described.

1.2 GEOMAGNETIC EFFECTS ON COSMIC RADIATION

Measurement of the directional properties of the flux indicate that the intensity arriving from the geomagnetic west direction is generally greater than that from the east. This is a consequence of the influence of the geomagnetic field upon the trajectories of the charged cosmic ray particles.

The theory of the geomagnetic effect is complicated by the fact that it has been found necessary to take account of the non-dipole character of the field in order to predict correctly the distribution of the cosmic ray flux on the earth's surface. In addition the perturbing effect of electric currents in the exosphere is not yet fully understood.

Subject to these uncertainties it is in principle possible to deduce the rigidity spectrum of the primary radiation from directional measurements of the primary flux at various locations on the earth's surface. In particular, a study of the azimuthal dependence of the intensity at high latitudes should provide information about that part of the primary spectrum which is subject to considerable variation due to the influence of the sun. An account of an experimental and theoretical study of the high latitude geomagnetic effect will be discussed in detail. This study requires a knowledge of the directional properties of the cosmic ray detectors used in the investigations. These properties will be discussed.

It will also be shown that the east-west asymmetry as measured

with geiger counter telescopes at high altitudes is not as useful as the east-west flux difference in relating geomagnetic effects to the primary rigidity spectrum. This is a consequence of the presence of a background flux of secondary particles at even the highest balloon altitudes.

1.3 THE ENERGY SPECTRUM OF PRIMARY COSMIC RAY PARTICLES

It is now recognised that the flux of cosmic ray particles incident upon the earth's atmosphere undergoes considerable fluctuations as a result of solar activity. The evidence suggests that all the observed intensity variations are either due to solar modulation of the galactic intensity or result from production of energetic particles at the sun itself.

The various intensity modulations, for example, the "Forbush decrease" and that related to the eleven year cycle of sunspot activity are accompanied by changes in the energy distribution of the primary particles. Near solar minimum, when the intensity is greatest the mean primary particle energy is lower than at solar maximum when the intensity is least. The differential energy spectrum at solar maximum peaks near 5 GeV/nucleon, while at sunspot minimum the peak is at 1 GeV/nucleon. The exact form of the spectrum modulation is uncertain, but the fact that the greatest changes occur at the lower energies suggests the utilization of high altitude geomagnetic effects in its determination. Investigation of these effects should therefore throw light on the solar-terrestrial relationship.

Spectral measurements and the potentialities of the geomagnetic methods are reviewed in a later chapter.

1.4 HIGH ALTITUDE NUCLEAR EXPLOSIONS

The detonation of a number of thermonuclear devices in the upper atmosphere during 1962 provided an opportunity to study the effects of the artificial injection of charged particles into the geomagnetic field. Observations of the Starfish explosion on July 9, 1962 explosion revealed unexpectedly intense geophysical effects at high latitudes.

Various experiments carried out at Hobart ($\lambda_m = 52^\circ$ S) revealed a close association between magnetic, ionospheric and radiation phenomena. It is believed that these observations allow a consistent description of the geophysical events following the "Starfish" shot.

The high altitude radiation enhancement recorded by a balloon borne geiger counter is of particular interest in that no comparable observations have been reported in the literature. The Hobart results are discussed in detail and compared with those obtained elsewhere.

These results are examined with regard to their geophysical implications and secondly in the context of the problem of the detection of nuclear detonations in the upper atmosphere. In this section, we discuss in general the detection of ionizing radiation by radiophysical techniques.

CHAPTER TWO

THE MOTION OF CHARGED PARTICLES IN THE GEOMAGNETIC FIELD

In this chapter we review current theories of the motion of charged particles in the earth's magnetic field. The main discussion is of the geomagnetic effects on particles of cosmic ray energies since a knowledge of these is required in interpreting the experimental results described in Chapters 3, 6 and 7 of Part I.

In recent years the Stoermer & Vallarta theories which form the basis of the calculations of the cosmic ray trajectories have been supplemented by the perturbation theory due to Alfven. Cosmic ray applications of the latter theory will be reviewed and the results will be used in the discussion of the effects of high altitude nuclear explosion in Chapters 12, 13 and 14 of Part II.

2.1 STOERMER THEORY

In a static magnetic field having axial symmetry the equations of motion of a charged particle possess two integrals. The first, applicable for static magnetic fields in general, states that the particle velocity, and therefore its kinetic energy, remains constant. The second, which is unique to the case of axial symmetry (Stoermer, 1955) is usually known as the Stoermer integral. This integral provides considerable information about the accessibility of particles to points in the field without requiring numerical calculation of the actual trajectories from the differential equations of motion. Since one of the main problems is the calculation of the energies of cosmic ray particles accessible to observers on the surface of the earth and since the earth's field is approximately that of a centred dipole, the

application is obvious.

Using spherical polar coordinates (r, λ) where r is the distance from the dipole centre, and λ is the geomagnetic latitude, the Stoermer integral (e.g. Fermi, 1949) gives an equation for the motion of the particle in the plane containing both the particle and the dipole axis, (the meridian plane),

$$2\gamma = R \cos\lambda \cdot \sin\alpha + \cos^2\lambda/R \qquad 2.1$$

γ is a constant of the motion, α is the angle between the current vector of the particle and the meridian plane, and is positive for westward moving positive particles. $R = r/C$ is the radial coordinate of the particle expressed in units of the Stoermer variable, $C = \sqrt{M/P}$ where M is the magnetic moment of the dipole and P is the magnetic rigidity (momentum per unit charge) of the particle (Stoermer, 1907). P has the dimensions of energy per unit charge in the mixed system of units customarily used and is usually expressed in volts.

Solving 2.1 for the rigidity, P we have

$$P = \frac{M \cos^4\lambda}{\gamma^2 r^2 \left[1 + \left(1 - \cos^3\lambda \cdot \sin\alpha \cdot \frac{1}{\gamma^2}\right)^{\frac{1}{2}}\right]^2} \cdot \qquad 2.2$$

For a given value of γ, this equation yields the rigidity of a particle incident at the point (r, λ) in the meridian plane in a direction specified by the angle α relative to this plane. It may be shown (Stoermer, 1955) from equation 2.1 that the condition $|\sin\alpha| \leq 1$ does not restrict the accessibility to infinity of particles at points (R, λ) in the plane provided $R > 1$. For points on the earth's surface this result holds for

$$R_e = r_e \left(\frac{P}{M}\right)^{\frac{1}{2}} > 1$$

That is, for $P > \frac{M}{r_e^2} = 59.6$ GV .

For $R < 1$ the particles are not accessible unless $|\gamma| \leq 1$ and from equation 2.2 it may be seen that the minimum permissible rigidity, i.e. found by putting $\gamma = 1$ is

$$P_o = \frac{M \cos^4 \lambda}{r^2 \left[1 + (1 - \cos^3 \lambda \,.\, \sin \alpha)^{\frac{1}{2}}\right]^2} \qquad 2.3$$

This value of the rigidity is the Stoermer cut off rigidity. Particles with rigidities below P_o are not accessible to the regions (r, λ) from outside the field. At any point of observation the Stoermer integral defines a circular cone, the Stoermer cone, with axis in the east-west direction. Trajectories inside this cone of angle $\frac{\pi}{2} - \alpha$ where $-\sin \alpha = \cos \lambda / R^2 + 2\gamma / R \cos \lambda$ (from equation 2.1) are forbidden.

With the centred dipole approximation the geomagnetic cutt off rigidity at the surface of the earth is therefore

$$P_{\theta,\phi,\lambda} = \frac{M \cos^4 \lambda}{r_e^2 \left[1 + (1 - \sin \theta \,.\, \sin \phi \,.\, \cos^3 \lambda)^{\frac{1}{2}}\right]^2} \qquad 2.4$$

where θ is the zenith, ϕ the azimuth, measured clockwise from geomagnetic north, λ the geomagnetic latitude of observation. M is the dipole moment $(8.06 \,.\, 10^{25}$ Γcm$^3)$ and r_e is the radius of the earth $(6.4 \,.\, 10^3$ km) .

The vertical cut off rigidity $(\theta = 0)$ is then

$$P_{0,\phi,\lambda} = \frac{M}{4R^2} \cos^4 \lambda = 14.8 \cos^4 \lambda \text{ GV} \qquad 2.5$$

at the top of the atmosphere. Comparing cut offs in the north-south plane,

$$P_{\theta,\phi,\lambda_o} = P_N = P_{\theta,\pi,\lambda_o} = P_S = P_o$$

In the east-west plane

$$P_{\theta,3\pi/2,\lambda_o} = P_W < P_E = P_{\theta,\pi/2,\lambda_o}$$

for positively charged particles. By expanding the RHS of equation 2.4 as a power series, it may also be shown that the rigidity difference

$$P_{\theta,\pi/2,\lambda_o} - P_{\theta,3\pi/2,\lambda_o} = P_E - P_W \qquad 2.6$$

$$\doteq \frac{M}{4R^2} \sin\theta \cdot \cos^7\lambda$$

$$= P_o \sin\theta \cdot \cos^3\lambda \qquad 2.7$$

This approximation underestimates the difference by less than 7 % at latitudes greater than 40° and zenith angles less than 60°. The error is approximately $(-43 \sin^2\theta \cos^6\lambda\ \%)$.

In figure 2.1 the vertical (rigidity) cut off, the cut off for 45° East and the east-west cut off difference for zenith angles of 30°, [illegible] and 45° are plotted as functions of geomagnetic latitude.

The discussion has been limited to positive particles reaching the earth from outside the field. Since the primary cosmic rays are of predominantly one sign (+ve), the dependence of cut off rigidity upon the angle of incidence will produce an anisotropy in the observed flux distribution, which will be determined by the place of observation and the rigidity spectrum of the primary particle. The so called "East-West asymmetry" will be discussed in later sections. For negative

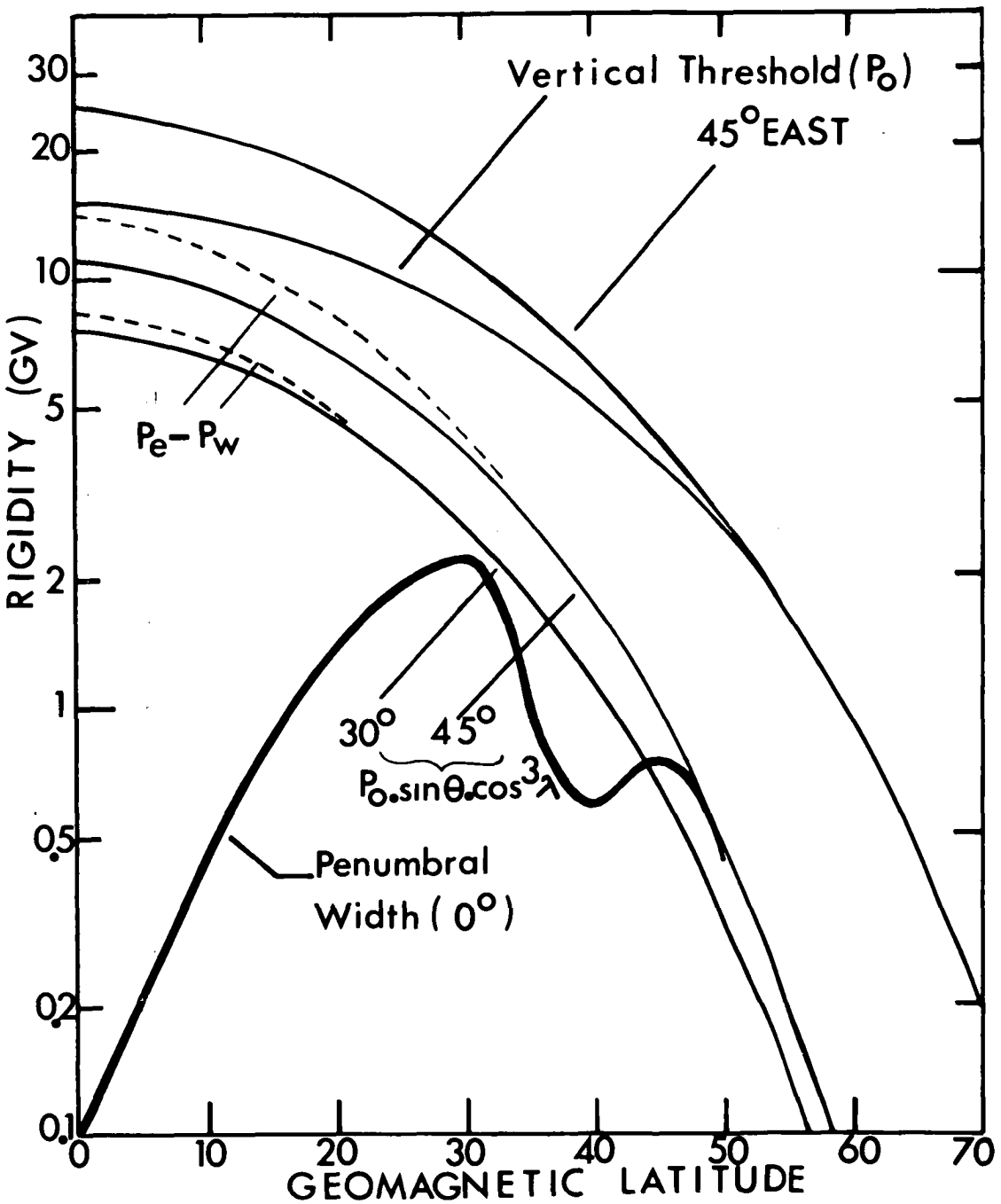

Fig. 2.1 STOERMER THRESHOLD RIGIDITIES
AND VERTICAL PENUMBRAL WIDTH
AT THE EARTH'S SURFACE FOR THE DIPOLE FIELD

primary particles the east and west cut off values calculated above are simply interchanged and the upper curve of Figure 2.1 then gives the latitude dependence of the cut off rigidity for negative particles coming from the direction 45° W.

2.2 THE THEORY OF LEMAITRE AND VALLARTA

The simple Stoermer theory outlined in Section 2.1, gives the minimum rigidity a cosmic ray particle must possess to be accessible at a given latitude from a given direction (θ, ϕ). This theory does not take into account the presence of the solid earth. Lemaitre and Vallarta (1936) showed that the presence of the planetary absorbing mass places further restrictions on the accessibility of charged particles to points on the earth's surface. At a given location on the earth's surface the field of view of a particle detector may be divided into the following regions. The first of these, the Stoermer cone has been mentioned and is derived from a first integral of the equation of motion. The second, the main cone, contains only those trajectories which come directly from infinity and which do not intersect the earth's surface other than at the point of observation.

The region between the main and Stoermer cones, the penumbra, contains both allowed and forbidden trajectories. Simple shadow-cones also exist and are defined so that the region between the shadow and Stoermer cones consists solely of forbidden trajectories.

The simple shadow cones calculated by Schremp, (1938) have been found to be in error. Schwartz, (1959) has recalculated the shadow and penumbral cones for a limited number of geomagnetic latitudes. Unlike Schremp he finds no simple shadow cone cut off for zenith angles

less than 70° for latitudes from 40° to 45°. These conclusions are supported by experiments conducted by Winckler et al., (1950) and Danielson and Freier, (1958). The results of Schwartz apply only if the geomagnetic field is assumed to be due to a geocentred dipole.

The main or "allowed" cone (M.C.) within which all particle trajectories reach infinity has been investigated (Lemaitre and Vallarta, 1933, 1934-5, 1936) by detailed calculation of trajectories in the centred dipole field approximation. The allowed cone cut offs are of interest in the present investigations because, together with the Stoermer cut offs, they determine the width (in terms of rigidity) of the penumbra. At medium latitudes certain penumbral rigidities are allowed and others are forbidden.

Calculations of the main cone cut offs have not been extended to high latitudes and an expression analogous to the Stoermer equation does not appear to have been obtained. Detailed conclusions concerning the penumbral width, and "transparency" (Schwartz) can be made for particular latitudes and directions of incidence. In general the penumbra is transparent at high latitudes, and opaque at low latitudes. The penumbral width in the direction of the zenith is plotted in Figure 2.1 as a function of latitude using results of Lamaitre and Vallarta and Schwartz.

In order to emphasise the complexity of the penumbra at medium latitudes we examine the calculations of Schwartz for latitude 41° N. Given in Table 2.1 are the Stoermer and M.C. thresholds at 0°, 45° E and 45° W at $\lambda = 41^{\circ}$ N together with the penumbral widths and the total allowed rigidity interval lying between the main and Stoermer cut

off rigidities. Figure 2.2 shows the detailed structure of the penumbra for the two inclined directions. From these the rigidity bands allowed at 45° W but not at 45° E are derived (Figure 2.2 (C), (D)). Thus by subtracting the primary eastern flux from the primary western flux we obtain the flux of those particles which have rigidities lying within a number, here nine, of adjacent rigidity intervals. Figure 2.3, taken from Schwartz, 1959, shows the penumbral bands in the east-west plane.

..... TABLE 1 ..... $\lambda = 41^{\circ}$ N (after Schwartz)

	STOERMER CUT OFF	MAIN CONE CUT OFF	PENUMBRAL WIDTH	ALLOWED PENUMBRAL WIDTH	FRACTION OF PENUMBRAL WIDTH ALLOWED
	(GV)	(GV)	(GV)	(GV)	(%)
$\theta = 45^{\circ}$ E	5.691	6.653	0.962	0.440	45.74
$\theta = 0^{\circ}$ (Zenith)	4.788	5.384	0.596	0.356	59.73
$\theta = 45^{\circ}$ W	4.173	4.815	0.642	0.342	53.27

EAST-WEST STOERMER THRESHOLD DIFFERENCE = 1.518 GV
EAST-WEST M.C. THRESHOLD DIFFERENCE = 1.838 GV
EAST-WEST TOTAL ALLOWED BAND WIDTH (δP_{EW}) = 1.740 GV

The widest allowed rigidity band lies between the eastern Stoermer cut off and the western main cone cut off. It constitutes 52% of the total penumbral width. At low latitudes where the penumbra is completely dark the width of the allowed rigidity band is just the difference in the main cone cut offs. At high latitudes where the penumbra is

Fig. 2.2 (a) Allowed rigidities of cosmic ray particles arriving from the directions :
(A) 45°W
(B) 45°E
(C) 45°W but not 45°E
at latitude 41°

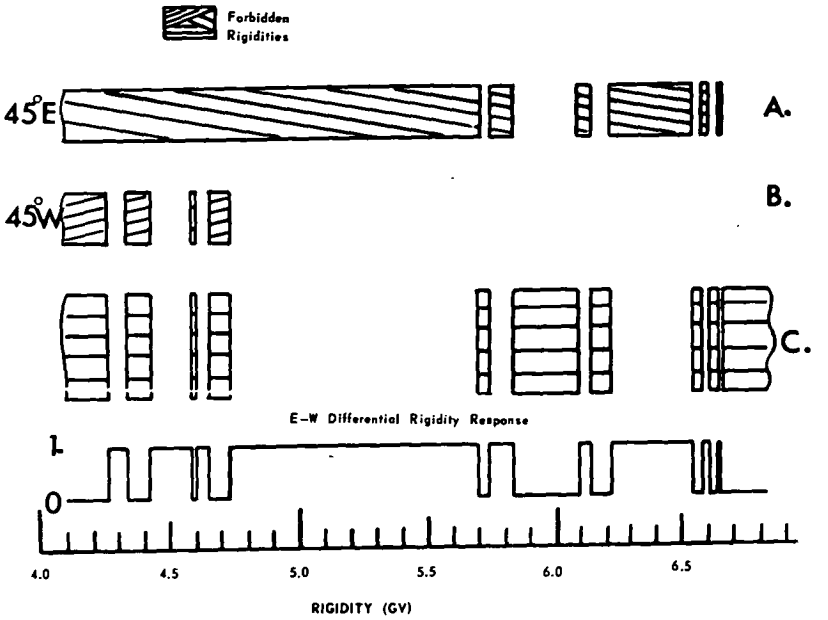

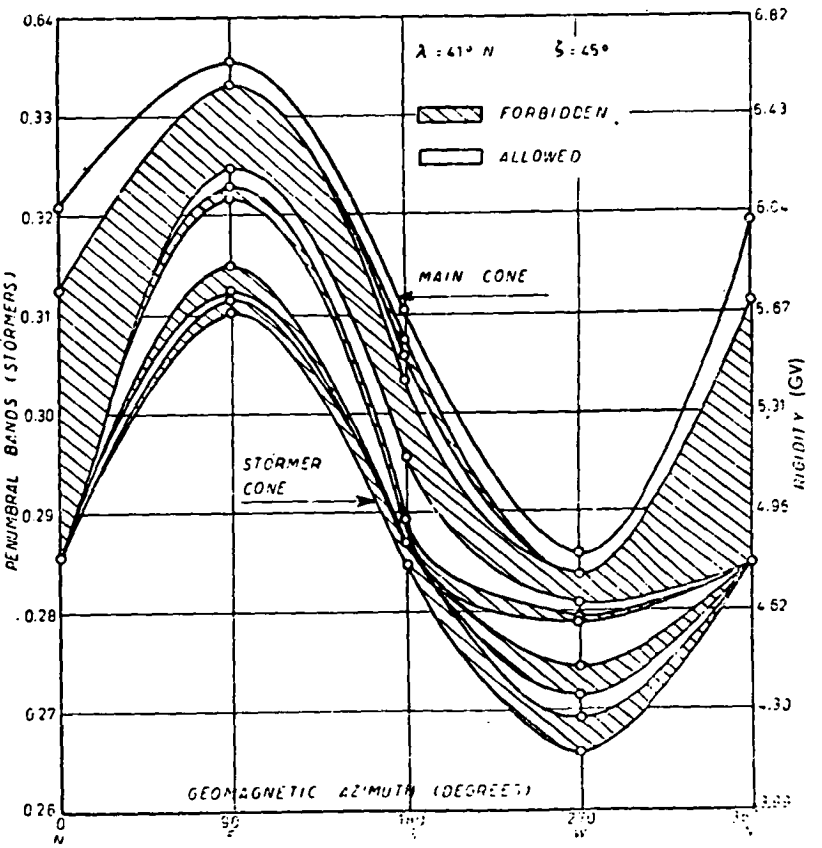

Fig. 2.3. Penumbral bands for 45° zenith angle at λ = 41°.

completely transparent, the width is equal to the E-W Stoermer cut off difference. The allowed rigidity band width does not always lie between the M.C. and Stoermer cut off differences as respective upper limits. For example, according to Schwartz, at the same latitude (41° N) the main cone cut off for 45° N is 0.425 GV above that for 45° S. On the other hand, the 45° NS rigidity band width is 0.533 GV, about 25 % greater than the M.C. difference.

Consider two local directions of incidence and let the higher M.C. cut off be $P_m(1)$, the lower, $P_m(2)$. The corresponding Stoermer width of the spectral window obtained by selecting those particles allowed in direction (2) but not in direction (1),

$$\delta P(1, 2) = (P_S(1) - P_m(2)) + (P_m(1) - P_S(1))(1 - \alpha_1) + (P_m(2) - P_S(2))\alpha_2$$

for $P_S(1)$ $P_m(2)$, where α_1, α_2 are the fractions of the rigidity width allowed between $(P_m(1), P_S(1))$ and $(P_m(2), P_S(2))$ respectively. The α may conveniently be thought of as transmission coefficients. They are approximately equal for zenith angles less than 45° in the EW plane at latitudes greater than about 40°. Under these circumstances,

$$\begin{aligned} \delta P(1, 2) &= P_m(1) - P_m(2) \quad (1 - \alpha) + P_S(1) - P_S(2) \quad . \alpha \\ &= P_S(1) - P_S(2) \quad \text{for} \quad \alpha = 1 \\ &= \tfrac{1}{2}\left[P_m(1) - P_m(2)\right] + \tfrac{1}{2}\left[P_S(1) - P_S(2)\right] \quad \text{for } \alpha = 0.5 \end{aligned}$$

Putting $\alpha = 0.5$ for $\lambda = 41^{\circ}$, $\theta = 45^{\circ}$, $\phi = \pi/2, 3\pi/2$ we obtain

$$\delta P_{EW} = 1.678 \text{ GV},$$

which compares favourably with the value quoted in Table 2.1.

In concluding this brief discussion of main cone theory we note that the main cone cut off, unlike the Stoermer cut off, is a function

of the direction of incidence in the North-South plane. The penumbral transmission coefficients also depend on zenith in the NS plane.

2.3 THE GUIDING CENTRE APPROXIMATION

In the preceding sections of this chapter we outlined the Stoermer and Lemaitre-Vallarta theories of the motion of charged particles in the field of a uniformly magnetised, impenetrable sphere. Calculation of the actual particle trajectories is particularly laborious for particles with low rigidities because of their highly looped orbits. In recent years the discovery by satellites of low energy particles trapped in the geomagnetic field has stimulated interest in the perturbation theory of Alfven (1950). This theory is useful, not only for deducing the motion of the Van Allen particles, but also in calculating cut off rigidities and trajectories of cosmic ray particles at medium high latitudes in the earth's field. (Sections 2,4; 2.5).

The fundamental assumption is that the dimensions of the loops of the trajectories are small compared with the scale size of inhomogeneities in the field. During a single loop the particle then moves in an approximately uniform field. In Alfven's theory the motion is therefore calculated for a homogeneous field and the inhomogeneity is introduced as a perturbation.

For a uniform static field the particle motion may be conveniently resolved into a uniform translation parallel to B and a circular motion perpendicular to B . The orbit is a helix of radius

$$r = \frac{p\,C}{ZeB} = \frac{pC}{Ze} \cdot \frac{\sin\psi}{B} \qquad 2.8$$

$$= \frac{P}{B} \cdot \sin\psi \qquad 2.9$$

$$= a \sin\psi \qquad 2.10$$

where ψ is the pitch angle of the helix, $(\tan\psi = v_\perp/v_{//})$, $P = \frac{pC}{Ze}$, the rigidity is defined in Section 2.1; $a = \frac{P}{B}$ is the gyroradius of the particle. The angular frequency of the circular motion, the gyrofrequency (A.G.F.),

$$\omega_B = \frac{ZecB}{E} \qquad 2.11$$

where E is the total energy of the particle. The above equations may be written:

$$a(\text{km}) = \frac{P(\text{MeV/c})}{30\ B\ (\text{gauss})} \qquad 2.12$$

$$\omega_B = 9.10^6 \cdot \frac{Z}{E(\text{MeV})} \qquad 2.13$$

$$f_H = \frac{\omega_B}{2\pi} = \frac{1.435Z}{E(\text{MeV})} \quad \text{Mc/sec} \qquad 2.14$$

The magnetic moment,

$$\mu = \frac{p_\perp^2}{2\gamma mB} = \frac{p^2 \sin^2\psi}{2\gamma mB} \qquad 2.15$$

is constant from equation 2.8.

The particle motion may therefore consists of a circular gyration about a moving guiding centre. In the present case the guiding centre has uniform velocity $v_{//}$ in the direction of the field. In general the application of a small force $\tilde{F}$ to a gyrating particle results (Alfven, 1950) in a drift of the guiding centre with velocity

$$\tilde{V}_D = \frac{\tilde{F} \times \tilde{B}}{Ze \cdot B^2} \qquad 2.16$$

Providing $\frac{|\nabla\tilde{B}|}{B} \ll \frac{1}{a}$ (Alfven) 2.17

the guiding centre concept holds for non uniform fields. The particle motion is then specified by the gyration about a drifting guiding centre. The field gradients give rise to inertial and magnetic forces on the

particle and the drift velocity perpendicular to the field may be written

$$\tilde{V}_D = \frac{\tilde{B} \times \nabla_\perp \tilde{B}}{ZeB^3} \left(\tfrac{1}{2}mv_\perp^2 + mv_{//}^2\right) \qquad \ldots 2.18$$

$$= \frac{E(2+\varepsilon)}{1+\varepsilon} \cdot \frac{\tilde{B} \times \nabla_\perp \tilde{B}}{ZeB^3} \cdot (1 + \cos^2\psi) \qquad \ldots 2.19$$

E = Kinetic energy

ε = Kinetic energy in units of the rest energy.

These equations may be used to find the motion of particles trapped in the geomagnetic field. The constancy of the magnetic moment (Equation 2.15) shows that as the particle moves to regions of higher field strength along a line of force the pitch steepens and the parallel component of the velocity decreases and becomes zero for $B_m = B_o \sin^2\psi_o$. Alfven shows that the parallel component of the field gradient then causes reflections of the particle. In a dipole field the motion of guiding centre may therefore be oscillatory in latitude. It may also be shown that the perpendicular drift (Equation 2.19) gives rise to periodic longitudinal motion of the guiding centre. The motion of a trapped particle is therefore associated with three periodicities. These are the gyro oscillation, the "mirror" oscillation parallel to the field, and, for fields with axial symmetry, the azimuthal oscillation about the axis. For each periodic coordinate p_i the action integral

$$J_i = \oint p_i dq_i$$

will be constant provided the system perturbation is adiabatic. It may be shown (e.g. Obayashi, 1961) that the action integrals associated with

the gyro and mirror oscillations in an axial field are respectively

$$J_1 = \mu$$

$$\text{and} \quad J_2 = \oint p_{//}\, dS \qquad 2.21$$

where the latter integration is made along the line of force. A third invariant (Northrop & Teller, 1960)

$$J_3 = \int B \cdot dA \qquad 2.22$$

is associated with the periodicity in longitude of the mirror points. The integration is over the surface bounded by the trajectory of either mirror point.

The adiabatic invariants have been frequently discussed in the literature in connection with the stability of motion of particles trapped in the earth's field. It is often assumed e.g. Singer, 1959, 1960 that breakdown of one or more of the invariants violates the condition for trapping. However, Gall (1963) points out that stable Stoermer orbits exist for which J_1 is certainly not constant. Harris, 1963 shows that non conservation of μ may in fact raise and not lower the altitude of the mirror points. The theory of particle trapping is currently being developed on more rigorous lines (Gall, 1962, 1963; Hayakawa & Obayashi, 1963; Stone, 1963; Harris, 1963).

For particles trapped in a dipole field conservation of the first two invariants shows that the particle gyrates about a guiding centre which mirrors at constant latitude and drifts longitudinally on a surface of revolution of a line of force about the dipole axis.

For the earth's dipole field the mirror period T(m) (Hamlin et al (1961)) is

$$T_m \doteq \frac{4Lre}{V}(1.30 - 0.56 \sin \psi_o) \qquad 2.23$$

ψ_o = Equatorial pitch angle

L = geocentric equatorial distance to the line of force in earth radii

V = Particle velocity

$$\therefore\ T_m = \frac{2.55 \cdot 10^9 L}{V}(1.30 - 0.56 \sin \psi_o) \text{ seconds} \qquad 2.24$$

where

V = Velocity (cm/sec)

The longitudinal drift period (T_a) is found by integration of equation 2.19 . It is given by Lew, (1961) as

$$T_a = \frac{172.4}{\mathcal{E}} \cdot \frac{1+\mathcal{E}}{2+\mathcal{E}} \cdot \frac{m_e}{m} \cdot \frac{1}{L} \cdot \frac{G(\lambda_m)}{F(\lambda_m)} \cdot Z \qquad 2.25$$

where

$\mathcal{E}$ = Kinetic energy in natural units

$\frac{m}{m_e}$ = Mass in units of the electron mass (m_e)

$\frac{G(\lambda_m)}{F(\lambda_m)}$ = Ratio of the drift period of a particle with mirror latitude (λ_m) to the equatorial drift period. (Tabulated by Lew)

= 1 at $\lambda_o = 0$; 1.5 at $\lambda_o = \pi/2$; $\frac{G}{F} = 0.35 + 0.15 \sin \psi_o$

Z = Charge in units of the charge on the electron.

For non relativistic energies ($\mathcal{E} \ll 1$) we have therefore

$$T_a = \frac{0.047\ ZG}{\mathcal{E}\ A.L.F} \text{ minutes}$$

$$= \frac{2.81\ ZG}{\mathcal{E}\ A.L.F} \text{ seconds} \qquad 2.26$$

where

A = Particle mass in a.m.u.

L = r_o/r_e

$\mathcal{E}$ = Particle Kinetic Energy in units of 931 MeV

More simply,

$$T_a = \frac{43.8}{(E/Z) \cdot L} \cdot \frac{G}{F} \text{ minutes} \qquad 2.27$$

where E/Z = Kinetic Energy per unit charge (MeV per electron charge). The drift is westward for positive particles, eastward for negative particles. The drift period is generally much longer than the mirror period.

Using Hamlin's results, the ratio

$$\frac{T_m}{T_A} = \frac{6\gamma mcv}{B_o L r_e Ze} E(\psi_o) \qquad 2.28$$

$$= \frac{P(MeV/c) \cdot L^2}{10^4 \cdot \pi} E(\psi_o) \qquad 2.29$$

is proportional to rigidity and to the square of the equatorial distance to the field line. The function

$$E(\psi_o) \doteq 0.47 + 0.34 \sin\psi_o - 0.43 \sin^2\psi_o \qquad 2.30$$

changes slowly with the equatorial pitch angle. For a particle mirrored at latitude λ_m,

$$\sin^2\psi_o = \frac{\cos^6 \lambda_m}{1 + 3 \sin^2 \lambda_m}$$

$$\therefore \sin\psi_o \doteq \cos^4 \lambda_m$$

If the particle mirrors at the surface of the earth on the field line labelled by L,

$$L^2 = \cos^{-4} \lambda_m$$

from the equation to a line of force, $r/r_e = L \cos^2 \lambda$ ... 2.31

Also $L^2 E(\psi_o) \doteq 0.47L^2 + 0.34 - 0.43L^{-2}$

and $$T_m/T_A \doteq \frac{P(MeV/c)}{10^4 . \pi} (0.47L^2 - 0.43L^{-2} + 0.34) \quad \ldots 2.32$$

Also from Equations (2.24) and (2.25),

$$T_m \doteq \frac{2.55.10^9}{V} (1.30L - 0.56L^{-1}) \text{ seconds} \quad \ldots 2.33$$

$$T_a \doteq \frac{43.8}{(E/Z)} \cdot \frac{1 + \varepsilon}{2 + \varepsilon} (0.35L^{-1} + 0.15L^{-3}) \text{ minutes} \quad \ldots 2.34$$

2.4 McILWAIN'S L PARAMETER

Early measurements of the spatial distribution of the intensity of geomagnetically trapped radiation revealed that the centred dipole representation of the earth's field cannot adequately account for the observed distribution. The constancy of the adiabatic invariants of the particle motion (Northrup and Teller,1960) allows a simple magnetic coordinate system to be used (McIlwain, 1960).

The longitudinal invariant (I) is defined at a point A in the field by

$$I = \int_A^{A'} (1 - \frac{B}{B_A})^{\frac{1}{2}} dS \quad \ldots 2.35$$

and is derived from $J_2 = \oint p_{\parallel} dS$ (Equation 2.21)by assuming $J_1 = \mu$ = constant, and p = constant, where A' is the conjugate point of A.

The points in the earth's field for which I, B have the same value lie on two closed curves, one in each magnetic hemisphere. The previous section shows that the guiding centre of a trapped particle

mirroring at the point (I, B) will remain on the surface containing the lines of force which connect the two curves. The problem of labelling such a surface is that of finding a function F (B, I) that has a constant value along a line of force. This function could be found by examining $I_i = F_i(B)$ along lines of force calculated from some representation of the real field. McIlwain states that the average values of the functions F_i (B) around the surface will be well represented by the functions obtained for the dipole field component alone.

The invariant I for a dipole field is

$$I = r_o \, h_1 (\lambda)$$

where $h_1(\lambda)$ is a function of λ, r_o = equatorial distance to the field line in earth radii.

Also
$$\frac{r_o^3 B}{M} = \frac{(4 - 3\cos^2\lambda)^{\frac{1}{2}}}{\cos^6\lambda} = h_2(\lambda)$$

$$\therefore \quad \frac{I^3 B}{M} = h_3\left(\frac{r_o^3 B}{m}\right)$$

$$\text{or} \quad F\left(\frac{I^3 B}{M}\right) = \frac{r_o^3 B}{M}$$

Hence the parameter (L) may be defined:

$$L^3 \frac{B}{M} = F\left(\frac{I^3 B}{M}\right) \qquad 2.35$$

where I and B are calculated at the point from an approximation to the real field. If the real field were due to a dipole of moment M, then $L = r_o$, the equatorial radial distance. The function $F(\frac{I^3 B}{M})$ may be quickly evaluated by an approximate method described by McIlwain

if I and B are known. However the calculation of I is lengthy. Some values of I and L have been computed from the Jensen & WHittaker (1960) field representation by McIlwain. It is found that L usually varies by less than 1 % along a line of force. It is also found that trapped particle intensity measurements are well organised when plotted in B, L coordinates and that the Argus shells were coincident with surfaces.of constant L .

Singer, (1962), points out that the mapping of the point (I, B) in the real field to the point (L, B) in the dipole field, is unique only for particles which mirror at the point (I, B). Stone, (1963), suggests that L be redefined to apply only to particles which mirror at that point. The redefined value of L is then an invariant of the particle motion and not necessarily constant along a real line of force. The values of L are within 5 % of the equatorial radius of the field line. This fact, coupled with the redefinition of L as an invariant, shows that the radial separation of particles initially trapped on the same field line is approximately proportional to the difference in their L values. Thus the L parameter has a physical significance for particles of constant magnetic moment trapped in the geomagnetic field. In view of the near equality of L along a geomagnetic line of force, the equations of the last section, in which L was identified with r_o , may be used with small resultant error.

2.5 CUT OFF RIGIDITIES IN THE GEOMAGNETIC FIELD.

Having surveyed various approaches to the calculation of charged particle motion in magnetic fields we now review the application of these theories to motion in the actual geomagnetic field.

Observational evidence shows that the centred dipole approximation to the earth's magnetic field is inadequate to account, through geomagnetic theory, for the distribution of the cosmic ray intensity over the surface of the earth. The close relation between the sea level cosmic ray intensity and the local value of the field strength (Rothwell & Quenby, 1957) suggests the importance of the non dipole components of the field in determining the cut offs. Significant discrepancies remain when the eccentricity of the real dipole is taken into account.

Assuming that a knowledge of the surface magnetic field is sufficient to compute the orbits of charged particles in the vicinity of the earth, cut offs may be found by computing numerous trajectories using surface field measurements. This has been done by McCracken (1962) for a number of selected observatories using the 6th degree spherical harmonic expansion of the magnetic potential due to Finch and Leaton (1957), McCracken's results refer primarily to asymptotic directions of incidence, and only in a few cases do they allow the cut off rigidity to be estimated with high accuracy.

A different approach, based on Stoermer theory is due to Sauer (1963), who also uses the field derived from the Finch & Leaton coefficients. The influence of an external field due to a "ring current" in the exosphere is also calculated.

A direction and point of incidence are chosen on the earth's surface for a particle of given rigidity. The equations of motion of the particle in the real field are then integrated to determine the position and direction of the particle at a radial distance from the centre of the earth, the "transition radius", where the non dipole field

components are negligible and where the particle may be assumed to move in the dipole part of the real field. Simple Stoermer theory is then used to determine whether or not the particle can have arrived from infinity. The procedure is repeated until the minimum rigidity allowed by the Stoermer criterion is reached. This is then the cut off rigidity.

The first part of the calculation is solved in the guiding centre approximation, i.e. the magnetic moment of the particle is assumed to be an adiabatic invariant of the motion. This places an additional restriction on the choice of the transition radius and limits the calculation to latitudes above 45° . The effect of a ring current may be easily taken into account since the Stoermer integral exists for all axially symmetric fields.

The initial calculations of Sauer refer to the cut off for vertical incidence only and being based on the simple Stoermer model, do not provide any information on the width or transparency of the penumbra. The effective cosmic ray cut offs might therefore be expected to be greater by 5 - 10 % than those calculated by this method.

Sauer compares the cut offs obtained in this manner with the frequently used Quenby-Wenk (1962) and Quenby-Webber (1959) figures. In addition a comparison is made with cut offs defined by the expression

$$R = 14.9L^{-2} \text{ GV} \qquad 2.36$$

where L is the "magnetic shell" parameter obtained from the Jensen & Whittaker (1960) field representation at the point of incidence. It was found that the L derived cut-offs differed by as much as 30 % from the cut offs obtained at the transition radius.

In a second paper (Sauer & Ray, 1963) the discrepancy is examined in some detail. It is stated that the L derived cut-offs agree with the results obtained in the first paper with an error of not more than several percent, provided that L is calculated at the guiding centre rather than the point of observation and that the guiding centre approximation holds at distance sufficiently great to make the non-dipole terms negligible. (The original discrepancies are due in part to an underestimate of the effect of the non-dipole field components at large distances.)

Sauer also states that a consequence of equation 2.36 is the approximate constancy of the cut offs in the direction of the field along a line of force. This statement is verified at several latitudes below those at which the guiding centre approximation holds, by numerical integration of the equations of motion using the Finch & Leaton field. The authors conjecture that the L expression holds at all latitudes, but state that this must be verified by numerical integration.

In connection with these statements we note that a consequence of equation (2.1) (the Stoermer integral) and equation (2.31) (the equation of a dipole line of force) is the invariance of the Stoermer threshold in a given direction to the meridian plane at all points on a dipole line of force. In the centred dipole approximation the Stoermer threshold in the plane of the line of force is thus constant and equal to the vertical threshold rigidity at the intersection of the line with the earth's surface.

In the earth's dipole field, equation 2.36 therefore holds exactly if L is the equatorial distance in earth radii to the field line on

which the observation is made. This result is independent of the validity of the guiding centre approximation.

Webber (1963), using a method by Schluter (1958), has also elegantly applied the Stoermer and Alfven methods to an investigation of high latitude particle trajectories. Previous methods of finding the directions of particles outside the earth's field (the asymptotic directions) corresponding to particular directions of incidence at points on the earth's surface required lengthy machine calculations (McCracken et al., 1962).

The vertical cut-off rigidities in the real field of the earth have been calculated by Quenby and Webber (1959) and Quenby and Wenk (1962). These authors consider perturbations of the dipole trajectories in the real field and find the "equivalent Stoermer latitude" λ_s for points on the earth's surface. Replacement of the geomagnetic latitude λ by λ_s in the Stoermer cut-off expression (Equation 2.5) then yields the vertical threshold rigidity. In the latter paper experimental results are used to find also the penumbral width and transmission (Section 2.2). These results for the vertical thresholds appear to be in good agreement with observation (Pomerantz et al., 1962). In determining the thresholds in directions other than the vertical, the results of Quenby and Wenk and Quenby and Webber will be used to find the equivalent Stoermer latitude. The results of Sections 2.2 and 2.3 for the dipole field will then be used. This procedure may be questionable, particularly when the field is disturbed.

CHAPTER THREE

DIRECTIONAL CHARACTERISTICS OF THE COSMIC RAY FLUX AT BALLOON ALTITUDES

INTRODUCTION

In the preceding chapter we discussed the influence of the geomagnetic field upon charged particle motion. In this chapter we discuss the cosmic ray observations in the light of the geomagnetic theory. In particular, the predictions from the Stoermer & Lemaitre-Vallarta theories of anisotropies in the cosmic ray flux are compared with high altitude observations. We assume that the primary cosmic radiation is isotropic in space outside the earth's magnetic field, and that Liouville's theorem holds for the motion of cosmic ray particles above the atmosphere.

3.1 LIOUVILLE'S THEOREM

This theorem states, in the absence of particle collisions, the density in phase space of the representative points of the particles is constant along a trajectory of any point in phase space. It has been shown (Swann, 1933, Fermi & Rossi, 1933) that the theorem holds for static electric and magnetic fields, also that it implies the constancy of the directional intensity at any point on the dynamic trajectories of the particles in a static magnetic field.

If the flux of particles of rigidity (P) is isotropic outside the earth's field (assumed static) the observed intensity in the vicinity of the earth is then, in the absence of electric fields, either equal to that at the source or zero, according to whether (P) is an allowed or forbidden value of rigidity. The flux of particles

of a particular rigidity consequently remains isotropic in the allowed cone, although the total flux of particles is clearly anisotropic, the directional flux distribution at any point being controlled by the rigidity spectrum of the primary particles.

If the flux is not isotropic at infinity the trajectories of the particles must be calculated in detail. The theorem may then be applied at any point on the calculated trajectories. This situation arises in the case of particles injected into the terrestrial field following solar flares. Anisotropy in the galactic radiation (Jacklyn, 1963) may be treated in the same way. Assuming isotropy outside the field, we need to know the rigidity spectrum of the primary particles in order to predict the directional effects observable with detectors situated near the surface of the earth.

3.2 THE PRIMARY COSMIC RAY-RIGIDITY SPECTRUM

The proton spectrum at sunspot minimum derived from measurements made in 1954, (Webber, 1962) may be described by a power law:

$$N(P) = KP^{-\gamma} \text{ peters/GV}^{*} \qquad 3.1$$

with exponent $\gamma = 2.48 \pm 0.05$ in the range 5-16GV. Below 3GV the spectrum begins to flatten and reaches a peak in the region 1-1.5GV. From the result of McDonald & Webber (1958) that

$$N(P \quad 4.5GV) = 730 \pm 30 \text{ peters},$$

the constant K may be determined as

$$K = 1.00 \cdot 10^{4} .$$

The α-particle spectrum appears to be similar in shape to the proton spectrum in the region 1-5GV. The power law exponent in

* 1 peter = 1 m^{-2} $sterad^{-1}$ sec^{-1}

the region 5-16GV, given by Webber as 2.45 ± 0.04, is not significantly different from that for protons in this range.

No heavy particle measurements in the range (1-5GV), were made during the 1954 sunspot minimum. Other measurements (Evans,1960), (Ellis et al., 1954) suggest that the spectrum is similar to the proton and alpha particle rigidity spectra.

Summarising the differential rigidity spectra for the year 1954 we have for $(5 < P < 16)$GV,

$$N(P) = K_Z P^{-\gamma} \text{ peters/GV},$$

where $K(Z = 1) = 100.10^4$; $\gamma = 2.48 \pm 0.05$

$K(Z = 2) = 1.39.10^3$; $\gamma = 2.45 \pm 0.04$

$K(Z = 6) = 1.1.10^2$; $\gamma = 2.44 \pm 0.06$

During the previous solar minimum (1944) the sea level ionization was higher than in 1954. However long term instrumental drifts do not allow any definite statement regarding the relative primary fluxes. The question of whether the 1954 spectrum represents the actual galactic spectrum may be answered when observations made during the present minimum (1963) are analysed.

If it is assumed that the peak in the spectrum at sunspot minimum is due to a residual solar modulation of form $(K(t)/P$, it has been shown by Webber that the true galactic spectrum would still not be a simple power law below 5GV. The form of the spectrum in this region is therefore of interest in establishing the processes of acceleration

and propagation of the primary radiation.

The spectrum at solar maximum is appreciably harder than at solar minimum. This result has been established by (a) latitude surveys, the interpretation of which depends on the geomagnetic theory; (b) by energy sensitive detectors, and (c) by examination of the atmospheric depth dependence of the intensity. The higher mean energy of the observed radiation near solar maximum is accompanied by a reduction in the total intensity. These two facts suggest the preferential screening of the lower rigidity particles at times of maximum solar activity. In figure (3.1) the integral rigidity spectra of cosmic rays obtained at times of sunspot maximum and minimum are plotted (after Webber, 1962). Transient increases in the charged particle intensity frequently occur following optical flares on the sun. The rigidity spectrum of the flare produced radiation has been investigated by Freier & Webber (1963) who show that the spectrum is well represented by

$$N(P) = K_s \exp(-P/P_o) \qquad 3.2$$

where P_o in the exponent is of the order of 10^2 MV .

3.3 COSMIC RAY EFFECTS IN THE GEOMAGNETIC FIELD

Use of the geomagnetic theory (Chapter 2) in conjunction with Liouville's theorem, enables the cosmic ray rigidity spectrum to be deduced from observations of the cosmic ray flux. Neglecting atmospheric effects and assuming the primary particles to be positively charged, the following effects are expected at the surface of the earth.

A. The Latitude Effect

In a given direction of incidence the threshold rigidity falls as

Fig.3.1

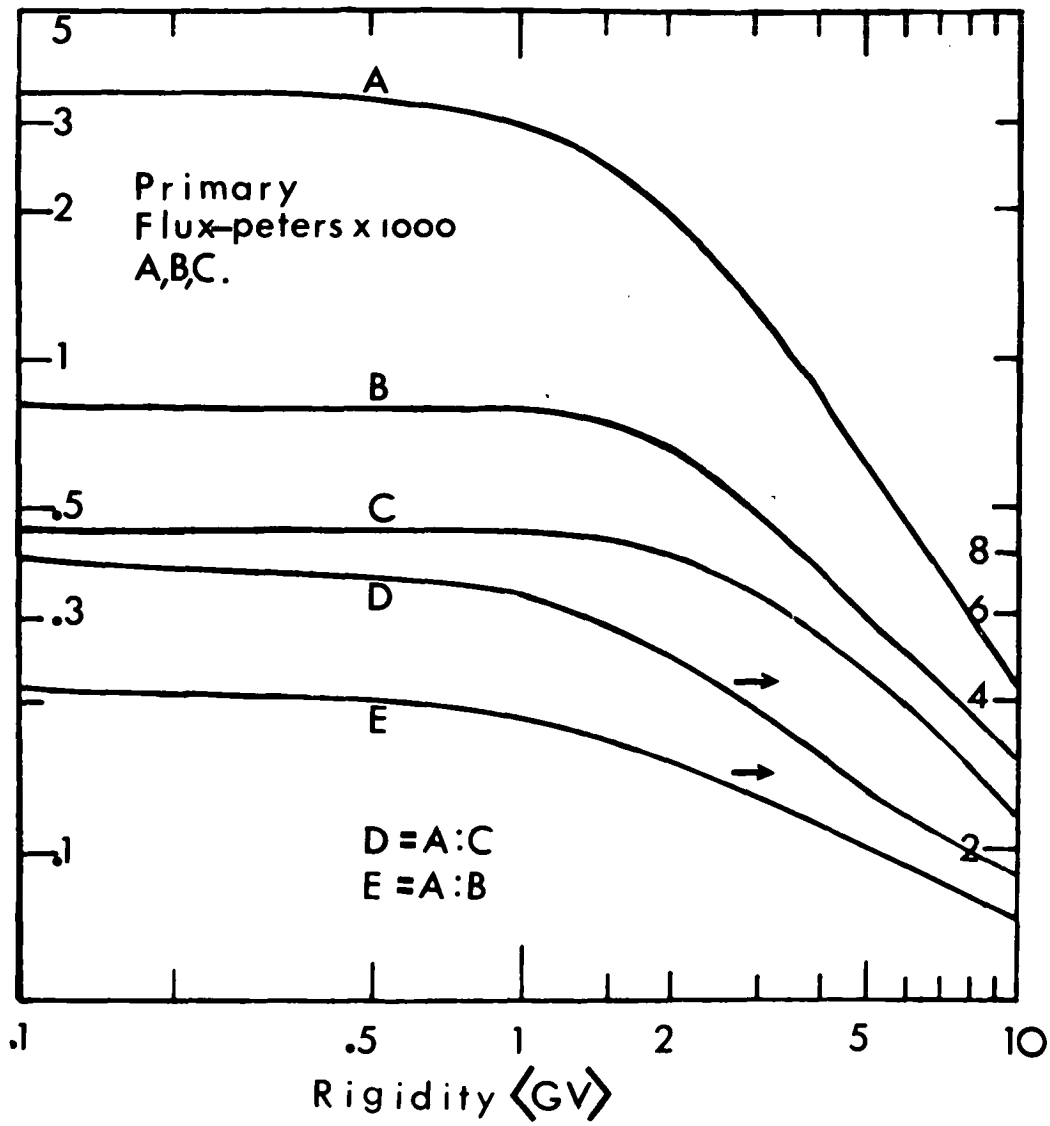

Integral Rigidity Spectrum of Cosmic Ray Protons:
A; At Solar Minimum
B; At Solar Maximum
C; During Forbush Event of July 18,1959

the geomagnetic latitude of observation is increased. The cosmic ray intensity therefore rises with latitude as particles of progressively lower rigidity are admitted by the field.

B. The Longitude Effect

The eccentricity of the dipole field and the non-dipole components field produce a longitude dependence of the threshold rigidity and hence of the cosmic ray intensity.

C. The East-West Asymmetry

The dependence of threshold rigidity upon the direction of incidence give rise to a directional asymmetry in the intensity. Since the threshold for positive particles is higher in the eastern than in the western direction the intensity is higher in the west than in the east. The east-west asymmetry (α_{ew}) is defined by

$$\alpha_{ew}(\theta) = \frac{J_w - J_e}{\frac{1}{2}(J_w + J_e)} \qquad 3.3.$$

where J_e, J_w are the directional fluxes measured in the east-west azenuths at the same zenith angle.

From equations (2.4) (2.7) and (3.1),

$$J_w - J_e = \delta J_{ew}(\theta)$$
$$\doteq \left(\frac{M}{4r^2}\right)^{1-\gamma} \cdot K \sin\theta \cdot \cos^{(7-4\gamma)}\lambda \qquad 3.4$$

and approximating $\frac{1}{2}(J_e + J_w)$ by $J(\theta = 0^\circ)$ we find

$$\alpha_{ew}(\theta) \doteq (\gamma - 1) \sin\theta \cdot \cos^3\lambda \qquad 3.5$$

These equations show that the asymmetry, at middle latitudes where both equations (2.7) and (3.1) approximately hold, is a linear function of the spectral index, γ, and a sensitive function of the geomagnetic

latitude. The "east-west excess", δJ_{ew}, unlike the asymmetry, increases with latitude (for $\gamma > 7/4$) and therefore might be expected to reach a maximum at a latitude determined by the flattening of the spectrum below 3GV. In figure (3.2) the east-west excess and the east-west asymmetry have been plotted for the spectra of Figure (3.1) using the exact Stoermer relations and neglecting the effect of the penumbra.

D. The North-South Asymmetry

Although the Stoermer threshold in the NS plane is independent of zenith, the main cone threshold is not. At latitudes 41° the resultant NS asymmetry is negligible for zenith angles below 30°. For $30^{\circ} \quad \theta \quad 45^{\circ}$, α_{ns} is a maximum at 45° and then decreases to zero as θ is increased. α_{ns} changes sign between 50° and 60° and again at $\theta = 70^{\circ}$ as the simple shadow cone cut off dominates for $\theta \quad 70^{\circ}$. At $\lambda = 41^{\circ}$ S, the asymmetry

$$\alpha_{ns} = \frac{J_s - J_n}{\frac{1}{2}(J_s + J_n)} \qquad 3.6$$

$$\doteq 0.1 \quad \text{for} \quad \theta = 45^{\circ}.$$

3.4 OBSERVATIONS OF THE EAST-WEST ASYMMETRY AT BALLOON ALTITUDES

All of the geomagnetic effects of the preceding section have been observed. The latitude effect has been often used to determine the spectrum of the primary radiation, (e.g. Johnson, 1938). In this section we review high altitude measurements of the directional effects.

A comprehensive investigation by Winckler (1949, 1950) of the azimuthal effects at balloon altitudes, while revealing significant asymmetrics at lower latitudes, failed to reveal an east-west asymmetry

FIGURE 3.2 : Primary East-West Asymmetry

(a) $\gamma = 2.5,\ \theta = \pi/2$

(b) - upper branch

$\gamma = 2.5,\ \theta = \pi/4$

(b) - lower branch

solar min. $\theta = \pi/4$

Primary East-West Flux Difference

(c) $\gamma = 2.5,\ \theta = \pi/2$

(d) - upper branch

$\gamma = 2.5,\ \theta = \pi/4$

(d) - lower branch

solar min.

Fig. 3.2

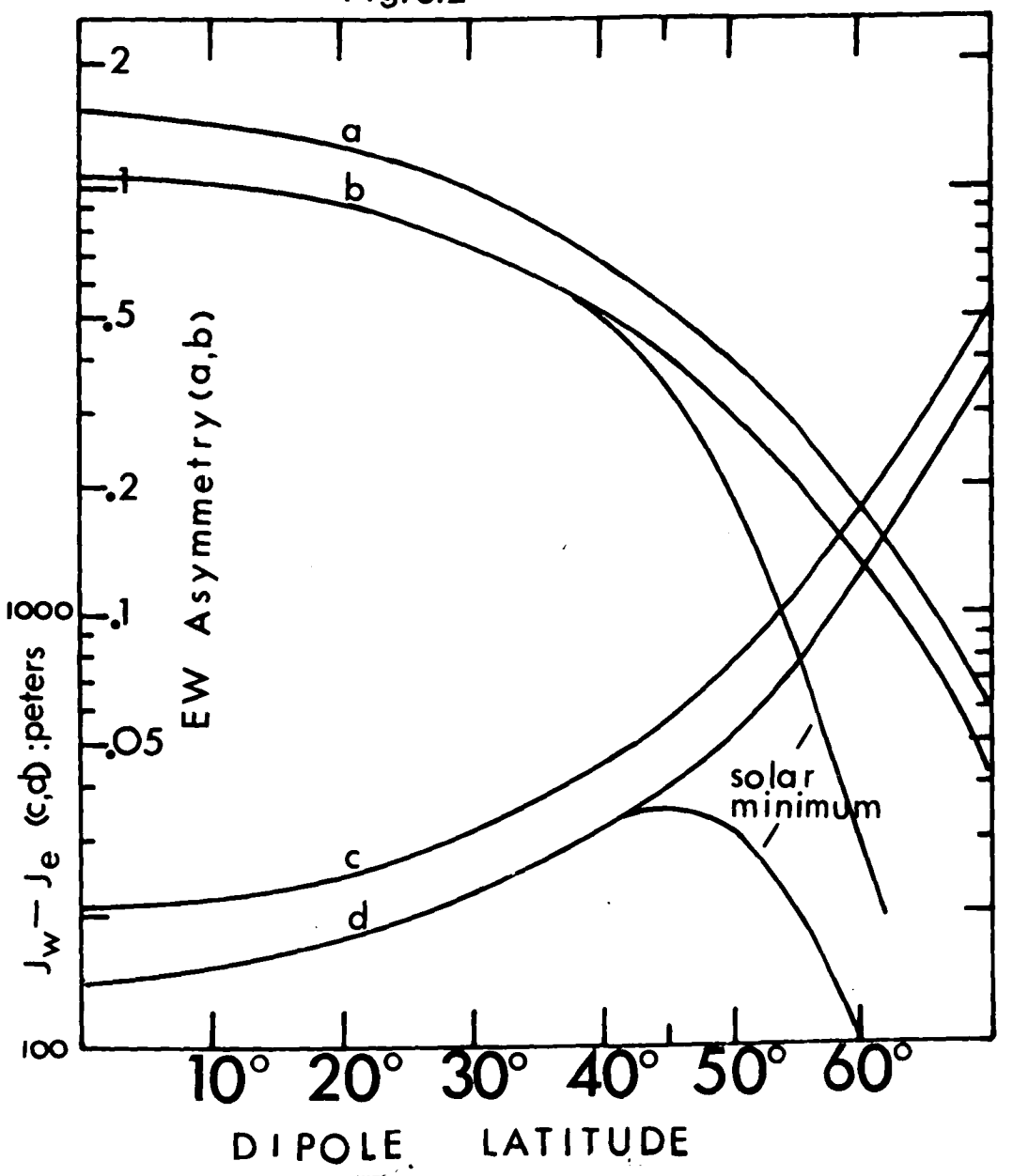
2
1
.5
.2
.1
.05
a
b
c
d
EW Asymmetry (a,b)
$J_w - J_e$ (c,d) :peters
100
10
solar minimum
10° 20° 30° 40° 50° 60°
DIPOLE LATITUDE

at geomagnetic latitude $\lambda = 56^{\circ}$ N . Had such an asymmetry been present its magnitude must have been less than 5% in magnitude.

The measured asymmetry (0.26 ± 0.06) at $\lambda = 40^{\circ}$ was shown by Anderson (1955) to be in consistent with the shadow cone calculations of Schremp (1938) after atmospheric effects had been taken into account. Schwartz, (1959) recalculated the shadow cones for a centred dipole field at a number of selected latitudes. He concluded that the asymmetry at $\lambda = 40^{\circ}$, $\theta = 60^{\circ}$ as measured by Winckler and Anderson with a directional Cerenkov counter to be (0.39 ± 0.2), was in agreement with the value predicted $(0.35 < \alpha < 0.52)$ for a differential spectrum $P^{-\gamma}$ with $(2 < \gamma < 2.5)$. In general the cut off rigidities predicted by Schwartz lie between the Stoermer and main cone values Sect. 2.2. The result quoted above is obviously not of sufficient accuracy to yield useful spectral information, even assuming the dipole calculations to be applicable. On the other hand the value obtained with a geiger telescope, although of higher statistical accuracy clearly errs on the low side due to the presence of the secondary background. If it is assumed that the background flux counted by the geiger telescope is the same for both east and west directions it must exceed one half the primary flux from the east. On this basis the measurements at $\lambda = 56^{\circ}$ indicate a primary asymmetry less than 8 %. In fact, assuming a 1/P spectral law, a primary asymmetry of no more than 8 % might be anticipated so that the experimental results are not in conflict with the assumption that the cut offs are given by the Stoermer model. If (as seems to be

the case), the differential intensity at 1.5 GV is no greater than at 3 GV at sunspot maximum (when the experiments were carried out) the primary asymmetry at $\lambda = 56^{\circ}$, ($P_o = 1.45$ GV) would be about 5.5 %, so that the measurable asymmetry would be less than 3.5 %. The absence of a measurable asymmetry at $\lambda = 56^{\circ}$ might therefore be expected irrespective of the phase of the solar cycle from observations of similar statistical accuracy to those of Winckler. Photographic emulsions have been used to measure the directional effects. Figure 3.4 reproduces the azimuthal variation in the intensity of the heavy ($Z \geqslant 5$) cosmic ray component at $\lambda = 42^{\circ}$ N observed by Danielson & Freier in 1956. These observations are in general agreement with the telescope results of Winckler & Anderson, but suggest the azimuth of maximum flux to be 20° south of geomagnetic west.

It is clear from the work of Neher (1948) that significant directional asymmetries are measurable with both shielded and unshielded telescopes at large atmospheric depths. For example over Peru, $\alpha(\theta = 45^{\circ}) = 0.23 \pm .01$ at $x = 310 g/cm^2$. The values are slightly higher for telescopes shielded with 10cm or more of lead. The Quenby-Webber vertical cutoff rigidity is 9 GV and the geomagnetic asymmetry is 0.8 for a P integral spectrum. The measured asymmetry is therefore about one quarter of the predicted Stoermer value.

Johnson and Barry (1939) carried out a number of flights with inclined telescopes at $\lambda_m = 20^{\circ}$ N. The measured east-west asymmetry averaged over the depth interval 50 - 150 g/cm^2 was found to be 0.072. That this value is anomalously low can be seen by comparison with the results of Neher ($x = 310 g/cm^2$) and Winckler ($x = 13.5 g/cm^2$)

$\alpha(\theta = 60^{\circ}) = 0.58$ at the same latitude. It is difficult to reconcile Johnson's value of α with the latter results, despite the fact that it was obtained with an unshielded telescope of wide aperture, averaged over 180° azimuthal sectors and at depths close to the transition maximum. Winckler found that similar azimuthal averaging reduced his value of α from 0.58 to 0.32. He concluded also that at a depth of 100 g/cm^2 α would be further reduced to about 20 %.

Winckler's results did not reveal a consistent depth dependence of the asymmetry, because of the poor statistics of the ascent data. Flights at the equator with unshielded telescopes did show however that the east-west difference did not change appreciably with depth below $x = 200$ g/cm^2, although the directional fluxes increased by a factor greater than three in going from $x = 15$ g/cm^2 to $x = 200$ g/cm^2. Moreover the asymmetries obtained were less than 10 % below those measured with 3 cm of Pb absorber. This latter result agrees with the observations of Neher at greater depths. Inspection of the graphed Winckler data for higher latitudes suggests that the asymmetry decreases slowly with increasing depth until the transition maxima are reached where upon the asymmetry drops rather more rapidly with further increase in depth.

The east-west difference increases with depth, reaches a maximum near the transition maxima and then decreases rapidly. The difference between the east and west transition depths is noticeable, the greatest western flux being observed at a lower depth, as might be expected.

Although it is not possible to obtain an accurate $\alpha(x)$ relation from the above results, it is clear that the asymmetries are preserved at considerable depths in the atmosphere. The results of the present

experiments are discussed in Chapter 8. These results have reasonable statistical accuracy, having been obtained during the floating periods of the flights.

In a recent review, Kane (1962), has examined the azimuthal measurements of many observers at sea level and at high altitudes. He concludes that the high altitude measurements at high latitudes are statistically inadequate to allow any detailed comparison with the theoretical effects.

3.5 THE SPLASH ALBEDO

The experiments of Anderson (1955) with Cerenkov detectors have yielded useful information on the depth and latitude dependence of the splash albedo, the presence of which prevents a direct comparison between the theory and observations of the azimuthal variations.

In Anderson's experiments the absolute flux of the "fast" vertical splash albedo ($P > 1.4$ GV) was a weak function of latitude, increasing from 70 to 110 peters at 20 g/cm^2 for a latitude range from 10^o to 55^o. The statistical errors are such, that the increase may not be significant. Expressed as a percentage of the total telescope flux, the fast splash albedo at the zenith decreases from 15 % at $\lambda = 10^o$ to no more than 2 % at $\lambda = 55^o$.

At latitude 40^o the azimuthal dependence of the splash albedo was found to be small. This result indicates that the fast albedo is produced by field insensitive primaries (protons of energy greater than 10 GeV) at this latitude. Near the equator the flux increased with zenith angle as might be expected. In going from 0^o to 60^o zenith the flux increased by about 70 %. No increase was observed at 40^o latitude.

The albedo at latitude 55° decreased by a factor of three in going from 20 to 55 g/cm^2 atmospheric depth.

The albedo flux below 1.4 GV was not obtained directly in this work. However the proton flux in the momentum band 0.64 to 1.4 GV, that is, those protons producing no Cerenkov light but capable of being detected by the geiger telescope, was obtained. This flux contains a contribution from the lower energy splash albedo which at high latitudes is greater than the fast albedo flux. At latitude 55° its intensity is greater by a factor of 10 at 20 g/cm^2. At greater depths the factor increases rapidly and the fast splash albedo becomes an insignificant fraction of the slow proton flux.

McDonald and Webber directly measured the proton intensity at $\lambda = 55°$ in 1955 to be 2600 peters. Single counter data obtained at the same time (van Allen and McIlwain, 1956) indicated an average indirectional flux of 4200 peters at the top of the atmosphere. By assuming the re-entrant and splash albedo fluxes to be equal (Meredith et al., 1955) the total splash albedo becomes 800 peters, about 30% of the primary flux. This result is in agreement with Anderson's work and suggests that it is the low energy part of the splash albedo which is most significant in reducing the directional asymmetries at high latitudes.

3.6 AIM OF THE PRESENT EXPERIMENTS

Having surveyed the theoretical and observational background to the directional cosmic ray effects, it is now possible to state the objects of the present work. The review of the literature reveals a dearth of high altitude asymmetry measurements - particularly at high latitudes where the geomagnetic effects, although small, ought to be

most sensitive to modulation of the primary spectrum. In recent years attention has been directed towards obtaining more accurate predictions of the distribution of cosmic ray flux over the surface of the earth, (e.g. Quenby & Webber, 1959; Quenby & Wenk, 1962; Pomerantz, 1962; McCracken, 1962). These investigations have not yet been finalised, even for radiation incident from the zenith. However, availability of accurate field representations, high speed digital computers and more advanced experimental techniques suggests that the geomagnetic effects might, in the near future, be sufficiently well known to allow the rigidity spectrum of the primary radiation to be deduced from directional measurements at a number of fixed locations on or above the earth's surface. The first of the geomagnetic effects used to provide spectral information, namely the geographic dependence of the intensity, has recently been re-examined (McCracken, 1962) and it has been shown for instance that the daily variation of the sea level intensity is probably independent of energy. It seems likely that advances in elucidating the energy dependence of other intensity variations may also result from the application of similar methods.

The immediate aim of the present experiments was therefore the acquisition of directional charged particle fluxes at high latitudes and altitudes. The main emphasis will be placed on measurements of the east-west excess flux (δJ_{ew}) as the preceding sections suggest this quantity to be more significant than the east-west asymmetry (a_{ew}) when measured with directional geiger telescopes. It was hoped that these data, would provide spectral information at low rigidities. Some contributions to the understanding of the geomagnetic effects might

also be expected. In the following chapter, experimental results on the azimuthal distribution of the high altitude flux will be presented. The extent to which these results are consistent with present estimates of the primary spectrum and the geomagnetic effects will be described.

CHAPTER FOUR

ACQUISITION OF DATA

INTRODUCTION

The aim of the experiment was discussed in the previous chapter. In this chapter we examine the techniques of measurement. The cosmic ray flux may be obtained with a variety of instruments. Economic considerations suggested the geiger counter telescope to be a suitable directional instrument. It was hoped that cosmic ray data could be obtained by suspending an inclined telescope below an elastic balloon, valved to float at a constant atmospheric depth using the method of Hopper (1957). The natural rotation of the balloon and pay load was relied upon to provide azimuthal scanning. The azimuth of the telescope was obtained with solar sensors. As a result of difficulty with the balloon valving technique at Hobart (geomagnetic latitude, 52° S) it was decided to fly equipment at Mildura on the Australian mainland. An air sampling program (Project Hibal of the U.S. Atomic Energy Commission) utilizing plastic balloons was being carried out at Mildura (geomagnetic latitude, 44° S) by the Australian Department of Supply. A number of telescopes were included with Hibal pay loads and successful flights were made.

In the following two chapters we discuss the techniques of data acquisition, recording and read out associated with the Hobart and Mildura experiments.

4.1 TELESCOPE DESIGN FOR DIRECTIONAL COSMIC RAY EXPERIMENTS

Directional measurements of the primary flux at a given location may be used to obtain, using geomagnetic theory, a differential rigidity

spectrum of the primary radiation. Assuming that the geomagnetic theory presents no obstacles, the greatest problem lies in discriminating between the primary and secondary components of the cosmic ray flux.

The simplest method is to make measurements of the heavy particle flux. Alpha-particle flux measurements using photographic emulsions are one example of this method. Since the secondary background of α-particles must constitute a very small fraction of the primary intensity, such measurements are virtually uncontaminated by the splash albedo and other secondary components.

Large geiger tube telescopes suitable for balloon work cannot eliminate the secondary background because of the large mass of absorber required. The time resolution of these tubes is also too low by several orders of magnitude to discriminate between up and down coming particles.

The Cerenkov detector exhibits a marked "anti-directional" property and may therefore be used to eliminate the fast splash albedo contribution to the charged particle flux. In addition, since this type of detector is velocity and charge sensitive, further discrimination against the re-entrant albedo and soft secondary particles is possible.

Unfortunately the preservation of the anti-directional characteristics of the detector is incompatible with the requirement of high geometric sensitivity. This situation arises principally because the limited optical aperture of economic photon detectors reduces the permissible volume of the Cerenkov radiator, and hence the area-solid angle product of the detector. In the experiments to be described the total

period of data collection in any one flight was too short to allow accurate directional flux measurements with Cerenkov detectors using conventional photo multipliers. The view was taken that the directional measurements were most efficiently obtained using geiger telescopes of high sensitivity.

The Cerenkov counter technique was first applied to the albedo problem by Winckler (1952). Later work by Winckler and Anderson (1952, 1954, 1955) resulted in reliable estimates of the background radiation. Anderson considers the east-west asymmetry observed by a geiger telescope to be

$$a'_{EW} = \frac{(I_W + X_W + Y_W) - (I_E + X_E + Y_E)}{\frac{1}{2}(I_W + I_E + X_W + X_E + Y_W + Y_E)} \qquad \ldots 4.1$$

where $I_{W(E)}$ = Ionising particle flux from the West (East), calculated from geomagnetic and nuclear collission theory (at the depth of observation)

$X_{W(E)}$ = Measured fast splash albedo flux from the West (East)

$Y_{W(E)}$ = Measured slow proton flux from the West (East)

He found the fast splash albedo and slow proton fluxes to be independent of azimuth and was therefore able to rewrite Equation 4.1 in the form

$$a'_{EW} = \frac{\delta I_{EW}}{\frac{\delta I_{EW}}{2} + (X + Y) + I_E} \qquad \ldots 4.2$$

Equation 4.2 shows that the measured asymmetry will in general be less than the geomagnetic ("primary") value.

Now the differential flux δI_{EW} evidently contains little or no background contribution. At depth $x g/cm^2$ we therefore write,

$$\delta I_{EW}(x) \doteq m(x).\delta J_{EW} \qquad \ldots 4.3$$

From Equation 3.4,

$$\delta I_{EW}(x) \doteq K\left(\frac{M}{h_r^2}\right)^{i-\gamma}.m(x).\sin\theta.\cos^{(7-4\gamma)}\lambda \qquad \ldots 4.4$$

The factor $m(x)$ may be found by experiment or by calculation. The primary differential flux may then be obtained after extrapolating $m(x)$ to zero depth. To find K and γ separately, some assumption must be made about the background contribution to the measured flux. We are now in a position to consider the design of the telescope. The basic limitation to the accuracy of the directional measurements is imposed by statistical fluctuations in the counting rates. Assuming the counting rate in a given direction to be a Poisson variable, the variance of the east-west difference rate is

$$\delta^2(\dot{N}_W - \dot{N}_E) = (\dot{N}_W\tau_W + \dot{N}_E\tau_E) \qquad \ldots 4.5$$

$$\text{Hence} \quad \frac{\delta(\dot{N}_W - \dot{N}_E)}{\dot{N}_W - \dot{N}_E} = \left(\frac{\overline{\dot{N}}}{\tau}\right)^{\frac{1}{2}} \cdot \frac{1}{\delta\dot{N}_{EW}}$$

$$\text{therefore} \quad \frac{\delta(\delta I_{EW})}{I_W - Y_E} = \left(\frac{\overline{I}}{\tau G}\right)^{\frac{1}{2}} \cdot \frac{1}{\delta I_{EW}} \qquad \ldots 4.6$$

where τ is the duration of the measurements, $(\tau_E = \tau_W = \tau/2)$,

and G is the geometric factor of the telescope. If the background were absent and the measurements were made at the tops of the atmosphere, then

$$\delta I_{EW} = \delta J_{EW}$$

$$\overline{I} = \overline{J} \doteq J_o$$

and

$$\frac{\delta(\delta \dot{N}_{EW})}{\delta \dot{N}_{EW}} = \frac{(\delta I_{EW})}{\delta I_{EW}}$$

$$= \frac{\delta(\delta J_{EW})}{\delta J_{EW}}$$

$$= \left(\frac{J_o}{\tau G}\right)^{\frac{1}{2}} \cdot \frac{1}{\delta J_{EW}}$$

$$= \left(\frac{1}{\tau G}\right)^{\frac{1}{2}} \cdot \frac{(M/4\pi r^2)^{(\gamma-1)/2}}{(\gamma-1)^{\frac{1}{2}} \cdot K^{\frac{1}{2}} \cdot \cos^{(5-2\gamma)}\lambda \cdot \sin\theta} \qquad \ldots 4.7$$

$$= F(\gamma, \lambda, K) \cdot \frac{(\tau G)^{-\frac{1}{2}}}{\sin\theta} \qquad \ldots 4.8$$

Since $\gamma \doteq 2.5$ for $P > 3GV$, the duration and geometric factor required for a given statistical error in δJ_{EW} will be independent of latitude at low and medium latitudes. The quantity $\tau G \sin^2\theta$ is then approximately $\frac{35}{k^2}$ cm^2-sterad-sec. For $k = 0.1$ (10%), $\sin\theta = 45^\circ$, $G = 100$ cm^2-sterad, the required period of data collection is therefore about one minute. At high latitudes longer flights or larger telescopes are required because of the reduction in the spectral

intensity and the reduction in the east-west rigidity difference. The quantity $(\sin^2\theta . \tau G)$ is plotted in Figure 4.1 for a standard error in δJ_{EW} of 1% using the spectrum of Section 3.2. The ordinate of this curve may be scaled to a standard error of k% by multiplying by $1/k^2$. The discussion above neglects the background contribution and consequently over estimates the statistical accuracy attainable with geiger telescopes.

4.2 ANGULAR RESOLUTION

Azimuthal intensity studies with telescopes do not yield directly the flux in the direction (θ,ϕ). Due to the finite opening angle of the telescope and the angular resolution of the associated compass device, the particle flux deduced from the telescope counting rate is effectively averaged over non-zero zenith and azimuth intervals.

We have seen that to any given direction of incidence, it is possible to find an effective threshold rigidity which depends only weakly on the primary spectrum. In order to investigate the influence of azimuthal resolution upon the expected directional effects, we consider a simplified model of an experiment designed to measure the east-west asymmetry (G), the east-west asymmetry ratio (J_W/J_E), and the differential flux $(J_W - J_E)$.

The threshold rigidity at high latitudes is well approximated by

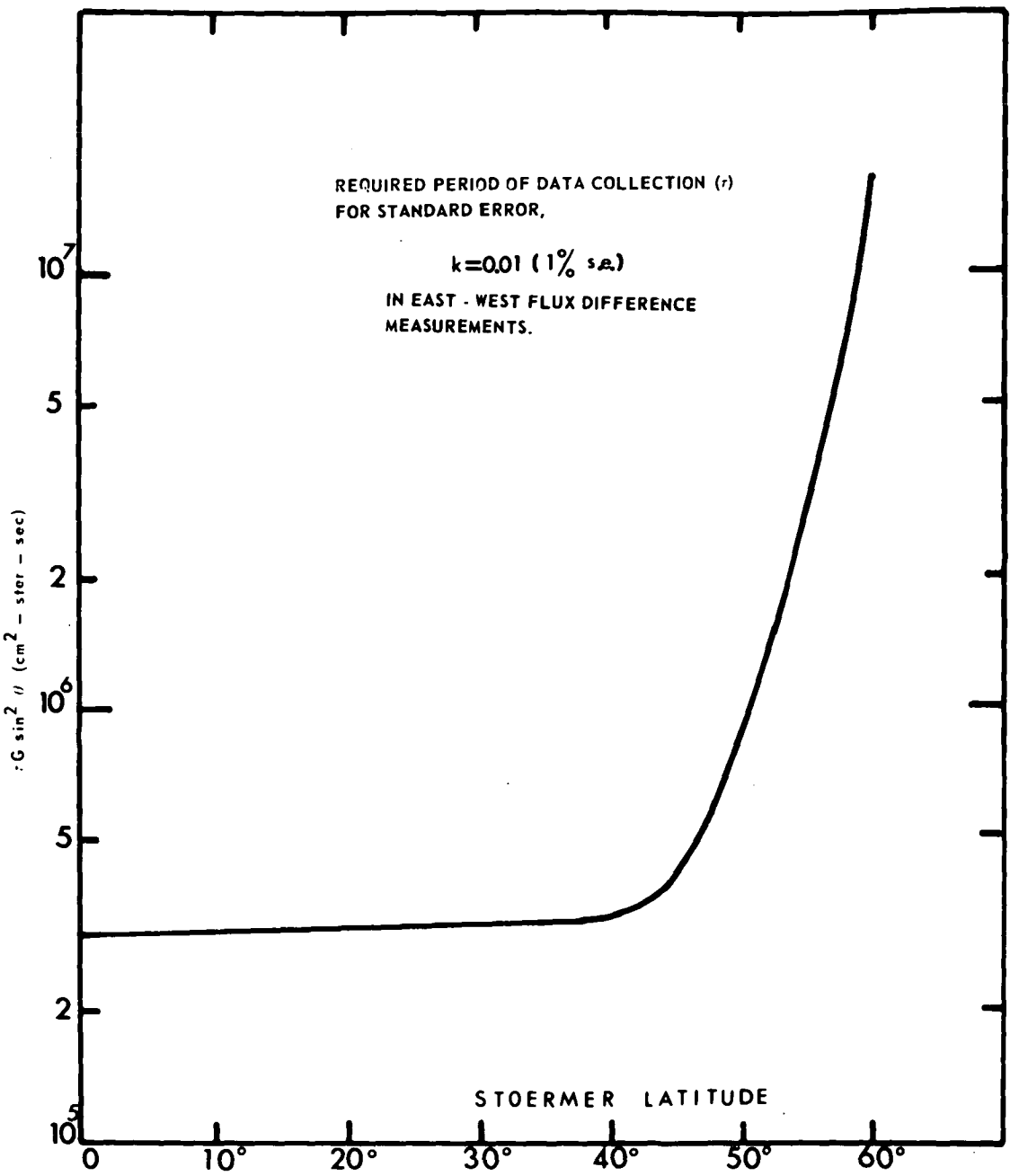
REQUIRED PERIOD OF DATA COLLECTION (τ)
FOR STANDARD ERROR,
k=0.01 (1% s.e.)
IN EAST - WEST FLUX DIFFERENCE
MEASUREMENTS.
10^7
5
2
10^6
5
2
10^5
$G \sin^2 \theta$ (cm^2 – ster – sec)
STOERMER LATITUDE
0
10°
20°
30°
40°
50°
60°

Fig 4.1

the expression,

$$P_o(\phi) = P_1 + P_2 \sin\phi$$

then $$P_o(\pi/2) = P_E = P_1 + P_2$$

and $$P_o(3\pi/2) = P_W = P_1 - P_2$$

$$\therefore \bar{P}_o(\langle\phi_o - \delta, \phi_o + \delta\rangle) = \frac{1}{2\delta}\int_{\phi_o-\delta}^{\phi_o+\delta}(P_1 + P_2 \sin\phi)\,d\phi = P_1 + P_2 \sin\phi \cdot \left(\frac{\sin\delta}{\delta}\right)$$

$$\therefore \bar{P}_o(\langle\pi/2 - \delta, \pi/2 + \delta\rangle) = P_1 + P_2 \cdot \frac{\sin\delta}{\delta} \qquad 4.9$$

and $$\bar{P}_o(\langle 3\pi/2 - \quad, 3\pi/2 + \delta\rangle) = P_1 - P_2 \cdot \frac{\sin\delta}{\delta}$$

It may be seen that the aperture effect is quite small. For example, if $2\delta = \pi/2$, the eastern threshold would be lowered by an amount $P_2\left(1 - \frac{\sin\delta}{\delta}\right) = 0.10\,P_2$, while the western threshold rigidity would be raised by the same amount. The effective cut off rigidities at latitude 41° (Schwartz, 1959),

$$\left.\begin{aligned} P_E &= 6.13 \text{ GV} \\ P_W &= 4.46 \text{ GV} \end{aligned}\right\}, \quad \theta = 45^\circ$$

therefore become, when averaged over 90° azimuth intervals,

$$\left.\begin{aligned} \bar{P}_o E &= 6.05 \\ \bar{P}_o W &= 4.54 \end{aligned}\right\} \text{GV}$$

values, which differ from the true threshold by little more than 1 %. Taking an integral rigidity spectrum of the form P_o^{-1}, the "primary" asymmetry,

$$\alpha = \frac{2(J_W - J_E)}{J_W + J_E} = 2 \cdot \frac{P_2}{P_1}$$

$$= 0.316$$

becomes

$$\alpha' = \frac{2P_2}{P_1} \cdot \frac{\sin\delta}{\delta} \qquad 4.10$$

$$= 0.285$$

while the asymmetry ratio

$$\frac{J_W}{J_E} = \frac{P_1 + P_2}{P_1 - P_2} = 1.37$$

becomes

$$\frac{\bar{P}_E}{\bar{P}_W} = 1.33$$

The differential intensity,

$$J_W - J_E = K \frac{(P_E - P_W)}{P_E \cdot P_W} = \frac{2K \cdot P_2}{(P_1 - P_2) \cdot (P_1 + P_2)}$$

$$= 0.061\ K$$

is reduced to

$$\bar{J}_W - \bar{J}_E = \frac{2K\ P_2 \frac{\sin\delta}{\delta}}{P_1^2 - P_2^2 \cdot \frac{\sin^2\delta}{\delta^2}} \qquad 4.11$$

$$= 0.055\ K$$

The required zenith angle resolution is comparable with that required in the azimuth plane. In the absence of a simple shadow cone cut off, the penumbral transmission will not change rapidly with zenith angle, and the sin θ dependence of the east-west effects given by the Stoermer expressions, (equations 3.4, 3.5) show that

$$\frac{\bar{\alpha}_{EW}(\theta - \delta, \theta + \delta)}{\alpha_{EW}(\theta)} = \frac{\overline{\delta J}_{EW}(\theta - \delta, \theta + \delta)}{\delta J_{EW}(\theta)}$$

$$= \frac{\sin\delta}{\delta} = 0.9 \quad \text{for } \delta_\theta = \pi/4$$

The generally small magnitude of these differences suggests that extremely high angular resolution is not required for an investigation of the type to be described. This allows the use of wide angle telescopes and compasses of limited resolution, in order to improve the statistical accuracy of the telescope count totals without introducing large bias to the directional flux data. For the same reason however, accurate determination of the directions of maximum and minimum flux cannot easily be made at high and medium latitudes. The presence of a secondary particle contribution to the telescope counting rate reinforces these conclusions. In determining the permissible zenith angle resolution it is clear however that large zenith angles should be avoided if a bidirectional detector, such as a geiger telescope, is used.

4.3 THE GEOMETRIC SENSITIVITY OF COUNTER TELESCOPES

The great variety of geometrical arrangements of the counting tubes in telescopes, and the various approximations used by different workers in calculating the telescope response to charged particle fluxes, has in the past led to some confusion. The problem of normalising measurements made with differing telescope geometries is aggravated when, as is often the case, the telescopes simply consist of an array of single cylindrical counting tubes. This is due to (a) the complicated cylindrical geometry, (b) uncertainties regarding the angular distribution of the incident flux and (c) the dependence of the geiger efficiency upon the path length of the particle in the sensitive regions of the tubes.

If the unidirectional intensity of detectable particles in the direction (θ, ϕ) is $I(\theta, \phi)$ cm^{-2} sterad^{-1} sec^{-1}, then $I(\theta, \phi)\, da.d\Omega.dt$

is the number of particles incident upon area da normal to the direction $(\theta,,\phi)$ from within the solid angle $d\Omega$ at (θ, ϕ) in the time interval dt . Let $A(\theta, \phi)$ be the cross section presented by the telescope normal to (θ, ϕ) . The counting rate is then

$$\dot{N} = \int\int_{\Sigma} I(\theta, \phi) \cdot A(\theta, \phi) \cdot d \qquad 4.12$$

where Σ is the solid angle over which $A(\theta, \phi)$ does not vanish. If the intensity is uniform over the aperture of the telescope, this equation may be rewritten in the form

$$\dot{N} = I_o G \qquad 4.13$$

where $$G = \int_{\Sigma} A(\theta, \phi)\, d\Omega$$

is the geometric factor (G.F.) of the telescope. This representation of the telescope sensitivity is also useful when the flux is non uniform, providing the telescope aperture is sufficiently small to allow an average value of the direction intensity to be used in the calculation. The most frequently used approximation to the G.F. is,

$$G = \frac{A^2}{l^2} = \left(\frac{db}{l}\right)^2 \qquad 4.14$$

where A is the cross sectional area of either of the end trays (assumed parallel, coplanar and equal in area) of the telescope, and l is their separation. This expression is the area-solid angle product $(A\Sigma)$ if the dimensions (d, b) of the counter trays are negligibly small compared with the separation (l) .

If (4.14) accurately gives $(A\Sigma)$ then the aperture of the telescope will necessarily be so narrow that the flux distribution will

usually be constant over its width and the counting rate will be given by

$$\dot{N}(\theta_o, \phi_o) = (\frac{db}{l})^2 \cdot I(\theta_o, \phi_o) \qquad 4.15$$

where the direction of the telescope axis is (θ_o, ϕ_o), and $I(\pi + \theta_o, \pi + \phi_o) = 0$.

If the flux is isotropic, the finite width of the aperture will not introduce any error in the determination of the incident flux. In this case the errors will depend on the accuracy of the expression for G. For telescopes made up of cylindrical counters the separation (l) is generally taken to be the perpendicular distance between the counter axes. Montgomery (1949) has shown that this procedure tends to overestimate the geometric factor.

Pomerantz (1949) has calculated G for isotropic, $(\cos\theta)$, and $(\cos^2\theta)$ distribution and gives,

$$G_{iso} = J_o d^2 \left[\frac{b}{l} \tan^{-1} \frac{b}{l} + \frac{d}{4l} \left(1 - \frac{l^2}{l^2 + b^2}\right)\right] \qquad (a)$$

$$G_{\theta_o = 0}(\cos\theta) = \frac{2J_o}{3} d^2 \left[2 \left(\frac{l^2 + b^2}{l^2}\right)^{\frac{1}{2}} - 1 - \left(\frac{l^2}{l^2 + b^2}\right)^{\frac{1}{2}} + \frac{d}{4l} \left(1 - \frac{l^2}{l^2 + b^2}\right)^{\frac{3}{2}}\right] \qquad (b)$$

$$G_{\theta_o = 0}(\cos^2\theta) = \frac{J_o}{4} d^2 \left[\frac{2b}{l} \operatorname{artan} \frac{b}{l} + \frac{b^2}{l^2 + b^2} + \frac{d}{2l} \left(1 - \left(\frac{l^2}{l^2 + b^2}\right)^2\right)\right] \qquad (c)$$

These formulas apply to vertically pointing telescopes with geometry defined by two parallel cylindrical tubes of diameter (d), length (b) and axial separation (l). Newell (1949) has also studied the geometry of the two counter telescopes and has presented his results in graphical form. The results derived by him allow G to be located between upper and lower bounds which differ by several percent.

Use of equation 4.14 shows that the volume (bdl) occupied by a telescope of given geometric factor G is proportional to l^2. It is therefore desirable to reduce l and widen the aperture in order to obtain maximum sensitivity. The results of Section 4.2 show that the telescope opening angles may be widened considerably before the aperture correction becomes excessive. In Chapter 7 we shall use geometric factor calculations in conjunction with numerical integration of equation 4.12.

4.4 THE GEIGER COUNTERS

The geiger counting tubes used in the balloon flights were similar to those used in the meson telescopes operated at ground stations by the University of Tasmania (Parsons, 1957). These tubes are of the self quenched, maze type. They are filled with an Argon-ether gas mixture to a total pressure of about 6 cm Hg. The anode is a 0.07 mm diameter tungsten wise and the cathode is an "Aquadag" coating on the external surface of the soda glass envelope. The nominal internal diameter of the envelope is 3.8 cm. The tubes are operated at voltages between 1000 and 1300 volts. The main disadvantages of this type of tube arise from the resistance of the soda glass cathode wall. The resulting dependence of the pulse amplitude on temperature and counting rate (Edwards, 1960) makes the tube unsuitable as a balloon borne detector.

In order to remove these defects, tubes were constructed with an internal nickel cathode. Satisfactory performance was then achieved at temperatures above -30° C. To further reduce the temperature dependence the proportion of ether in the gas mixture was

reduced from 11 % to 5 %. Counters of this type performed at - 60° C and were successfully flown at night. The internal cathode counters were found to have higher background counting rates and were more photosensitive than the maze counters. Considerable improvement resulted when the tubes were constructed of pyrex and baked under vacuum at 420° C for several hours. Table 4.1 below lists typical characteristics of the geiger tubes used in this investigation.

TABLE 4.1

TYPICAL GEIGER COUNTER CHARACTERISTICS

	1.	2.	3.
Anode Length (cm)	10	10	30
Anode Diameter (mm)	0.07	0.07	0.07
Cathode Diameter (cm)	3.90	3.85	3.90
Gas Mixture: Ether: Argon;	1:9	1:13	1:9
Gas Pressure (cm Hg)	5.6	6.0	8.0
Starting Voltage	920	1000	1000
Dead Time (μs)	300	300	300
Plateau Slope (%/100 volts)	4.2	5.0	4.4
Plateau Length (volts)	250	200	300
Background Rate (sec^{-1})	2	3	10

Unfortunately it was not possible to construct nickel counters of length greater than 10 cm. It was necessary therefore to use the longer maze counters for the telescope flights in which high counting rates were required.

Before the counters were placed in the telescope, their dimensions

were accurately measured. They were then sprayed with an opaque paint to exclude light, the ends of the cathode having previously been marked to facilitate telescope alignment.

Experience gained in the construction of single geiger counter balloon sondes at Hobart (Edwards, 1960) was useful in devising methods of preventing corona discharge at high altitude. Several methods were originally used, both involving "potting" techniques. Complete encapsulation of E.H.T. supplies in wax or epoxy resin was found to be necessary to prevent corona discharges. All high voltage leads to the counting tubes were kept as short as possible and were protected by several thicknesses of polyethylene or polyvinyl-chloride tubing. Resin encapsulation of all high voltage points was carried out. This was necessary at the external connections to the geiger counter anodes. Where batteries were used to provide the counter voltage, the cells were dipped in a low melting point paraffin wax.

All high voltage connections were smoothly soldered in order to minimuse the field strength in their neighbourhood. For the same reason the E.H.T. leads, covered with material of high dielectric strength, were kept away from sharply edged conductors. These techniques were all vacuum tested in the laboratory. It was found that if sharp edges were avoided, mere separation of high voltage conductors was sufficient to prevent discharge at pressures above 3 cm Hg ($h < 70{,}000$ feet) providing the separation was greater than about $\frac{\pi}{2}$". At lower pressures, corona prevention becomes increasingly difficult and complete potting or pressurization appear the only solutions.

Experimental difficulties with geiger counters due to corona discharge are small because of the high amplitude of the pulses (5 volts) from these counters. The correspondingly high discrimination levels prevents interference from corona noise pulses. Corona cannot be tolerated in a Cerenkov telescope however, where the output pulses may be comparable in amplitude with the corona pulses. The problem is also greater because of the high voltage $\doteq$(2 KV) required to operate the photo multiplier.

4.5 CONSTRUCTION AND OPERATION OF THE TELESCOPES

The telescopes were constructed on the basis of the design considerations of the previous sections. The permissible volume of the Mildura telescopes was limited so that wide apertures were necessary. Three telescope types were used. The geometries are shown in figures 4.2 and 4.3.

It was intended to rely primarily on Telescope A for the Mildura data. Telescopes B and C were flown at Hobart and Mildura when the initial flights of telescope A proved unsatisfactory due to cooling of the Maze counters below 0° C . Redesign of the package and the inclusive of a heating element allowed this telescope to be used in later flights. Each tray (fig. 4.2 (A)) contained 3 (4 x 30) cm Maze counters. The trays were bolted to the diagonal members of the tubular aluminium instrument frame. The outputs of each counter in a tray were added and applied to the pulse shaping circuit of fig. 4.4 (a) . The pulse shapers were constructed as plug in modules. Coincidence circuits with a resolving time of 2.5 sec were developed and used. Fig. 4.2 (B) shows the double telescope with geometry B .

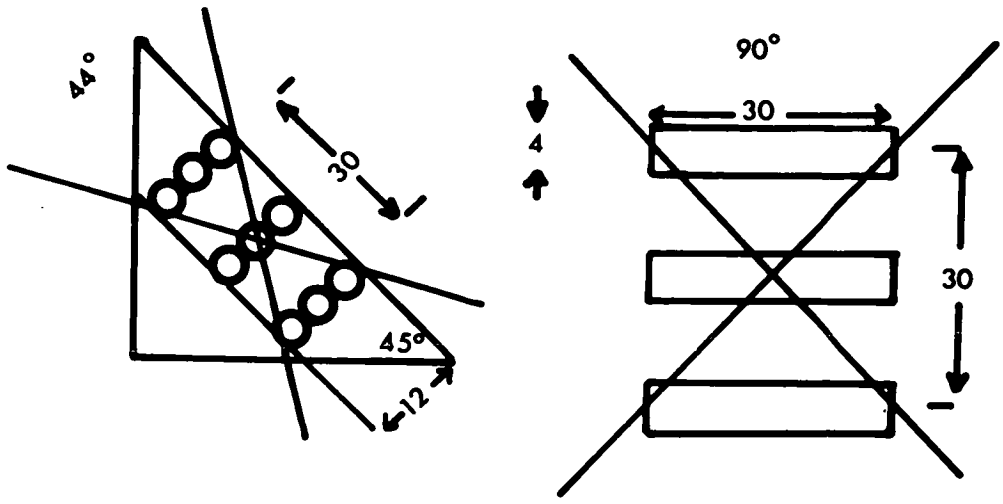

"A"

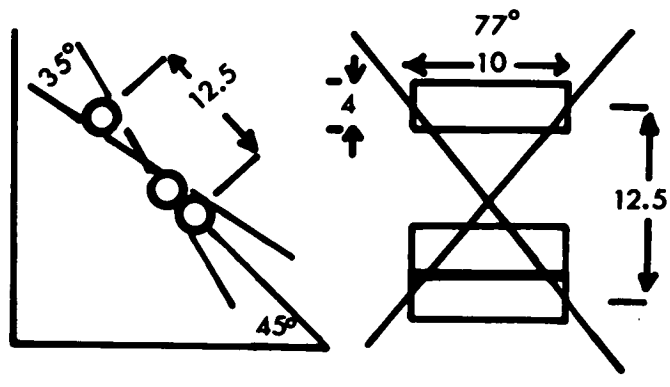

"B"

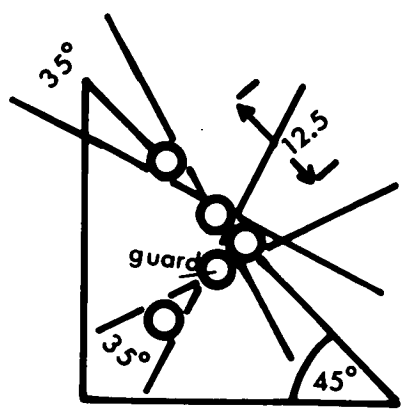

"C"

FIG. 4.2 Telescope geometries

The Cerenkov telescope geometry is shown in fig. 4.3. The array of five counters constituted telescopes defined respectively forming by coincidences between counters G_1, G_2, G_3, G_4 and G_1, G_4, G_5. The Cerenkov telescope output was obtained by placing the N.A. output pulses in coincidence with the amplitude discuminated photomultiplin pulses. The Cerenkov telescope logic circuity is shown as a block diagram in fig. 4.5 (a). The circuit board is shown in fig. 4.5 (b).

The telescopes were operated for several days in the laboratory before each flight to allow accurate intercomparison of flight results. The laboratory meson telescope rates were used as references. The relative counting rates of the various telescopes were in good agreement with the ratios calculated from equation 4.1 (c) using the measured dimensions of the counter arrays. However it was found that an appreciable correction (-24 %) had to be made to the geometric factor of telescope A to take account of the reduction in sensitive tray area, due to the thickness of the counter walls. In deducing absolute flux values from the experimental data, calculation of the reduction in counter efficiencies due to the high background rate and non zero dead time was necessary. Details of the telescope efficiency calculations are given in appendix 1.

4.6 DETERMINATION OF AZIMUTH

At balloon altitudes the sun is an optical source of approximately $\frac{1}{2}°$ angular width situated in a dark sky-background. The sun therefore provides a convenient reference in determining the magnetic azimuth of a balloon borne directional instrument, since the magnetic declination and the hour angle of the sun may both be found if the geographic coordinates of the balloon are known at any given time.

FIGURE 4.3 : Cerenkov-Geiger Telescope Geometry

Narrow Angle (N.A.) : G_1. G_2. G_3. G_4

Wide Angle (W.A.) : G. G_4. G_5

$a = 3.9$ cm

$b = 10$ cm

$L_4' = L_2 - L_3$

$= 34.5$ cm

$L_1 = 25.7$ cm

B : Cerenkov Radiator

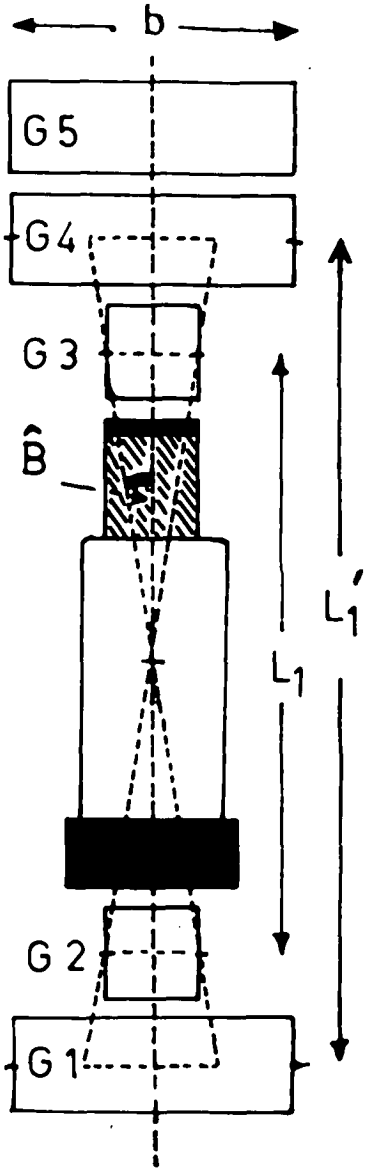

Fig. 4.3(a)

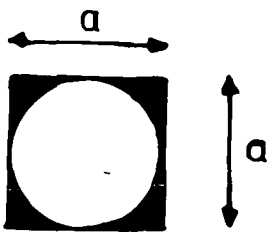

Fig 4.3(b)

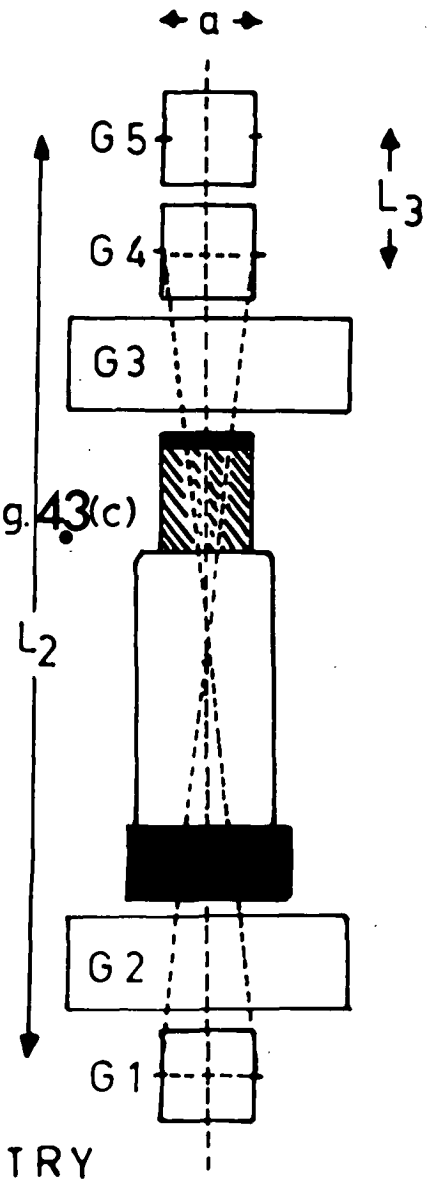

Fig. 4.3(c)

TELESCOPE GEOMETRY

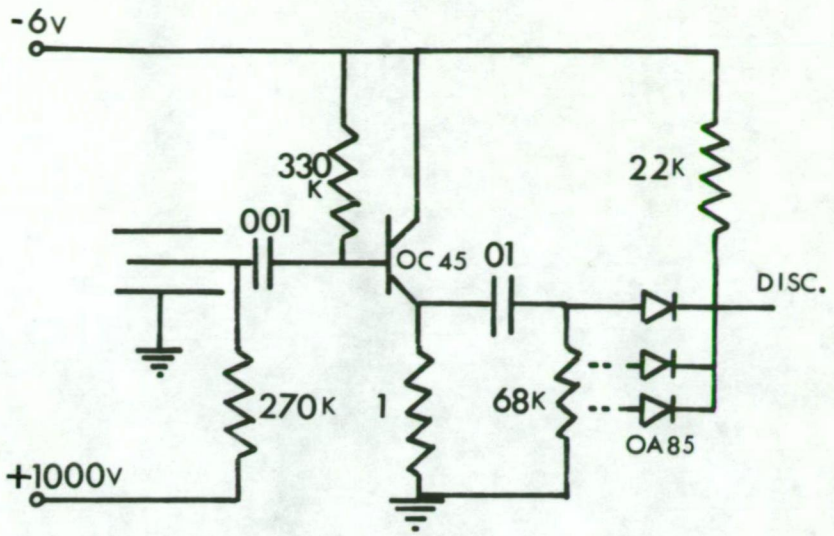

FIG. 4.4a PULSE SHAPER—COINCIDENCE

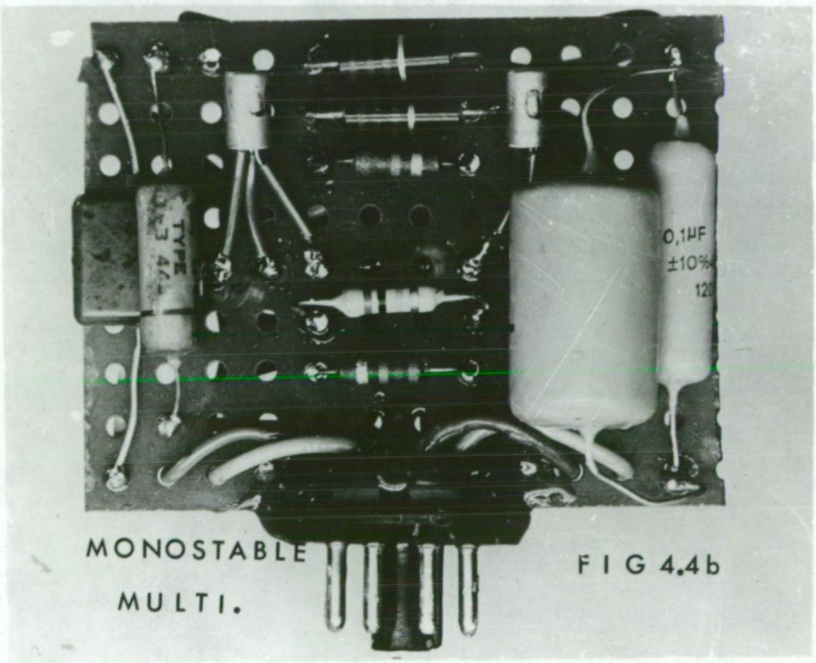

FIG 4.4b

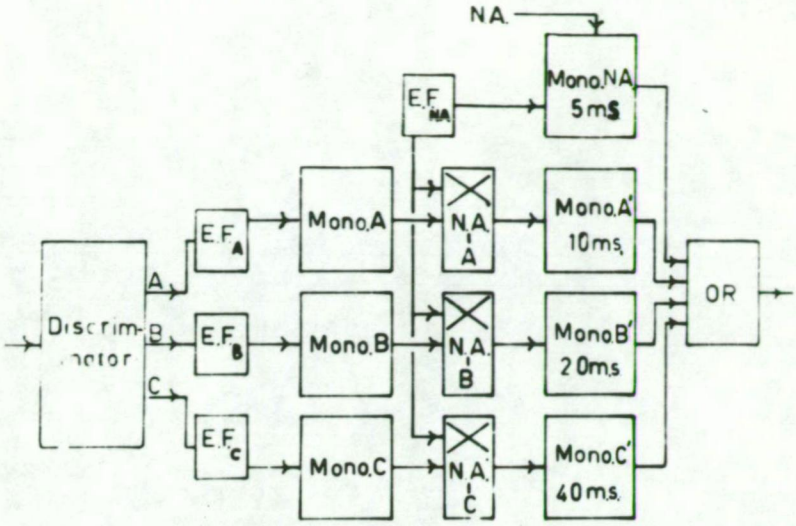

ČERENKOV PULSE DISCRIMINATOR & GATE

Fig. 4.5a

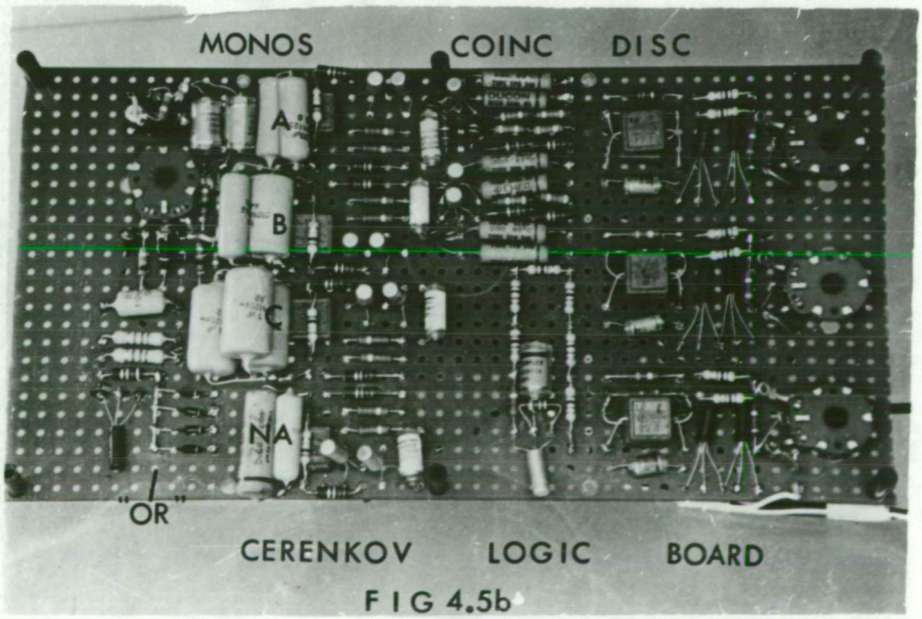

FIG 4.5b

The solar azimuth may be determined by a number of methods. The Nautical Almanac annually lists the apparent right ascension and apparent declination of the sun at Greenwich together with the equation of time. This information is sufficient to calculate precisely the position of the sun in altitude and azimuth at any point on the earth's surface at any instant. Neglect of the equation of time is permissible only if an azimuthal resolution of no better than about 10^{o} is required at medium latitudes.

The labour of solving the oblique spherical triangle involved in each calculation may be reduced by constructing a circular nomogram. This allows the solar azimuth to be obtained with an accuracy of one half degree from a knowledge of the apparent solar hour at a given latitude. The equation of time, together with the longitude then relates this value of the azimuth to the local meridian time of observation.

The values obtained in this way at hourly intervals may be interpolated to give the azimuth at all times during the solar day. Similar interpolation is necessary between monthly values. The hourly interpolation introduces the greatest error at solar noon during the solstitial periods when the rate of change of azimuth is highest. The overall accuracy of this method in determining solar azimuth at any arbitrary time is of the order of several degrees at medium latitudes. This was considered to be adequate for the present experiments.

The maximum rate of change of solar azimuth occurs at meridian transit when the elevation is also greatest. At Hobart (42.5^{o} S), the maximum rate is 38^{o} per hour, on December 22nd while at Mildura (34^{o} S)

it is 56° per hour. At lower latitudes the nomogram as described may not provide sufficient accuracy near noon because of the rapid change at azimuth. Any change in location of the balloon must also be taken into account in computing azimuth.

The greatest error introduced by balloon drift at Mildura is less than four degrees in azimuth per degree of latitude or longitude change. Where necessary a correction was made. This correction was generally somewhat greater than that made to the magnetic declination. Similar corrections were made to the Hobart data.

Direct calculations were made using the Nautical Almanac for those flights in which the azimuth was required more precisely.

The majority of the Hobart flights were launched shortly before local noon. The Mildura launchings were usually carried out near dawn. Most of the latter flights were terminated well before noon and consequently the rate of azimuthal variation of the sun was generally similar to that at Hobart.

The Solar Compass

The azimuth of the telescope axis relative to the sun was determined with an array of phototransistors (fig. 4.6) mounted on the instrument package. These sensors were situated near the centre of the horizontal disc, each being placed at the base of the line of intersection between two vertical sectorial surfaces inclined at angle δ'. The azimuthal field of view of each sensor was thus restricted to the angle δ', generally $\pi/4$ radians, by the shadow cast by these surfaces. The vertical field was restricted near the zenith by a second horizontal disc placed above the transistors to prevent response to reflected light from the balloon. The compass was constructed of tin plate sections,

Fig. 4.6

A: TOP VIEW

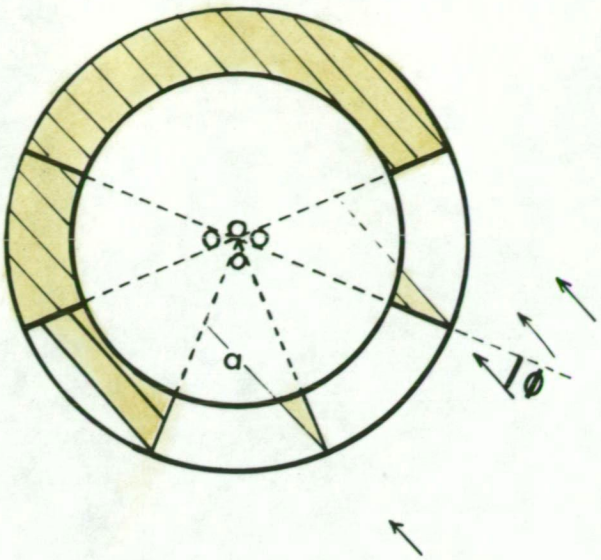

B: SIDE VIEW

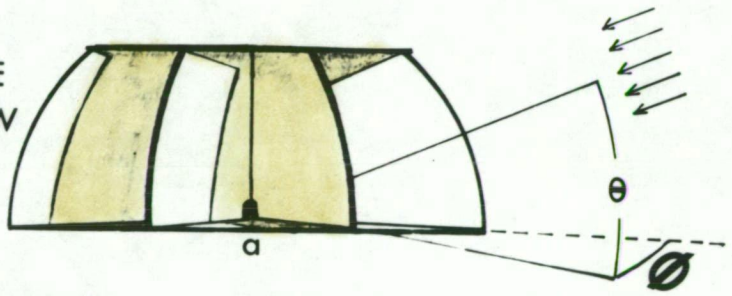

C: CIRCUITRY

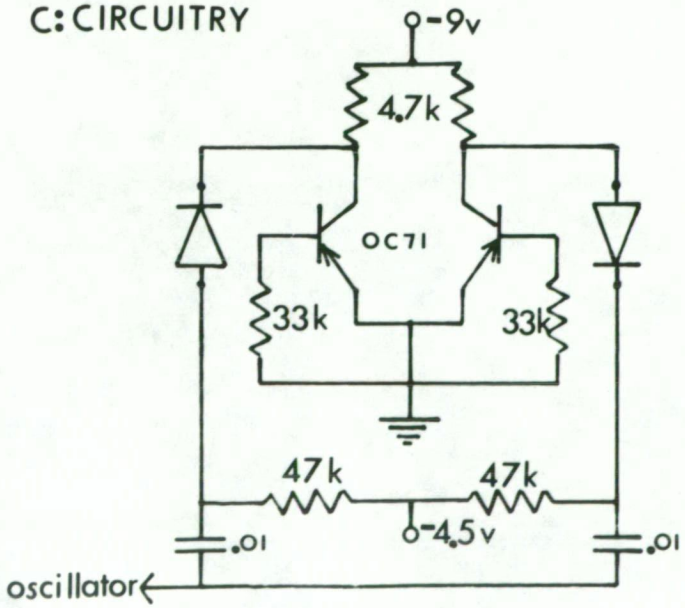

sprayed with a flat black paint to minimise reflection. The expected range of solar azimuth was calculated prior to each flight and the compass then iolated accordingly. Since the primary purpose of the experiments was to acquire east-west data, two photo transistors looking in opposite directions were always used. In several flights a third sensor was included to provide more detailed information.

The compass was connected by shielded cable to the power supply and modulator. The circuit diagram is shown in Figure 4.6 (c).

4.7 PRESSURE AND TEMPERATURE MEASUREMENT

Aneroid "baroswitch" elements were used as pressure transducers for the Hobart flights. The baroswitches were set to indicate the laboratory pressure prior to each flight. Laboratory calibrations, performed on several of these instruments, showed the pressure measurements to be reproducible within several millibars. The pressure data obtained during the floating period of the Hobart flights is therefore likely to be in error by as much as 10%. The contact arrangements were such that it was not possible to determine directly whether a change in pressure contact indicated a rise or fall in altitude. It was therefore difficult to obtain meaningful directional flux data from those flights in which the altitude of the balloon fluctuated markedly during the floating period.

Baroswitches were also flown with the Mildura payloads. In most flights the Hibal pressure data obtained by aneroid transducers of the Olland type were relied upon.

No temperature measurement was necessary in those flights in which internal cathode geiger counter telescopes were flown since the counters and electronic circuitry were tested at temperatures well below

those anticipated in day time flights. Thermistors were taped to the Maze telescope for some Mildura flights, these being usually launched before dawn.

4.8 LEVEL FLIGHT BALLOON TECHNIQUE

The experiments required the accumulation of data at constant atmospheric pressure for periods of the order of six hours. Because of the prohibitive cost of plastic balloons it was necessary to use elastic balloons for the flights from Hobart. Since the balloon would, unless regulated, continue to rise until bursting, the balloon ascent was arrested at a predetermined altitude. The method used was devised and successfully tested by V.D. Hopper (1957) and adapted by K.B. Fenton for balloon flights at Hobart. A valve is inserted in the neck of an expansible meoprene balloon. The valve, normally closed, is pulled open by a string attached to the top of the balloon when the balloon diameter exceeds the length of the string.

Assuming the balloon to be a sphere of diameter d(cm) equal to the length of the string (ls), the valve will open at an altitude at which the density of the atmosphere is

$$\rho_o = 6G/\pi d^3 \qquad 4.17$$

where G = gross (gm) load (weight of payload plus balloon and gas). The required string length is

$$l_s = \left(\frac{6G}{\pi \rho_o}\right)^{\frac{1}{3}}$$

$$= \left(\frac{1.62G}{p_o} \cdot \left(\frac{T_o}{290}\right)\right)^{\frac{1}{3}}$$

$$= \left(\frac{1.4 \cdot 10^6 G}{p_o}\right)^{\frac{1}{3}} \quad \text{for } T_o = 257^\circ \text{ K}$$

$$= 112\ (G/p_o^{\,2})^{\frac{1}{3}} \qquad 4.18$$

where p_o = atmospheric pressure (g/cm^2)

T_o = atmospheric temperature (^{o} K)

The pressure level at which the balloon valve opens is assumed to be the floating level. For a given load (G) and desired float pressure (p_o) the string length is therefore cut to the length (ls) calculated from equation 4.18.

The maximum permissible string length is determined by the bursting diameter of the balloon. A convenient safety factor (F) (K. B. Fenton, private communication) is the ratio of the excess skin thickness ($t_o - t_b$) at the floating level to the skin thickness (t_b) when the balloon diameter is equal to the average bursting diameter

$$F = \frac{t_o}{t_b} - 1$$

$$= \left(\frac{d_b}{d_o}\right)^2 - 1\ , \qquad 4.19$$

providing the balloon remains spherical. The (J11 - 28 - 2400) Darex daytime sounding balloon has a bursting diameter of 12.5 metres. Table 4.2 below lists safety factors, floating pressures and string lengths for this balloon,,carrying a total payload of 15lb (G = 9.2 Kgm).

Experience at Hobart suggested that the distortion of the 2400 gm balloon would be proportional to the load and equal to about 10 % in diameter for a 20lb payload. If the distortion of the balloon were neglected in the string length calculation the valve would open at a lower altitude and the balloon would consequently float at a higher

TABLE 4.2

String Length ls (cm)	Safety Factor F (%)	Floating Pressure (28P) p_o (mB) (28)	
1250	0	7.0	6.6
1200	4.5	7.8	7.4
1150	18	9.0	8.5
1100	29	10.2	9.6
1050	42	11.8	11.2
1000	56	13.7	13.0

pressure level (and with a higher safety factor) than intended. If the distortion were overestimated and the string length made 10 % longer than the "effective diameter" (d_o) calculated from equation 4.18 the balloon would float at a higher altitude and its skin thickness would be less than anticipated. For p_o = 8.5 mB , a 10 % over correction for distortion would result in the valve opening at 6.6 mB and a safety factor of zero.

The rate of ascent is given by the manufacturers (Dewey & Almy) as

$$V = 436\, F^{\frac{1}{2}}/(F + G)^{\frac{i}{3}} \text{ ft/minute} \qquad 4.20$$

where F = free lift in grams

G = gross load in grams

For the Jl1 - 28P - 2400 balloon carrying a 15lb payload

F (gm)	F/G	V (ft/min)
1000	10 %	625
1500	15 %	753
2000	20 %	858
2750	28 %	985

The ascent rate was usually kept below 800 ft/min to reduce the risk of balloon failure due to turbulence.

The gross lift $F + G = P$

$$\dot{=} 7.6\ Vg \quad . \qquad 4.21$$

where P = required lifting force (lb wt) of the gas

$= 7.6\ Vg$ for hydrogen at 0^{0} C .

and Vg = volume of gas required (units of 10^{2} cu. feet)

$F + G$ = gross lift (lb) .

Although several successful telescope flights were made at Hobart using the valve technique the level flight periods were generally shorter than anticipated.

The Mildura flights were made with plastic balloons designed to carry the Hibal payload to nominal altitudes of 65,000; 80,000; 90,000 and 105,000 feet. A successful level flight was also carried out at Hobart with a plastic balloon provided by N. R. Parsons.

4.9 PACKAGING OF THE INSTRUMENTS

The Mildura instrument frame consisting of tubular aluminium members to which the telescope, electronic circuity and battery power pack were attached, was enclosed in a polyethylene bag before packaging. The frame was placed in a foamed polystyrene box with 2" thick walls. The box was internally lined with aluminium foil to provide shielding from the Hibal talemetry transmissions. The outside surface was painted black and covered with a second polyethylene sheet. The package was carried in a light steel cradle and crated to Mildura where the cradle was bolted to the gondola. Figure 4.7 (a) shows a photograph of the

frame, box and cradle prior to packaging.

Figure 4.7 (b) shows the same package (the Cerenkov telescope) in the laboratory during the period of calibration. (The Hobart instrument packages were insulated in a similar manner.)

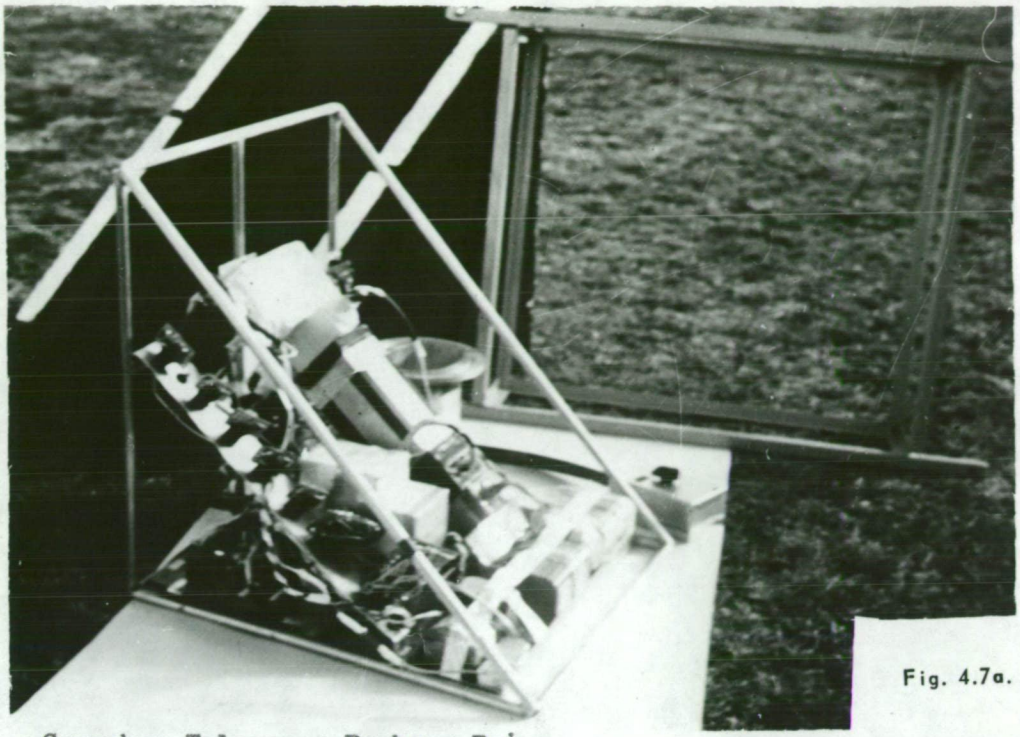

Fig. 4.7a.

Cerenkov Telescope Package Prior
to Installation in Container.

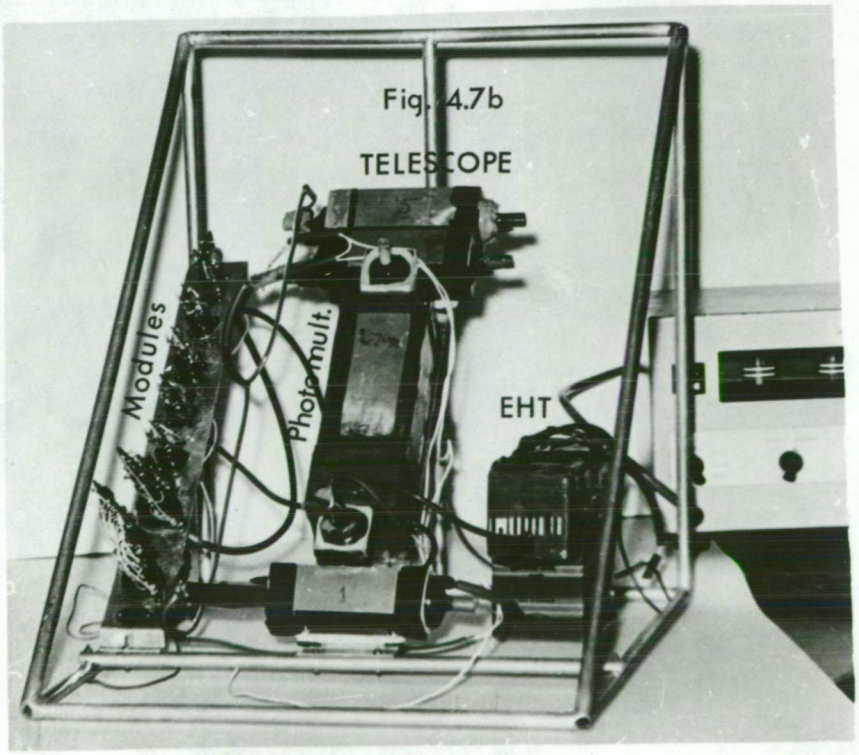

Cerenkov Telescope Frame

CHAPTER FIVE

DATA HANDLING

INTRODUCTION

The design and operation of the equipment directly concerned with the acquisition of data was discussed in the last chapter. This chapter discusses the methods by which the outputs of the various measuring instruments were stored and read out. The Mildura flights were recoverable and consequently the instrument outputs were converted to a suitable form and stored by inflight recorders. The flight packages launched from Hobart were not recovered and radio telemetry was therefore necessary. The cost of the Hobart flights had to be minimised and some effort was therefore spent in the design of simple and economic radio sondes.

5.1 IN-FLIGHT DATA-STORAGE: WIRE RECORDING

Because of the lack of personnel and telemetry facilities at the "HIBAL" Balloon Launching Station at Mildura and the existence of advanced recovery techniques it was decided to include an in-flight data store in the instrument package. The maximum flight time of over six hours (5 hours of level flight) together with the requirements of minimum weight and maximum information capacity considerably restricted the choice.

A suitable instrument, the P55(L) "MINIPHON" wire recorder manufactured by PROTONA GmbH. of Hamburg was purchased. This recorder weighs two lbs with batteries, has a quoted half power bandwidth of 3 Kc/s and a nominal recording time of 5 hours. The motor speed is regulated and flutter and wow were measured to be less than

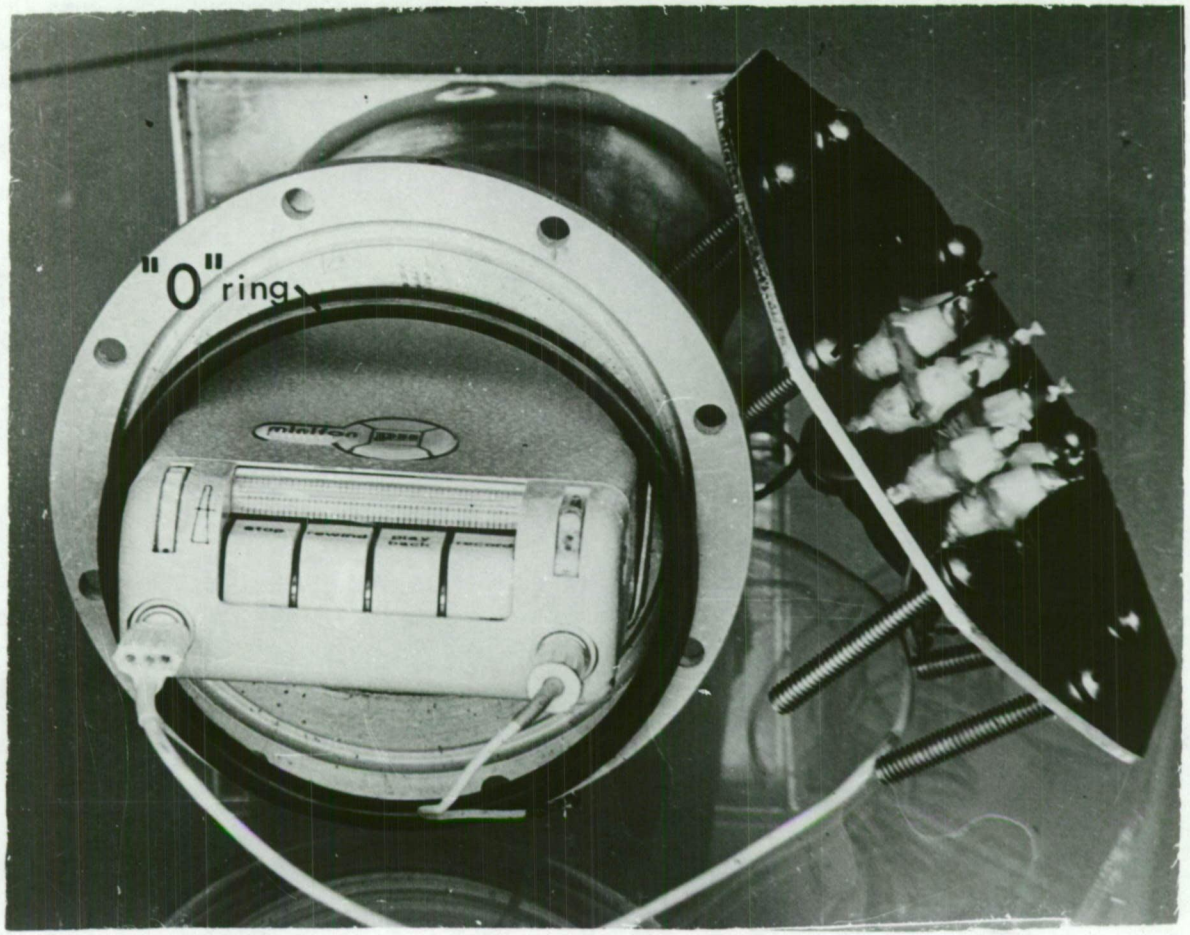

Fig. 5.1. Wire Recorder positioned in Flight Container.

1%. The instrument used was in fact found to record for only four hours, and complete records of most flights were not obtained. The major problems of the recorder were associated with its limited dynamic range, non linearity, and high noise level (maximum signal to noise voltage 16 db). These problems were overcome and satisfactory operation was obtained.

Tests at reduced pressure and temperature established the reliability of the machine at temperatures above 0°C and altitudes below 90,000 feet. The original instrument was unfortunately damaged beyond repaid when the first flight package landed in a fresh water lake in north-west Victoria. A considerable delay in purchasing a second recorder of this type occurred and the first successful in-flight recording was made in February 1963. A pressurised and shock-proofed container was constructed for the 1963 flights (Figure 5.1) and proved to be entirely satisfactory. Use of a rubber "O" ring seal provided easy access to the recorder. Ceramic lead through connectors allowed the recorder to be remotely switched. Modifications were made to the power input terminals to enable remote control of the machine.

In order to remove any uncertainty in timing during a flight and also to provide pressure information a baroswitch was included and its readings cross checked with those obtained by another baroswitch in the "HIBAL" gondola, from which the data was routinely telemered and recorded during each flight. This allowed a check on the motor speed during the ascent. An independent check was also made by measuring the frequencies of the sub-carrier oscillators throughout each flight. Both checks were consistent in showing the absence of any long term

speed variations exceeding ½%. For those flights in which the recording period included both the time of float and the time of cut down, the count data gave a further check.

Figures 5.2(a), 5.2(b) show block diagrams of the data handling circuitry used in the flights with the wire recorder. In the flight with the Cerenkov counter three sub-carrier oscillations and a set of univibrators were used for multiplexing the eleven pieces of data. The oscillators were deviated in frequency by the compasses and the thermister and gated on by single shot multivibrators triggered by the telescope pulses. The temperature controlled oscillator was amplitude modulated by the baroswitch. The East-West compass oscillator was simultaneously pulsed on by either both or one of two single shots according to whether or not a $G_4 \cdot G_5$ coicidence was accompanied by a $G_1 \cdot G_4 \cdot G_5$ coicidence. The output of the 3Kc/s oscillator consisted therefore of a sequence of long $(G_1 \cdot G_4 \cdot G_5)$ and short $(G_4 \cdot G_5)$ trains of a sinusoidal oscillation with frequency determined by the east and west sun sensors. Pulse width multiplexing was also employed in recording the Cerenkov and narrow angle telescope outputs. In this case four single shots were required, providing four different pulse widths. The shortest pulse corresponded to a N.A. output unaccompanied by a Cerenkov output. The remaining three single shots, A',B',C' in figure 4.5(a), generating progressively longer pulses, were triggered by photomultiplier with amplitudes respectively greater than the discriminator levels A,B, or C . The single geiger telescope and associated instruments provided data in similar form (fig. 5.2(b)) to the wire recorder. The single pulse channel allowed simpler

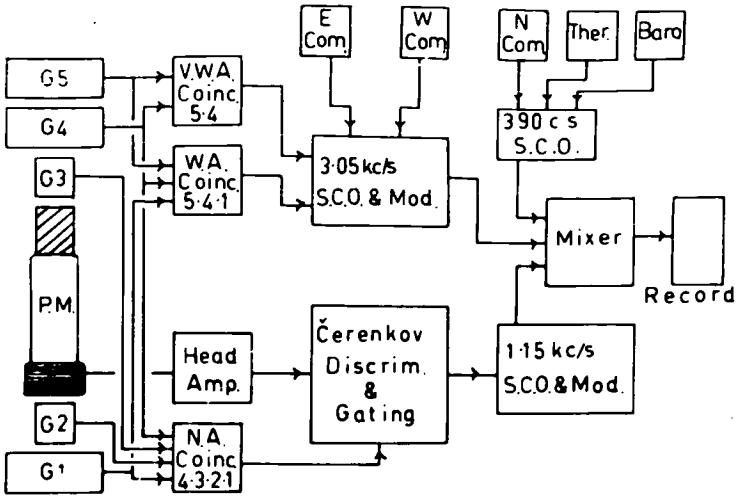

Fig. 5.2(a). Block Diagram, Cerenkov Telescope Flight Instrumentation.

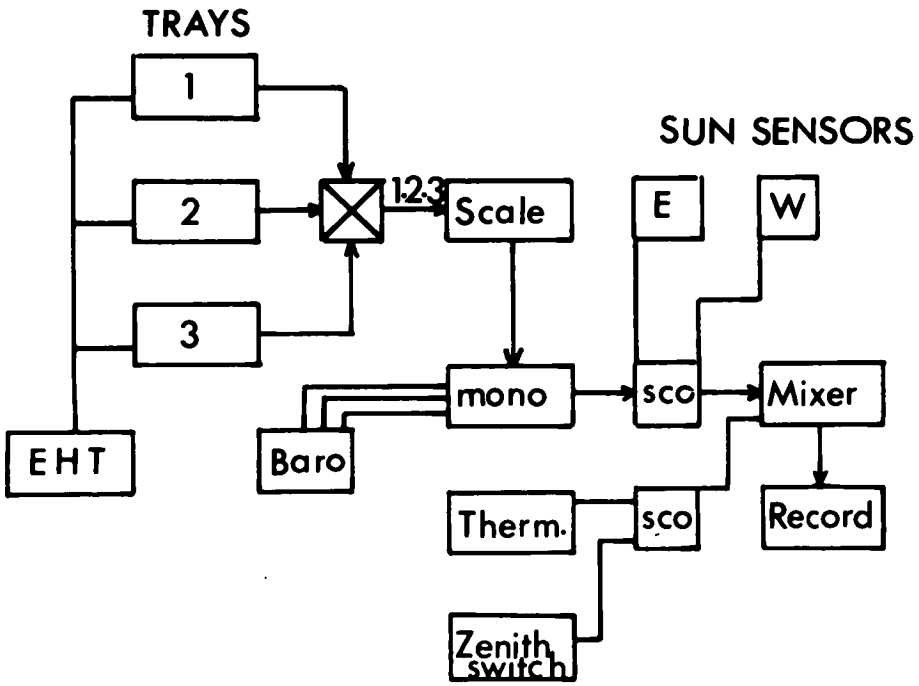

Fig. 5.2(b). Block Diagram, Single Geiger Telescope Flight Instrumentation.

multiplexing. The triple contact baroswitch was used to change the time constant of a single univibrator, thus providing telescope pulses of width determined by the three sets of pressure contacts. A mercury switch, used to indicate variations in the zenith angle of the telescope, was included in several flights. The non-uniform frequency response of the wire recorder required the relative amplitudes of the sub-carrier oscillators outputs to be adjusted at the mixer.

5.2 IN-FLIGHT RECORDING: REGISTER BANK

Mechanical malfunction of the wire recorder resulted in some loss of data. A second in-flight recorder was therefore constructed and flown with two inclined telescopes to enable east and west count rates to be obtained simultaneously. This recorder consisted of a set of mechanical registers, gated with relays by the east and west sensors and automatically switched on by a baroswitch at an altitude slightly below the floating altitude. A block diagram of the system is shown in fig. 5.3. Ten shock mounted registers were used. Six of these accumulated the east, west and complete level flight count totals from the two telescopes. Three registers, driven by a stable oscillator, indicated east count and west count accumulation times and total duration of level flight. The tenth register was left unconnected. It provided an estimate of the effect of mechanical vibration due to impact upon the register totals.

The "clock" oscillator was a simple neon tube relaxation device using stable RC elements and deriving H.T. from a 180V battery pack stabilized with a VR 105 voltage regulator tube. The voltage excursion at the anode of the neon tube was differentiated and applied through a transistor amplifier to trigger a univibrator. A frequency of $\frac{1}{3}$ sec^{-1}

5.3 IN-FLIGHT REGISTER RECORDER.

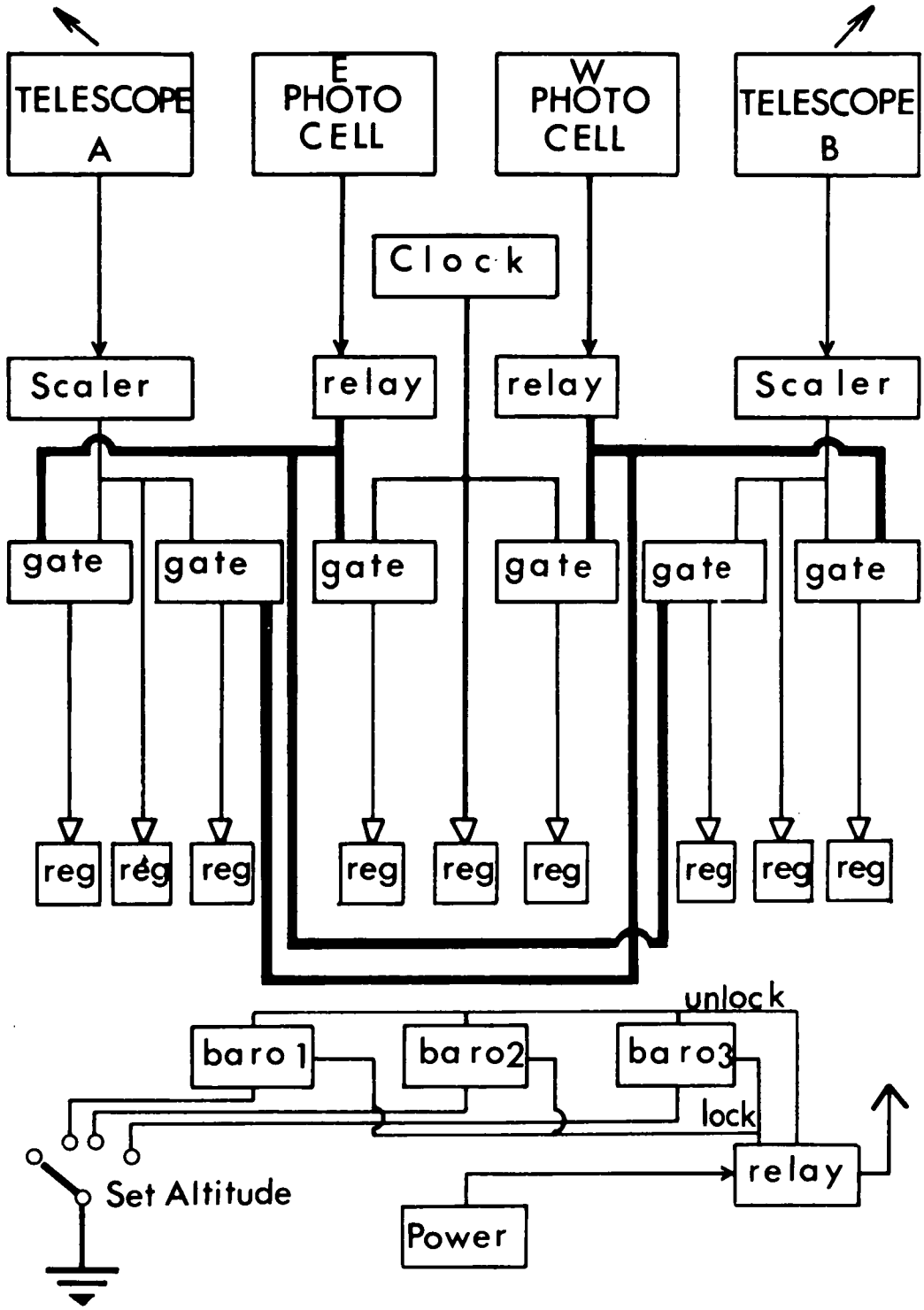

was chosen to provide adequate time resolution. Ground tests established the frequency to be unaffected by ionizing radiation at the level likely to be encountered in the flights. The neon tube was light shielded. The repetition rate of the clock remained constant to within 0.02 % in extended laboratory tests using the in-flight battery pack. The main source of drift, once the neon tube and voltage regulator had been run for several days, was due to the effect of changes in temperature and battery voltage on the operation of the transistor coupling circuit. The circuit diagram is shown in fig. 5.4(a).

The telescope logic circuits were identical with those used in the other flights and were constructed in modular form. Univibrators providing pulses of 10 ms width were used to gate the OC76 register driving transistors. Reliable register counting rates of 10 sec^{-1} were obtained with this arrangement, fig. 5.4(b). The scale factor of the telescope scaling circuits was adjusted so that the 100ms resolving time of the register circuit introduced negligible counting loss. (Appendix 2).

The instrument package was made more versatile by including a number of baroswitches set to operate at various floating levels. The appropriate level was selected by a remote switch before the balloon was launched. In the first flight of the register bank the instrument was switched on at impact due to mechanical vibration of the self locking relay. A time delayed locking device was devised for later flights. The circuit diagram is shown in fig. 5.4(c). When the upper baroswitch (U) contact is earthed by the moving arm

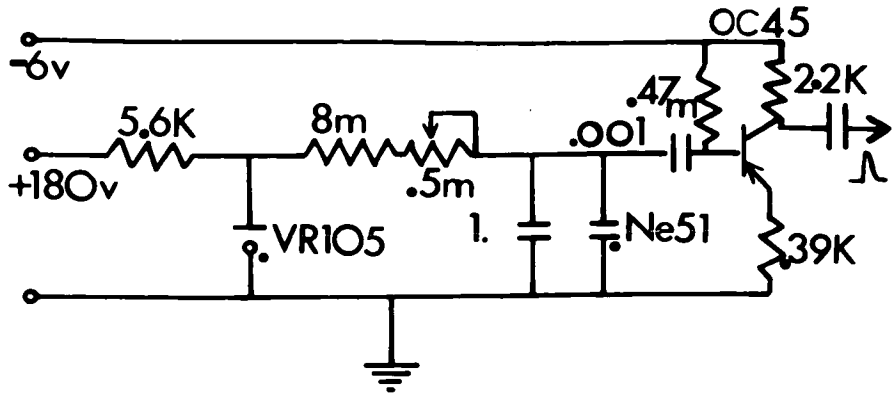

Fig. 5.4a. Clock Oscillator.

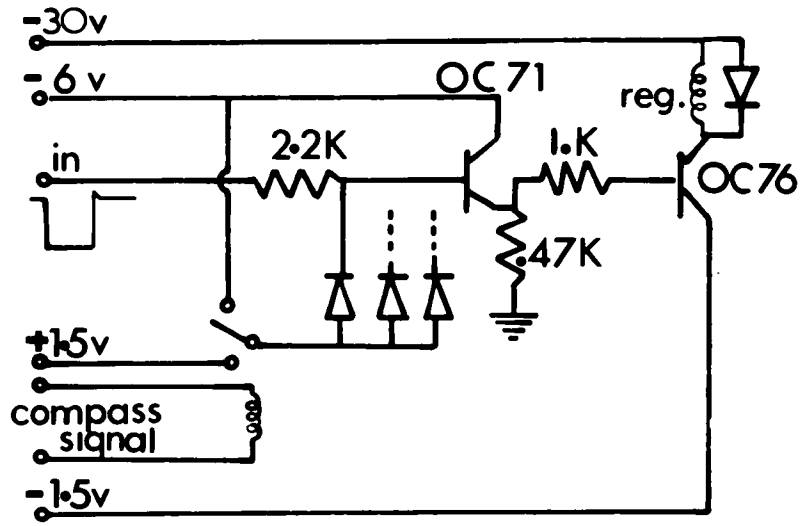

Fig. 5.4b. Register Drive.

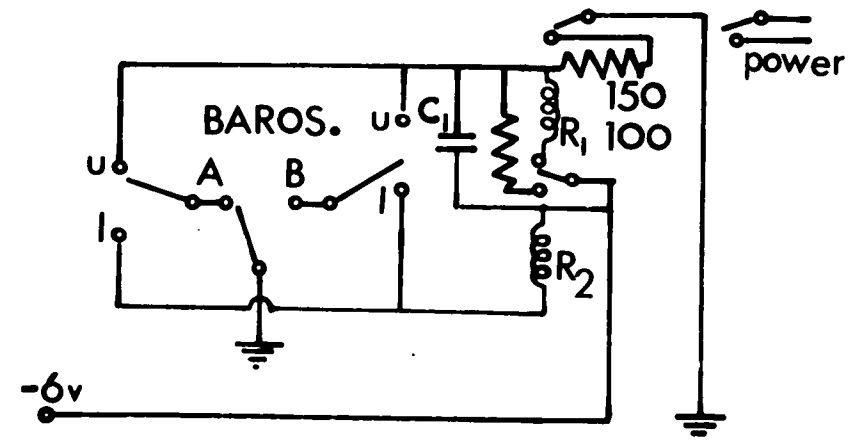

Fig. 5.4c. Baroswitch Lock

at the selected pressure level, relay R_1 is closed. If the contact remains closed for a period of at least three seconds, condenser C_1 will have charged sufficiently through the 150 Ω resistance to allow R_1 to remain on when the baroswitch contact is opened as the balloon continues to rise. At the end of the flight, contact L is momentarily earthed during the descent, and the operation of relay R_2 then removes power from the locked relay R_1, and simultaneously discharges C_1 to prevent relocking.

5.3 RADIO TELEMTRY: MODULATION AND MULTIPLEXING

The principal requirement of a suitable radio sonde was that it be simple and cheap. The maximum information capability of the telemeter was set by the need to accomodate data from at least one geiger telescope, a baroswitch and an azimuthal indicator. The design of these instruments has already been discussed. To simplify the read out and interpretation of data the Hobart measurements were telemetered in the same form as the Mildura data were wire recorded.

The first system to be used was a modification of a simple two channel telemeter designed by the author to handle the data from a hypsometer and the unscaled output of a single geiger counter, these being the instruments used in the initial Hobart balloon flights (Edwards, 1960; Greenhill, 1960). In this system the geiger output pulses were developed across the low capacity input circuit of a cathode follower, the cathode being directly connected to the screen grid of the radio frequency power oscillator. This oscillator was thereby gated off for the duration ($\doteq 300\mu s$) of each geiger pulse. The hypsometer signal, a sinusoidal audio frequency voltage, was applied to the control grid of the oscill-

ator, thus amplitude modulating the transmitter at a low level. The pressure dependent hypsometer oscillator frequency was measured at the receiver by comparison with a local oscillator of known frequency. The counter pulses were recovered at the output by amplitude discrimination preceded by low pass filtering.

The resolving time of the geiger telemeter was fixed at the receiver by allowing the discriminated pulses to trigger a 1m sec univibrator. A block diagram of the instrument package is shown in Figure 5.5 (a).

In the modified system, (Figure 5.5 (b)) the vacuum tube modulator was replaced by a transistor and the hypsometer by a baroswitch. The pressure signal was a tone of three well separated frequencies, determined by the particular baroswitch contact in circuit. Multiplexing in the first telescope flight was similar to that described in Section 5.1 (Figure 5.5 (c)). Pressure contacts were recognised by the width of triggered univibrator pulses and the frequency of the low level signal was made dependent on azimuth. Although this system operated satisfactorily, the adjustment of the modulation level was unduly critical. The transmitter was accordingly modified in such a way (Figure 5.6 (a)) that the azimuth oscillator was directly gated by the variable width telescope pulses. The gated oscillator signal was then used to pulse the transmitter off. This pulses system is quite uncritical in adjustment, the amplitude of the modulating signal needing only to be sufficiently great to switch off the RF oscillator during the negative excursions of the compass oscillator wave form. A marked increase in efficiency could be achieved by pulsing the (normally off) transmitter on for the duration of the pulses. This was not done because the self

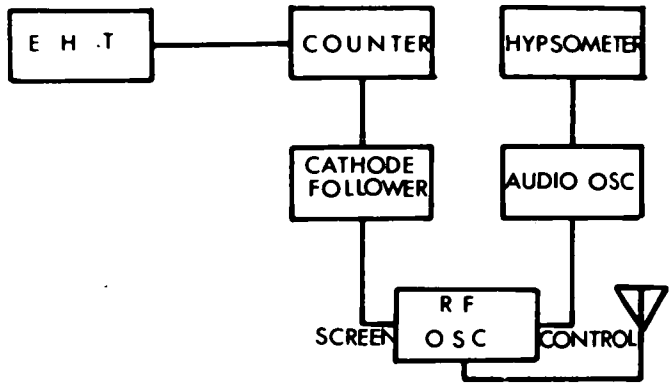

Fig. 5.5a. Single Counter Sonde

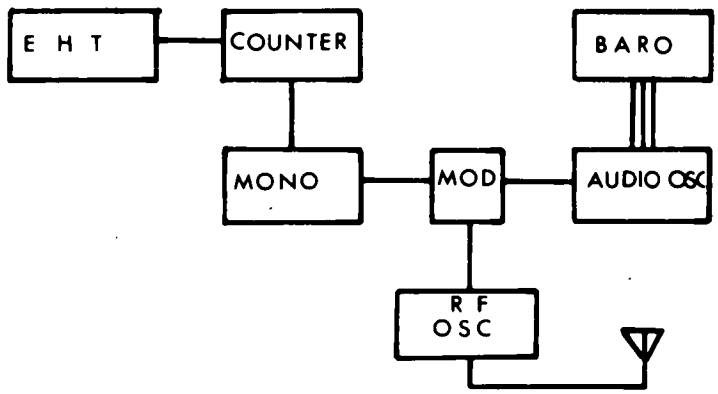

Fig. 5.5b. Modified Single Counter Sonde

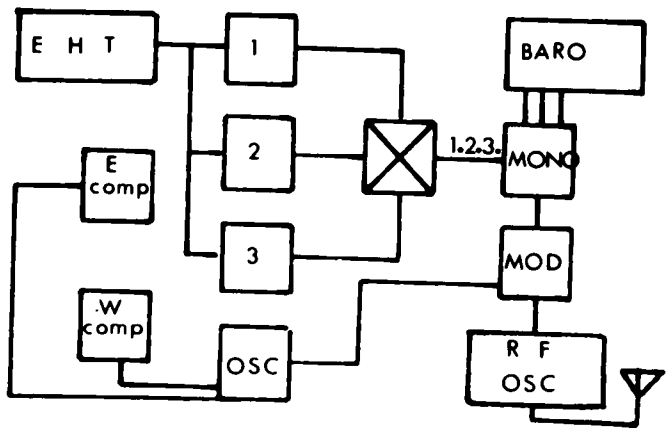

Fig. 5.5c. Single Telescope Sonde.

quenched superregenerative receivers (Section 5.5) available for the Hobart flights required the presence of a carrier signal for optimum performance in the presence of external noise.

This telemeter will accomodate additional digital information using the methods of Section 5.1. The same restrictions apply, namely it is possible to multiplex data from channels $1,\ldots,r$, using pulse width identification, providing the set of interchannel time coincidences,

$$S_\nu \cdot S_{\nu-1} \cdot \ldots\ldots\ldots S_2 \cdot S_1 = S_\nu \qquad \nu = 2,\ldots,r \qquad 5.1$$

and providing the channel pulse widths are arranged so that

$$\tau_\nu > \tau_{\nu-1}, \qquad \nu = 2,\ldots,r \qquad 5.2$$

Subject to this condition, the τ_ν may be tapered in any way consistent with the requirements of the pulse width discriminator at the receiver. The method is applicable to the telemetry of data from a variety of particle detectors. Examples include the output from multichannel integral pulse height analysers (Section 5.1) and the single counter and ν-fold coincidence rates of counter arrays for which equation 5.1 is satisfied. Where independent detector outputs are to be multiplexed by this method time devision may be used without degrading the performance.

A simple system designed to accomodate data from two independent detectors is shown as a block diagram in fig. 5.6(b). The two binary pairs, S_1, S_2 driven by these two detectors, are alternately interrogated by a free running multivibrator. If, upon interrogation, either binary is found to be in the "on" state, it is reset and the

channel univibrator generates a pulse of characteristic width which is passed to the modulator. No synchronising pulse is needed and the read out facilities of the basic system are used.

Both channels may carry data from additional detectors using the methods of the basic system. The third detector in Figure 5.6 (b), (d.e.f.g.) might for example be a side shower detector or a narrow angle telescope. The resolving time of the two channels is the same and equal to the repetition period of the multivibrator (τ_S). The counting loss due to channel resolving time is then (Appendix 2)

$$1 - c \doteq \dot{n}_o \tau_S \qquad \ldots 5.3$$

Scaling prior to interrogation by a factor m reduces this to

$$1 - c_m \doteq e^{-\dot{n}_i \tau_S} \cdot \frac{(\dot{n}_i \tau_S)^m}{m!} \qquad \ldots 5.4$$

It is clear that the methods of modulation and multiplexing described here allow the use of simpler and cheaper flight equipment than are required with more conventional telemeters. This is particularly evident when the criterion of Equation 5.1 is satisfied by all particle detectors. For example, the basic single telescope system 5.6(a) can easily accommodate three related telescopes and a shower detector, requiring the addition of three univibrators to the multiplexing circuit. A frequency division multiplex carrying the same data would require four scaling circuits, at least four subcarrier oscillators and a mixer. Also, since it is a pulsed time division system, cross talk and linearity requirements are both small and no critical adjustments are necessary as in the case of frequency division. The characteristics of the system are discussed further in Section 5.7. In the following two sections we discuss the problems of transmission, propagation and reception, associated with radio telemetry.

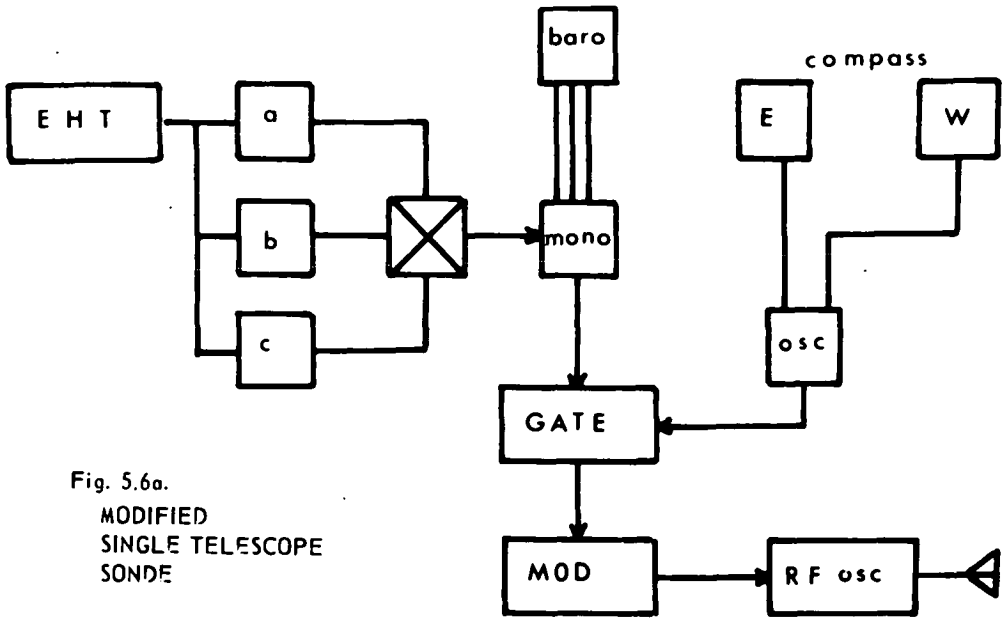

Fig. 5.6a.
MODIFIED
SINGLE TELESCOPE
SONDE

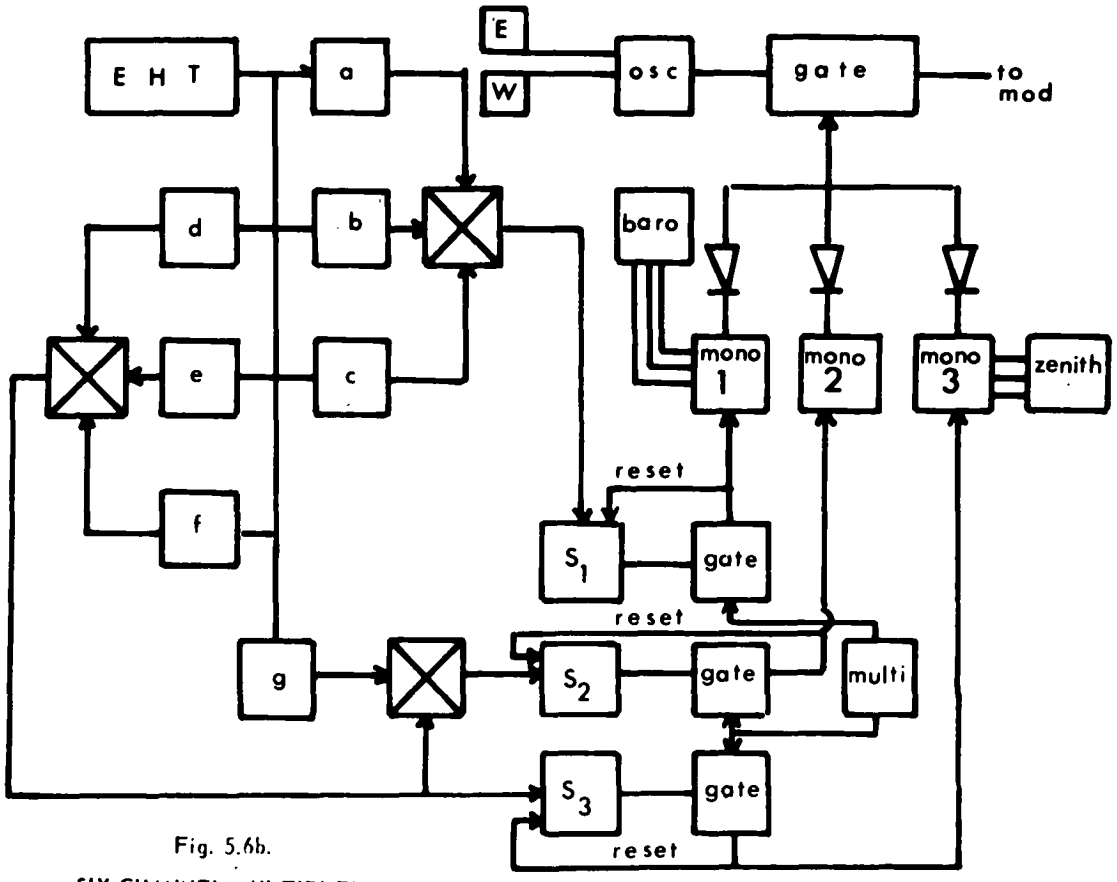

Fig. 5.6b.
SIX CHANNEL MULTIPLEX

5.4 THE CHOICE OF CARRIER FREQUENCY FOR BALLOON TELEMETRY SYSTEMS

In this section we examine the frequency dependent factors which determine the optimum carrier frequency for a communication link. The discussion is limited to line of sight propagation of signals with carrier frequencies in the range 50 - 1000 Mc/s. The results are applicable to the design of air to ground links such as balloon telemetry systems in which transmitter weight must be minimised.

A number of papers (Pratt, 1960; Perlman, et al, 1959) have recently dealt with the choice of optimum frequencies for earth-space links. The frequency dependent factors have been examined by Pratt (1960) who concluded that the optimum frequency lies between 1000 and 10,000 Mc/s. It was considered desirable to make a similar analysis to include situations in which the presence of the earth's surface influences the system performance. The existence of an optimum frequency may be anticipated simply from consideration of the total noise in the link. This may be divided into two components, one generated in the receiver and the other contributed by the receiving antenna. The sum of these components, respectively increasing and decreasing functions of frequency in the range considered, will have a minimum value at some frequency. In the absence of other frequency dependent factors, operation at this frequency will ensure a maximum signal to noise ratio. The present objective is the minimisation of the transmitter input power required to maintain the signal to noise ratio above some threshold value under the specified conditions of link operation.

The frequency dependent factors to be discussed are:

1. Receiver noise.

2. External noise.

3. Transmission loss.

4. Transmitter efficiency.

The transmitter input power required to give a threshold signal is

$$P_i = \frac{S_o.N'.k.T_o.B}{\mathcal{E}.A} \qquad 5.5$$

where S_o = Minimum permissible RF signal to rms noise power ratio at the receiver input in the bandwidth (B).

N' = Effective receiver noise factor.

kT_o = $10^{-20.4}$ Joules.

B = Receiver noise bandwidth.

$\mathcal{E}$ = Transmitter power efficiency.

A = Power attenuation factor (P_R/P_T).

P_R = RF power available from matched antenna.

P_T = RF power radiated by transmitting antenna.

Both (A) and (N') are strongly frequency dependent. In general (N'), which contains antenna noise and receiver noise terms, falls to a minimum at metre wavelengths for vacuum tube receivers. The transmission loss, (1/A) is a monotonic function of frequency as are the transmitter efficiency and the noise bandwidth. The functions A, B, therefore determine the difference between the frequency for which N' is a minimum (f') and the optimum frequency of the link (f_o). These two frequencies will be equal only if A and B do not depend on frequency.

The optimum frequency might have been found by differentiating Eq. 5.5 with respect to frequency. However, since the expression

obtained in this way is analytically cumbersome, graphical means will be used instead.

Noise

The noise in the link determines the minimum usable signal power available at the receiver input terminals. The noise internally generated in the receiver will be specified by the noise figure (N) while the total link noise will be described by an "effective" noise figure (N') .

Now by definition

$$N = \frac{(S_i/N_i)}{(S_o/N_o)} \qquad 5.6$$

where S_i/N_i = Input signal to noise ratio

and S_o/N_o = Output signal to noise ratio.

The receiver input is assumed matched to a resistance at $T_o = 290^\circ$ K . Hence the receiver effectively adds noise power $(N - 1)kT_oB$ to the signal at the input terminals. Now the external noise presented to the receiver is kT_AB , where T_A is the noise temperature of the receiving antenna. The total link noise, referred to the receiver input, is therefore $kB(T_A + (N - 1)T_o)$ and the effective noise figure

$$N' = (T_A/T_o) + (N - 1) \qquad 5.7$$

expresses the total link noise per unit bandwidth, referred to the receiver input terminals in units of kT_o . It should be noted that N' is greater than or equal to N only if T_A is greater than or equal to T_o and that N' is a noise figure as previously defined if the signal to noise ratios are measured at the input and output of the link. The input measurement is made on the attenuated signal power (AP_T) available

from a resistance at temperature T_o .

Receiver Noise

The contribution of receiver noise to the total link noise may be made smaller by the use of master and parametric amplifier techniques. These techniques, particularly useful in the microwave range, will not be considered here as they do not yet appear to be sufficiently developed for use in routine telemetry operation.

In assessing typical receiver noise a linear dependence of noise figure on frequency, characteristic of low noise triodes, is assumed. An examination of vacuum tube data shows that the expression

$$N = 1 + \frac{f(Mc/s)}{150} \qquad 5.8$$

is representative of noise figures currently attainable in the range 50 to 1000 Mc/s .

Antenna Noise

The noise temperature of the VHF receiving antenna has a diurnal variation associated with the motion of the earth. The maximum and minimum values of the antenna temperature due to galactic emission as summarised by Kraus and Ko (1957) and Shklovski (1960) have been used in calculating the effective noise figure for receivers with directional antennas. The dipole noise temperatures used are based on figures obtained by the National Bureau of Standards (1952).

In order to take some account of the thermal radiation from the ground absorbed by horizon-looking antennas, the minimum antenna temperature is set at 150° by adding this figure to all cosmic noise temperatures. The above procedure may overestimate the antenna temperature

at the lower frequencies where the sky is brighter than the ground but it is considered adequate in view of the other uncertainties involved in the calculations. No explicit account will be taken of man made noise. It will be assumed either that this noise is absent or that it has been removed by suitable techniques. In figures 5.7.1, 5.7.2, the curves (a) and (b) show the effective noise figure (N') as a function of frequency. The curves are plotted for both minimum (a) and maximum (b) sky noise. The dotted curves will be described below.

Propagation

With isotropic or fixed gain antennas the free space transmission loss increases by 6 db per octave. The propagation of a signal from an airborne transmitter however differs significantly from that in free space. Due to the presence of the earth's surface, which acts as a reflector and absorber, the free space attenuation is modified by diffraction below the horizon, and by interference between the direct and ground reflected waves above the horizon.

Consider a transmitter at constant altitude (h_T) travelling away from the receiving antenna situated at altitude (h_R). As the angle of elevation (θ) decreases the field strength oscillates about the free space value until the transmitter nears the horizon. The free space power transfer between the dipole antennas varies inversely as the square of both the frequency ($1/\lambda$) and distance (d) (Bullington, 1957).

$$A = P_R/P_T = (0.13\lambda/d)^2 \cos^4 \theta \qquad 5.9$$

The ($\cos^4 \theta$) term applies to vertical antennas. For horizontal polarization this term should be omitted.

Interference between the direct and reflected components of the

FIGURE 5.7 1. Frequency Dependence of Telemeter Performance

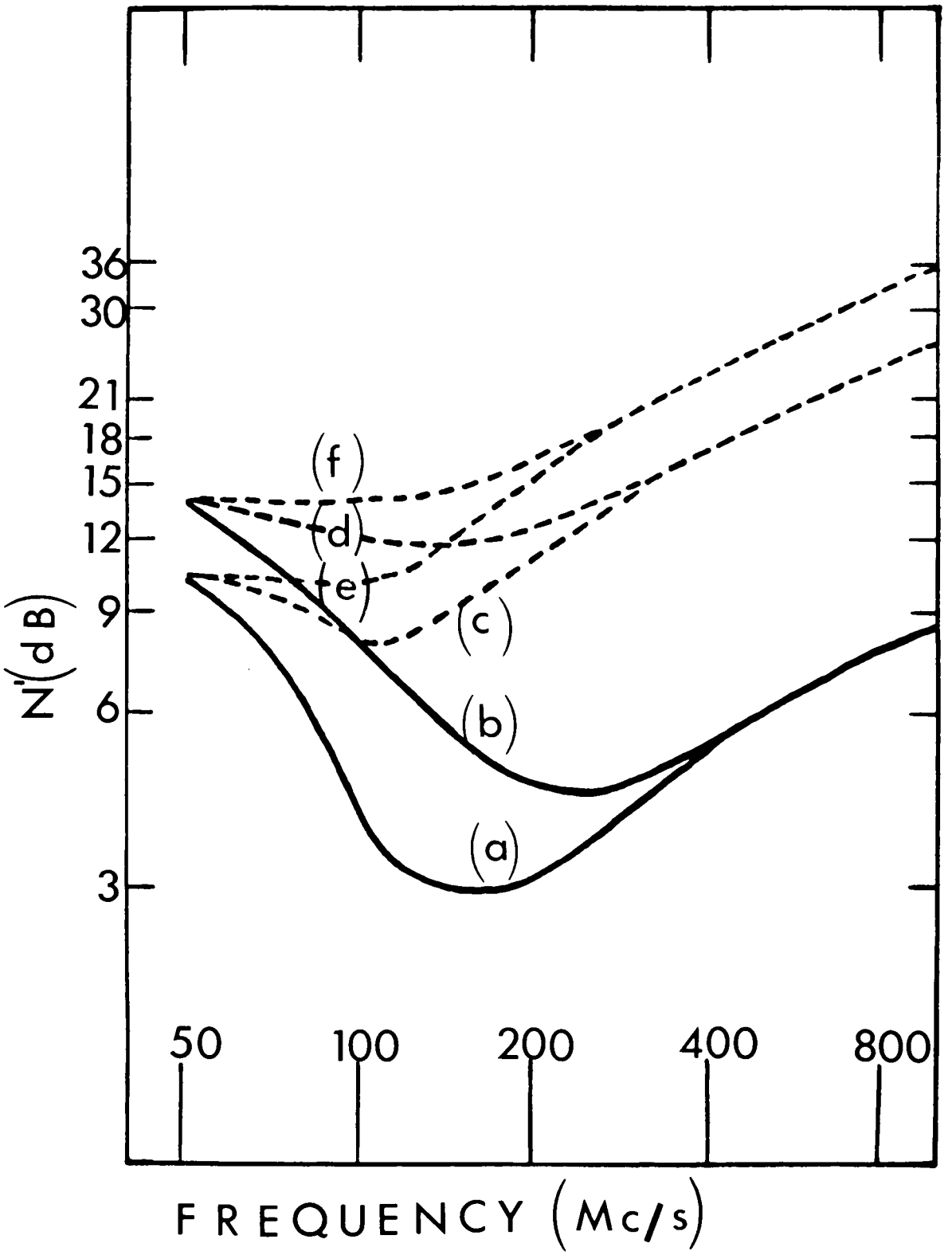
36
30
21
18
15
12
9
6
3
N' (dB)
(f)
(d)
(e)
(c)
(b)
(a)
50
100
200
400
800
FREQUENCY (Mc/s)

FIGURE 5.7 2. Frequency Dependence of Telemeter Performance

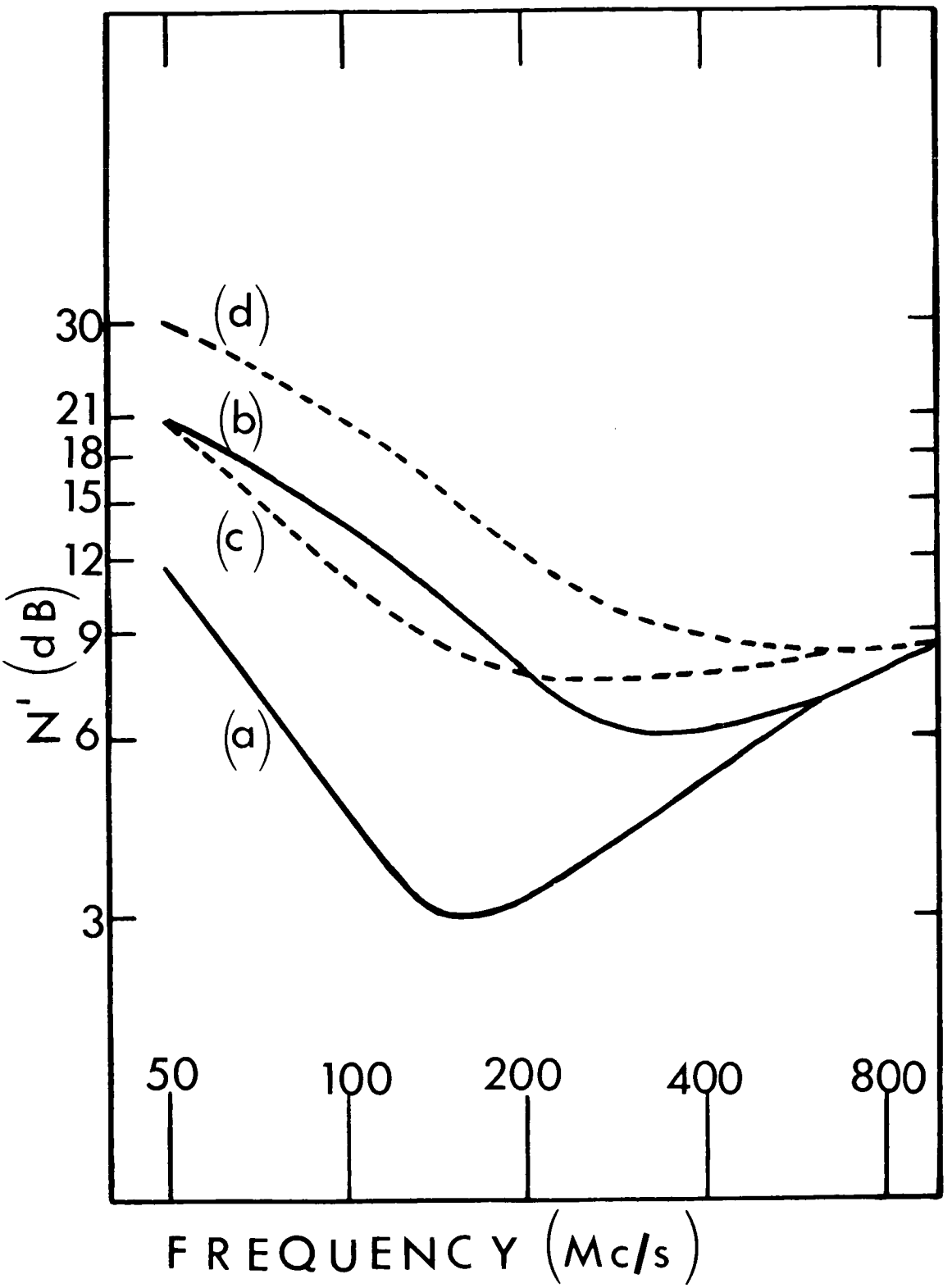
30
21
18
15
12
9
6
3
(d)
(b)
(c)
(a)
$\bar{Z}$ (dB)
50
100
200
400
800
FREQUENCY (Mc/s)

signal will, at most, raise the received power by 6db but may also cause complete signal drop out if the ground acts as an efficient reflector. By assuming that these interference minima produce gaps in air-ground coverage, Norton (1952) has shown that for a given value of h_T there exists a value of h_R which permits maximum coverage. The link performance then steadily deteriorates as the frequency is raised since the optimum h_R value, and therefore the distance to the horizon, varies inversely with frequency. In the present discussion this view is not taken since destructive interference will not drop the signal below that at optical cut off unless horizontally polarized antennas are used over smooth terrain. With vertical polarisation or over a "rough" surface the coefficient of reflection does not approach unity except at low elevations.

As the angle of elevation of the transmitter drops, the ground reflection coefficient becomes independent of polarization and tends to the value of -1. At elevations of the order of several degrees the earth may be considered as a perfectly reflecting plane and the (dipole) transmission loss becomes independent of frequency. At the optical horizon the transmission loss again becomes frequency dependent owing to diffraction effects. It follows from the equation due to Domb and Pryce (1947), for the field strength at optical cut off, that the dipole transmission loss increases as $f^{4/3}$. This result strictly applies only to smooth terrain below a standard atmosphere. Since the propagation loss increases rapidly as the transmitter passes below the horizon the discussion will be limited to optical paths.

Antenna Limitations

A directional receiving antenna is useful in reducing fading due to multipath propagation and in reducing the transmission loss. Although the maximum effective noise figure will be raised at the lower frequencies (compare Figures 5.7.1 and 5.7.2), this is not serious because of the shortened duration of the daily maximum. For a given type of antenna, the ratio of physical to electrical aperture is a constant in the absence of frequency dependent losses. In the frequency range under discussion the antenna losses are small so that mechanical considerations, in fixing the maximum permissible antenna area, also fix the available capture area. The only other limitation, that of angular resolution, is imposed by tracking difficulties. If the beam width is predetermined by acquisition and tracking considerations then the antenna gain will be constant, regardless of frequency. The use of an area-limited antenna will reduce the transmission loss at the rate of 6 db per octave. Since control over the aspect of the transmitting vehicle is not possible, an omnidirectional transmitting antenna is generally required, which will not contribute to the frequency dependence of the transmission loss.

Transmitter Efficiency

At the power level of interest (of the order of several hundred milliwatts), the choice of transmitter lies between directly heated vacuum tubes and low power transistors. As the "state of the art" is rapidly changing, it is difficult to generalise the frequency dependence of the power efficiency of these devices. It is reasonable to assume

that operation above about 600 Mc/s is prejudiced because of reduced efficiency and increased cost. Another factor associated with the transmitter and prejudicial to UHF operation is that of frequency instability. If the information bandwidth of the link is very much greater than the fluctuations in transmitter frequency, then the noise bandwidth (B) will not depend on frequency. On the other hand, if the noise bandwidth is determined solely by frequency instability then a loss in effective radiated power of 3db per octave would result from the use of oscillators of fixed stability, that is (B/F = constant). For convenience in curve plotting, a loss of 2 db per octave ($B/f^{2/3}$ = constant) will be assumed in plotting narrow band link performance.

Applications

The results of the preceding discussion will now be applied in determining the optimum frequency for a number of practical situations. The frequency dependence of the link performance is determined graphically from Eq. 5.5 . The effective noise figure (N') expressed in decibels is plotted (Curves (a) and (b) in Figures 5.7.1 and 5.7.2). The contribution to frequency dependence due to the bandwidth (B) and link attenuation (A) is given by a power law of exponent α . The overall link performance is therefore found by applying a linear bias to the N'(f) curves of magnitude 10 α db per decade. Each curve then expresses the required transmitter power in decibels above an arbitrary level as a function of frequency under the conditions specified for the link in question. The optimum frequency is then found by inspection and is tabulated in Table 5.1.

For a simple baloon-ground telemetry link in which horizon coverage

is not required, the plane earth approximation to the path loss suffices. Dipole antennas and vacuum tube receivers are used in the interests of operating simplicity. For a broad band system the only frequency dependent factor is then the effective noise figure (N') . The frequency at which the required transmitter output power is a minimum is then determined solely by link noise. In Fig.5.7.1 the (N') curves (a) and (b) show the relative power requirement in the range (50 to 1000) Mc/s. The optimum frequency (f_o) lies between 150 and 250 Mc/s , depending on sky noise conditions. The curves, being relatively broad, allow considerable latitude in the choice of frequency. For maximum sky noise the link performance is degraded by no more than 3 db from the optimum by a choice of frequency in the range 100 to 570 Mc/s . For a horizon limited system these curves must be weighted by the propagation loss factor (4 db per octave). In Fig.5.7.1 curves (c) and (d) are derived in this way. Optimum frequencies are lowered by 50 and 100 Mc/s respectively and the system becomes more sensitive to deviations above, than below (f_o) . The "3 db handwidth" is also reduced by a factor of more than two. In practice the tolerance in (f_o) will be less than the figures quoted because of reduced transmitter and antenna efficiencies at the higher frequencies. In order to take some account of frequency instability an additional bias of - 2 db per octave has been applied and plotted as curves (e) and (f) in Fig. 5.7.1 These curves, as well as applying to the narrow band horizon link also represent the broad-band, free space performance with isotropic (or constant gain) antennas. The system performance remains unchanged from 50 to 100 Mc/s but rapidly deteriorates above this range.

Turning to Figure 5.7.2 N' curves (a) and (b) show the frequency dependent performance of a narrow band telemeter using a fixed receiving aperture for horizon coverage. These curves apply to also a broad band free space link. The optimum frequency lies between 150 and 350 Mc/s , depending on sky noise. The broad band link performance, derived as before, is plotted in Fig.5.7.2as curves (c) and (d). In this case the full advantage of operation in the optimum region (300 to 1000 Mc/s) is conditional upon the use of high efficiency transmitters. These results are summarised briefly in Table 5.1.

TABLE 5.1

	Figure Reference	Optimum Frequency f_o(Mc/s)	System
5.7	1 (a) 1 (b)	150 250	A
5.7	1 (c) 1 (d)	100 150	B
5.7	1 (e) 1 (f)	70 70	C, D
5.7	2 (a) 2 (b)	150 350	E, F
5.7	2 (c) 2 (d)	250 800	G

A : Broad band (dipole to dipole) plane earth link.
B : Broad band (dipole to dipole) horizon link.
C : Narrow band (dipole to dipole) horizon link.
D : Broad band (dipole to dipole) free space link.
E : Broad band (dipole to fixed aperture) free space link.
F : Narrow band (dipole to fixed aperture)horizon link.
G : Broad band (dipole to fixed aperture) horizon link.

On the basis of these results it is clear that a choice of optimum frequency is possible for line of sight communications systems.

With the increasing use of low-noise solid state devices, the optimum frequencies will be raised until transmitter efficiency and stability become the limiting factors.

5.5 R.F. DESIGN FOR BALLOON TELEMETRY

In the preceding section we discussed general considerations governing radio telemetry design with special reference to the choise of carrier frequency. It was shown that optimum performance might be expected from a choice of frequency in the range 150-350 Mc/s (System F). Unfortunately it was not possible to choose a frequency in this range, a frequency of 72 Mc/s being allocated for the Hobart flights. This frequency was shared with the meteorological radio sonde transmitters operated by the Commonwealth Meteorological Bureau.

At this frequency, equation 5.9 shows the free space path loss (A) to be approximately 120 dB for a distance of 690 KM, the distance to the horizon from a balloon at an altitude of 30 KM. For a bandwidth of 100 Kc/s, minimum signal to noise ratio of 10 db and effective noise figure $N' = 10$ db from figure 5.8 we find the necessary radiated power from equation 5.5 to be approximately 40 mW . This is a lower limit to the required power since the attenuation at the optical horizon is actually about 20 dB greater than the free space loss (Domb & Pryce, 1947). When a directional receiving antenna with 10 db gain is used, figures 5.7, 5.8 show that about 0.8W of radiated power is required under average sky noise conditions. These figures suggest several hundred milliwatts of radiated power to be adequate for balloon telemetry since, in a practical situation, lower signal to noise ratios could be tolerated

and horizon coverage may not be necessary. From fig.5.7.2it may be seen that the power requirements could be reduced by a factor of at least ten if operation at the optimum frequency were possible. The desirability of elevating the receiving antenna is also clear. Not only is the distance to the horizon increased, but more significantly since the path loss for low angles of elevation is in the "plane earth" approximation,

$$A = \frac{P_R}{P_T} = 2.7 \left(\frac{hr\theta}{d}\right)^2 \qquad 5.10$$

where hr = height of receiving antenna

θ = angle of elevation

d = distance

the loss is reduced by 6dB by doubling the height of the antenna.

A primary design consideration in balloon telemetry is the weight of the transmitter power pack. Since the transmitter is the major consumer of battery power, it is desirable to reduce the transmitter power drain as much as possible. The preceding discussion shows how this may be done by choosing an appropriate frequency and by using elevated high gain antennas.

The problem of minimising weight is accentuated by the fact that the power requirements <u>increase</u> during a flight as the balloon drifts away from the receiver towards the horizon, while the power supplied to the transmitter by a dry cell battery pack decreases continuously as the terminal voltage drops due to polarization. A considerable saving in battery weight would result if the input power to the transmitter, initially low at the beginning of a flight, was allowed to

FIGURE 5.8 : The Transmission Loss (Attenuation) of a Dipole-Dipole radio Link at Optical Cut Off as a Function of Frequency. (Curves A, B, C).

h_r = Receiving Antenna height

h_T = Transmitting Antenna height

The "free space" and "flat-earth" attenuations are Shown for Comparison.

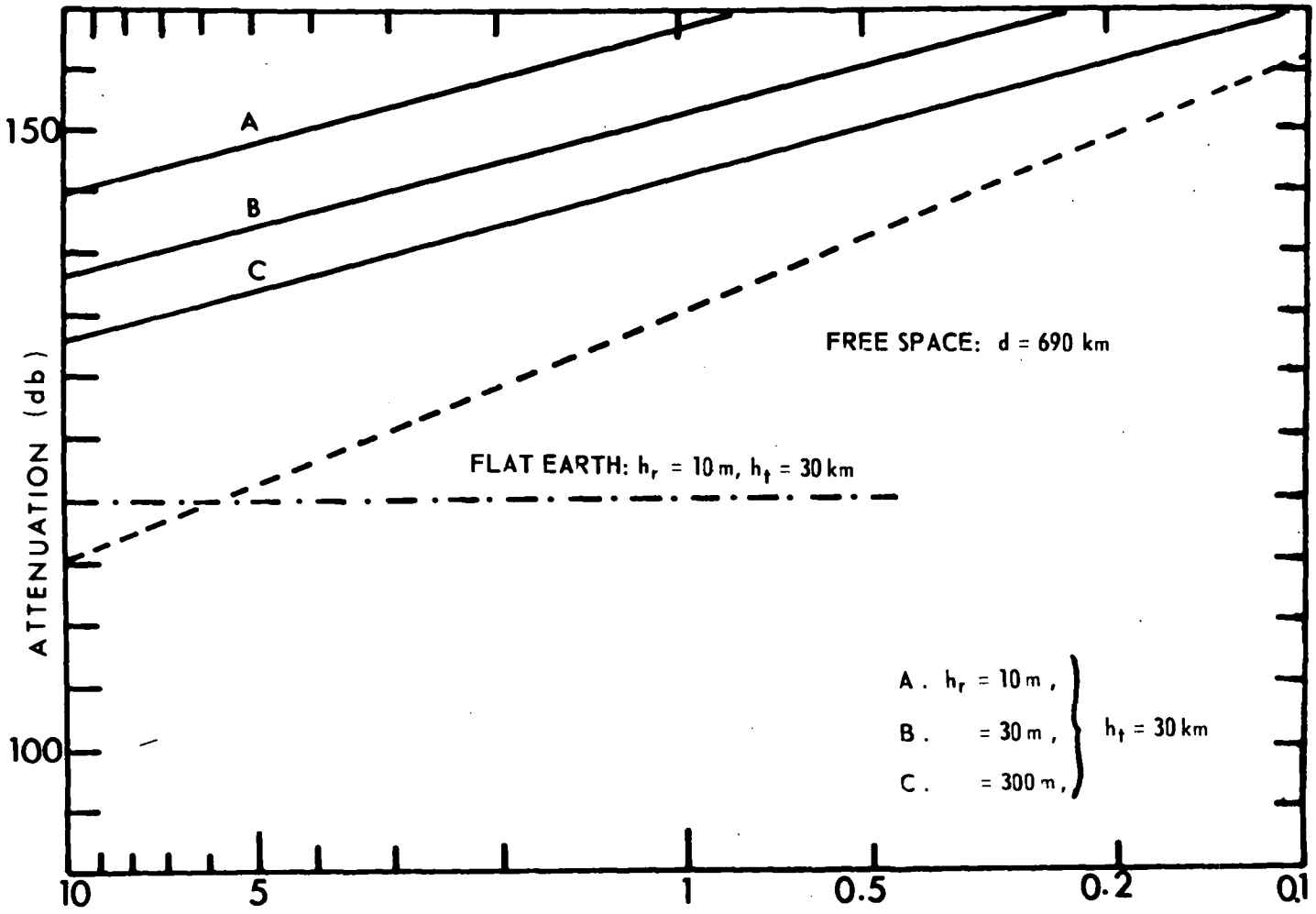

Fig. 5.8. ATTENUATION (P_t / P_r) AS A FUNCTION OF WAVELENGTH.

increase gradually during the flight to compensate for the increase in path loss due to balloon drift. This would be possible with a vacuum tube transmitter using a loaded grid bias battery. Laboratory tests showed the general feasibility of this method. It was not used because of the resultant frequency drift and change in modulation characteristics of the simple transmitters used in the project.

The power efficiency of the transmitter was also considered to be of major importance. A comparison between the performance of transistor and tube power oscillators showed their efficiencies to be similar. The efficiencies were generally low, 30 % being a typical figure obtained in practice. The smaller frequency drift, higher power dissipation and relative cheapness of suitable vacuum tubes indicated their use in the Hobart flight packages. Circuit diagrams of the two types of transmitter used are presented in figs. 5.9(a) and (b). The 958 oscillator provided 150 mW of radiated power [illegible] with an anode efficiency of 35 % and the 3A5 oscillator provided 400 mW with an efficiency of 30 %.

Vertical antennas were used for transmission and reception. An end fed transmitting antenna suspended below the package was used initially. Fading due to antenna swing was experienced on a number of flights. A centre fed half wave dipole attached to the balloon load line cured the fading problem completely.

5.6 DATA READ OUT

The same read out facilities were used for both the wire recorded and radio telemetered data. The main telemetry station used a vertical four element Yagi antenna connected by coaxial cable to the receiver.

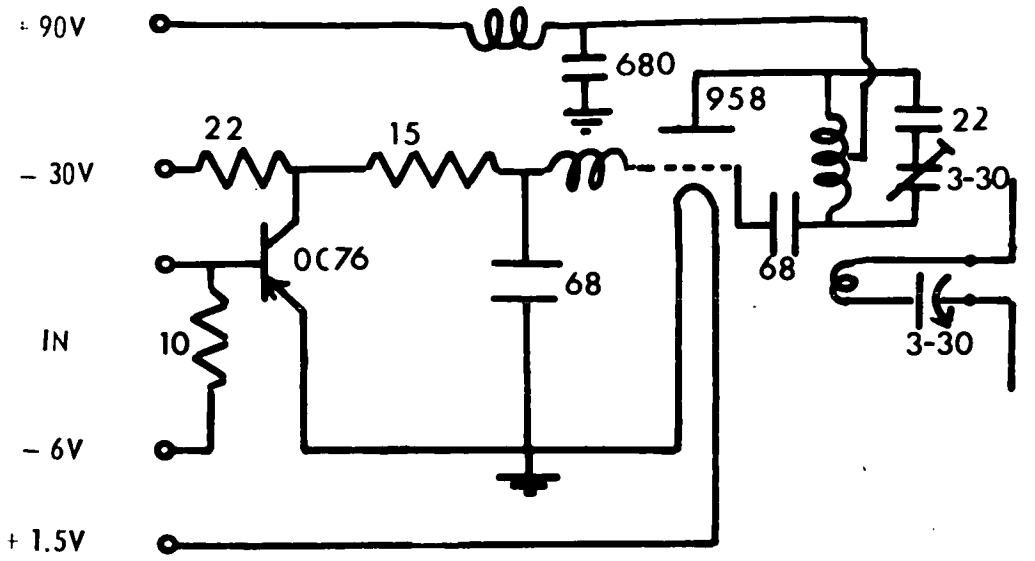

Fig. 5.9a. PULSE MODULATOR AND R F OSCILLATOR (I)

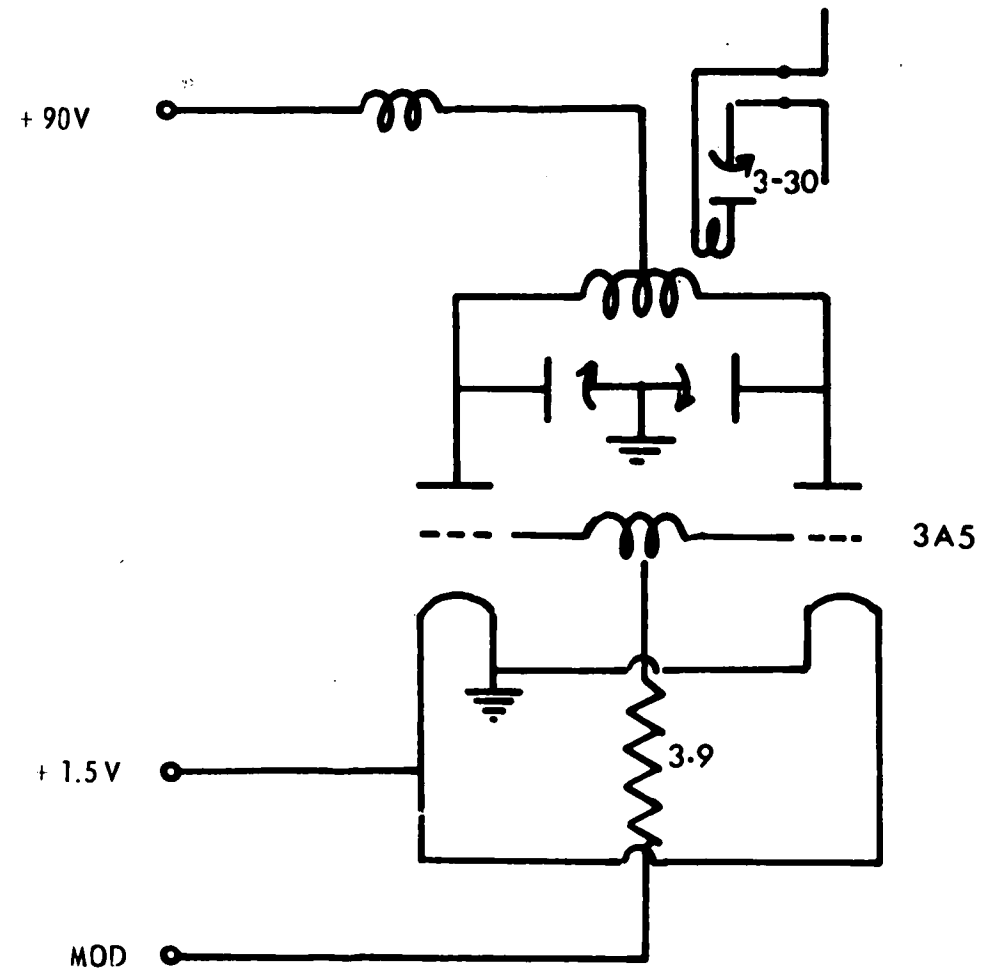

Fig. 5.9b. R F OSCILLATOR (II)

The receiver was of the superregenerative type, designed and built (Edwards, 1960) in the initial stages of the Hobart cosmic ray balloon flight programme. The receiver output was directly recorded on magnetic tape. The Mildura wire records were also transferred to tape. Figure 5.10 shows the read out facilities for the telescope flights.

In order to reduce the time and labour involved in read-out, as much data as possible were tabulated during a flight or wire-tape dubbing. Pressure-time data, and minute count totals were obtained in this way from the visual monitor displays. The tape records were used when malfunction of the pen recorder or associated circuitry occurred. The multiplexing method already described allowed the east and west counting rates to be automatically recorded by different pens. Pulse width discrimination allowed the pressure data to be directly recorded on the chart when required.

Error free read out was possible with signal pulse amplitudes below the average noise level. The system thus compares favourably with comparable FM/FM multiplex systems which exhibit high video noise thresholds.

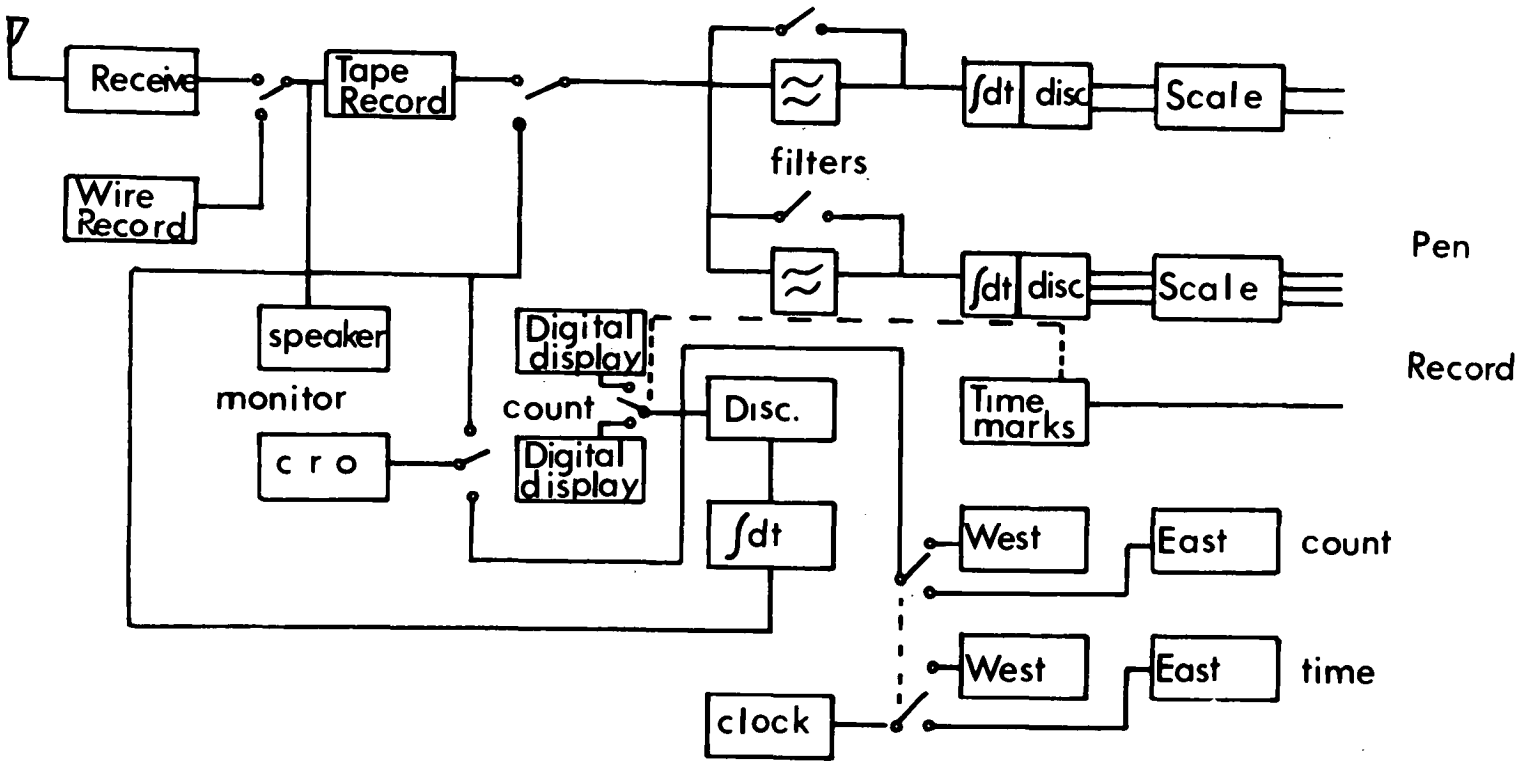

Fig. 5.10. Block Diagram, Read-out Facility.

CHAPTER 6

DIRECTIONAL MEASUREMENTS OF THE COSMIC RAY INTENSITY AT HOBART ($\lambda_m = -52^\circ S$) AND MILDURA ($\lambda_m = -44^\circ S$)

In the preceding chapters the design and construction of the experimental equipment was described. In this chapter we present the experimental data obtained from the Hobart and Mildura flights. In the following Chapters the results are discussed and interpreted.

6.1 Summary of the Flight Programme

The first flights were made in early 1962 at Mildura on the Australian mainland. The initial flight was not successful due to water immersion of the in-flight wire recorder prior to recovery of the gondola. Several additional flights were made using a telemetry system constructed at the launching site when it became apparent that the wire recorder would not be available for further use. Information concerning the rotation characteristics and temperature of the gondola was obtained in this way. The telescope (geometry "A", Section 4.5) did not function satisfactorily at floating altitude. The temperature measurements established that the package was insufficiently insulated against heat loss, leading to temperatures below $0^\circ C$, with consequent malfunction of the external cathode geiger counters. The package was redesigned at Hobart to improve thermal insulation and several internal cathode telescopes were constructed. In 1963 the instrument packages were dispatched from Hobart to the launching

site at Mildura. Successful flights were then achieved with the maze counter telescope and a number of internal cathode telescopes. The nominal floating altitude of 105, 90, 80 and 65 thousand feet provided directional intensity data in a range of atmospheric depths from 9 to 60 g/cm^2. All data were obtained at locations within a distance of 70 KM from Mildura.

The Hobart flights commenced in 1962. It was hoped to achieve floating periods of the order of half a day at floating altitude using the valving technique described in Section 4.8. This technique was not successful and although four flights were made with neoprene balloons during 1962-1963, in only two of these did the telescope remain at a reasonably constant altitude for more than one hour. The last flight was launched from Hobart in December 1963 and carried telescope (A) used in the Mildura flights. A plastic balloon was used and this stayed aloft for more than 36 hours. This flight was successful and provided asymmetry and directional flux data of good statistical accuracy over a range of atmospheric depths. The Hobart data were obtained at distances of less than about 200 Km S.E. of Hobart.

In the following Sections the Hobart and Mildura data are separately presented. All telescopes were inclined at a zenith angle of 45°.

6.2 Mildura Flights Data : Hibal Flights 138; 148

In this Section we present data obtained during the ascent and level flight periods of the two flights in which the nominal floating

altitude was 105,000 feet. In this and the succeeding sections the flight number is that used by the Balloon Launching Station at Mildura (geomagnetic co-ordinates 43°40'S, 142°E).

Flight 138

This flight was launched at 2125 UT on April 22, 1963. The balloon rose at an average rate of 1040 feet/min, commenced floating at 2313 UT at an altitude of 104K ft and was cut down at 0226 UT, April 23, 1963. The instrument package contained a single three counter telescope (geometry "B", Figure 4.2(b)), a solar sensor covering the magnetic east and west quadrants, and the wire recorder and associated equipment. The total recording period was nearly four hours, including two hours of the floating period, during which the balloon remained at an atmospheric depth of 9.0 ± 0.3 g/cm^2.

The gondola rotated with a period of less than one minute during ascent. During level flight the azimuthal rate was considerably slower, of the order of several degrees a minute. The telescope counting rate is shown as a function of pressure and time in Figure 6.1. From this figure may be seen the enhanced counting rate at the start, middle and end of the floating period when the compass signal indicated westerly orientation of the telescope. The depressed rates were recorded when the telescope pointed east. The east-west asymmetry, averaged over 45° azimuth intervals centred on the geometric east and west directions was determined to be $a_{ew} = 0.35 \pm 0.05$. The east-west asymmetry ratio, $\frac{J_w}{J_e} = 1.43 \pm 0.07$, the differential flux, $J_w - J_e = 570 \pm 50$ peters, and the flux from the east $J_e = 1340 \pm 35$ peters. The flux at the transition maximum (at an atmospheric depth of approximately 90 g/cm^2) averaged over 360° in azimuth,

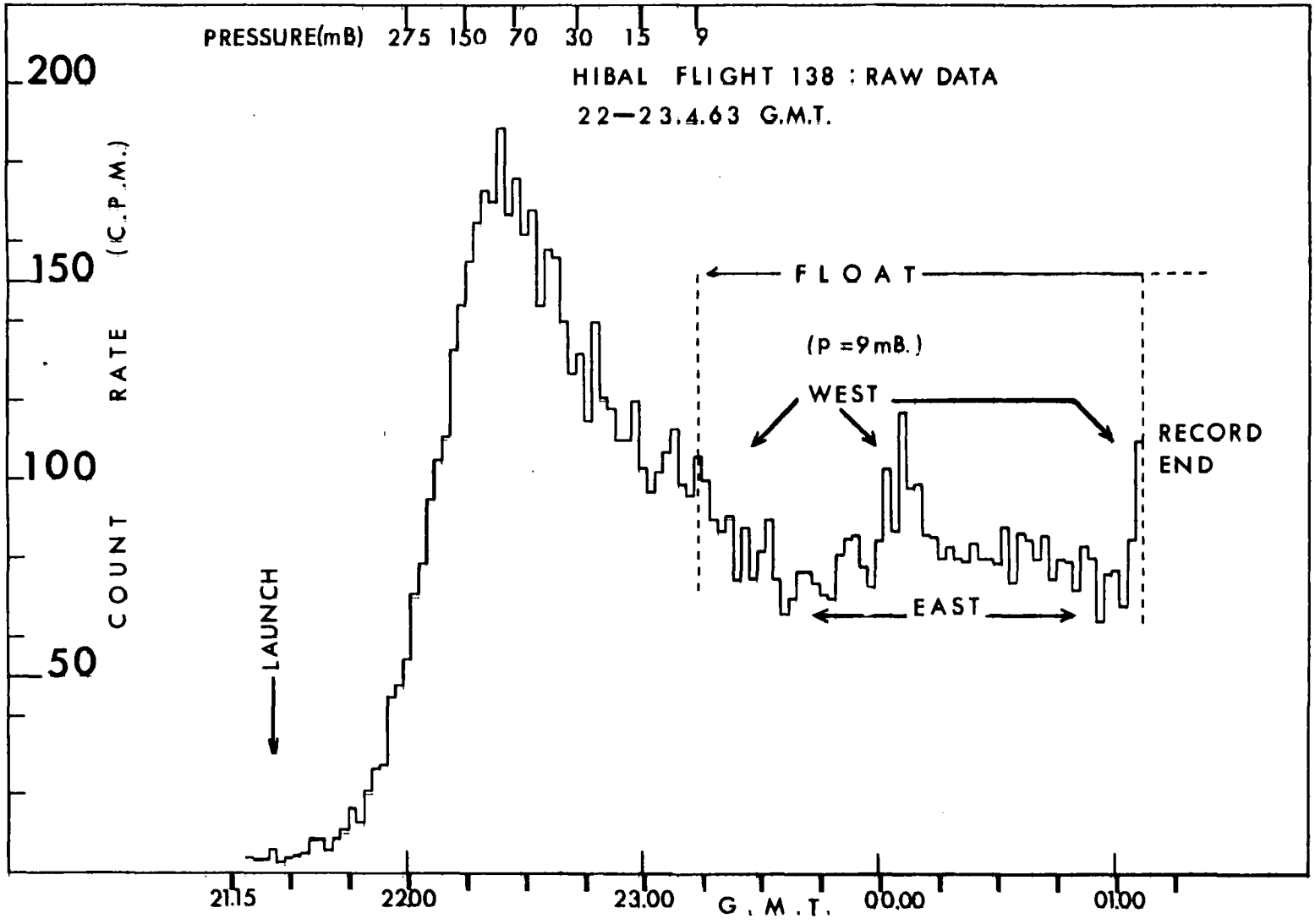
PRESSURE(mB) 275 150 70 30 15 9
HIBAL FLIGHT 138 : RAW DATA
22—23.4.63 G.M.T.
200
150
100
50
COUNT RATE (C.P.M.)
FLOAT
(P =9mB.)
WEST
EAST
RECORD END
LAUNCH
21.15
22.00
23.00
G.M.T.
00.00
01.00

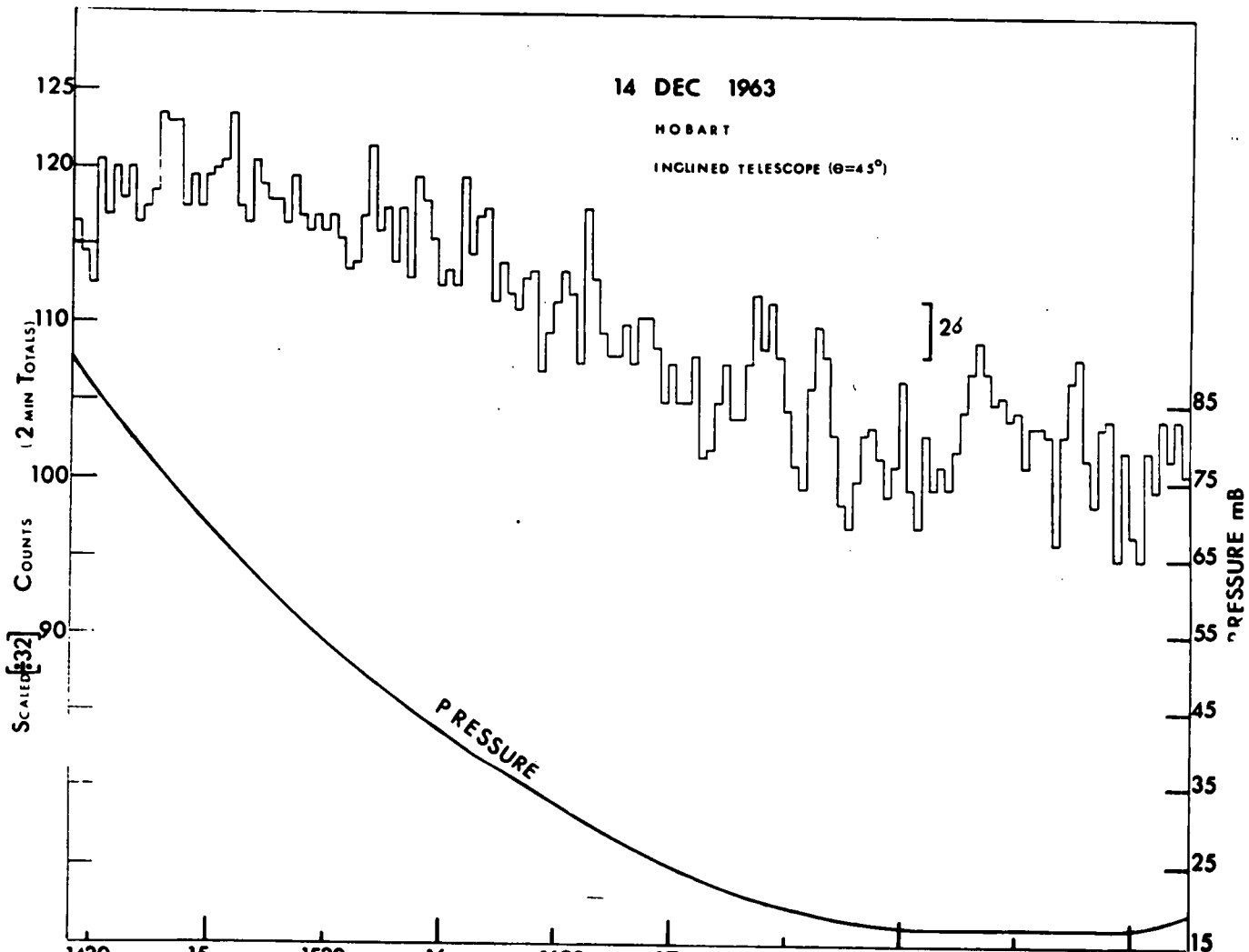

FIG. 6.2: HOBART FLIGHT 5.

was found to be $J_m = 3350 \pm 100$ peters. The errors quoted above are statistical and do not take into account possible errors in the geometric factor which was taken as 8.75 cm^2 sterad.

Flight 148

This flight was launched at 2206 UT on July 23,1963, four months after Flight 138. The mean ascent rate of the balloon was 825 feet/min and the floating depth of 9.5 ± 0.3 g/cm^2 was reached at 0011 UT, July 24, 1963. Telescope ("A", Figure 4.2(a)) was flown in conjunction with a solar sensor covering the east and west quadrants. Due to a mechanical malfunction of the wire recorder, only one hour of level flight data was recorded. However, because of the higher geometric factor (120 cm^2 sterad), the directional data is statistically more accurate than that obtained in the previous flight, although the gondola did not rotate as regularly.

The east-west symmetry averaged over 45° sectors was 0.36 ± 0.03 and the asymmetry ratio, $\frac{J_w}{J_e} = 1.64 \pm 0.04$. The differential flux, $J_w - J_e = 550 \pm 30$ peters and $J_e = 1300 \pm 20$ peters. The quoted intensities may contain a residual error because of the large correction to the counting rates necessitated by the low counting efficiency of the telescope due to counter resolving time. This correction was attempted using two methods. The first method involved calculation of the counter tray efficiencies and (Appendix 1) using laboratory resolving time measurements. The second correction was obtained by comparing the counting rate during the ascent with the counting rate at corresponding depths of several different telescopes for which the resolving time loss was small and had been computed by the first method. The first method gave an efficiency 15% higher than

that obtained by the second method. In view of the uncertainties in the resolving time calculations, the counting efficiency used in the intensity calculations was determined by the second method.

6.3 Mildura Flight Data : Mibal Flight 158

In this section data is presented from Flight 158, launched at 1954 UT on October 9, 1963. The balloon reached floating depth at 2132 UT, October 10,1963. Telescope "A" was flown with a three quadrant solar sensor covering the east, west and north magnetic quadrants. Due to recorder malfunction, no ascent data was obtained, but a total of 50 minutes of level flight data was recorded. The baroswitch on board the Mibal gondola indicated an initial level flight pressure of 23.3 mb, slowly increasing to reach 25.3 mb at the end of the floating period. The pressure deduced from radar soundings was 17.1 mb. It was established that the baroswitch was in fact in error and the mean atmospheric depth was taken as 17.5 g/cm^2. This figure is uncertain by several g/cm^2.

The east-west asymmetry was determined as 0.40 ± 0.02 and the asymmetry ratio, $\frac{J_W}{J_E} = 1.50 \pm 0.03$. The differential flux, $J_W - J_E = 760 \pm 35$ peters, and the flux from the east, $J_E = 1520 \pm 20$ peters.

6.4 Mildura Flight Data : Mibal Flights 132, 153, 157

In this section we present the intensity data obtained in three level flights at a nominal altitude of 80,000 feet.

Flight 132

Flight 132 was launched at 2016 UT on March 18,1963. The mean

ascent rate of the balloon was 990 feet/min and level flight commenced at 2134 UT, March 18,1963. The geometric factor of the telescope (Figure 4.3) was 0.97 cm^2 ster. A three quadrant solar sensor provided azimuth information. A baroswitch was included with the pay load in order to check the Hibal pressure measurements. The total recording period of four hours covered the ascent, two hour level flight at 32.5 ± 0.5 $g/cm^2$and twentyfour minutes of the descent. The telescope counting rate is plotted in Figure 6.2. The low counting rate of this telescope and the irregular rotation of the gondola do not allow the azimuthal variation of intensity to be clearly seen from the graph.

The east-west asymmetry averaged over 90° in azimuth was 0.286 ± 0.06. The asymmetry ratio, $\frac{J_w}{J_e}$ = 1.33 ± 0.08. The differential flux, $J_w - J_e$ = 790 ± 160 peters, and the east flux, J_e = 2370 ± 110 peters.

Flight 153

This flight was launched at 2034 UT on September 17, 1963. The package contained two inclined telescopes, 180° apart in azimuth with geometric factors of 10.9 and 10.4 cm^2 sterad (Geometry "C",Figure 4.2). Mechanical registers separately accumulated the east and west counts and the total count from each telescope for the period of level flight. The mean ascent rate of the balloon was 660 feet/min and the floating level (30 g/cm^2) was reached at 2233 UT, September 17,1963. The baroswitch was arranged to start the registers counting at a depth of 37 g/cm^2(74,000 ft) and to terminate the count when the balloon descended to 70,000 feet (46 g/cm^2). The register indicating the total counting period did not function but the period of 116 minutes, estimated from the flight curve,

commenced at 2222 UT and ended at 0018 UT. The period of level flight was 103 minutes, 11 minutes of data were accumulated during the ascent (37-30 g/cm^2) and the remaining two minutes of recording time covered the descent from 30 - 46 g/cm^2.

The east-west asymmetry averaged one 180° in azimuth, was 0.078 ±0.015 and the asymmetry ratio $\frac{J_w}{J_e}$ = 1.08 ± 0.02. The flux from the east measured with the two telescopes was 2330 ± 25 peters and 2220 ± 30 peters respectively. The mean differential flux was 186 ± 36 peters. The flight was made during the progress of a Forbush decrease which commenced at Hobart at 0200 UT, September 17, 1963. Comparison between the two telescope count totals suggests that intensity variations occurred during the flight.

Flight 157

The flight was launched at 2006 UT on October 7, 1963. The average ascent rate was 856 feet/min and the maximum altitude of 79,000 feet was reached at 2140 UT, October 7,1963. The balloon burst prematurely five minutes later. The register bank commenced counting at 0732, eight minutes before the balloon stopped rising. Counting ceased at 0750 when the balloon depth had increased to 46 g/cm^2. The counting period was too short to provide accurate directional data. Subject to the uncertainties introduced by the variation in depth (46 - 30 g/cm^2), the following results were obtained with the telescopes used in Flight 153. One of the telescopes was placed in anti-coincidence with a single counter (Figure 4.2). The results are averaged over 90° in azimuth.

The east-west asymmetry was 0.11 ± 0.06 for the unpoliced telescope and 0.16 ± 0.08 for the policed telescope. The asymmetry ratios were respectively 1.12 ± .06 and 1.17 ± 0.09. The east fluxes were respectively 2300 ± 110 peters and 2030 ± 107 peters and the differential fluxes, 266 ± 156 peters and 316 ± 155 peters. The results show that the anti-coincidence counter reduced the telescope counting rate by about 11%. The statistical accuracy is not sufficiently high to allow a comparison between the directional flux measured in this flight and that measured in Flight 153 during the Forbush decrease.

6.5 Mildura Flight Data : Flight 128

This flight was launched at 1935 UT on February 12,1963. The mean ascent rate was 795 feet/min and level flight at 66.5 g/cm^2, lasting 65 minutes, commenced at 2053 UT. The instrument package contained a Cerenkov detector associated with four internal cathode geiger counters (Figure 4.3). Figure 4.5 (a) shows the instrumentation in block diagram form. The photomultiplier output pulses were discriminated at three amplitude levels, corresponding to proton momenta of 1, 1.16 and 4.4 GV.

The flight was the first in 1963 and a baroswitch and thermistor were included to provide pressure and temperature information in order to check the Hibal pressure data and the adequacy of the thermal insulation of the package. Figure 6.3 shows the temperature, pressure and altitude during the flight. The baroswitch readings indicated on the graph by open circles, are in good agreement with the Hibal data. The temperature

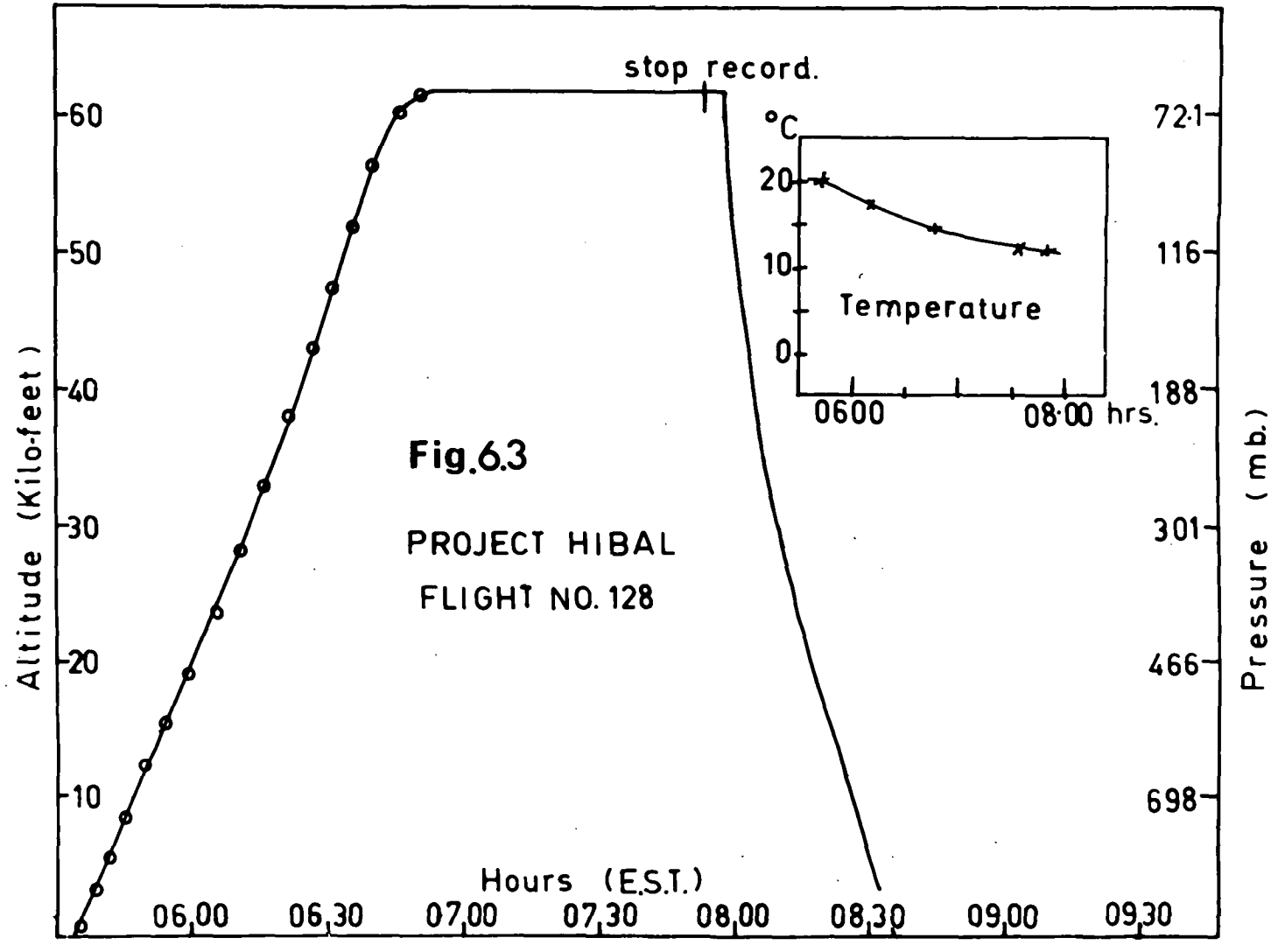

Fig.6.3

PROJECT HIBAL

FLIGHT NO. 128

of the pay load dropped by less than 10°C. This was considered to be satisfactory since the balloon was launched before local sunrise and the low altitude of the sun throughout the flight suggested that solar heating was small.

One of the sub carrier oscillators, which were constructed as plug in modules (Figure 4.4, Section 4.5) was jarred from its socket during rail transport to Mildura. The data were consequently restricted to that from the pressure and temperature transducers, the "north" solar sensor, the "narrow angle" (N.A.) telescope and the Cerenkov detector. Figure 6.4 shows the N.A. telescope counting rate during the flight.

The counting rates and flight duration were too low to provide reliable estimates of the azimuthal flux distribution, the main purpose of the experiment being the acquisition of "housekeeping" information for the design of further flights. Of particular interest was the contribution of non-primary particles to the geiger telescope counting rate.

Particles traversing the telescope encountered an absorber thickness of 15 g/cm^2. The momentum threshold was therefore 0.52 GV for protons and 0.12 GV for μ-mesons. Table 6.1 lists the N.A. and Cerenkov telescope fluxes obtained during level flight.

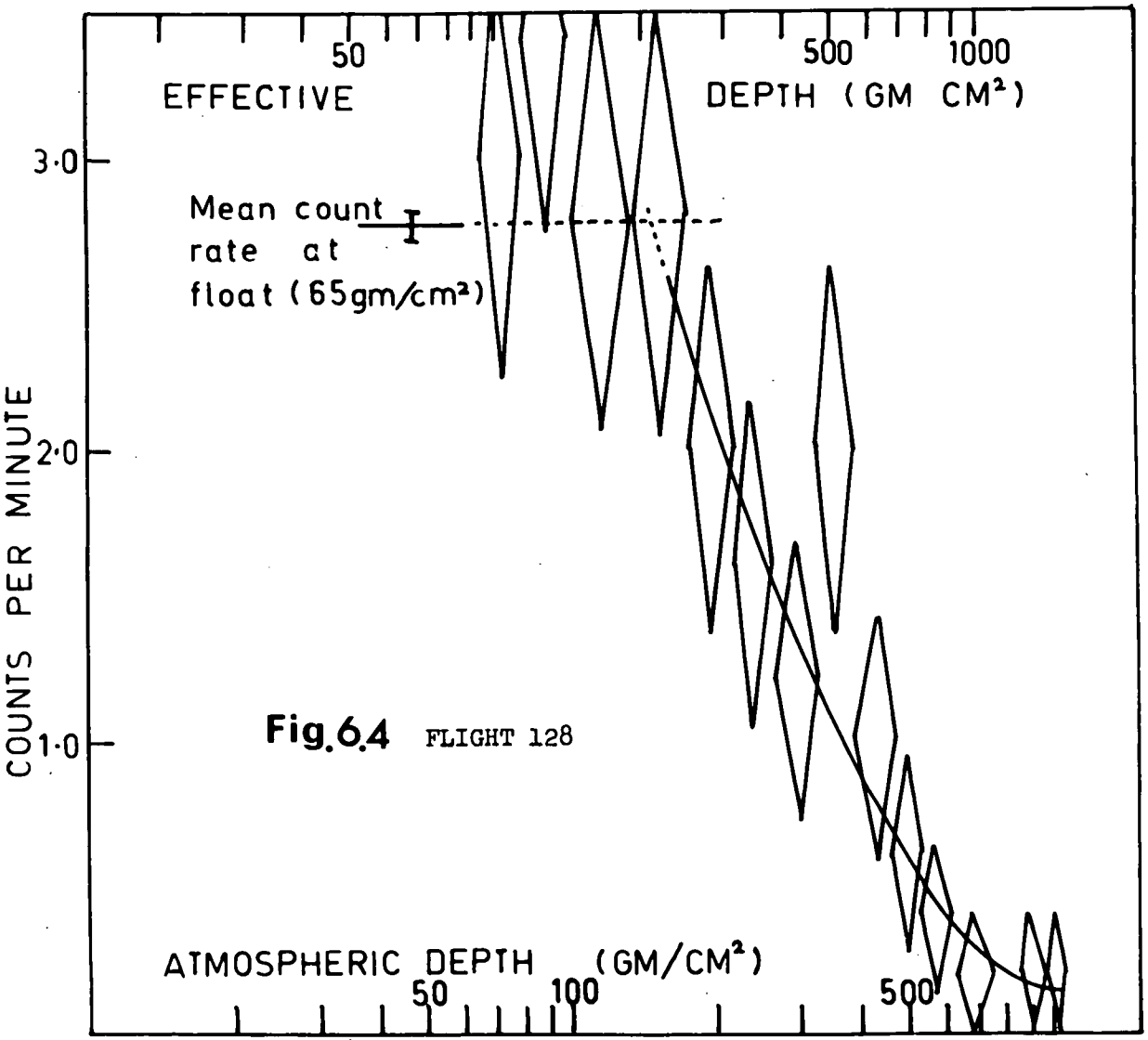

Fig.6.4 FLIGHT 128

TABLE 6.1

Channel	Momentum Range (GV)		Flux (Peters)
	Proton	μ-Meson	
NA ($\overline{A}.\overline{B}.\overline{C}.$)	0.52 - 1.0	-	524 ± 85
A	1.0 - 1.16	-	198 ± 42
B	1.16 - 4.40	0.12 - 0.47	354 ± 75
C	≥ 4.40	0.47	803 ± 113
NA	≥ 0.52	0.12	1879 ± 205

Particles counted by the telescope but giving no detectable Cerenkov light (NA.$\overline{A}.\overline{B}.\overline{C}.$) Comprise: (a) Protons with momenta between (0.52 and 1.0) GV entering the telescope from above.

(b) Fast splash albedo protons.

(c) Side shower particles which trigger the four fold coincidence set but not the Cernkov discriminator.

Channel A counts are predominantly due to down coming secondary protons. A small contribution is due to proton collissions with the photomultiplier structure.

Channel B counts down coming protons and μ-mesons.

Channel C counts down-coming primary protons, heavier nuclei and mesons. Nuclear collisions in the Cerenkov radiator will also contribute pulses to this channel.

The sum of the splash albedo flux and of the slow proton flux in the momentum interval (0.52 - 1.0) GV, N.A.($\overline{A}.\overline{B}.\overline{C}.$) in Table 6.1, is 28% of the total N.A. flux.

6.6 Hobart Flight Data : Flights 2, 4

In this section the data from two flights launched from Hobart in 1963 is discussed. Flight 1, launched in 1962 did not provide useful directional data owing to a telemetry fault. Flight 3 in April,1963 did not reach floating altitude, and burst prematurely. The ascent data from this flight was examined and established as asymmetry of the order of 10% in the depth interval (100 - 50) g/cm^2.

Flight H.2

This flight was launched at 0149 UT on April 2, 1963. The balloon reached floating depth (30 g/cm^2) at 0310 UT but began to sink 15 minutes later. Irregular fluctuations in depth continued for one hour and the balloon rapidly lost altitude after 0420 UT. The instrument package contained a single bellows baroswitch, wide angle telescope of geometric factor 13.8 cm^2 sterad inclined at 45° zenith angle and a two quadrant sun sensor. Ambiguity in the identification of the baroswitch contacts necessitated rejection of some data. The east-west asymmetry at 32 $\pm$ 3 g/cm^2 was 0.095 $\pm$ 0.04 and the differential flux, $J_w - J_e = 400 \pm 160$ peters. The flux from the east was 3600 $\pm$ 130 peters.

Flight H.4

The flight was launched at 0051 UT on September 5, 1963. The instrumentation was identical with that used in Flight 2. The telescope had previously been flown at Mildura (Flight 138). A depth of 32.5 ± 3 g/cm^2 was reached at 0223 UT and remained within these limits until 1242 when the balloon began to lose altitude. The telemetry signal was lost at 1410 when the balloon apparently passed below the radio horizon.

The asymmetry at 32.5 ± 3 g/cm^2 was 0.103 ± 0.045, the differential flux was 378 ± 160 peters, and the east flux 3520 ± 300 peters.

6.7 Hobart and Telescope Flight Data : Flight 5

Flight H.5

A plastic balloon carrying telescope "A", east and west quadrant sensors, a baroswitch and associated telemetry equipment, was launched from Hobart at 0106 UT on December 14,1963. The ascent rate was considerably lower than had been intended, and the balloon reached its maximum altitude of 90,000 feet (17.5 g/cm^2) at 0800 UT. The low ascent rate enabled directional intensity data to be obtained with reasonable statistical accuracy over a wide range of atmospheric depth. The balloon remained at constant altitude for 60 minutes and then commenced to sink at 0900 UT following local sunset. The telescope rate dropped as the package cooled during the night and although data was obtained on the following day it is not reported here because of uncertainty regarding the atmospheric depth of the balloon.

Figure 6.2 shows the telescope counting rate and pressure for the first day of the flight. The azimuthal flux variation is evident from the two minute count totals during the latter part of the flight. Owing to the slow ascent, the sun sensors did not directly indicate the east and west directions during this later stage of the flight. It was possible however to interpret the compass data with reasonable confidence.

The east-west asymmetry at an atmospheric depth of 17.5 g/cm^2 was determined to be $= 0.097 \pm 0.02$ and the asymmetry ratio, $\frac{J_w}{J_e} = 1.10 \pm 0.02$. The east flux, $J_e = 3270 \pm 50$ peters, and the east-west differential flux, $J_w - J_e = 330 \pm 60$ peters. These results were averaged over an azimuth interval of approximately 45°.

The directional data at greater depths is discussed in Section 7.1.

CHAPTER 7

DISCUSSION OF THE DIRECTIONAL MEASUREMENTS

7.1 The East-West Asymmetry at 52°S.

The E-W asymmetry obtained in the three Hobart flights is plotted as a function of depth in Figure 7.1. The asymmetry increases monotonically with decreasing depth, from about 5% at the transition maximum to 10% at the lowest depth attained, 17.5 g/cm^2(15 g/cm^2 atmospheric stopping power at 45° zenith angle). Extrapolation to zero depth suggests a primary asymmetry of 0.13 ± 0.03.

Observations of the east-west asymmetry were reviewed in Section 3.4. The observations reported here appears to be the first in which a measureable high altitude asymmetry has been obtained at a geomagnetic latitude above 45°. Reference to Figure 3.2 (Section 3.3) shows the extrapolated asymmetry to be in agreement with the primary asymmetry expected at latitude 52°S at solar minimum.

7.2 The Dependence of the East-West Intensity Difference at 52°S upon Atmospheric Depth

The data from Hobart Flight 5 has been used to plot the depth dependence of the east and west intensities in Figure 7.1. The east-west intensity difference is also plotted.

The intensity difference curve is well represented as an exponential function of atmospheric pressure in the range 17 - 150 mb.

$$\delta \text{ Jew} = J_W(\theta=\pi/4) - J_E(\theta=\pi/4) = 400 \exp(-P/67) \text{ peters}$$

This relation implies an absorption mean free path of $68\sqrt{2} = 96$ g/cm^2 for

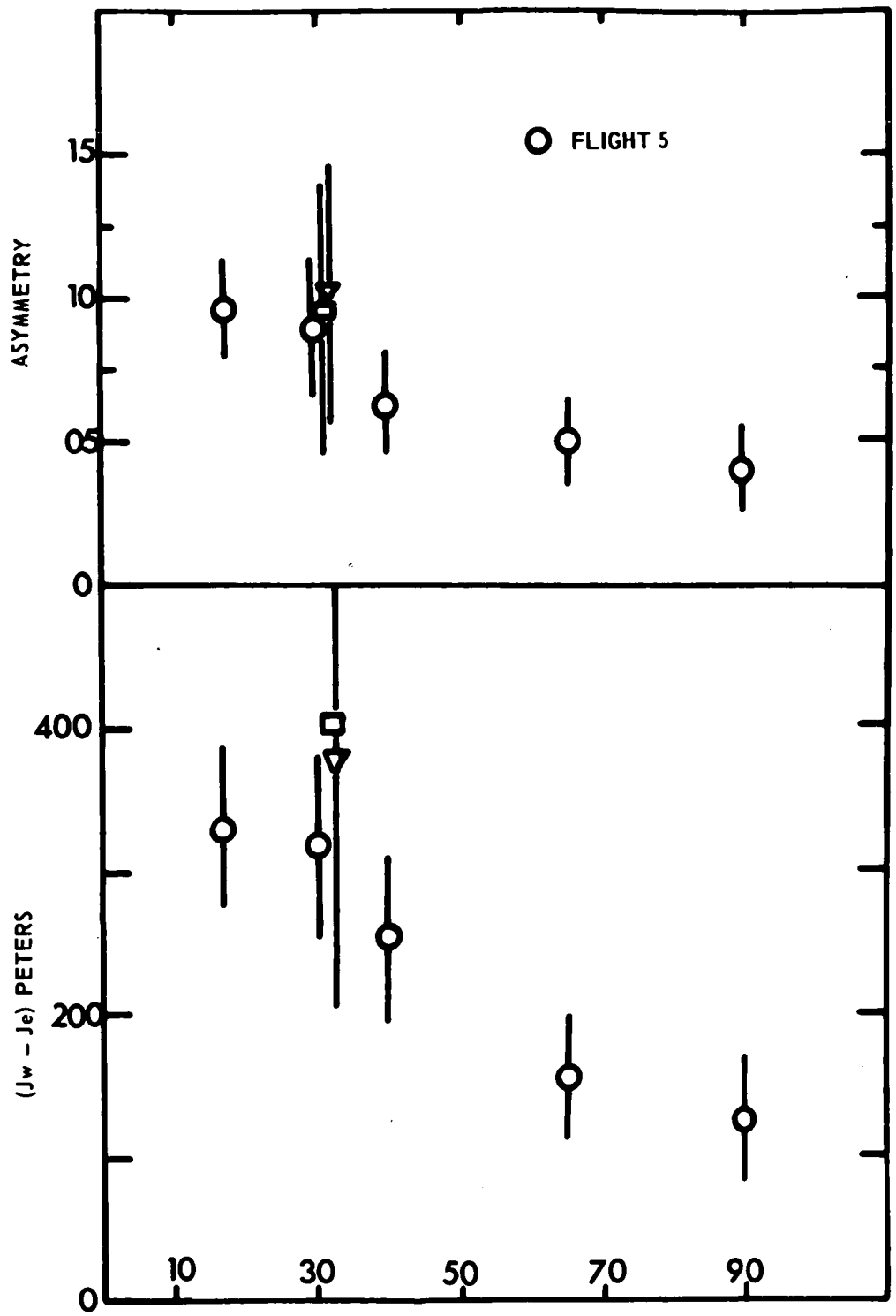

Fig. 7.1. EW ASYMMETRY AND
EW FLUX DIFFERENCE
AT HOBART (52°S)

the radiation producing the east-west difference, principally protons with a near energy close to 1000 MeV (Section 2.1). The agreement with the proton mean free path of 100 g/cm^2 in air suggested by emulsion measurements at 900 MeV (Millburn et al., 1954) is probably fortuitous in view of the statistical uncertainties in the east and west counting rates.

The transition depth of the east and west intensities is not significantly different at Hobart and lies in the range 70 ± 5 g/cm^2.

7.3 The East-West Asymmetry at 44°S

As expected, (Section 3.3) the east-west effects at Mildura (44°S) were appreciably greater than at Hobart (52°S). Figure 7.2 shows the depth dependence of the asymmetry obtained from the Mildura flights. Although several different telescope geometries were used, no geometry correction has been made. The agreement between the values obtained at 9.5 g/cm^2 with telescope "A" and "C", and the considerations of Section 4.2, together suggest that the magnitude of these corrections would be less than the statistical errors.

The asymmetry at 44°S, unlike that at 52°S, does not decrease monotonically with increasing depth, but appears to reach a maximum of 0.40 at 17.5 g/cm^2. At 9.5 g/cm^2 the asymmetry has dropped to 0.35, although the decrease is not highly significant statistically.

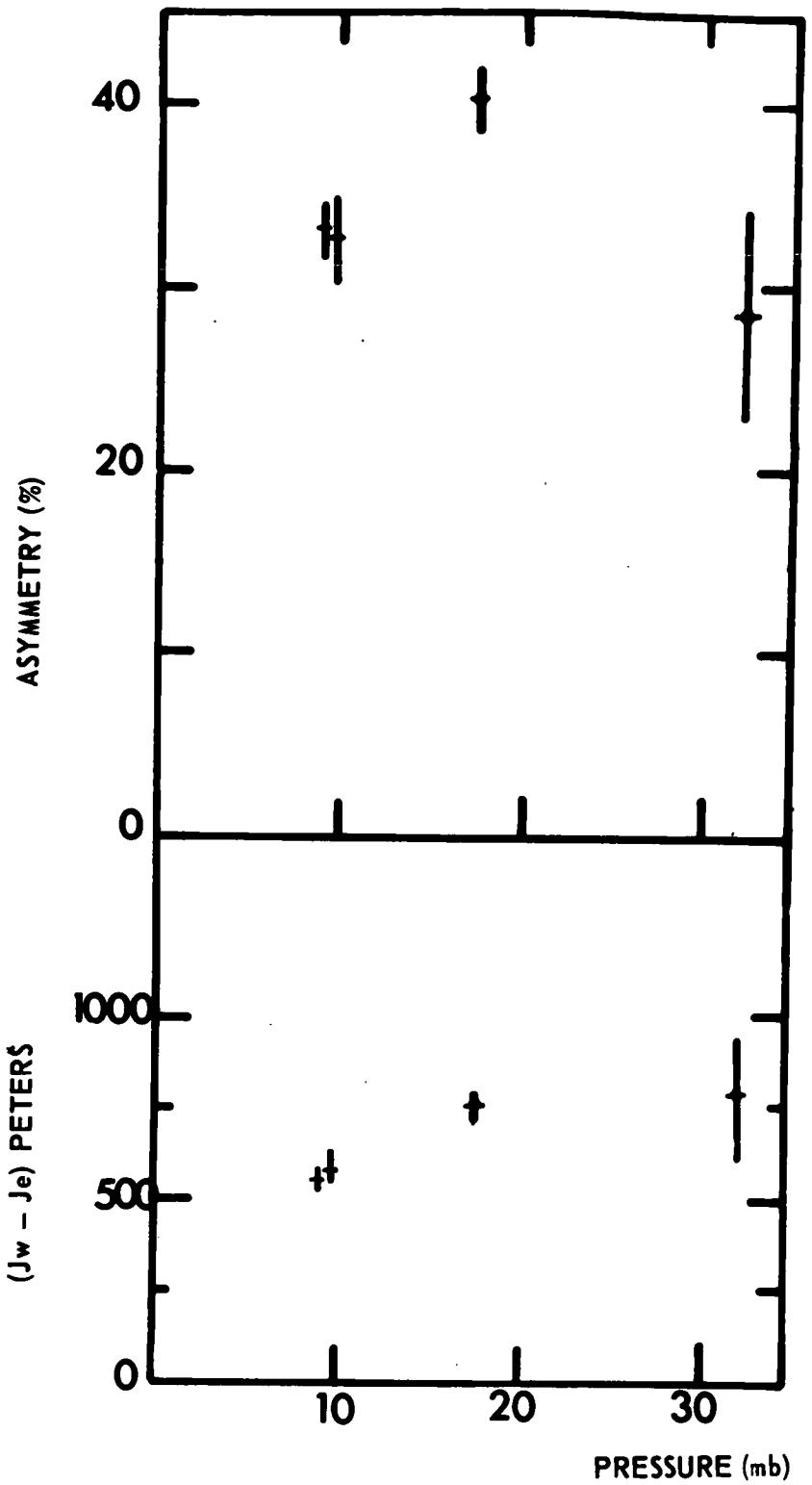

Fig. 7.2. E W ASYMMETRY
+ E W FLUX DIFFERENCE
AT MILDURA (44°S)

A primary asymmetry of 0.40 is expected at solar minimum (Figure 3.2). Comparisons may be made with the investigations of Winckler and Anderson (op.cit. Section 3.4) in which the asymmetry at 60^{o} zenith angle and latitude 40^{o} at comparable atmospheric depths was found to be 0.26 ± 0.06. This is certainly significantly less than that obtained from the present investigations. The geomagnetic theory (Chapter 2) shows that the asymmetry ought to be greater at larger zenith angles and lower latitudes, as was in fact confirmed by Winckler's experiments.

The anomalously high asymmetry obtained at 44^{o}S latitude is therefore consistent with the existence of a softer primary energy spectrum in 1963 than in 1949. Evidence supporting this view is presented in Sections 7.5 and 7.6.

7.4 THE DEPENDENCE OF THE EAST-WEST INTENSITY DIFFERENCE AT 44^{o}S UPON ATMOSPHERIC DEPTH

The east-west intensity difference is plotted in Figure 7.2.

The intensity difference increases with depth, reaches a broad maximum at about 35 g/cm^2 and decreases rapidly at depths greater than the west intensity transition depth ($\triangleq$ 90 g/cm^2). The transition depth of the east intensity cannot be accurately determined from the ascent data but is approximately 100 g/cm^2.

Protons allowed from the west but not from the east (Section 7.6), have rigidities between approximately 3.7 and 4.8 GV. Taking the primary rigidity spectrum of Section 3.2, the mean energy of protons

responsible for the east-west difference at Mildura is approximately 3 GeV. The occurrence of a transition maximum in the east-west intensity at 44°S but not at 52°S (Section 7.2) is therefore not unexpected in view of the increased production of penetrating secondary particles at higher primary energies.

7.5 The Primary Cosmic Ray Rigidity Spectrum in 1963.

(A) Hobart Observations

The directional measurements at Hobart and Mildura allow certain deductions concerning the cosmic ray rigidity spectrum in 1963. It has already been pointed out that the observed asymmetries are considerably greater than would be expected by extrapolating similar measurements made by Winckler in 1949, near solar minimum. Direct comparison between the directional intensities has been shown by Anderson (op.cit. Chapter 3) to give misleading results because of the presence of the secondary background. However, as discussed in Chapter 3, the differential intensities ($J_W - J_E$) at a given location ought to allow the intensity of primary cosmic rays in a narrow range of rigidity to be deduced. This rigidity interval (Chapter 2) is approximately centred at the vertical Stoermer threshold value with width approximately the difference between the east and west Stoermer thresholds.

The vertical rigidity threshold at Hobart according to Quenby and Webber (op.cit. Section 2.5) is 1.70 GV. The equivalent Stoermer latitude at the top of the atmosphere above Hobart, using Equation 2.5,

is therefore 54.5°. The actual threshold will in fact be higher because of the neglect of the penumbra. Quenby and Wenk (op.cit. Section 2.5) quote the effective threshold as 1.79 GV.

The machine calculations of McCracken (op.cit. Section 2.5) suggest a somewhat higher vertical threshold. Since the east-west rigidity difference at high latitudes varies as the seventh power of the Stoermer latitude (Equation 2.6), the deduced primary differential intensity is clearly sensitive to the latitude assumed for Hobart. From Figure 2.1 the east-west rigidity interval for zenith angle 45° varies from 250 MV at $\lambda_s = 54°$ to 470 MV at $\lambda_s = 50°$. Assuming the penumbra in the east and west to be transparent, the rigidity difference $\delta P_{ew}(\theta = 45°, \lambda = 54.5°) = 230$ MV. From Section 7.2 the primary differential intensity is therefore

$$\int_{1.60}^{1.83} \frac{dN}{dP} \cdot dP \Big/ \delta P_{ew} = \frac{\delta J_{ew}(x=0)}{\delta P_{ew}} = 1740 \text{ peters/GV at 1.7 GV} \quad \ldots\ldots 7.2$$

For a Stoermer latitude of 50°

$$\frac{\delta J_{ew}(x=0)}{\delta P_{ew}} = 850 \text{ peters /GV at 2.6 GV.} \quad \ldots\ldots 7.3$$

In view of the possible errors in the east-west rigidity band width associated with the uncertainty in the Stoermer latitude of Hobart, it is not possible to set accurate limits to the deduced intensity. The errors introduced by counting statistics and uncertainty in telescope geometrical sensitivity probably do not exceed ±30%.

The differential rigidity spectrum at the 1954 solar minimum (Webber, 1962) reached a maximum of about 1460 peters/GV at 1.5 GV (protons plus alpha particles). The balloon measurements (December, 1963) therefore suggest a differential primary intensity at least as high as that expected from the previous solar minimum. However, at the time of the present measurements the Mawson and Mt.Wellington neutron monitor rates (private communication, Dr.A.G.Fenton) were still rising towards the level anticipated from observations in 1954.

7.6 The Primary Cosmic Ray Rigidity Spectrum in 1963: (B) Mildura Observations

The vertical threshold rigidity at Mildura according to Quenby and Webber (op.cit. Section 2.6) is 3.73 GV. By the method of the previous section the east and west Stoermer thresholds at 45° zenith angle were found to be respectively 4.28 and 3.31 GV. The penumbral calculations of Schwartz (Section 2.2) at Stoermer latitude 41° may be approximately extrapolated to latitude 45° to give

$$P_E(\lambda_s=45^{\circ},\ \theta=45^{\circ}) = 4.78 \text{ GV and } P_W(\lambda_s=45^{\circ},\ \theta=45^{\circ}) = 3.69 \text{ GV.}$$

We thus find

$$\int_{3.69}^{4.78} \frac{dN}{dP} \cdot dP/\delta P_{ew} = 330 \text{ peters / GV}$$

The predicted intensity using the solar minimum spectrum given by Equation 3.1 is 320 peters/GV. However, the statistical error in the east-west differential intensity measured in the Mildura flights is approximately ±20%.

We note that the extrapolated intensity from the east (Section 7.4) (900 peters), and the west (1250 peters) are both about 175 peters above the primary intensities deduced from the solar minimum spectrum.

7.7 The Primary Cosmic Ray Rigidity Spectrum

(C) Comparison Between the Hobart and Mildura Data

In Figure 7.3 the atmospheric absorption curves of the azimuthally averaged intensity obtained at Mildura and Hobart are plotted together with the difference curve. The data was obtained with the two telescopes (A and B) which were flown at both locations. The radiation allowed at Hobart but not at Mildura is initially absorbed with a mean free path of approximately 100 g/cm^2. At depths greater than about 150 g/cm^2, the intensity decreases less rapidly with depth with an apparent mean free path of 230 g/cm^2.

Taking the near rigidity thresholds to be 4.2 GV and 1.7 GV, the differential intensity, extrapolated to zero depth,

$$\left(\int_{1.7}^{4.2} \frac{dN}{dP}\, dP\right)/\delta P = 650 \text{ peters / GV}$$

From Figure 1.7, the expected primary intensity at solar minimum is approximately 560 peters GV. Although the secondary background contribution is uncertain, this result is therefore in reasonable agreement with the intensity separately deduced from the directional measurements.

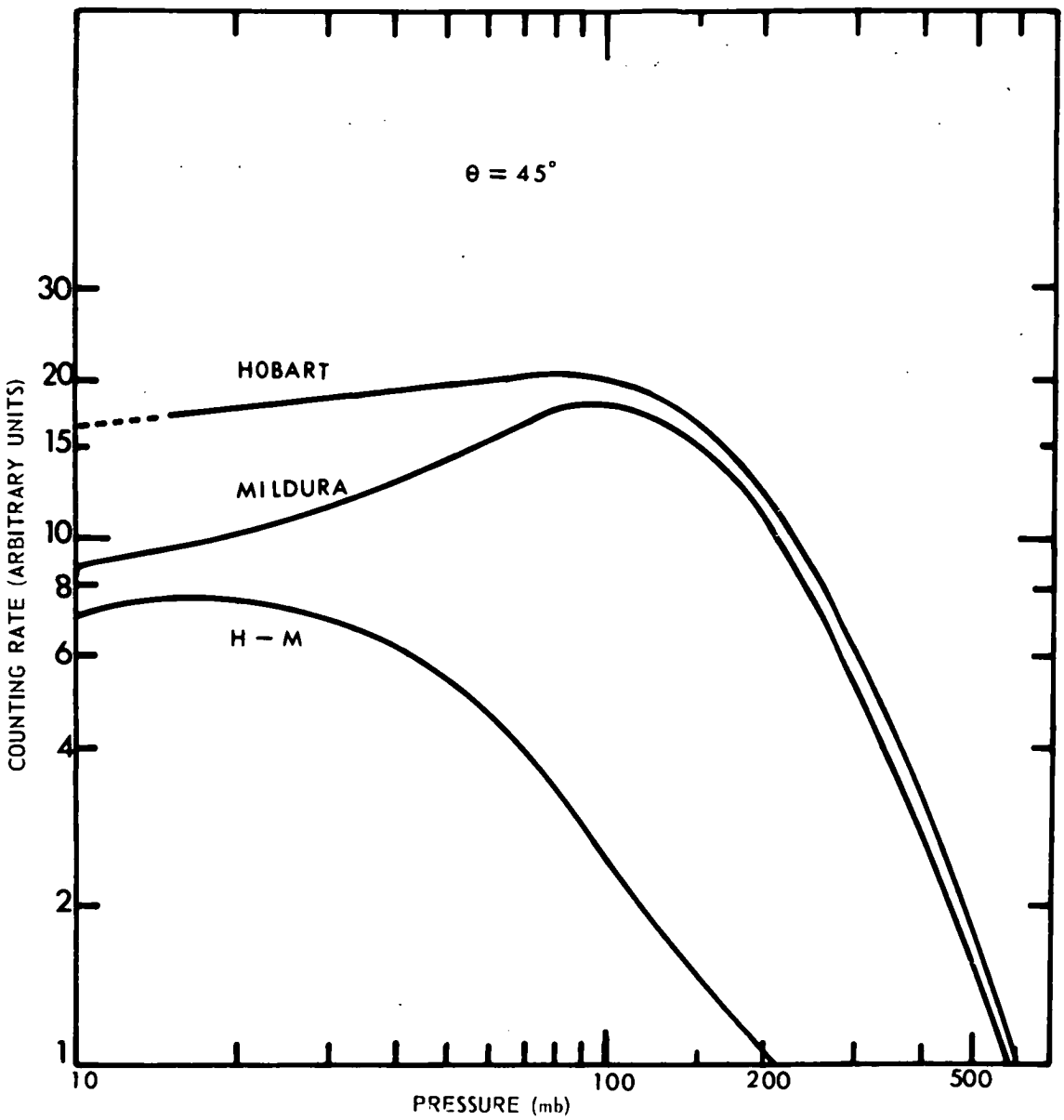

Fig. 7.3. DEPTH DEPENDENCE AT HOBART (52°S) AND MILDURA (44°S) OF INCLINED TELESCOPE (θ = 45°) COUNTING RATE, AVERAGED OVER 360° IN AZIMUTH.

PART II

In the second part of this thesis we discuss measurements obtained with balloon borne geiger counters launched from Hobart. The phenomena to be discussed include changes in the intensity and energy spectrum of cosmic rays during the period 1959 - 1963, the detection of radioactive material in the stratosphere in 1961, and the observation of a radiation enhancement following the "Starfish" nuclear explosion on July 9 1962. Experimental results from other instruments will also be presented and discussed in relation to the balloon observations.

CHAPTER EIGHT

OMNIDIRECTIONAL MEASUREMENTS OF IONIZING RADIATION WITH BALLOON BORNE DETECTORS

INTRODUCTION

A programme of single geiger counter balloon flights commenced at Hobart in 1959 (Edwards, 1960; Greenhill, 1960). These experiments continued during the period 1960 - 1963. In this chapter the results of these flights are discussed in conjunction with those of other workers. The radiation enhancement following the Starfish shot is discussed in Chapter 10.

8.1 THE ATTENUATION OF IONIZING RADIATION IN THE LOWER ATMOSPHERE.

Balloon flights of omni-directional cosmic ray detectors have been made over a period of thirty years and the general form of the atmospheric absorption curves has been well established with ionization chambers and geiger counters. One of the features of the absorption curve, its exponential slope in the lower atmosphere, has been neglected in the literature, although it is well known (e.g. Simpson, 1951) that the intensity of the nucleonic component of cosmic radiation decreases approximately exponentially with atmospheric depth in the interval $(200 < x < 600)$ g/cm^2 . A latitude dependence of the nucleonic attenuation length (L_n) has also been reported by a number of investigators, (Simpson, 1951; Pomerantz, 1960) and attempts have been made to link changes in L_n at fixed latitudes with changes in the energy spectrum of the primary radiation.

An analysis (Appendix 8) carried out on the high altitude ion

chamber measurements of Neher et al (1937, 1938, 1939, 1942, 1953, 1961) showed that curves of the form (e^{-x}/L) accurately express the ionization-depth relation in the region $(250 < x < 500)$ g/cm^2. The absorption in this part of the atmosphere may therefore be specified by a single parameter, the "attenuation length", (L) which may be accurately and easily computed by a least squares fit to the data from a single balloon ascent. It should be pointed out that the ionization over a wider depth interval may be expressed (Bowen, 1933) as the sum of three Gold integrals (involving three parameters) and that the one-parameter representation discussed here must be regarded merely as a close approximation suitable for computational purposes.

Further examination of the ion chamber results shows that the value of the absorption length as defined above decreases monotonically from about 220 g/cm^2 at geomagnetic latitudes above the cosmic ray "knee". The latitude dependence of (L) is plotted in Fig. 8.1. Due to the lack of data at low latitudes, fast neutron attenuation lengths (Simpson, 1951; Soberman, 1955) have been included to aid in extending the curve to the equator. It may be seen that the value of (L) above the knee is raised significantly during 1958, a year of high sunspot activity, a result consistent with the well accepted hardening of the primary spectrum during solar maximum.

Analysis of data obtained by Neher at high Northern latitudes in July - August 1951 suggests an inverse relation between the attenuation length (L) and the intensity of the nucleonic component measured at climax (Simpson et al, 1952). This result indicates the fluctuations in the cosmic ray intensity to be energy dependent during this period.

FIGURE 8.1 Latitude Dependence of the Attenuation Length (L_1) Derived from the Ionization Chamber Measurements of Neher et al. (Inset) Variations in the Climax Neutron Monitor Rate and the High Latitude Attenuation Length (L_1)

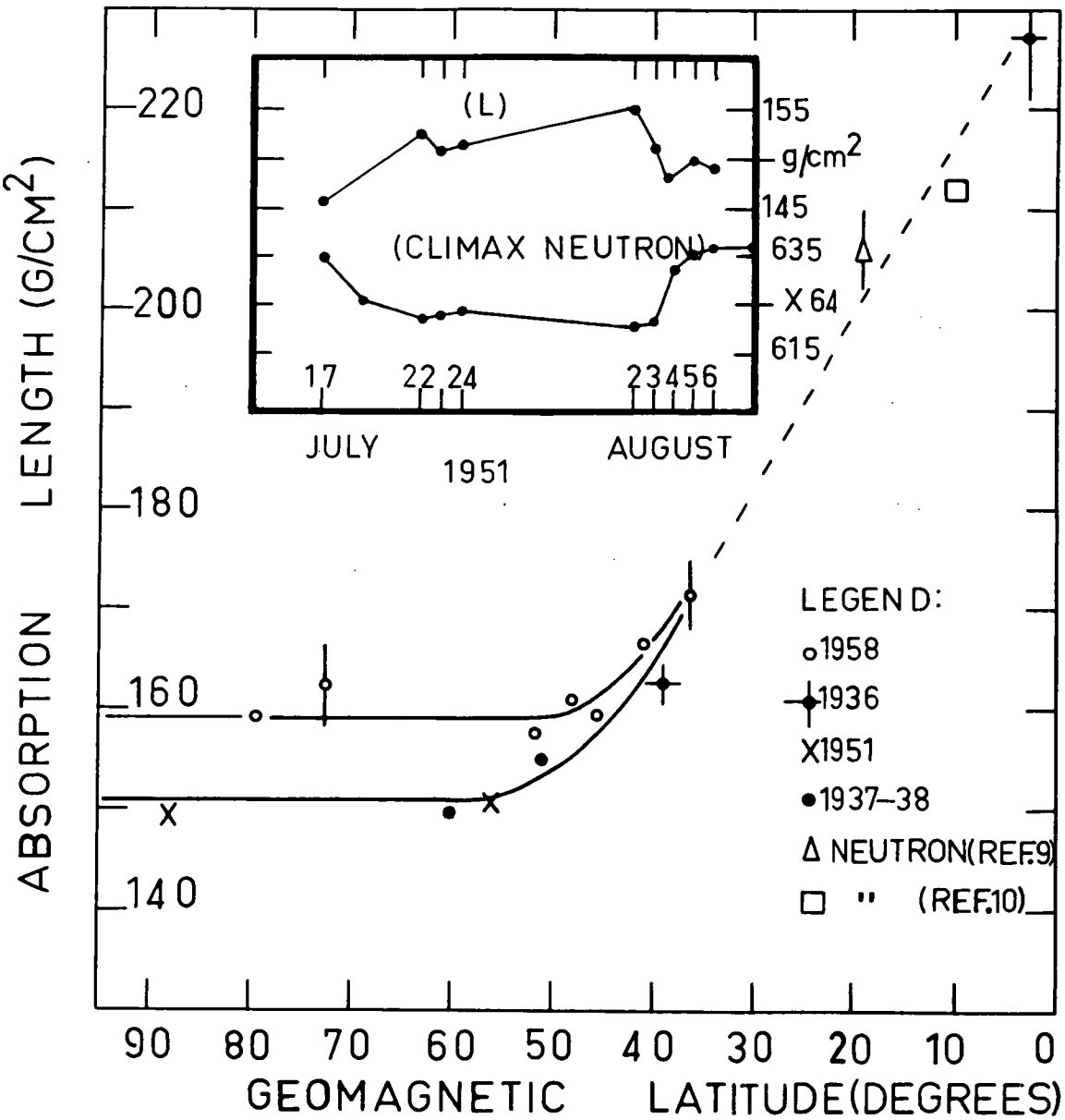
ABSORPTION LENGTH (G/CM^2)
220
200
180
160
140
(L)
155
g/cm^2
145
(CLIMAX NEUTRON)
635
X 64
615
17
22 24
23456
JULY
AUGUST
1951
LEGEND:
o 1958
+ 1936
X 1951
• 1937–38
Δ NEUTRON (REF.9)
□ " (REF.10)
90 80 70 60 50 40 30 20 10 0
GEOMAGNETIC LATITUDE (DEGREES)

TABLE 8.1

Flight No.	Date of Flight	Period of Data Collection (U.T.)	Attenuation Length g/cm^2	Geophysical & Solar Activity
1.	28 Oct 59	0700 - 0730	157.1 ± 2	Importance 2 Flare: 0340 U.T.
2.	31 Dec 59	0230 - 0300	168.0 ± 3	-
3.	7 Oct 60	0249 - 0311	174.0 ± 2.5	Forbush Decrease commenced on 6 Oct 60. In progress during flight
4.	14 Oct 60	0210 - 0233	172.5 ± 2	Forbush Decrease commenced during flight
5.	15 Nov 60	0700 - 0721	142.0 ± 5	Forbush Decrease in progress; Sea Level Flare increase commenced at Hobart during hour 03 U.T.
6.	20 Apr 61	0604 - 0630	164.9 ± 2.5	-
7.	7 Aug 61	0420 - 0437	165.2 ± 2.5	-
8.	6 Jul 62		163 ± 4	-
9.	20 Nov 63	1349 - 1414	161.0 ± 2.5	-

Analysis of data from the Hobart geiger counter flights also showed the counting rate to be an exponential function of atmospheric depth in the range $(200 < x < 500)$ g/cm^2. Table 8.1 shows the attenuation lengths obtained from the Hobart flights. 95 percent fiducial errors are quoted. [illegible]

The attenuation lengths (L_i) are compared with hourly values of the Mt. Wellington Neutron Monitor counting rate at the times of the flights in Fig. 8.2(a). We note:

(a) The attenuation lengths obtained from flights made during geophysically "quiet" periods show a general decrease from 1959 to 1963. This is

consistent with the change in the primary cosmic ray spectrum expected during the approach to solar minimum.

(b) Flights (3) and (4) made during Forbush events are characterised by unusually high values of L, consistent with a transient hardening of the spectrum. These data therefore support the hypothesis (e.g. McCracken, 1959) that the energy dependence of the short term intensity variations differs from that of the long term variations.

(c) The attenuation lengths from flights (1) and (5), made shortly after the occurrence of solar flares, are unusually low as might be expected from the softening of the incident radiation during cosmic ray flare events.

It is concluded, therefore, that the value of the attenuation length derived from balloon flights of single geiger counters does in fact reflect changes in the energy spectrum of the primary radiation. Consideration of the attenuation length derived in this way may be worthwhile in determining changes in the primary spectrum. No attempt to do this is made in the present work because of the lack of data from other latitudes.

Kamphouse (1963) has shown that the nucleonic attenuation length (L_n) at College, Alaska decreased from 147.1 ± 2.4 g/cm^2 in 1958 to 135.9 ± 1.8 g/cm^2 in 1962. Philips (1961) found the Hobart attenuation length (L_n) to change from approximately 139 g/cm^2 in 1958 to 135 g/cm^2 in 1960. These results suggest L_n and L_i, to be roughly equally sensitive to spectral changes, since the Hobart L_i values changed from about 168 in 1959 to 163 g/cm^2 in 1962, a change comparable with the change in L_n.

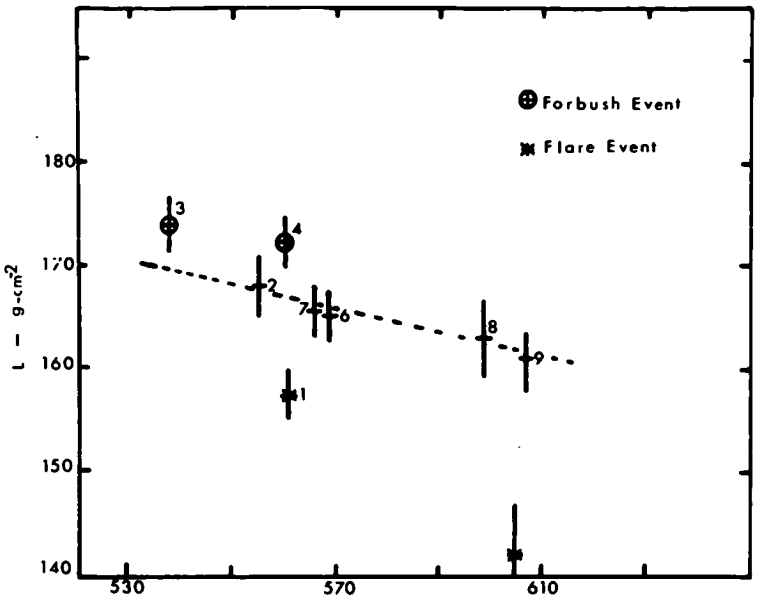

Fig. 8.2(a). ATTENUATION LENGTH (L) FROM HOBART SINGLE COUNTER FLIGHTS (1959 – 1963)

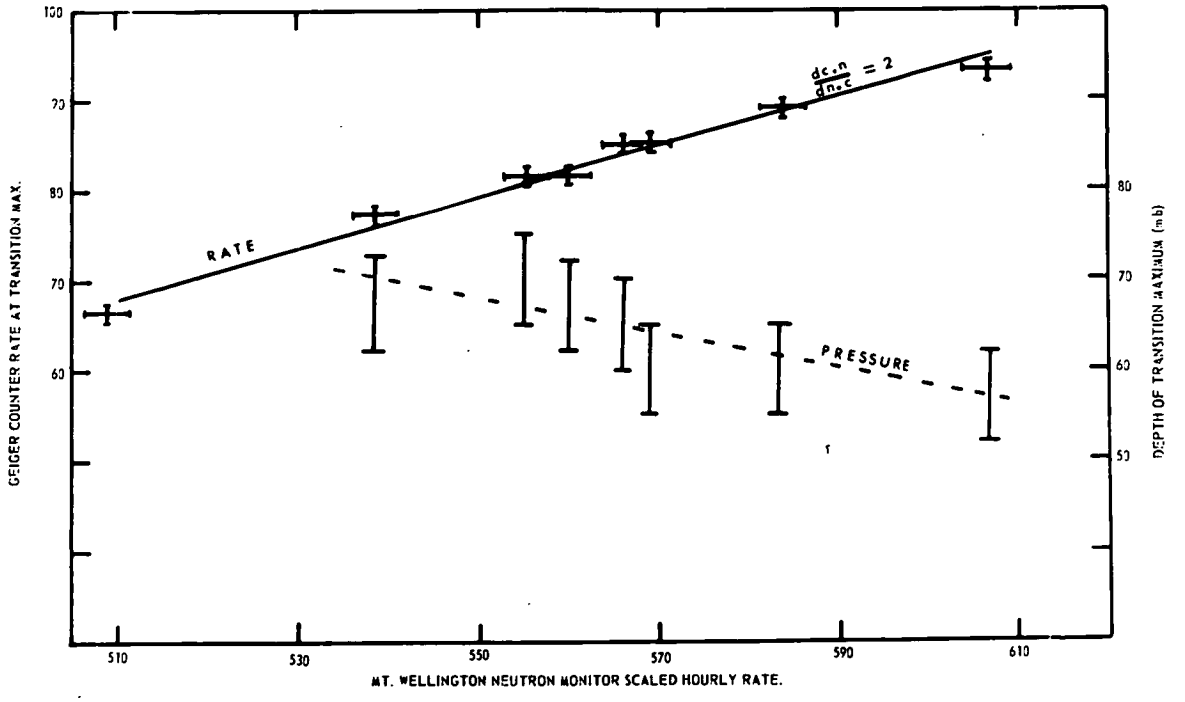

Fig. 8.2 (b). SINGLE COUNTER TRANSITION CHARACTERISTICS (1959 – 1963), HOBART.

8.2 HOBART BALLOON GEIGER COUNTER MEASUREMENTS 1959 - 1963

In the previous section we discussed the attenuation length (L_i) derived from geiger counter and ionization chamber balloon flights. It was shown that the value of L_i derived from the Hobart flights decreased during the period 1959 - 1963. In this section we examine changes in other characteristics of the atmospheric absorption curves obtained from the Hobart flights during this period.

Depth of the Transition Maximum

Examination of the ionization chamber data of Neher et al. shows that the atmospheric depth (x) at which maximum ionization occurs (the transition maximum) varies with latitude from $x \doteq 0$ near the poles in years of low sunspot number to $x \doteq 100$ g/cm^2 near the equator. This may be compared with the corresponding variation from $x = 80$ g/cm^2 to $x = 130$ g/cm^2 for the nucleonic component according to Soberman (1955). Since the depths of the ionization and geiger counting rate maxima appear to be more sensitive to threshold energy than the nucleon transition depths it may be possible to investigate spectral changes by observing the fluctuations in x_{max} from geiger counter measurements. The data of Henkel & Lockwood (1959) for example suggest a general depression in the depth of the maximum when the intensity rises above the mean.

The depths of the counting rate maxima were extracted from the Hobart data by fitting parabolic regression curves to the minute count totals. The pressure and hence the atmospheric depth at the maximum was then determined from the pressure-time ascent data. The early flights (1959 - 1961) used a hypsometer for pressure measurements and

these are considered to be more reliable than in the later flights in which baroswitches were used. The errors in x_{max} due to barometric errors and time variations in the counting rates are comparable with the magnitude of the long term change. It is clear however that the depth of the transition maximum decreased from about 65 g/cm^2 in 1959 to below 60 g/cm^2 in 1963.

Intensity Fluctuations

The geometric factors of the counters were intercompared by means of a laboratory calibration using a Radium gamma ray source. The earlier flight counters of the Maze type were replaced by internal nickel cathode counters in 1962. The two types of counters differed considerably in gamma efficiency and although an attempt has been made to take this into account, the laboratory calibrations may be in error by several percent. Other uncertainties concern the rise in β particle threshold energy due to the change in wall material and the assumption that the geometric factor of the counter is proportional to its counting rate when calibrated with the point source. In Figure 8.2(b) the normalised counting rates and the approximate pressures at the transition maxima are compared with the hourly rates of the Mt. Wellington neutron monitor. The fractional change in the transition counting rate is about twice that in the Mt. Wellington neutron monitor rate but the uncertainties in the counter normalization do not allow any more detailed conclusion. Subject to these uncertainties, the relative amplitude of the geiger counter and neutron monitor counting rate changes is the same for both the long and short (Forbush) term modulations, and is equal to

one at an atmospheric depth.of 250 g/cm^2. The counting rate at the transition maximum increased by 12% over the period October 1959 to November 1963.

8.3 THE OBSERVATION OF SOLAR RADIO NOISE BURSTS

In 1960 it became evident that immediate access to information concerning umusual solar activity would be useful in planning cosmic ray balloon flights from Hobart. Since the interests of the Hobart Cosmic Ray Group lay in time variations in the intensity and spectrum of corpuscular radiation, warnings of solar flare occurrence were of particular value.

A study of the relevant literature suggested that detection of Type IV continuum radio noise storms would provide the necessary information in view of their high degree of association (Thompson & Maxwell, 1960) with solar particle radiation increases observed at the earth.

The continuum radiation is characterised (Thompson & Maxwell, 1960, 1962) by an increase in solar radiation over a wide frequency range, typically 50 - 500 Mc/s, generally lasting for a period of minutes or, when associated with optical flares of high importance, often for several hours. The intensity of a Type IV noise storm does not usually fluctuate rapidly and the flux density is of the order of $10^{-20} W/m^2/cps$ at metre wavelengths. The larger bursts are usually more intense at lower frequencies and the considerations of Section 5.4 therefore suggest the optimum operating frequency of a fixed frequency radiometer to be in the V.H.F. range.

The Type II "slow drift" bursts (Roberts, 1959) are also of interest as precursors of geomagnetic activity. These are of geophysical sig-

nificance when associated with contimuum noise and their occurrence is restricted.to metre wavelengths. Although of shorter duration (minutes) than the Type IV storms when observed at a single frequency, the maximum intensity is usually an order of magnitude greater than that of the associated continuum and detection is correspondingly easier.

Consideration of the spectra of the Types II and IV bursts and of the sky background and receiver noise levels, suggested that a frequency in the range 100 - 200 Mc/s would be a suitable operating frequency for a fixed frequency total power radiometer.

Neglecting man made noise, the required aperture of the receiving antenna may be estimated by requiring the detectable noise storm power per unit bandwidth to be comparable with the background noise level. The antenna aperture must then exceed

$$A = \frac{2kT_o N'}{G_s} m^2$$

where G_s is the noise storm flux density. From Figure 5.8 the background noise power at 100 Mc/s, $N'kT_o \triangleq 4.10^{-21}$ watts/m^2/cps. (Janskys) The required antenna aperture is then $A = 10\ m^2$. The required gain, relative to an isotropic antenna, is 10 db and the corresponding beam area, $3.9 . 10^3\ deg^2$. (1.2 sterodians). If a fixed antenna were used, the angle of acceptance would need to be at least 180^o in one plane. A suitable antenna is the abtuse angled corner reflector (Kraus, 1940) which has a wide angle of response in the E plane.

A 108 Mc/s radiometer was constructed using a corner reflecting antenna and, later, a motor driven Yagi antenna. A block diagram of the instrument is shown in Fig. 8.3(a). The radiometer was operated

at the Cosmic Ray laboratory in Hobart and the high man made noise level necessitated the use of a minimum reading detector.

A number of flare increases were observed at sea level following outbursts recorded by the radiometer and checks with data obtained by the Sydney Radio Astronomy Group established that the instrument was functioning satisfactorily. Typical chart records of solar noise bursts obtained with the radiometer are reproduced in Fig. 8.3( ). Several balloon flights were launched by the Cosmic Ray Group following the detection of enhanced solar noise and during one of these (Flight 3, Section 8.1), flare produced radiation was observed.

8.4 THE RADIATION INCREASE OF AUGUST 7, 1961

Data from a single counter balloon flight launched from Hobart at 0346 UT on August 7, 1961 showed that the counting rate was enhanced by about 10% between 0456 and 0500 UT in the depth interval 110 - 95 g/cm^2. There was no evidence of intensity fluctuations during the rest of the flight. Therefore it does not seem likely that malfunction of the balloon equipment occurred. Figure 8.4(a) shows the counting rate derived from minute count totals with the corresponding pressure readings during the latter part of the flight. Four minutes of count data were lost at the transition maximum due to a malfunction of the 60 second count total transfer switch on the ground equipment (section 5.3). The balloon burst at 0547 UT and pressure data could not be used during the rapid descent. However the descent rate, as deduced from a comparison of the altitude profiles of the ascent and descent transition counting rates, suggests that the high minute count total at 0554 UT occurred at the same altitude 50 - 55 K ft as did the enhancement

FIG. 8.3

SOLAR RADIO NOISE (108 MC/S)

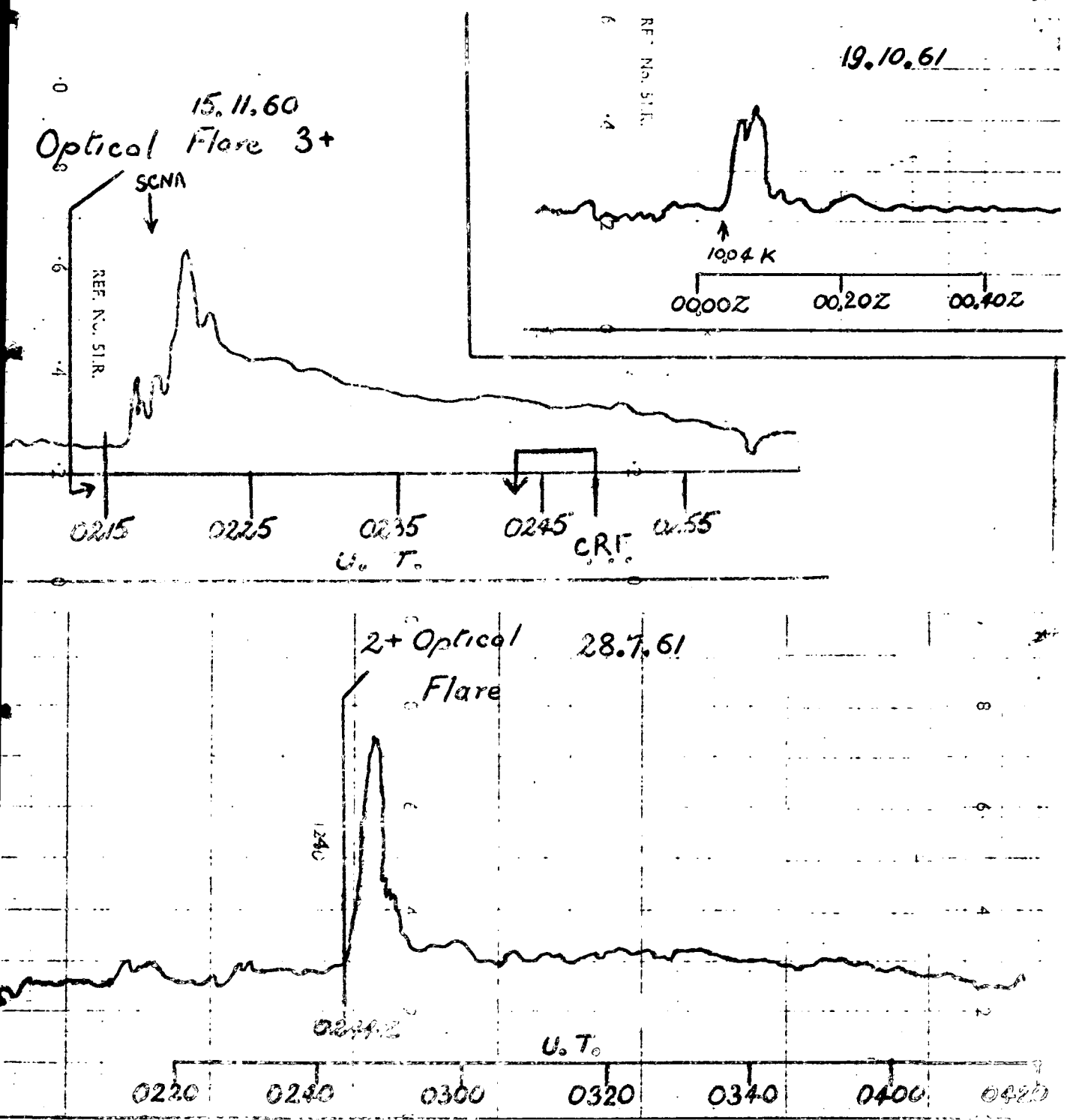

at 0456. There is no evidence of a solar radio noise event, either at 1420 Mc/s or in the range 5 - 210 Mc/s during the flight (private communication, Dr. J. P. Wild). The Hobart 108 Mc/s radiometer (Section 8.3) did not record any significant noise burst during the day, and no VLF noise storm occurred at Hobart (private communication, Prof. G.R.A. Ellis). The Toolangi magnetograph trace was undisturbed throughout the day of the 7th which was selected (CRPL - F 206 (B), October 1961) as one of the 5 quiet days of the month on the basis of the geomatnetic activity indices. Apart from the enhancement the atmospheric absorption curve was normal (Sections 8.1 and 8.2) and did not otherwise indicate the presence of excess radiation.

In view of the lack of solar and geomagnetic activity we do not believe this event to be due to a solar disturbance such as a gamma ray burst as inferred by Winckler et al (1959) from similar observations with balloon equipment. The most likely explanation appears to lie in the presence of radioactive debris at an altitude in the vicinity of 53000 feet. The excess counting rate during the descent supports this wind maximum at the same altitude.

Mantis & Winckler (1960) observed radio-active debris at the 350 mb and 140 mb levels in two flights launched from Minneapolis in 1958. On the assumption that their radiation detectors (geiger counter and ion chamber) were responding to fission γ-rays the specific activities were calculated to be respectively 0.8×10^{-5} and $0.4 \cdot 10^{-5}$ cm^{-3} sec^{-1}. The excess radiation levels were observed within a week of Soviet nuclear explosions in the Arctic region and the trajectories of the debris were traced back to the test site.

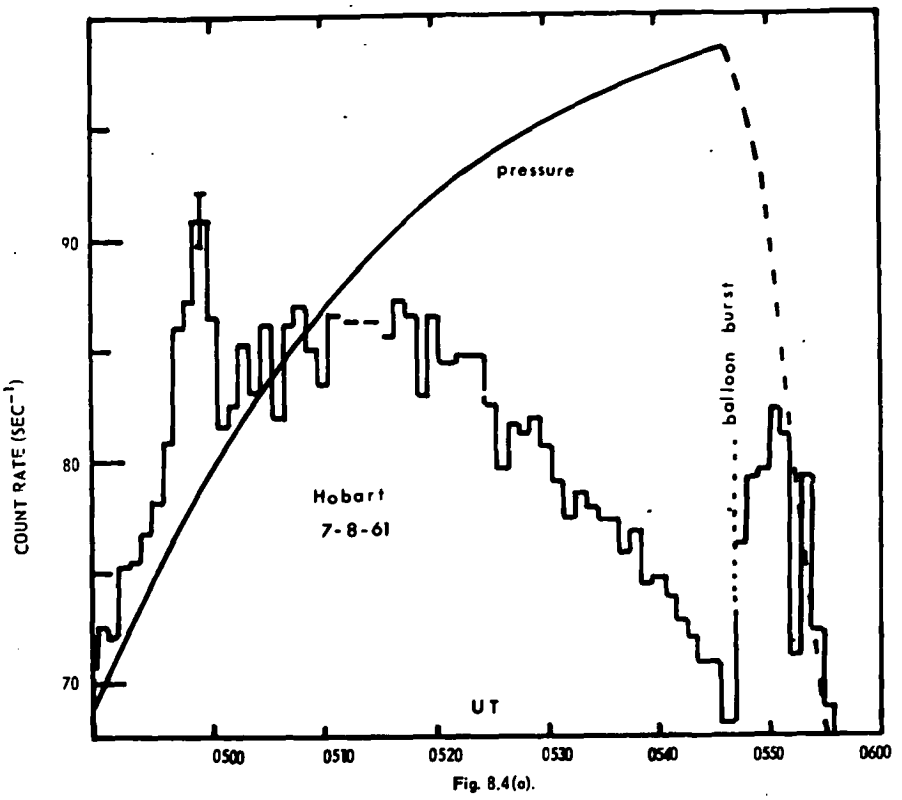

Fig. 8.4(a).

The Radiation Increase of Aug.7, 1961

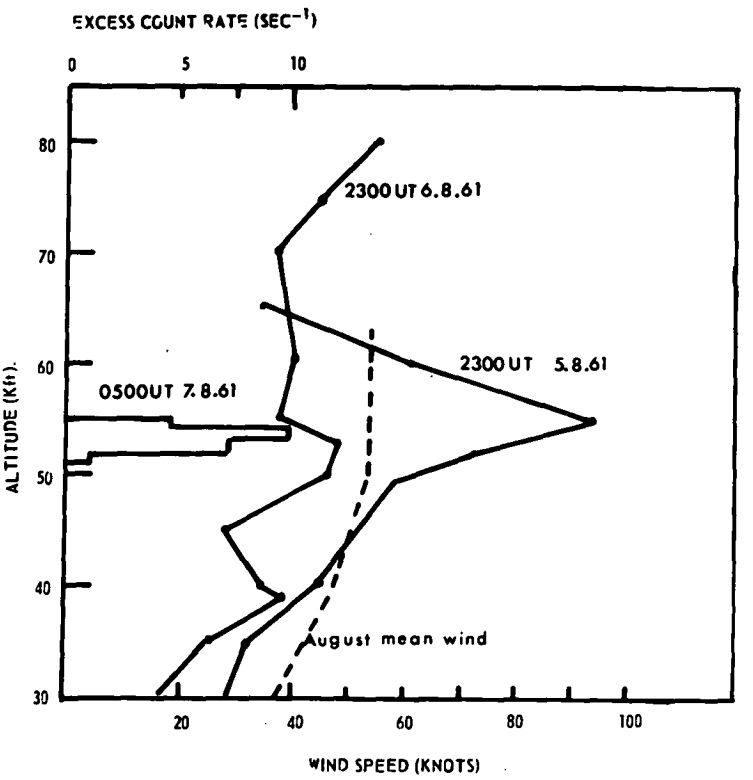

Fig. 8.4(b).

Altitude dependance of the Radiation Increase compared with horizontal wind speed profiles.

If the Hobart increase were due to γ-active debris, the specific activity is given by

$$I_\gamma = \frac{\mu \dot{N}}{G_\bullet \eta} \qquad \ldots 8.2$$

where μ = Linear γ-ray absorption coefficient (cm^{-1})

$\dot{N}$ = Excess geiger counting rate (sec^{-1})

$G_\bullet$ = Effective area of detector (App.3)

η = Gamma-ray detection efficiency

if it is assumed to be uniform over a sphere of radius large compared with $\frac{1}{\mu} \doteq 10$ km at the altitude of detection. On this basis, putting

$G_\bullet = 36\ cm^2$, $\eta = 0.5 \times 10^{-2}$ we obtain

$I = 5.6.\ 10^{-4} cm^{-3} sec^{-1}$.

This value is a lower limit since the layer would certainly need to be less than 2 km thick in order to account for the small depth interval (15 g/cm^2) in which the counting rate was enhanced.

If the increase were due to β particles of energy greater than 0.6 MeV, the threshold energy due to the finite counter wall thickness, the specific activity is

$$I_\beta(E_m) \doteq \frac{\mu \dot{N}}{G_\bullet} \cdot e^{\mu_m \cdot x_o} \qquad \ldots 8.3$$

where μ_m = Mass absorption coefficient (cm^2/g) for a β emitter of maximum energy E_m(MeV)

$= 22\ E^{-4/3} cm^2/g$ (Price, 1958)

μ = Linear absorption coefficient (cm^{-1})

x_o = Mass thickness of counter wall and other shielding material

$\doteq 0.3 g/cm^2$

Assuming the β emitter to be Yttrium 90 in equilibrium with Strontium 90, E_{max} = 2.27 MeV and the specific activity,

$$I_\beta = 3.6.\ 10^{-3} cm^{-3} sec^{-1}$$

The concentration of Sr^{90} would then be at least $5.\ 10^6 cm^{-3}$ if it originated in nuclear tests carried out before the 3-year moratorium which began in October 1958 and ended in the month following the Hobart observation.

In view of the low sensitivity of the measurements to β-action debris it seems that γ activity is a more likely cause of the event. In any case the relatively high activity and narrow altitude range is unexpected in view of the Minnesota measurements on fresh debris.

Measurements of the specific β-activity of rainfall carried out by the Division of Meteorological Physics, C.S.I.R.O., outside Melbourne (private communication, B.Hicks) suggest a Spring increase in the tropospheric air activity concentration, beginning in August 1961, and reaching a maximum in November of about 300% above the February-July average for the year. The activity in August was estimated to be 30 - 40% higher than the 6-month Melbourne average. The results of the sampling program of the Atomic Weapons Tests Safety Committee (Blake et al., 1962) suggest a considerably smaller Spring increase. Using the same parameter,

$$\frac{\text{Total Deposition (mc/km}^2\text{)}}{\sqrt{\text{Rain Fall (inches)}}}$$

to indicate tropospheric air concentration, the latter measurements suggest a Spring maximum of only 20% above the February-July average at Hobart and about 100% at Melbourne. The discrepancy between the AWTS and C.S.I.R.O. measurements and the difficulty in relating sea level

precipitation activity to the upper air concentration, prevents any firm association between the balloon observation and the surface measurements.

CHAPTER NINE

EFFECTS OF THE NUCLEAR EXPLOSION "STARFISH PRIME" OBSERVED AT HOBART, TASMANIA ON JULY 9, 1962

INTRODUCTION

In this chapter we present an account of geophysical observations of the effects of the nuclear explosion "Starfish Prime". The data were obtained at Hobart (147°E, 43°S geographic; 224.5°E, 52°S geomagnetic) on July 9, 1962.

The observations to be described include the following:-

1. A radiation enhancement recorded by a balloon borne geiger counter at 80 g/cm^2 atmospheric depth.
2. The occurrence of magnetic micropulsations in the vertical (Z) component of the earth's field.
3. Fluctuations in the geomagnetic field components (X,Y,Z) recorded by a flux gate magnetograph.
4. A sudden ionospheric absorption (S.C.N.A.) recorded by wide and narrow beam equipments at 4.7 Mc/s.

9.1 RADIATION ENHANCEMENT

A balloon borne geiger counter and associated equipment was launched from Hobart on July 9, 1962 with the object of monitoring the ionizing radiation level at high altitudes following the expected detonation of a megaton yield nuclear device in the ionosphere above Johnston Island. As any radiation increase was expected to be rapidly attenuated in the

atmosphere the balloon was designed to rise to a depth of 15 g/cm^2 and remain at this depth for several hours. Owing to delays in launching the detonation occurred (at 090009 UT) before the maximum altitude had been reached. At this time the balloon was about 50 km SE of Hobart. The signal from the sonde was monitored at Hobart and in addition was recorded on magnetic tape at a remote receiving station. Following the detonation a marked increase in the minute count totals was observed by the monitor station, the increase first being noticed in the minute count beginning 0900.30 UT. The enhancement persisted for several minutes, the minute totals reaching a maximum of about 30% above the cosmic ray background level at a depth of 77 g/cm^2. The balloon burst prematurely at 0927Z at an atmospheric depth of 40 g/cm^2. A brief description of the enhancement has already been reported (Edwards et al, 1962). In the following sections the observations will be examined in detail.

The instrument package contained horizontally mounted internal cathode (0.1mm Ni) counter of the type described in section (4.4) designed and tested for operation at temperatures above ($-60^{\circ}C$). The pressure transducer was a single bellows baroswitch. This instrument was checked against a laboratory barometer prior to the flight. The radio transmitter was a modulated triode oscillator operating at a frequency of 71.5 Mc/s coupled to a vertical antenna. Dry cells provided power to operate the transmitter, geiger counter and the associated transistor circuitry.

All circuits were designed for low temperature operation as the

FIGURE 9.1 : Raw Data Showing the Geiger Counter Increase Over Hobart (52°S) Following the "Starfish" Explosion.

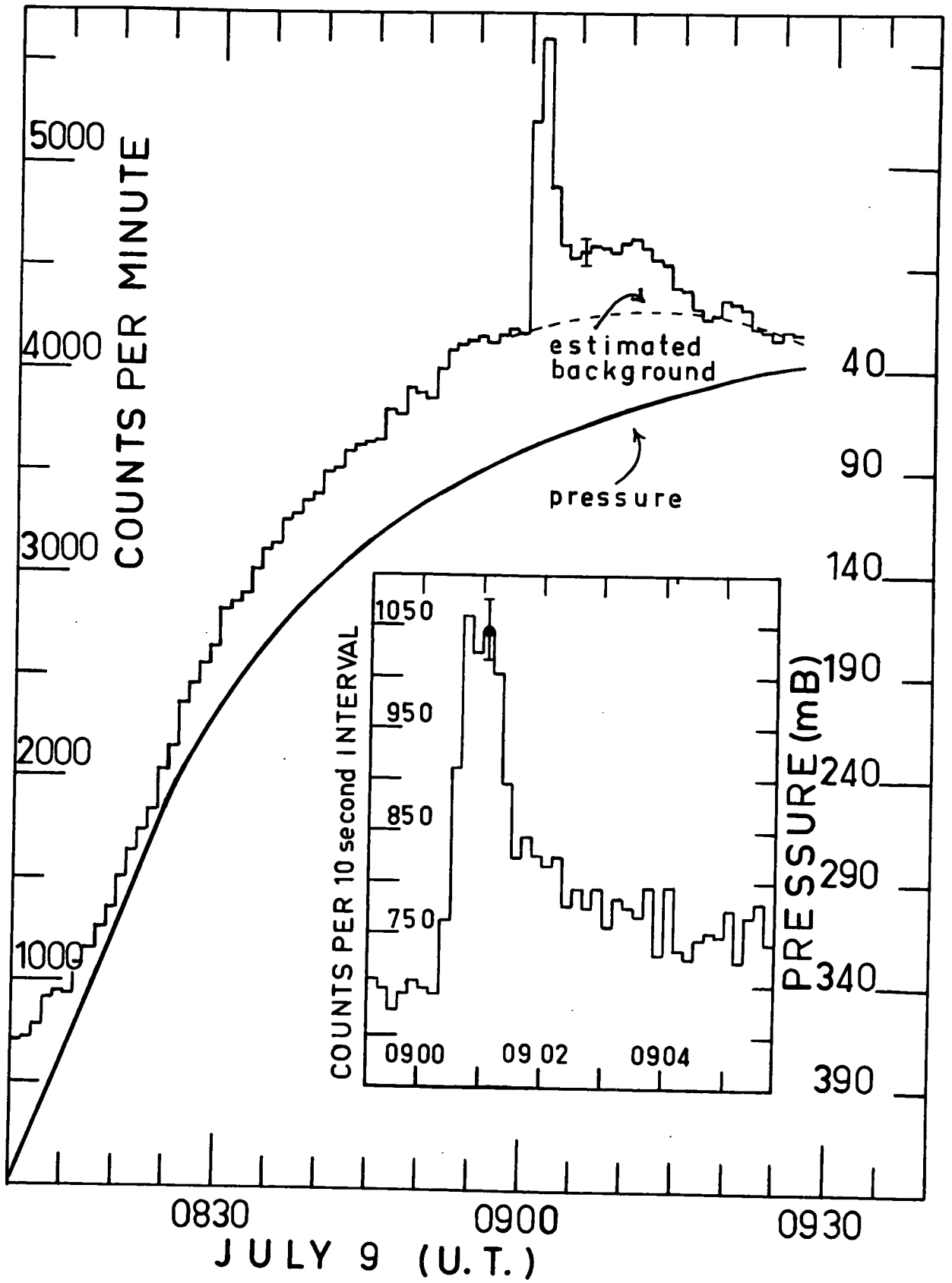
5000
4000
3000
2000
1000
COUNTS PER MINUTE
estimated
background
pressure
40
90
140
190
240
290
340
390
1050
950
850
750
COUNTS PER 10 second INTERVAL
PRESSURE (mB)
0900
0902
0904
0830
0900
0930
JULY 9 (U.T.)

flight was launched shortly before local sunset. The payload was enclosed in a 2" thick foamed polystyrene container which was itself covered with polythene sheet to minimise heat loss. The pulses from the geiger counter were lengthened and used to gate the oscillator off for a period of $\frac{1}{2}$ mS during each pulse. The baroswitch deviated the frequency of a 2Kc/s sinusoidal oscillator the output of which was applied to the modulator at a low level (Section 5.3). During the flight the pressure contacts were identified aurally and noted as a function of time. The clocks at both receiving stations were checked against WWV time before and after the flight. Time marks were made on the tape at intervals throughout the flight and the maximum timing error does not exceed $\pm$ second.

The raw data is shown in Figure (9.1).

Significant features of the enhancement are:-

(a) The considerable atmospheric depth (80 g/cm^2) at which the increase occurred.

(b) The time delay of 10 - 15 seconds between the instant of the detonation and the commencement of the increase.

(c) The rapid rise to a peak intensity of more than 70% above the cosmic ray level at 0901 UT, (H + 50 seconds).

(d) The slow recovery of the enhancement to a minimum at H + 200 seconds and the persistence of the enhancement until after 0915 UT.

Durney et al (1963) observed a radiation burst at about the same time with the shielded Anton 302 counter in satellite Ariel. They suggest that the satellite burst was due to hydromagnetic redistribution of the pitch angles of naturally trapped electrons. The Hobart

Fig 9.2

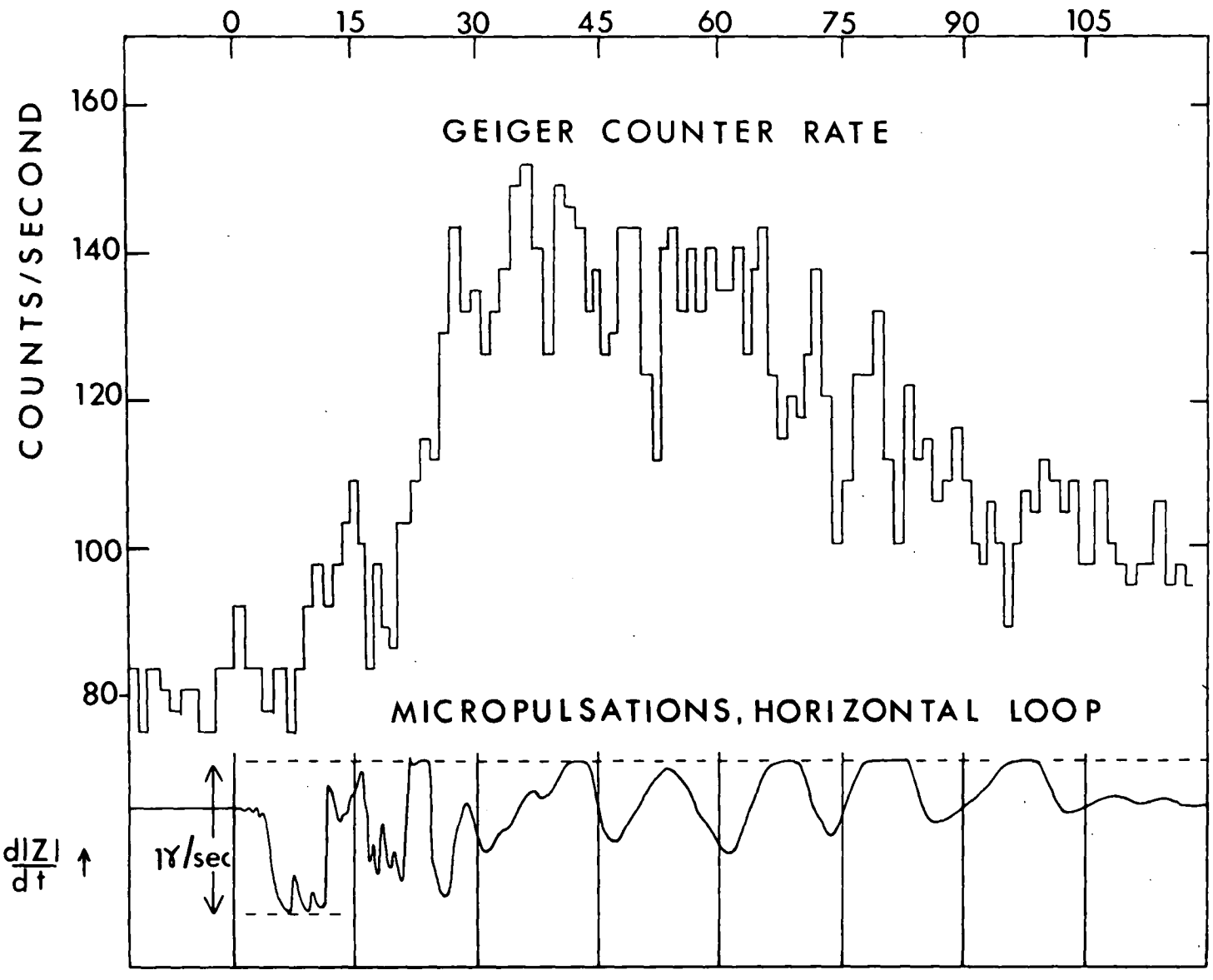
TIME , SECONDS AFTER 0900.09 U.T., JULY 9 1962
0
15
30
45
60
75
90
105
COUNTS/SECOND
160
140
120
100
80
GEIGER COUNTER RATE
MICROPULSATIONS, HORIZONTAL LOOP
d|Z|/dt
1γ/sec

observations might then be interpreted in terms of the bremsstrahlung radiation from dumped electrons. We shall postpone further discussion of the balloon result and consider it in relation to the other Hobart observations in chapter 10, since, in the absence of supporting data, the interpretations are necessarily open to question.

9.2 MAGNETIC MICROPULSATIONS ACTIVITY

A micropulsations recorder, installed at a field station 10 miles from Hobart was in operation at the time of the detonation. In addition to the normal chart record, the data were tape-recorded at $7\frac{1}{2}$ ips together with the Johnston Island count down. The detector was a horizontal loop coupled to a galvanometer and photocell unit. The response of this unit and the associated amplifier was flat up to a frequency of 0.05 cps and dropped by 4db per octave about this frequency.

Figure 9.2 shows the radiation increase and the micropulsation record plotted on the same time scale. The irregular pulsations which took place in the first 30 seconds are followed by a train of 5 quasi sinusoids of approximately 16 seconds period. Particular interest attaches to these oscillations because of their narrow frequency spectrum and their time relation to the radiation burst. Macdonald's (1961) low density model predicts a period of 16 seconds for the fundamental V mode oscillation of the field line through Hobart. Power spectrum and Chree analysis of the radiation and micropulsations data (presented in Chapter 10) confirm an association between these data.

In Figure 9.3 the onset of the artificial micropulsations is shown. The depression of the vertical (upward) component of the field within

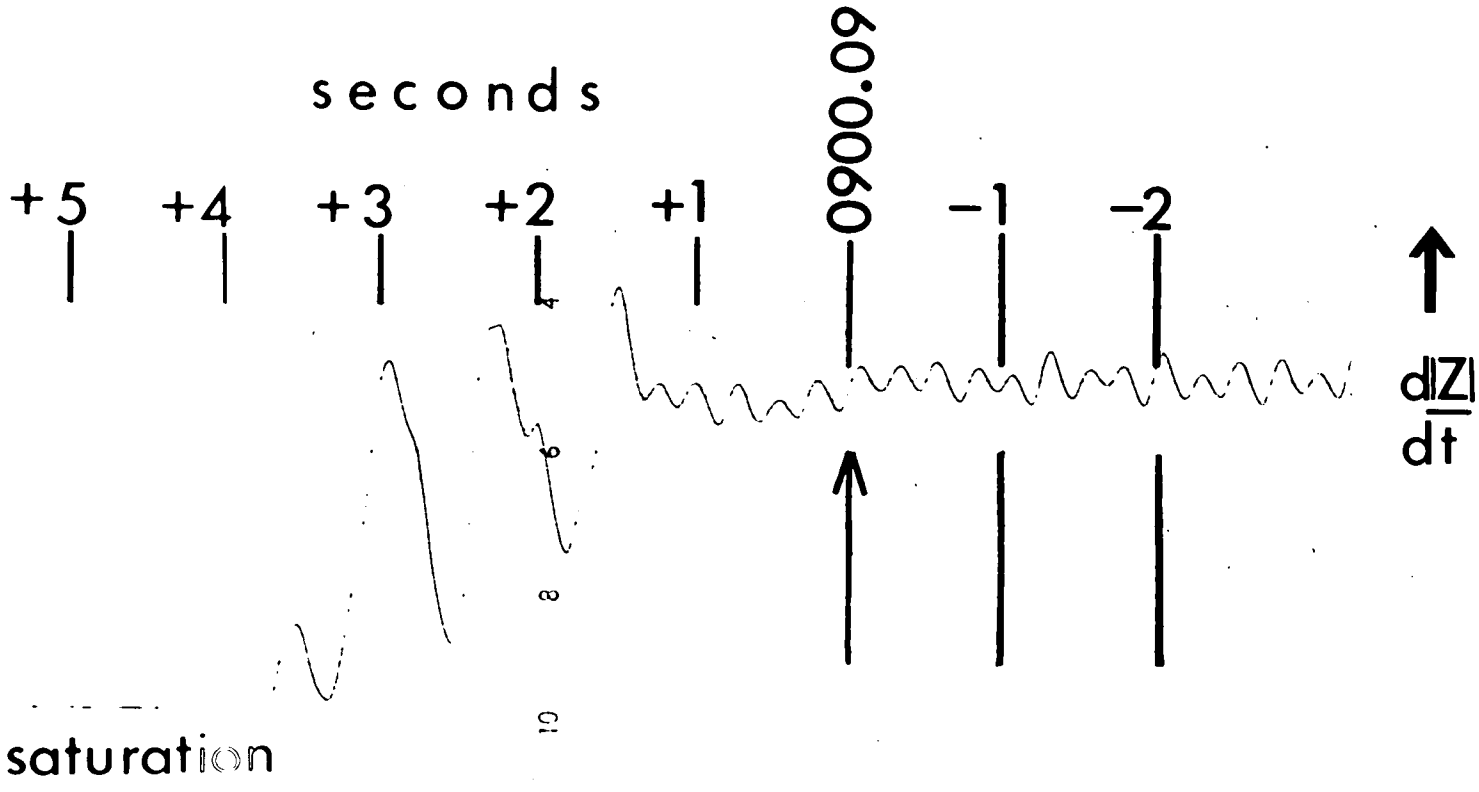

HOBART MICROPULSATION RECORD

9.3 July 9 1962

0.1 seconds of the detonation is clearly apparent. This effect, presumably due to an electromagnetic pulse propagated in the earth ionosphere cavity (Wait, (1960)) has been reported by other observers (Casaverde et al, (1963), Roquet et al, (1962), Odencrantz, (1963)). At H + 1.4 ± 0.1 seconds, a sharp increase in $\dot{Z}$ occurred and was the first peak in a train of 3 quasi sinusoids of period 0.7 seconds. Saturation of the recorder ($|\dot{Z}| > \frac{1}{2}$ gamma/sec) took place at H + 3.5 ± 0.1 seconds and rapid fluctuations continued until H + 20.9 seconds when a large positive excursion lasting 3 seconds again saturated the instrument. The regular oscillations already referred to began after +30 seconds and reached peak to peak amplitudes in excess of 1 gamma. The time delay of 1.5 seconds to the first peak of the short period oscillations is more than twice the delay (0.6 ± 0.2 sec) observed at Wellington, New Zealand (Christoffel, 1962). J. Roquet et al, (1963) have drawn attention to the world wide observation of a magnetic impulse at H + 2 seconds. There is some suggestion of an impulse at Hobart at this time (Figure 9.3) but its recognition is made somewhat uncertain by the prior arrival of the short period oscillations.

9.3 MAGNETOGRAPH RECORD

Flux gate variometers operated at Hobart by the Australian Bureau of Mineral Resources (private communication Dr. D. Parkinson) recorded variations in the X, Y, Z components of the field following the detonation (Figure 9.4; 9.5) The chart speed of $1\frac{1}{2}$" per hour restricted

FIGURE 9.4 : General Features of the Radiation Increase, Sudden Ionospheric Absorption and Magnetic Variations at Hobart Following the "Starfish" Explosion of July 9, 1962.

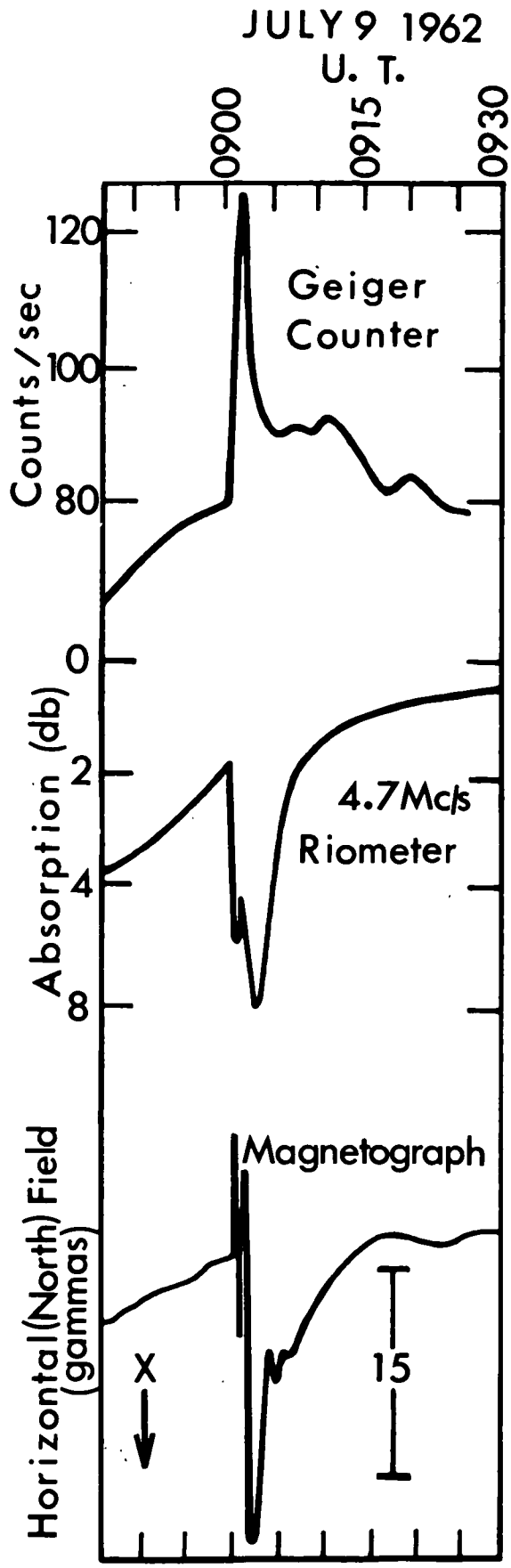
JULY 9 1962
U. T.
0900
0915
0930
120
100
80
Counts/sec
Geiger
Counter
0
2
4
8
Absorption (db)
4.7Mc/s
Riometer
Magnetograph
Horizontal(North) Field
(gammas)
X
15

the time resolution of the data but it is clear that the total field strength was depressed in the first minute following detonation and enhanced for the following period of about 15 minutes. The maximum deviations in the X(North), Y(East), Z(down) components were respectively -9, -13, +10 gammas during the first phase of the event and +20, +9, -9 gammas during the second phase.

This event is of more complex form than the bay like disturbance recorded by near-equatorial stations (Pisharoty, 1962; Glover, 1963; Casaverde et al, 1963). The mean Sq variations at Hobart for July at the time of the event have been estimated by Parkinson (private communication) as approximately +6, +4, -1 gammas respectively in X, Y, Z. The fluctuations in the horizontal field during the second phase of the event would therefore correspond to an increase of a factor of two or three in the strength of the local Sq current system.

9.4 SUDDEN COSMIC NOISE ABSORPTION

A number of cosmic noise receivers were in operation at the time of the detonation. These included the narrow beam (3° x 11°) and wide beam radio telescopes operated by the Radio Astronomy Group of the Physics Department at a frequency of 4.7 Mc/s and a 30 Mc/s vertical wide beam (80° x 120°) riometer, constructed by the author for the purpose of monitoring ionospheric absorption following the detonation.

No absorption greater than 0.5 db was observed with the 30 Mc/s riometer but a doubly peaked absorption event of amplitude 6.0 db was recorded with those narrow beam 4.7 Mc/s telescopes (declinations of -52°, -47°, -37°, -32°) which had been receiving appreciable cosmic noise

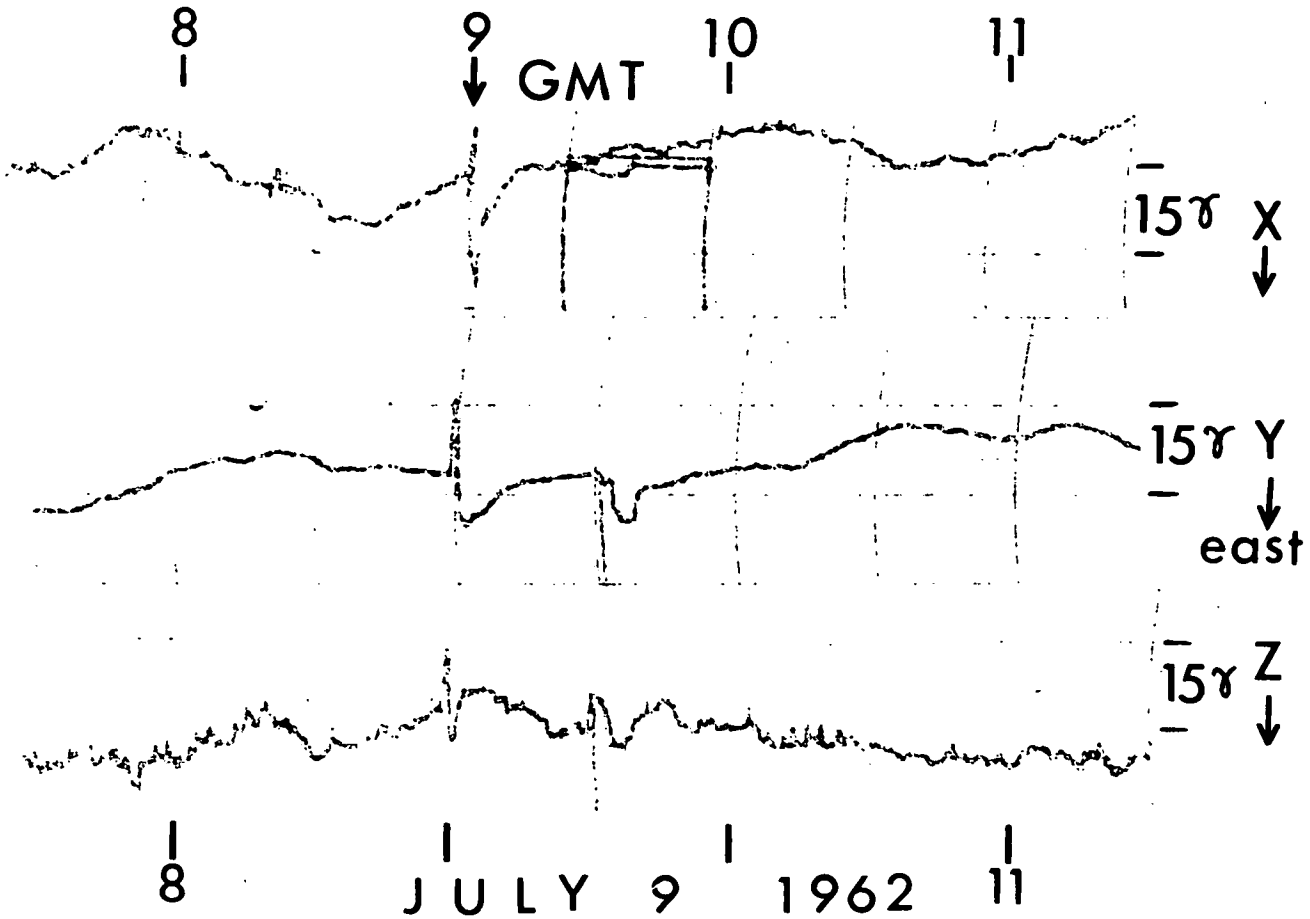
8
9
GMT
10
11
15γ X
15γ Y
east
15γ Z
8
JULY 9 1962
11
HOBART MAGNETOGRAPH

Fig 9.5

prior to the detonation. Figure 9.6 shows a typical chart record. The recovery after the initial (4 db) absorption peak was probably greater than that observed because of the long rising time constant (60 seconds) of the minimum reading circuitry. Owing to the slow chart speed it is difficult to assign an accurate onset time to these effects but the results are consistent with a time coincidence between the first absorption peak and the peak of the radiation burst. There is little evidence for a second radiation increase at the time (H + 2.5 minutes) of the second absorption. Within the limits of accuracy (± 0.5 db), (± 30 sec) all narrow beam equipments recorded equal absorptions at the same times. The wide beam absorption (5 db ± 0.5 db) was certainly not greater than the narrow beam absorption and although of the same duration (15 minutes) did not show a double peak.

The Hobart ionosonde was not operating at the time of the explosion so that no critical frequencies are available for this time. Comparison with the galactic noise profile obtained under quiet conditions shows however that the cosmic noise level was depressed by several decibels on the night of July 8 and until 1300 UT (2300 local time) on the night of July 9. The normal galactic intensity was recorded after H + 4 hours and also during the following night of July 10.

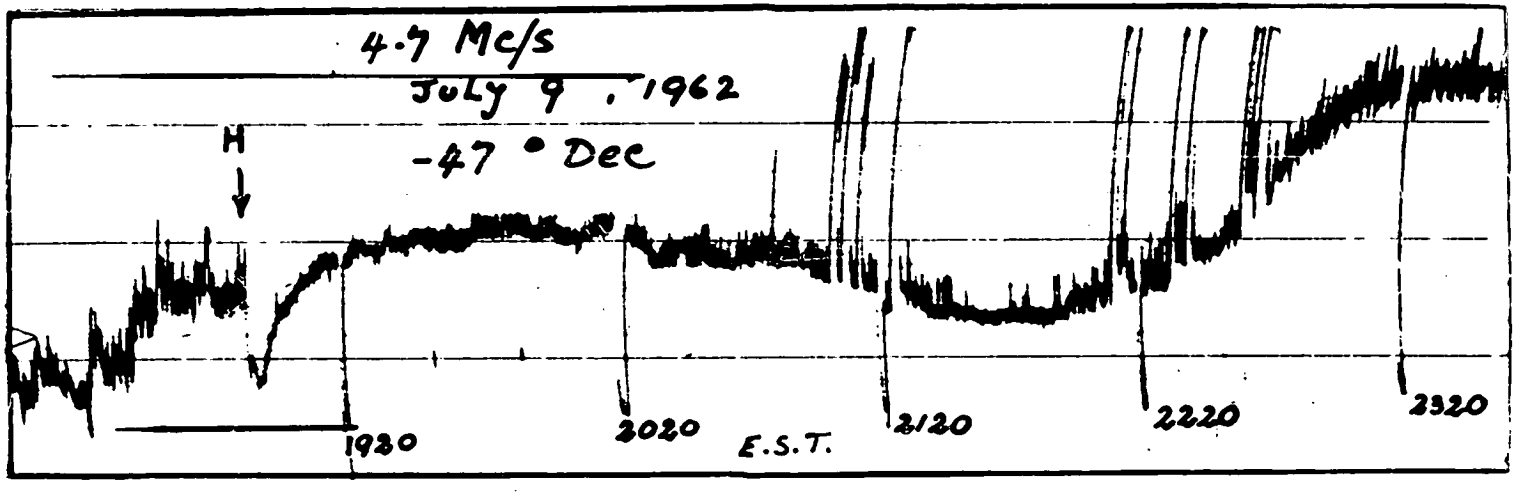

Fig. 9.6. Narrow Beam Riometer Absorption

CHAPTER TEN

INTERPRETATION OF THE RADIATION BURST OBSERVED ON JULY 9, 1962 AT HOBART

INTRODUCTION

Hobart observations of the immediate effects of the nuclear explosion "Starfish Prime" were presented in the previous chapter. The magnetic and ionospheric effects of high altitude nuclear explosions have been widely discussed (Obayashi, 1963; McNish, 1959; Matsushita, 1959) and the artificial injection of β-particles into the magnetosphere has been established by satellite and other observations following the Starfish shot and other earlier high altitude nuclear explosions (Van Allen et al, 1959, 1963).

Disagreement exists concerning the interpretation of the Starfish effects, in particular of the cause of the unexpectedly wide latitude distribution of the geomagnetically trapped electrons (Hess, 1963; Van Allen et al, 1963). The occurrence of generally larger magnetic, ionospheric and auroral effects near New Zealand (Gregory, 1962) than in the area magnetically conjugate to Johnston Island was also unexpected but well established.

The Hobart observation (Section 9.1) of enhanced radiation under 80 g/cm^2 of residual atmosphere is, as far as is known, the only reported measurement with a balloon born detector of excess ionizing radiation following the explosion. In this chapter the balloon observation will be examined in conjunction with other observations at Hobart and elsewhere.

10.1 THE RESPONSE OF THE GEIGER COUNTER TO IONIZING RADIATION

The general features of the geiger counter were described in Sections 4.4, and 9.1. The β-particle threshold energy due to absorption in the 1mm pyrex glass wall and 0.1 mm internal nickel cathode is estimated to be 0.8 MeV, being higher than that of the maze counters because of the presence of the nickel cathode. The minimum energy of a detectable proton entering the atmosphere vertically was 330 MeV due to the residual atmosphere above the balloon at the time of onset of the radiation increase. Twenty seven minutes after the detonation when the balloon burst, the proton threshold energy had dropped to 300 MeV, due to the ascent of the balloon during the intervening period.

A gamma ray calibration carried out on an identical counting tube after the flight with nominal 10 μc Cs^{137} and Co^{60} sources (photon energies of 0.66 and 1.2 MeV, respectively) established the photon detection efficiency (η) to be

$$\eta(\nu) \pm (0.75\nu\ (\text{MeV}) - 0.25)\%\ ,\ (0.5 < \nu < 3)\ \text{MeV} \qquad 10.1$$

assuming a linear relation (Price, 1958) between efficiency and photon energy (ν) in the Compton regime. The errors in the calibration are thought to be due mainly to departures of the source activities from their nominal value. The decay in activity of the Cobalt source which had taken place since the date of manufacture was taken into account. The errors in the quoted efficiencies probably do not exceed ± 25% .

A significant loss in counting efficiency (ϵ) arose from the finite resolving time of the counting tube and read out systems. The loss in efficiency due to this cause is given by

$$1 - \quad \pm \frac{\dot{N}\,(\sec^{-1})}{5}\,\% \,.$$

The effective area presented to a parallel vertical flux of radiation was $39 \pm 3\ cm^2$ and the geometric factor G, relating the counting rate $\dot{N}\ (sec^{-1})$ to the particle flux $J\ cm^{-2}\ sec^{-1}$, isotropic over one hemisphere, by

$$\dot{N} = \quad G \quad J \qquad 10.2$$

where = detection efficiency, was

$$G = \frac{\pi}{2} r\,(r + 1) \qquad 10.3$$

$$= 36.6 \pm 2.5 cm^2.$$

10.2 INTERPRETATION OF THE RADIATION ENHANCEMENT: PRELIMINARY DISCUSSION

We shall consider the radiation enhancement to consist of two phases. The initial burst, beginning at H + 15 ± 5 seconds and ending at H + 200 seconds will be referred to as burst A. The enhanced level which remained after H + 3 minutes and persisted till H + 20 minutes will be called enhancement B.

Hypotheses as to the cause of burst A will be primarily considered. These fall into two categories according to the proposed source of radiation:

(1) Natural radiation detected as an indirect result of the explosion, for example, Bremsstrahlung x-rays from dumped Van Allen particles.

(2) Artificial radiation, either directly produced by the explosion, generated as a result of radio active decay of the products of the explosion, or that arising from interaction between these products

and the terrestrial environment. Examples include gamma rays from fission debris, x rays from neutron decay electrons and gamma rays arising from the nuclear interactions of neutron decay protons.

Knowledge of the characteristics of the balloon borne detector enables certain interpretations to be rejected. For example the attenuation of radiation in the residual atmosphere is sufficiently great to rule out the direct detection of protons with energy below about 350 MeV. The gamma ray detection efficiency of the counter is small enough to prevent indirect detection of such protons via their nuclear interactions with sufficient efficiency to account for the magnitude of the burst in view of the inadequate flux of naturally trapped protons known to be available for precipitation into the atmosphere above Hobart.

Comparison with the magnetic and ionospheric observations (Chapter 9) allows a further restriction of tenable hypotheses. The unusually light ionospheric absorption accompanying the radiation burst was referred to in the previous chapter. This fact allows the interpretation of the burst in terms of dumped electron bremsstrahlung to be rejected with reasonable confidence. The restricted area at ionospheric heights to which both the balloon detector and the narrow beam riometer respond would however, introduce some uncertainty into the interpretation, were it not for their geographical proximity and the availability of the wide beam riometer records.

In the following sections the interpretations listed below will be examined.

1(a) An increase in the flux of galactic cosmic rays, detected as a result of temporary reduction in the geomagnetic cut off rigidity (Chapter 2).

1(b) The precipitation into the atmosphere of naturally trapped protons or alpha particles with ranges exceeding the residual depth of the balloon.

1(c) The production of gamma radiation arising from nuclear interactions of dumped protons and alpha particles which have insufficient energy to be directly detected by the counter.

1(d) Bremsstrahlung radiation from dumped Van Allen belt electrons.

2(a) Bremsstrahlung x-rays and gamma radiation from bomb-neutron decay electrons and protons respectively, produced in the magnetosphere and accessible to the atmosphere above Hobart.

2(b) Gamma rays from radioactive fission and fusion products.

10.3 THE PROTON RESPONSE OF THE GEIGER COUNTER AND THE MT. WELLINGTON NEUTRON MONITOR

The Mt. Wellington neutron monitor chart recorder was in operation during the radiation event. In deducing the energy spectrum of protons proposed (Edwards, Fenton, et al., 1962) as a possible interpretation of the burst we may make use of the monitor observations to set an upper limit to the mean energy per particle for a hypothetical proton flux.

On the assumption that the burst radiation was due to a modulation of the primary cosmic radiation having spectral dependence similar to that observed at Hobart during 1959-1963, the results of Section 8.2

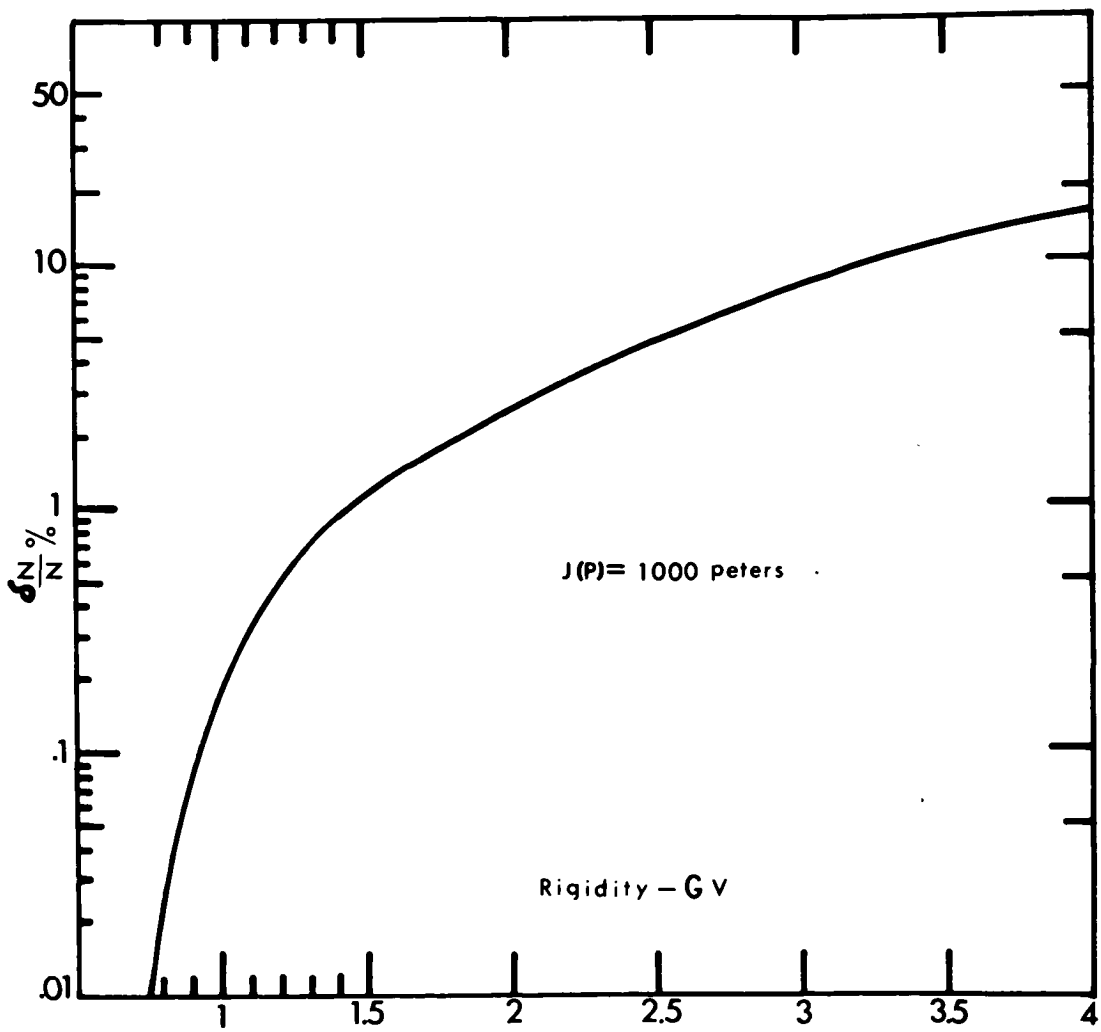

Fig. 10.1

PROTON RESPONSE OF SEA LEVEL NEUTRON MONITOR.

may be used to predict the resultant increase in the rate of the Mt. Wellington neutron monitor. Taking one minute averages, the 30% increase in counting rate at 80 g/cm^2 ought to be accompanied by an increase of at least 15% in the monitor rate, about five times the standard error in the minute totals. In fact, no significant fluctuations occurred in the monitor rate so that the hypothesis may be rejected.

The energy response of the monitor drops rapidly below 2 GeV (Webber, 1962) and the lack of any measurable monitor response does not therefore rule out an explanation in terms of protons with energies below this value. The vertical cut off energy at Hobart is about 1 GeV so that any reduction in this would probably be undetectable near sea level. However, the flux of cosmic ray particles with energies between 350 MeV and 2 GeV, even at solar minimum, (Section 3.2) is inadequate to produce the observed maximum increase of 70% in the rate of the geiger counter.

Response of the Neutron Monitor to Low Energy Protons

The differential counting rate of the neutron monitor at depth x due to primary protons with rigidities in dP at P may be written (Fonger, 1953)

$$\frac{dN(P,x)}{dP} = Sx(P)\,\frac{dJ(P)}{dP} \qquad 10.4$$

where $Sx(P)$ is the specific yield function and $\frac{dJ(P)}{dP}$ is the primary differential rigidity spectrum.

If the vertical rigidity threshold is P_o, the monitor rate may be written

$$N(P_o,x) = \int_{P_o}^{\infty} Sx(P) \cdot \frac{dJ}{dP} \cdot dP \qquad 10.5$$

The fractional increase in rate due to particles of rigidity P incident isotropically at the top of the stmosphere is then

$$\frac{\delta N}{N(P_o,x)} = \frac{S_x(P) \cdot J(P)}{\int_{P_o}^{\infty} S_x(P) \cdot \frac{dJ}{dP}\, dP} \qquad 10.6$$

where $J(P)$ is the unidirectional intensity (per unit solid angle). At Hobart $P_o = 2GV$, and near solar minimum, $\frac{dJ}{dP} \doteq 10^4 P^{-2.5}$ peters/GV (section 3.2), so that numerically integrating

$$\int_2^{\infty} S(P) \cdot \frac{dJ}{dP} \cdot dP$$

we have, using the yield functions as recently revised by Webber (op. cit.). Therefore

$$\frac{\delta N_o}{N}\% \doteq 0.8\, S(P)\, J(P) \qquad 10.7$$

Since the altitude correction to $S(P)$ is uncertain we shall calculate the sea level response with the understanding that this will underestimate the response of the Mt. Wellington monitor, particularly at the lowest rigidities. In the range $2 - 6$ GV, $S \sim KP^{+2.8}$ and therefore

$$\frac{\delta N}{N}\% = 3.5 \cdot 10^{-4}\, P^{2.8}\, J(P) \qquad 10.8$$

Thus if the differential flux at $P_o = 2GV$ were doubled at solar minimum ($J(2) = 10^3$ peters) the monitor rate would increase by 2.4%. The single counter rate at $x = 80$ g/cm^2, would in this case increase by approximately $\frac{10^3 \cdot G_o(\pi/2)}{10^4} \doteq 25$ counts per second. Since the minute averages during the event were enhanced by little more than this and the

corresponding monitor increase would probably be undetectable, we cannot definitely rule out protas of this energy (1 GeV) as the cause of the increase. Examination of the relative amplitudes of the monitor counting rates at Hobart and Mt. Wellington during the November 1960 flare suggests that use of the sea level yield functions underestimates the Mt. Wellington monitor response by about 10%. Other uncertainties in the calculation probably exceed this error. In Figure 10.1 the monitor response is plotted as a function of proton energy from equation 10.5 using the yield functions given by Webber (op. cit). We now examine the response of the geiger counter to a flux of protons isotropic at the top of the atmosphere.

Response of the geiger counter to low energy protons

The absorption mean freepath of protons deduced from absorption and interaction cross section measurements is 100 g /cm^2 in air and is nearly independent of energy in the range 100- 900 MeV. (Lees et al., 1953; Milburn et al., 1954; Freier and Webber, 1963). At higher energies the range of the secondary particles becomes appreciable and the absorption length becomes eager than the interaction length. A natural division between the response to protons exists according to whether their energies are less than or greater than about 2GeV. Above this energy the counter response may be deduced from galactic cosmic ray measurements, and compared with neutron monitor observations near sea level in order to deduce the approximate energy spectrum required to account for burst in terms of an

enhanced proton flux. At lower energies the enhanced neutron monitor response decreases rapidly and energy and solar proton measurements must be used to check the theoretical results.

The counting rate ($\dot{n}$) of an omnidirectional detector at depth x due to an isotropic flux of protons of energy E,

$$\dot{n}_x = 2\pi A \int_0^{\theta_o} J(E) \cdot e^{-\frac{x \sec\theta}{\lambda}} \sin\theta \, d\theta \qquad 10.9$$

where A = projected area of counter

J(E) = Flux (per unit solid angle) of protons with energy E and range $R > x$.

and $\sec\theta_o = \frac{R(E)}{x}$

λ = absorption near free path

= 100 g/cm^2 , $E \lesssim 900$ MeV.

Upon integration,

$$\dot{n}_x = 2\pi A \, J(E) \, \left(\mathcal{E}_1\left(\tfrac{x}{\lambda}\right) - \tfrac{x}{R}\,\mathcal{E}_1\left(\tfrac{R}{\lambda}\right)\right) \qquad 10.10$$

where $\mathcal{E}_1(y) = \int_1^\infty \frac{e^{-ys}}{s^2}\, ds$ is a Gold integral and is tabulated by Rossi (1952).

In the present case we approximate the counter response by considering it to be a sphere of radius

$$r = \left[\frac{a\ell}{2}\left(1 + \frac{a}{\ell}\right)\right]^{\frac{1}{2}} \quad \text{(appendix 3)}.$$

Then $$A = \frac{\pi a \ell}{2} + \frac{\pi a^2}{2}$$

$$= 36.6 \text{ cm}^2 \qquad \text{(section 10.1)}$$

In Figure 10.2(a) the normalised counting rate $\frac{\dot{n}_x}{2\pi A}$. sec^{-1} cm^{-2} is plotted as a function of energy for x = 80 g/cm^2 and a primary

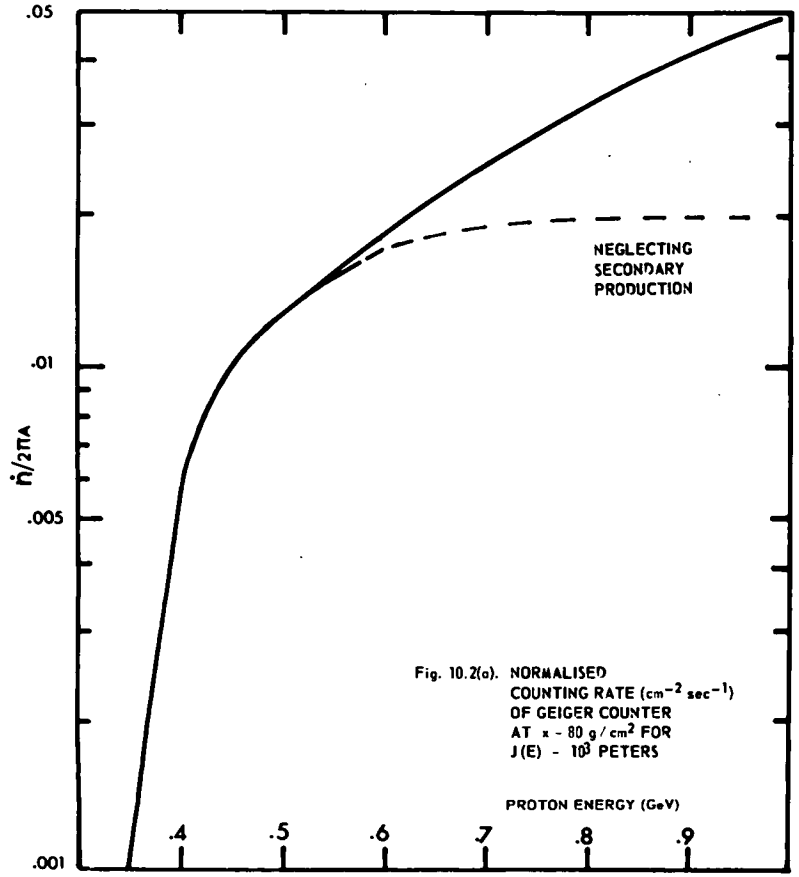

Fig. 10.2(a). NORMALISED COUNTING RATE (cm^{-2} sec^{-1}) OF GEIGER COUNTER AT $x = 80\ g/cm^2$ FOR $J(E) = 10^3$ PETERS

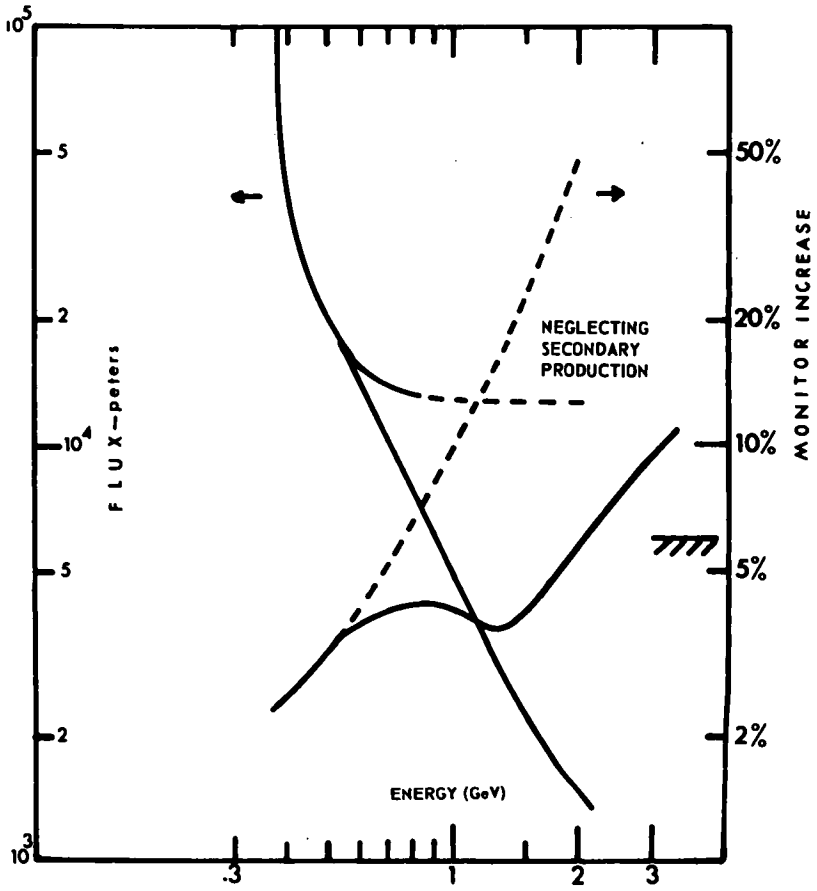

Fig. 10.2(b). MONOENERGETIC PROTON FLUX REQUIRED TO ACCOUNT FOR BURST A.

flux of 1000 peters. Neglecting secondary production as we have,, the counting rate is substantially independent of energy above 600MeV and drops rapidly below this energy. The omnidirectional intensity of primary protons at 80 g/cm^2 is therefore $\epsilon_1(0.8) \doteq 1/5$ of the omnidirectional intensity at the top of the atmosphere for $(600 < E < 10^3)$MeV. We take secondary particle production into account by making use of omnidirectional cosmic ray observations at various latitudes. For example, extrapolating the ionization curves of Nehar (Montgomery, 1948) to zero atmospheric depth, the ionization at $x = 809/cm^2$ is approximately one half that at $x = 0$ for primary particles with a mean energy of 1 GeV, and twice that at $x = 0$ for a mean energy of 2 GeV. In Figure 10.2(b) the primary intensity of protons required to produce the observed geiger counter increase is plotted as a function of energy. The corresponding percentage increase in the neutron monitor minute totals is also plotted. Taking the minimum detectable monitor increase to be 6%(2σ) it is clear that protons with energy as high as 2 GeV cannot be excluded on the basis of a comparison between the neutron monitor and the geiger counter measurements.

The maximum flux of photons required with energy 2 GeV is seen to be about 5.10^3 peters although, due to uncertainties in the response of a single counter to relativistic primary protons, this figure may be in error by as much as 50%. The required flux, however, is certainly at least several times the available cosmic ray flux. For this reason alone we reject the hypothesis that an enhanced cosmic ray flux was responsible

for the increase.

In the next section we examine the possibility that protons of lower energy were dumped from the radiation belts. To do this it is necessary to consider the response of the riometer to low energy protons.

10.4 PROTON PRECIPITATION : RESPONSE OF THE RIOMETER AND GEIGER COUNTER TO LOW ENERGY PROTONS

The ionospheric absorption of cosmic radio noise due to galactic and solar protons has recently been examined by Webber (1962). The night-time absorption at the poles is quoted as 0.6 db at 4Mc/s during solar minimum. Since the absorption in decibels is proportional to the path integrated electron density for a given spectrum, and the proton energy loss rate is nearly independent of energy for relativistic protons, an upper limit to the absorption at 4.7 Mc/s due to an isotropic flux of relativistic protons (stopping below the ionosphere) may be easily calculated. The absorption depends on the square root of the flux so that the 5000 peters of flux of 1 GeV protons ($\doteq 2.5 \times$ the cosmic ray flux at Hobart) compatible with the monitor and counter observations (Section 10.2) would result in an excess cosmic noise absorption of less than 1 db at 4.7 Mc/s. At lower energies the proton energy loss in the ionosphere increases and the absorption rises correspondingly.

Using the results of Webber (op. cit.,) and Freier and Webber (1963) it is found that the flux of monoenergetic protons needed to account for the magnitude of the counter increase would not produce a detectable increase ($\gtrsim 0.5$ db) in 30 Mc/s absorption for energies above 360 MeV, at which energy the proton range exceeds the atmospheric depth of the balloon. The greater sensitivity of the 47 Mc/s absorption to ionospheric ionization is compensated by the rapid decrease in the required flux with increasing energy in the region of the atmospheric cut off of the balloon detector. The flux of protons with energies above 360 MeV required for the counter increase would in fact produce less than half that observed at 4.7 Mc/s.

Since it is certain that other mechanisms, for example, the precipitation of neutron-decay electrons, could produce the bulk of the observed absorption, the proton dumping hypothesis is not contradicted by the absorption measurements. We conclude therefore that the hypothesis of an isotropic flux of monoenergetic protons proposed to account for burst A does not conflict with either the riometer or neutron riometer observations if the energy lies in the range 380- 2000 MeV. The required flux varies from 10^5 to 10^3 peters.

The energy spectrum of protons trapped on the magnetic shell ($L = 2.5$) accessible to the atmosphere above Hobart is given by McIlwain and Pizzela (1963) as $\frac{dN}{dE} \sim e^{-E/E_o}$ with $E_o \triangleq 2.5$ MeV.

Other observations (for example Fan et al., 1961) suggest an upper limit to the energy of trapped protons of several tens of MeV at L = 2.5. The burst cannot therefore be due to protons dumped from this shell because of the steep energy spectrum and inadequate flux available. An alternative mechanism is suggested by the proton observations on lower magnetic shells.

At L = 1.2 the differential proton flux (Heckman and Armstrong, 1962) exceeds 10^5 peters at 400 MeV and 10^4 peters at 600 MeV. The Hobart observations might then be explained if protons from lower L shells were scattered into unstable orbits at the L = 2.5 shell as a result of the explosion. This possibility will be examined in Section 10.8.

10.5 ELECTRON PRECIPITATION : THE RESPONSE OF THE GEIGER COUNTER AND RIOMETERS TO DUMPED ELECTRONS

In the previous two sections we examined the response of the counter, neutron monitor and riometers to an isotropic flux of protons and deduced an allowed range of proton energies which satisfied the observations. In this section we consider the response of the riometers and geiger counter to a vertical flux of electrons, the former as a result of enhanced ionization in the D layer, the latter through the production of bremsstrahlung x-rays. This interpretation is suggested by the time coincidence between the Hobart radiation burst and that observed with satellite Ariel, the latter burst being explained by Durney et al.(1963) in terms of a pitch angle redistribution of naturally trapped electrons.

The absorption of a radio wave passing through an ionized medium may be expressed by the relation,

$$I = I_o \exp(-Ks)$$

where I is the transmitted power, I_o is the incident power, K is the absorption coefficient, and s is the thickness of the medium traversed by the wave.

The absorption coefficient, K, may be calculated using magneto-ionic theory. In the ionosphere K is a function of altitude.

The ionospheric D layer absorption is given by the well known equation (Ratcliffe, 1959),

$$A = 10 \log \frac{I_o}{I} = \int K_h dh$$

$$= 4.6.10^4 \int \frac{n_e \nu dh}{\nu^2 + (\omega \pm \omega_L)^2} \quad \text{dB} \qquad \ldots\ 10.11$$

where n_e is the electron density, (cm^{-3}), ν the electron-neutral particle collision frequency, ω the angular frequency of the wave, ω_L the angular electron gyro frequency (Equation 2.11) about the longitudinal field component, and h the altitude in km.

The equilibrium electron density N_e is related to the ion production rate (q) by

$$q = \alpha_{eff} N_e^2 \qquad \ldots\ 10.12$$

where the effective recombination coefficient (α_{eff}) is a function of altitude. It may be derived from the ionization rate equations (e.g. Bailey, 1959) and lumps together the effects of various attachment and detachment processes involving electrons, ions and neutral particles. The values of the recombination parameters have been recently re-examined

by Webber (1962). In the following calculations (a_{eff}) has been calculated using Webber's figures.

The electron production rate at altitude h, $\{q(h)\}$ may be calculated from a knowledge of the rate of energy deposition from the electron beam. This is given by

$$w.q(h) = N(E).J\left(\frac{x(h)}{x_o}\right).\left(\frac{dE}{dx}\right)_o.\rho(h).MeV/cm^3 \qquad \ldots 10.13$$

where N(E) = Primary (vertical) flux, ($cm^{-2}sec^{-1}$) of mono energetic electrons

$\left(\frac{dE}{dx}\right)_o$ = Rate of energy loss ($MeV.cm^2g^{-1}$) at beginning of an electron of initial energy E MeV.

$\rho(h)$ = Air density at altitude (h)

$J\left(\frac{x(h)}{x_o}\right)$ = Weighting factor expressed as function of depth (x) in units of the residual range (x_o) g/cm^2. This is tabulated by Spencer (1959) for a plane parallel source of mono energetic electrons in air.

w = Energy required (36eV) to produce one ion pair.

Using the ionospheric parameters $\nu(h)$, $\rho(h)$, $a_{eff}(h)$, x(h) suggested by Webber (op.cit.), the absorption in the vertical direction is then found by numerical integration:

$$A(db) = C(E_o) \cdot \int_o^\infty \left[\frac{\nu\left(\frac{\rho}{\rho_o}\right)^{\frac{1}{2}}}{\nu^2+\omega^2}\right]_h \cdot \left[J\left(\frac{x}{x_o}\right) \cdot \left(\frac{dE}{dx}\right)_o\right]_{E_o,h} dh \quad \ldots 10.14$$

where $C(E_o) = 7.66\sqrt{N(E)}.10^{-3}$ with h in kilometres.

The vertical absorption is plotted in Figure 10.3 as a function of frequency and energy. At energies below 400 keV, the absorption occurs at altitudes where the collision frequency $\nu << \omega$ and the absorption in decibels is inversely proportional to the square of the observing frequency. The 30Mc/s absorption A'_{30} has been accordingly raised by a factor of 10^2 and it is seen that $A'_{30} \sim 10^2 A'_3$ below 400 keV. As the energy is increased the ionization at lower altitudes rises and the denominator in Equation 10.11 becomes a function of ν^2 as well as ω^2. As is evident from the curves, the total absorption becomes correspondingly less dependent on frequency above 400 keV. The total absorption at 30 Mc/s continues to rise with energy while the 3 and 6 Mc/s curves show shallow maxima in the range 1 - 5 MeV.

The maximum in the energy dependence is considerably less pronounced than for a proton flux. In the case of a proton beam (Section 10.4) the energy loss rises sharply at the end of the range and the ionization is consequently restricted to a smaller range of altitudes. Maximum absorption thus occurs at an energy for which the stopping altitude is close to the altitude (h) at which the specific absorption per unit ionization, $\frac{\nu(h)}{\nu^2(h)+\omega^2}$, is a maximum ($\nu = \omega$).

At sufficiently high energies the protons stop below the ionosphere where the high collision frequencies result in negligible

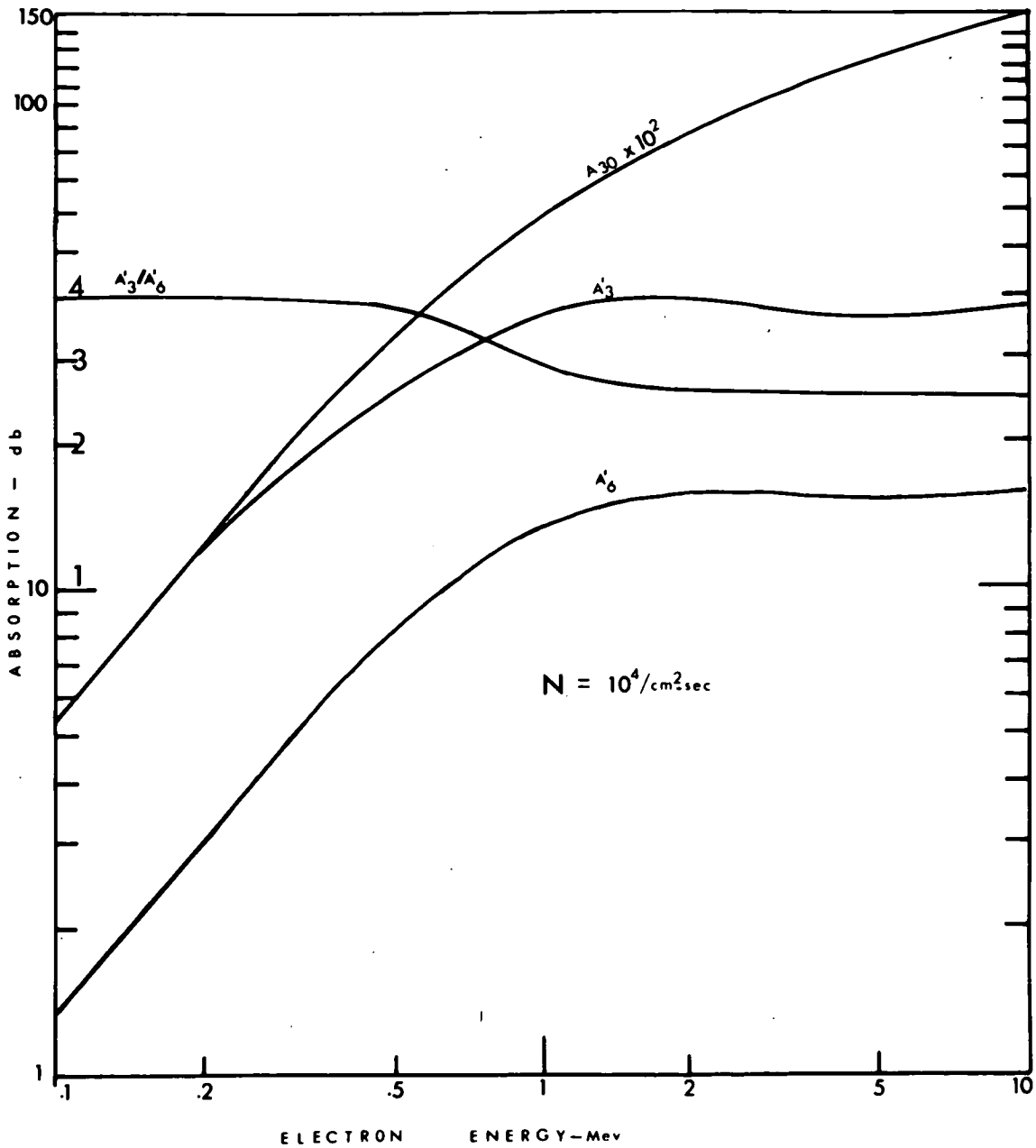

Fig. 10.3. VERTICAL COSMIC NOISE ABSORPTION FOR A MONO ENERGETIC FLUX OF ELECTRONS.

absorption and the total absorption increases slowly with energy due to the relativistic increase in the energy loss rate. The decrease in proton absorption with energy in the range from several tens of MeV up to several GeV allowed us to show in Section 10.4 that, in a restricted energy interval, the flux of protons required to account for burst A would not produce ionospheric absorption in excess of that observed. In the present case the electron produced absorption does not exhibit a marked maximum in its energy dependence, and the counter and riometer response both increase with energy. In the calculation of electron produced absorption, the ionization due to bremsstrahlung x-rays has been neglected.

The curves in Figure 10.3 therefore show lower limits to the absorption although the x-ray contribution is small below 1 MeV. The 30 Mc/s vertical absorption may be obtained directly from the upper curve. The lower curves, shown for $\frac{\omega'}{2\pi} = \frac{\omega \pm \omega_L}{2\pi}$ = 3 Mc/s and 6 Mc/s respectively, show the X and O mode absorption at a frequency of 4.5 Mc/s, ($\omega_L \doteq 2\pi.1.5$ Mc/s) this being the approximate operating frequency of tje radio telescopes. The vertical absorption at 4.5 Mc/s is found from the curves using the relation,

$$A_{4.5}(\text{db}) = 3 + 10 \log \frac{R_o R_x}{R_o + R_x} \qquad \ldots 10.15$$

where $A'_3 = A_{4.5}(X) = 10 \log R_x$

and $A'_6 = A_{4.5}(O) = 10 \log R_o$

$$\text{or,} \qquad A_{4.5}(\text{db}) = 3 + 10 \log \frac{R_o^n}{1 + R_o^{n-1}} \qquad \ldots 10.16$$

where $n = A(x)/A(o)$

$$= A'_3/A'_6$$

Thus, although the absorption in either mode is proportional to the square root of the flux and can be estimated from the curves for flux $n(E)\text{cm}^{-2}\text{sec}^{-1}$ by multiplying the ordinate by $\frac{N^{\frac{1}{2}}}{10^2}$, the net absorption observed at low frequencies with a linearly polarized antenna must be obtained from separate calculations of the ordinary and extraordinary mode absorption and it is not in general possible to plot the relative energy response of a low frequency riometer independently of the magnitude of the ionizing flux. From Equation 10.16, as R_o increases, $A_{4.5}$ tends to the limit $(A_o + 3)$db. As R_o goes to 1, $(A_o \to 0)$, A approaches A_x. Thus, for small absorption, A'_3 represents an upper limit to $A_{4.5}$ while for large absorption $(A'_6 + 3)$ is the upper limit. The total absorption at 4.5Mc/S always exceeds A'_6.

The maximum flux available for x-ray production may then be calculated on the assumption (a) that the observed absorption was due solely to ionization by monoenergetic electrons, and (b) that the wide beam and inclined narrow beam (Section 9.4) absorption does not exceed the vertical absorption. The effect of these assumptions is to overestimate the required flux by perhaps 50%.

The flux calculated in this way varies from $4.5.10^4\text{cm}^{-2}\text{sec}^{-1}$ at 100 KeV to $3.6.10^2\text{cm}^{-2}\text{sec}^{-1}$ at 10 MeV. We shall now investigate the response of the geiger counter to bremsstrahlung x-rays to see whether the electron dumping hypothesis is compatible with both the riometer and counter observations.

X-RAY BREMSSTRAHLUNG

The energy loss rate due to radiation of an electron of total energy $E + \mu$ is given by the relation (Bethe and Heitler, 1934)

$$\left(\frac{dE}{dx}\right)_{rad} \doteq \frac{Z(E+\mu)}{800}\left(\frac{dE}{dx}\right)_{ion} \qquad \ldots 10.17$$

where Z is the atomic number of the medium, μ is the rest energy of the electron, E the kinetic energy (MeV) and $\left(\frac{dE}{dx}\right)_{ion}$, the rate of energy loss ($MeVg^{-1}cm^2$) due to ionization and excitation of the medium.

The total amount of energy radiated per stopped electron is then

$$U_R \doteq \frac{ZE^2}{1600}, \text{ for } \frac{800}{Z} >> E >> \mu \qquad \ldots 10.18$$

For non relativistic energies ($E<<\mu$), Chamberlain (1961) has shown that the total energy $E_o = E + \mu$ in Equation 10.17 must be replaced by the kinetic energy E. Equation 10.18 then becomes valid at low energies. This Equation expresses the well known experimental fact (e.g. Compton and Allison, 1936; Petrauskas et al., 1943; Buechner et al., 1948) that the thick target bremsstrahlung efficiency (U/E) increases linearly with atomic number, Z and kinetic energy, E. The numerical factor in Equation 10.18, $1/1600$, is about 30% lower than that deduced from Kramer's equation (Compton and Allison, 1936, p.106) used by Cladis and Dessler (1961) to calculate the x-ray flux due to atmospherically scattered radiation belt electrons. The experimental results of Buechner et al. (1948) and Petrauskas et al. (1943) for relativistic energies are in good agreement with Equation 10.18.

The differential photon flux (Bothe and Ashkin, 1953) may be approximated by

$$\frac{dN}{dv} = \frac{1}{v}\left(1-\frac{v}{E}\right).C(E) \quad \text{photons/MeV/electron} \qquad \ldots 10.19$$

The constant $C(E)$ may be found from the requirement $\int_0^E v.\frac{dN}{dv}.dv = U_E$.

We may then rewrite Equation 10.19 as

$$\frac{dN}{dv}(E) = \frac{Z.(E-v)}{600v} \qquad \ldots 10.20$$

$\doteq (E-v)/10^2v$ in air

where $\frac{dN}{dv}.dv$ is the number of photons radiated with energy in dv at v (MeV) per stopped electron of initial kinetic energy E(MeV).

Neglecting the build up of photon flux due to scattering, and assuming the x-rays to originate in an infinite horizontal plane in the ionosphere, the flux of photons in dv at v at depth x in the atmosphere is then, assuming isotropic emission,

$$J(v,E) = \tfrac{1}{2}e_0(\mu(v).x).\frac{dN}{dv}(E).N(E) \ \text{cm}^{-2}\text{sec}^{-1} \qquad \ldots 10.21$$

where $\mu(v)$ is the narrow beam mass absorption coefficient. $N(E)$ is the primary flux of electrons of kinetic energy E.

The counting rate due to a mono-energetic flux $N(E)$ cm^{-2} sec^{-1},

$$\dot{n} = \frac{A.N(E)}{2}\int_0^E e_0(\mu(v).x).\frac{dN}{dv}(E).\eta(v).dv \ \text{sec}^{-1} \qquad \ldots 10.22$$

where A is the effective area of the horizontal counter (Appendix 3) and $\eta(v)$ is the photon efficiency of the counter (Section 10.1). The contribution of the scattered photon flux to the counting rate may be taken into account by including a "build-up" factor (Goldstein, 1957) in

the attenuation term. Since the mean energy of the scattered flux will be lower than that of the direct flux, inclusion of the build-up factor in the integration will lead to an overestimate of the counting rate because of the increase in η with energy. We take the build-up factor to be $B(\mu x) \doteq 1 + \mu x$ (Chappell, 1956) so that the attenuation term becomes $(1 + \mu x).\varepsilon_o(\mu x)$ and the counting rate, upon substitution of the various quantities, may be written

$$\dot{n} \doteq 0.5E(E).10^{-3} \int_{1/3}^{E} \left(1 + 80\mu(\nu)\right).\varepsilon_o\left(80\mu(\nu)\right).(E - \nu)(3\nu - 1)\frac{d\nu}{\nu} \qquad \ldots 10.23$$

The counter efficiency, according to Equation 10.1 is zero below 1/3 MeV. While this assumption is certainly not true, it leads to negligible error in the integration. The linear extrapolation of the efficiency to 10 MeV is not strictly correct but is also adequate for the present calculations. We note that the counting rate due to a constant flux N(E) will increase rapidly with electron energy (E) since the bremsstrahlung energy conversion efficiency (W_R/E) and the mean phton energy ($\bar{\nu}$) both increase with energy. The increase in $\bar{\nu}$ results in a corresponding increase in counter efficiency and reduction in atmospheric attenuation. As the primary electron energy increases, the conversion layer behaves less like an isotropic source and more like a plane parallel source since most of the x-rays are emitted in the forward direction. The atmospheric attenuation term then becomes

$$(1 + \mu x)e^{-\mu x} \sim \mu x\left((1 + \mu x).\varepsilon_o(\mu x)\right)$$

At 10 MeV, $\mu x \sim 1.6$, while at 1 MeV, $\mu x \sim 5$. The consequent reduction in attenuation by a factor of the order of (μx) on the extreme assumption

of forward emission is not sufficient to alter the conclusions of this section.

It is clear that at low energies the counting rate will be negligible for the electron fluxes calculated from the riometer measurements. At E = 1 MeV for example the energy in bremsstrahlung radiation is $W_R E(E) \sim 2.5$ MeV $cm^{-2}sec^{-1}$ from Equation 10.18. The primary x-ray flux is therefore only several photons/cm^2sec. Since the atmospheric alternation is of the order of 10^{-3} and the counter efficiency of the order of 10^{-2}, the flux of 1 MeV electrons required for the riometer absorption would not produce a detectable increase in the geiger counting rate. Upper limits to the electron flux required to account for a counting rate increase of 50 sec^{-1}, calculated from Equation 10.23 are $1.0.10^4 cm^{-2}sec^{-1}$ at 10 MeV and $2.3.10^8$ at 1 MeV. These values are respectively 30 times and 10^5 times the maximum allowable primary intensity deduced from the absorption observations. We may therefore confidently reject the hypothesis of wide-spread electron dumping since the electron fluxes required to produce the counting rate increase would produce absorption far in excess of that actually observed at either 4.7 or 30 Mc/S. Using the same argument we may also reject neutron decay $-\beta$ particles as a source of the increase.

The observation that all 4.7 Mc/S narrow beam antennas recorded about 6db absorption, independently of their inclination to the zenith (10^oN, 5^oN, 5^oS, 10^oS), suggests that the ionization covered an area of the order of at least several hundred square kilometres at D layer heights. The smaller absorption recorded by the wide beam 4.7 Mc/S riometer suggests that the excess ionization was smaller outside this zenith centred area.

The balloon was less than 50 km east of Hobart at the time of the observations so that it is unlikely that prolonged electron dumping could occur above the balloon without causing large ionospheric absorption above Hobart although the possibility of localised electron dumping cannot be entirely excluded by the measurements. The localised dumping of a sufficient flux of electrons to the east of the balloon might conceivably produce an x-ray flux at the balloon adequate to account for the observed increase.

Kenney and Willard (1963) predict the prompt neutron decay β flux from the Starfish explosion to have been about $10^3 cm^{-2} sec^{-1}$ over Tasmania. From Figure 10.6(a) it is seen that this flux (taking E = 350 KeV) would produce about 5db of absorption at 4.5 Mc/S if directed vertically. Although the effect of gyration about the inclined field lines (20^o to the zenith) has not been considered in this and other absorption calculations in this section, it appears likely that a major part of the observed absorption originated in the ionization produced by the electrons from the decay of fast neutrons.

10.6 GAMMA RADIATION : RESPONSE OF THE GEIGER COUNTER AND RIOMETER TO GAMMA RAYS

The efficiency of the counter to gamma rays is small, of the order of 1% (Section 10.2). Nevertheless its response, relative to that of a riometer, to a flux of gamma rays is considerably greater than for the case just considered, that of an electron flux. This is so because of the relatively small energy loss in air and long mean free path of gamma rays with energy above a few tens of KeV.

The atmospheric attenuation of photons was discussed in the previous section. The minimum attenuation of the narrow beam flux occurs for a monodirectional ("parallel") source and is just $e^{-\mu x}$. For a point isotropic source above the atmosphere at altitude h_s emitting $N(\nu)$ photons of energy ν per second, the counting rate at depth (x) is

$$\dot{n} = \frac{\eta(\nu).N(\nu).A}{4\pi} \cdot \frac{B(\mu(\nu).x \sec\theta).e^{-\mu(\nu).x \sec\theta}}{(h_s-h_p)^2\sec^2\theta} \qquad \ldots 10.24$$

where h_p is the altitude of the detector, θ the zenith angle of the source.

For an infinite plane isotropic source, of activity $N(\nu)cm^{-2}$

$$\dot{n} = \frac{\eta(\nu).N(\nu).A}{2} \cdot B(\mu(\nu).x).\varepsilon_0(\mu(\nu).x). \qquad \ldots 10.25$$

These expressions overestimate the counting rate, particularly at large depths where the scattered flux of lower energy photons predominates over the direct flux.

The intensity of the flux at great depths $(x>>\frac{1}{\mu})$ due to a monodirectional source is proportional to $e^{-\mu(\nu).x}.x^{K(\nu)}$ (Fano, 1953) providing the primary photon energy is less than the energy at which the narrow beam absorption coefficient attains its minimum value. This provision is satisfied in the present case. The quantity $K(\nu)$ may be adjusted for various source geometries.

At great depths the unscattered flux is much less than that of the secondary flux. The energy of the scattered photons becomes independent of x if x is large and the mean photon energy is degraded to an energy close to that at which photoelectric absorption predominates over Compton scattering. In air or water the photon energy spectrum at large depths therefore peaks at an energy of about 50 KeV. At this

energy the counter response is due to photoelectric absorption in the counter wall. The photon efficiency is then approximately 0.1%.

Gamma radiation, from the debris of the Starfish explosion or from the nuclear interactions of photons or neutrons stopping in the atmosphere, is a possible cause of the radiation burst. Proton interaction x-rays of sufficient intensity would, however, imply a primary flux of protons with energy below 380 MeV well in excess of that allowed by the riometer observations (Section 10.4; Bhavsar, 1962; Hofmann and Winckler, 1962).

The ionospheric absorption produced by fission-gamma rays has been examined by Latter and Le Levier (1963). Using these results it is found that the flux of 0.7 MeV gamma rays required for the radiation burst (of the order of $10^5 cm^{-2} sec^{-1}$) would produce less than 0.05 db absorption at 30 Mc/S and, from Figure 10.3, less than about 1 db at 4.7 Mc/S. At higher energies the absorption may be expected to increase approximately linearly with energy while the counting rate will increase at a more rapid rate because of the rapid decrease in $\mu(\nu)x$. The response of the counter relative to the riometer therefore initially increases with energy above 0.7 MeV. At lower energies, before photoelectric absorption predominates, the geiger counter response continues to fall relative to the riometer as the energy decreases. We conclude that monoenergetic gamma rays with energies in the range from several hundred keV to at least 10 MeV could produce the radiation burst without causing cosmic noise absorption in excess of that observed.

10.7 THE MAGNETIC OBSERVATIONS

In the preceding sections the responses of the balloon borne geiger counter, the Mr.Wellington neutron monitor and the cosmic radio noise monitors to ionizing radiation have been analysed. The analysis, though subject to various uncertainties, showed that the radiation detected by the geiger counter produced considerably lighter ionospheric absorption than would be expected from an electron, or low energy proton, dumping event. It was concluded, however, that the observations do not exclude either gamma rays with energies of the order of 1 MeV or protons with an energy spectrum intermediate between that of galactic and solar protons. In this section we briefly consider the magnetic observations.

The Hobart magnetograph (Section 9.3) recorded small fluctuations in the amplitudes of the magnetic field components which persisted for approximately the duration of the riometer absorption and the geiger counter enhancement. As already noted in Section 9.3, the total field was depressed during the first minute of burst A and the horizontal field vector moved to the west. The field then increased and the horizontal field component variations reached a maximum of two to three times the amplitude of the Sq variation. The magnitude of the vertical component during the second phase of the west (after H + 60 sec) 10γ, considerably greater than twice the Sq variation ($\simeq$ 2γ). This observation suggests that the ionization following burst A which apparently produced the persistent riometer absorption and

magnetic field enhancement, was less intense to the south of Tasmania than to the north. This is in general agreement with the hypothesis of a neutron decay -β source for the ionisation. The initial phase of the magnetic event is more complex. Although it is possible to state that the approach and passage of geomagnetically trapped particles from the east would be compatible with the observations. This interpretation has been suggested by Pisharoty (1962) to account for the bay-like depressions in the surface magnetic field in South India which occurred several minutes after the detonation.

The bays, of maximum amplitude - 40γ in H at near equatorial stations, lasted 12 minutes. The maximum depressions occurred at 2 and 3.3 minutes after the detonation. Pisharoty suggested that these were produced by a westward drift of positively charged ions generated by the explosion and trapped on the magnetic field shell (L = 1.2) upon which the detonation took place. From the longitude difference between Johnston Island and the observing stations, it was concluded that protons with energies of 5.5 and 3 MeV would account for the time delays to the two field depressions. A small error was made in this calculation and it appears that better estimates of the energies per unit charge are 4.1 and 6.7 MeV/Z, (from Equation 2.27).

An error also occurred in the computation of the diamagnetic effect of the trapped ions, these being assumed to constitute a semi-infinite current sheet. Pisharoty's estimate of the total number (N) of trapped particles that cross 80°E longitude in a 30° band of latitude

centred on the magnetic equator must, on this assumption, be raised by a factor of ten to give $N = 3.10^{26}/Z$. This number (for $Z = 1$) is of the order of 10% of the total number of light nuclei produced in a 1 megaton fusion explosion.

Other equatorial observations (Glover, 1963; Caseverde et al., 1963) show that large depressions in the horizontal field occurred at longitudes up to 207° west of Johnston Island. Smaller enhancements occurred to the east, Huancayo (90°E) recording an increase in H of 10γ. These observations were interpreted by Caseverde et al. as an enhancement of the equatorial electrojet current. It is certain, however, that the source of the equatorial magnetic field depression propogated to the west with an apparent angular speed between 0.5 and 0.8 °/second. The time of the maximum field depression in the Philippines (H + 90 sec) is in good agreement with the angular drift rate deduced from the South India observations. Depressions at longitudes greater than 207° west of Johnston Island might be explained by the precipitation of the trapped particles in the region of the South Atlantic anomaly (250°W of J.I.) if the hypothesis of Pisharoty were accepted.

The above discussion is included as an introduction to an interpretation of the Hobart radiation burst in terms of westward drifting, magnetically trapped, charged particles. Trapping of electrons from the Starfish explosion in the vicinity of the shell, $L = 1.2$ was

expected, (e.g. Singer, 1962) and established by satellite observations (e.g. Van Allen et al., 1963; McDiarmid et al., 1963). Pisharoty's hypothesis therefore appears reasonable in the light of known injection mechanisms and is indirectly supported by observation. The mode and spatial extent of the injection of charged particles at higher altitudes is not clear however.

The value of the magnetic shell parameter appropriate to Hobart is $L = \cos^{-2}\lambda_g$ (Sauer, op.cit., Section 2.5). Taking $\lambda_g = 54.5^\circ$ (Quenby and Webber, op.cit., Section 7.5), we find $L = 2.95$. Although the cosmic ray spectrum measurements (Section 7.5) suggest a somewhat lower "equivalent dipole" latitude, we take $L = 3$ to define the line of force through Hobart. If burst A were due to west drifting particles injected at $L = 3$ above Johnston Island, Equation 2.27 may be used to compute their energy per unit charge. Taking the time delay to the onset (≈ 15 seconds) and the longitude interval of 45° we find $E/_Z = 3.8$ MeV per unit charge. The peak intensity of the burst occurred at $H + 45$ seconds. Particles mirrored over Hobart at this time would therefore have the energy of 1.3 MeV per unit charge if injected at $L = 3$ at the time of the explosion. These values are close to those required to account for the equatorial magnetic field changes. The existence of two depressions in the horizontal field observed by Pisharoty suggests a doubly peaked distribution in the kinetic energy per unit charge of the trapped particles assumed responsible for the magnetic effects.

The initial kinetic energy of the fission products of uranium averages (Price, 1958) 97 and 65 MeV for the "light" and "heavy" fragments respectively. Since the initial mean charges are respectively +20 and +22, the distribution in energy per unit charge may be expected to peak in the vicinity of $E/Z = 4.85$ and 2.95 MeV per unit charge.

Since the longitudinal drift rate of non-relativistic particles depends linearly on their kinetic energy per unit charge (Section 2.3), the temporal distribution in the number of simultaneously injected trapped particles observed on a particular magnetic shell reflects their distribution in E/Z. It is possible therefore that the Indian magnetic observations might be explained on the basis of the westward drift of positively charged fission fragments. Thus, although the energies per unit charge required to explain the time delays are about 40% above those expected for fission products at the beginning of their range, the ratio of the time delays to the two field depressions (1.65) is very nearly equal to the ratio (1.64) of the estimated mean energies per unit charge of the light and heavy fission fragment groups. A total number of about $\frac{3.10^{26}}{20} = 1.5.10^{25}$ (5% of the number produced in a 1.4 Megaton yield fission explosion) would then be needed to account for the magnitude and duration of the equatorial magnetic effects. If fission products were injected at $L = 3$, the Hobart radiation burst might also be explained since the fission products are gamma active, emitting, on the average, $0.7\ t^{-1.2}$ photons of mean energy 0.7 MeV per second per fission product where $t(>1)$ is the time in seconds after the fission event (Latter and LeLevier,

FIGURE 10.4 : Three Diagrams and Auto-covariance Plots Showing the 7 - 8 Second Periodicity in Intensity : During Burst A (upper diagrams). The Lower Diagrams show the Absence of a Periodicity Immediately Prior to Burst A.

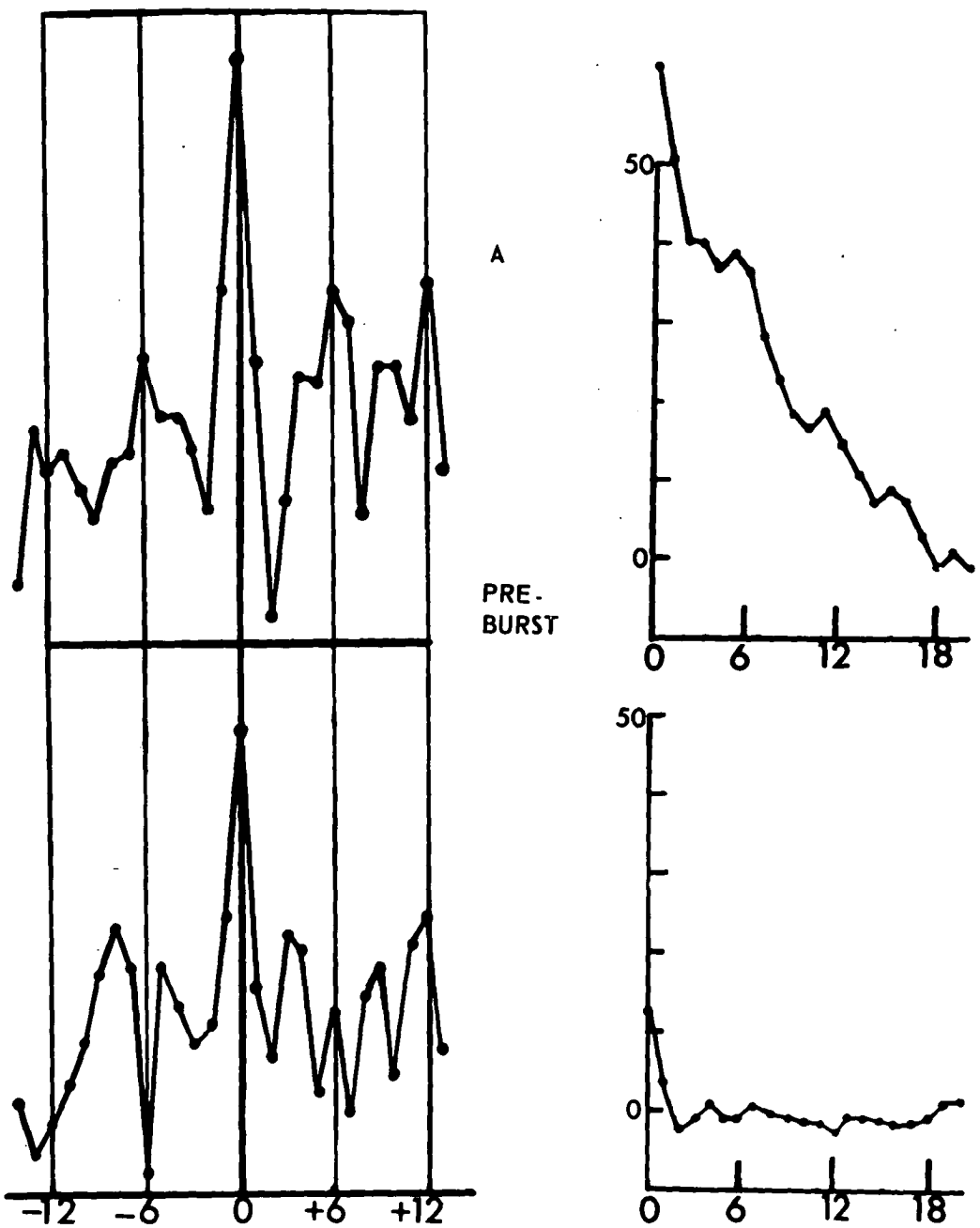

Fig. 104. CHREE DIAGRAMS (INTENSITY MAXIMA.) AUTO COVARIANCE

(LAG = 1.10 sec)

1963; Goldstein, 1957; Kothari, 1956). Before examining this interpretation further, we discuss the magnetic micropulsations observed at Hobart in relation to the radiation burst.

Micropulsations during Burst A

The micropulsations record was discussed in Section 9.2. A time association was noted between the onset and cessation of the 16 second quasi sinusoidal micropulsations and burst A. A Chree analysis was made of the counting rate during burst A. This showed (Figure 10.4) an apparent periodicity in the counting rate maxima during this period of 7 - 8 seconds. No periodicity was evident prior to the event.

Since the period of recurrence was found to be just half the micropulsations period it was decided to carry out an autocorrelation and power spectrum analysis to confirm the periodicity. The results of this analysis are presented in Figures 10.5 and 10.6. The short duration of the event limits the reliability of the spectral estimate particularly for the longer periods, but the presence of the strong peak in the spectral density at 7 lags (8 seconds) and to a smaller extent at 16 seconds is most noticeable. A second Chree analysis was then performed on the radiation record. The zero epochs were taken to be the zero crossing times of the micropulsations record ($\frac{dZ}{dt} = 0$). The times of maxima were not chosen because of the distortion of the chart record as the instrument approached saturation. This analysis showed (Figure 10.6) a clear tendency for the radiation intensity maxima to occur 4 seconds before and after the zero crossing times, that is at the

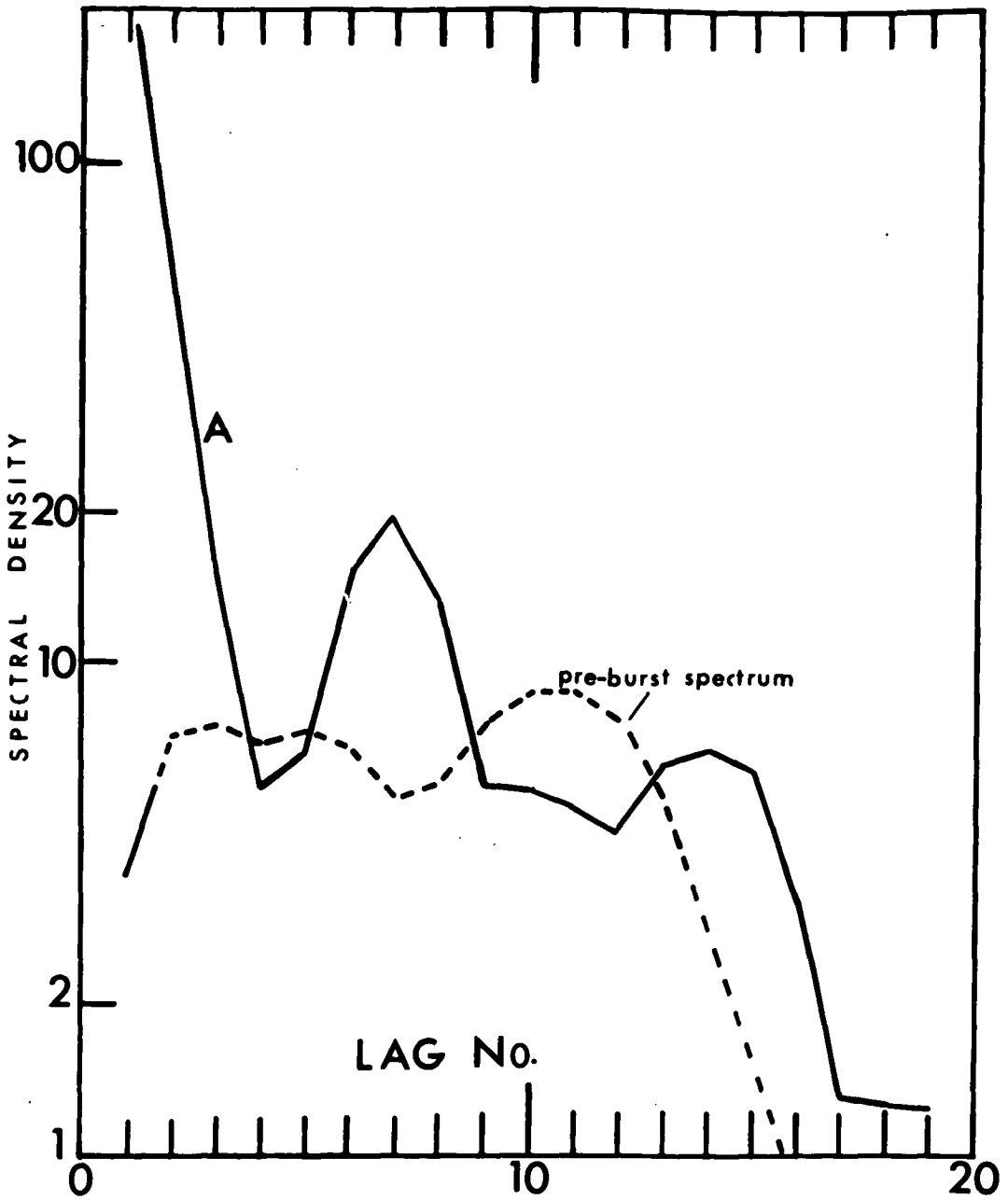

Fig 10.5

POWER SPECTRUM
(Lag = 1.10 sec
Duration = 90 sec)
OF GEIGER COUNTING RATE FLUCTUATIONS.

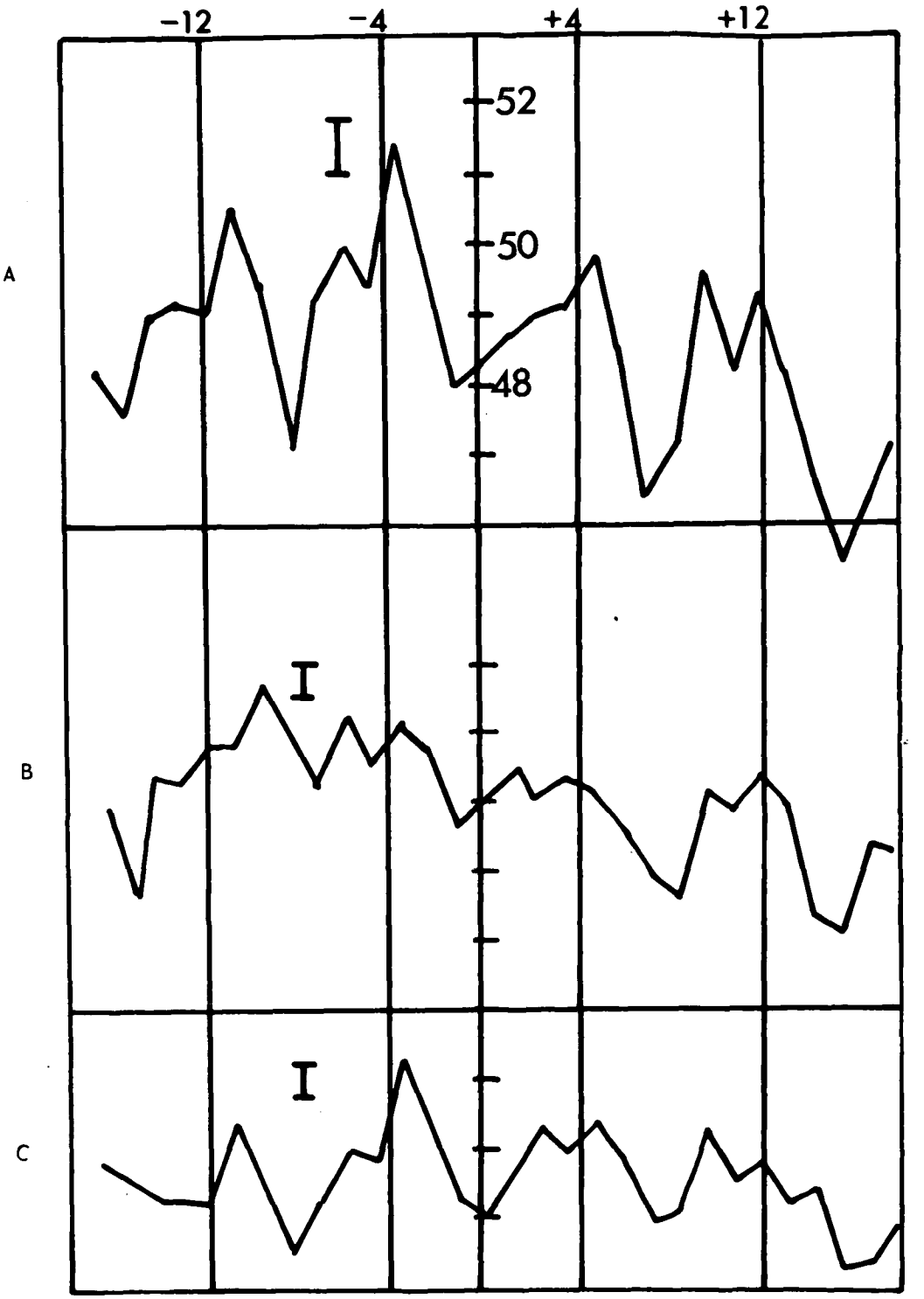

Fig. 10.6. CHREE DIAGRAMS SHOWING PERIODICITY IN BURST A INTENSITY WITH ZERO EPOCHS SELECTED FROM MICRO PULSATIONS ZERO CROSSINGS:
(A) ALL ZERO CROSSINGS; (B) POSITIVE GOING;
(C) NEGATIVE GOING.

times of maximum rate of change of the vertical field component. It was therefore concluded from the statistical analyses that a definite association existed between the magnetic and radiation phenomena. The presence of a periodicity in the radiation intensity at twice the micropulsations frequency and the existence of a consistent phase difference between the intensity and magnetic fluctuations strongly suggests magnetospheric origin of the radiation.

10.8 THE HOBART RADIATION BURST : POSSIBLE INTERPRETATIONS

In the previous sections of this chapter a number of possible origins of the radiation burst were examined. The magnetic, ionospheric and radiation measurements at Hobart were considered jointly in an attempt to determine the nature of the radiation responsible for burst A. It was concluded that the most likely cause of the increase was the influx of gamma rays or protons over Hobart. The discussion of the last section suggested the possibility of trapped particles as the source of the increase. The association demonstrated between the micropulsations and radiation events strengthens this hypothesis. It was suggested that the westward drift of radio active debris, injected at high altitudes over Johnston Island, might account for the Hobart burst.

The presence of artificially injected β particles at high altitudes (L as high as 5) following the explosion is confirmed by the data from satellites Ariel (Durney et al., 1962, 1964) and Telstar (Brown and Gabbe, 1963). Telstar observed a decrease of several orders of

magnitude in the electron intensity in the region $2.5 < L < 3.5$ in the four months following the explosion. This latter result suggests the loss of "Starfish" electrons from this region, although this interpretation has been disputed (Van Allen et al., 1963). It seems clear however that widespread injection of β particles did in fact take place. Assuming these to be fission-decay particles we therefore have indirect evidence for the presence of fission products on the magnetic shells passing through Tasmania. The possible mechanisms of injection at high altitudes have been examined by Colgate (1963), who suggests that neutralised fission products would provide the main source of β particles at $L > 1.3$. This mechanism is inadequate to account for the Hobart burst because of the excessive time required for the uncharged products to reach sufficiently high altitudes to be observed over Hobart.

As already mentioned, satellite Ariel observed a radiation increase at the time of the Hobart increase. If the Hobart and Ariel bursts had a common origin we may make use of the Ariel data to elucidate the cause of the Hobart event. Durney et al. (1963) used the relative responses of the shielded geiger counter and Cerenkov counter on board Ariel as an indication of the type of radiation responsible for the event. It was concluded from this and other characteristics of the event that naturally trapped electrons were responsible for the increase. It was shown in Section 10.5 that electron dumping, as would be expected on Durney's hypothesis, is not a likely cause of the Hobart increase. If the conclusions of Section 10.5 and the hypothesis of a common origin for

the Ariel and Hobart bursts are accepted, we may enquire whether the gamma activity of fission products might explain both events.

The emission of delayed gamma rays from the radio active plasma formed above the detonation was considered by Durney et al. as a possible cause of the Ariel burst. These authors found that 10% of the fission products formed would be required above the Ariel horizon at H + 20 seconds in order to account for the increase. It was also pointed out the Hobart increase would have been delayed by about 60 seconds, and not 15 seconds as observed, if both events were due to the gamma activity of a plasma bubble rising above Johnston Island. In addition it may be shown, using the results of Section 10.6, that the gamma activity of the bomb plasma would be insufficient to produce a detectable geiger counter increase at Hobart (8000 km distant) even if the atmospheric mass thickness were only 80 g/cm^2, the residual stopping power in the vertical direction.

The gamma ray hypothesis could be retained however if the fission products were able to reach the L = 3 shell in the charged state with energies per unit charge of the order of 1 MeV/Z (Section 10.7) and drift longitudinally towards the west. If the debris precipitated at 90 km (the minimum altitude for fission product deposition) above Hobart, equations 10.24 and 10.25, show that about 10^{21} fragments (3.10^{-3} of the total number of fragments produced in a 1 kT explosion) would be required to account for the magnitude and duration of burst A. The mirror period of fission products having their initial velocities

($\simeq 10^9$cm sec^{-1}) would be about 10 seconds at L = 3 (Equation 2.33). This period is of the same order as the magnetic and radiation periodicities and suggests the likelihood of a resonant interaction (Dragt, 1961; Dungey,1962) between the trapped particles and the hydromagnetic disturbance evidenced by the micropulsations record.

APPENDIX 1

The counting rate of a counter telescope is, from Equation 4.12,

$$\dot{n} = \varepsilon \int_{\Sigma} I(\theta,\phi).A(\theta,\phi).d\Lambda \qquad \ldots A\ 1.1$$

where ε is the efficiency of the telescope. The efficiency, $\varepsilon = \varepsilon_a.\varepsilon_b.\varepsilon_c$, assumed to be independent of the direction (θ,ϕ) of the particle arriving from within solid angle (Σ) is considered here to take into account the following sources of count loss:

(a) Insensitive area of counter trays.

(b) The finite probability that a particle which enters the sensitive volume of a counting tube will fail to initiate a discharge due to the statistical nature of the ionization process.

(c) The finite probability that a particle arriving at the counter at time (t) will not be detected owing to the prior initiation of a discharge at time $(t - \tau_r)$ where τ_r is the resolving time of the counting system.

(a) If, in the calculation of geometric factor, the dimensions of the sensitive area are used, then (a) introduces no count loss. This calculation presents no difficulty if each tray of the telescope consists of a single counter. In the case of telescope A, however, the nominal tray area was 360 cm^2, 14% of which was contributed by the walls of the three counters. Since three trays were used in the telescope, its efficiency $\varepsilon_a = (0.86)^3 = 0.64$. This is an underestimate of the efficiency since particles which travel in the direction of the telescope

axis and pass through the insensitive regions of one tray will necessarily traverse the same regions of the remaining trays. The geometric factor of telescope A was in fact deduced by comparing its counting rate in the laboratory with that of a number of accurately dimensioned single counter-tray telescopes.

(b) The reduction in telescope efficiency due to this cause was calculated to be less than 0.5% and was therefore neglected.

(c) The major source of count loss was due to the "dead time" of the individual counters.

If the counting rate is $\dot{n}_o$, the rate of occurrence of ionizing events, (Appendix 2)

$$\dot{n}_i = \dot{n}_o/1 - \dot{n}_o\tau_r \qquad \ldots \text{A } 1.2$$

Suppose a fraction $f_{1,2,3} = \frac{\dot{n}_{1.2.3}}{\dot{n}_i}$ of these events is due to particles capable of producing genuine 3-fold coincidences. $\dot{n}_{1.2.3}$ would then be the telescope counting rate providing the efficiency (ϵ) in A 1.1 were unity and if accidental coincidence were absent. If $f_{1.2.3} \ll 1$, and if the ionizing events in any one counter are independent of those in any other, the resolving time efficiency of the telescope,

$$\epsilon_c = (1 - \dot{n}_o\tau_r)^3 \qquad \ldots \text{A } 1.3$$

This expression was used by Biehl et al.(1948). The assumption that the counter backgrounds are independent is not valid, however, and A 1.3 overestimates the resolving time counting loss.

Consider a test particle passing through all three trays. The probability of detection in the first tray is just $\frac{\dot{n}}{\dot{n}_i} = (1 - \dot{n}_o\tau_r)$.

If the particle triggered tray one then it will also trigger tray two unless this tray has been rendered inoperative by the prior passage of a competing particle. This competing particle cannot have triggered tray one, since, if it had, the test particle would not have been detected by tray one. The probability of tray two detection of the (tray one detected) test particle is therefore $1 - (\dot{n}_o - \dot{n}_{1.2})\tau_r$. At tray three the particle competes for detection with particles that have triggered neither tray one nor tray two. The probability of tray three detection is then $1 - (\dot{n}_o - \dot{n}_{1.2.3} - \dot{n}_{2.3.\bar{1}})\tau_r$. The 3-fold resolving time efficiency is thus

$$\epsilon_c = \epsilon_{1.2.3} = (1 - \dot{n}_o\tau_r)(1 - \overline{\dot{n}_o - \dot{n}_{1.2}}\,\tau_r)(1 - \overline{\dot{n}_o - \dot{n}_{1.2.3} - \dot{n}_{2.3.\bar{1}}}\tau_r)$$

$$= (1 - \dot{n}_o\tau_r)(1 - \dot{n}_o - \dot{n}_{1.2}\tau_r)(1 - \dot{n}_o - \dot{n}_{2.3}\tau_r) \quad \text{A 1.4}$$

The total tray rate may be deduced from single counter observations. The two-fold coincidence rates, $\dot{n}_{1.2}$ and $\dot{n}_{2.3}$ may be approximately calculated from the telescope geometry and the observed three-fold rate, the Equation A 1.4 was used in calculating the efficiency of the three and four counter telescopes. The maximum resolving time loss for these telescopes was of the order of 10%.

Correction to the observed counting rates was also necessary because of the contribution of "accidental" three-fold coincidences to the observed rate. The accidental rate,

$$A_{1.2.3} \doteq 4(\dot{n}_{1.2.\bar{3}} \cdot \dot{n}_o) \cdot \tau_c$$

$$\doteq 12\, \dot{n}_{1.2.\bar{3}} \dot{n}_o \tau_c \quad \text{... A 1.5}$$

for equispaced trays having the same counting rates ($\dot{n}_o$) connected to a coincidence circuit of resolving time, τ_c. The fraction of the observed rate due to chance coincidences, $12\dot{n}_o\tau_c \leq 0.05$ for telescope A at Mildura

APPENDIX 2

Equation A 1.2 used in Appendix 1 and Section 5.3 has been rigorously derived by Blackman and Michiels (1948). In an alternative derivation of the same equation (Price, 1958; Curran and Craggs, 1949) the recording system is considered to be inoperative for a period τ_r following each recorded pulse. If the mean recorded rate is $\dot{n}_o$, the recorder is consequently off for a fraction $\dot{n}_o\tau_r$ of the recording period and a number $\dot{n}_i(\dot{n}_o\tau_r)$ of input pulses go unregistered in each second.

Since $\dot{n}_i - \dot{n}_o = \dot{n}_i(\dot{n}_o\tau_r)$ the efficiency is then

$$\frac{\dot{n}_o}{\dot{n}_i} = 1 - \dot{n}_o\tau_r \qquad \ldots \text{A 2.1}$$

The maximum recorded rate, $\dot{n}_o(\max) = 1/\tau_r$. Equation A 2.1 correctly gives the counting efficiency only if the resolving time is independent of the input pulse rate. If the system is such that the arrival of an input pulse during the inoperative period extends this period, without however giving rise to an output signal, the recorded rate $\dot{n}_o$ goes to zero as the input rate ($\dot{n}_i$) increases indefinitely. The efficiency is then (Price, 1958),

$$\frac{\dot{n}_o}{\dot{n}_i} = e^{-\dot{n}_i\tau_r} \qquad \ldots \text{A 2.2}$$

For input rates $\dot{n}_i \ll \frac{1}{\tau_r}$, the same values of efficiencies are given by A 2.1 and A 2.2. If $\dot{n}_i\tau_r \gtrsim 1$, A 2.2 is applicable to geiger counter efficiency. At lower rates A 2.1 is more accurate and was used in the efficiency calculations. A recording system with counting efficiency given by A 2.1 is termed a Type II recorder. A

monostable multivibrator with period (τ) followed by a recording device with resolving time $\tau_r \ll \tau$ (Section 5.3) constitutes a type II system. Type I systems with efficiency given by A 2.2 include pulse handling systems with limiting high frequency response.

The input rates have been assumed to be randomly distributed with mean value $\dot{n}_o$. If the rate is scaled by a factor n prior to Type II recording, the efficiency (Blackman and Michiels, 1948) is given by

$$\varepsilon_n = 1 - e^{-\dot{n}_i\tau} \frac{(\dot{n}_i\tau)^n}{n!}, \quad \frac{\dot{n}_i\tau}{n} \ll 1 \qquad \ldots \text{A } 2.3$$

where τ is the recorder resolving time.

APPENDIX 3

The omnidirectional particle intensity per unit sphere ($J_\bullet$), defined (Montgomery, 1948) by the relation,

$$J_\bullet . da = \int_0 J(\theta,\phi)\cos\theta\, da$$

$$= \int_0^{2\pi}\int_0^{\pi} J(\theta,\phi)\sin\theta d\theta d\phi da \qquad \ldots \text{ A } 4.1$$

is the number of particles per second incident upon the sphere of unit projected area. $J(\theta,\phi)$ is the unidirectional particle intensity defined in Section 4.3.

The counting rate of a spherical detector of radius r and unit efficiency is thus

$$\dot{n} = \pi r^2 J_\bullet \qquad \ldots \text{ A } 4.2$$

$$= G_\bullet J_\bullet$$

If $J(\theta,\phi) = J_0$ is isotropic over solid angle

$$\Omega_0 = 2\pi\int_0^{\theta} \sin\theta d\theta$$

and zero outside Ω_0,

$$\dot{n} = 2\pi J_0 . \pi r^2 (1 - \cos\theta_0)$$

$$= G_0(\theta_0) . J_0$$

where $G_0(\theta_0) = 2\pi\int_0^{\theta_0} A(\theta).\sin\theta d\theta \qquad \ldots \text{ A } 4.3$

is the geometric factor for a flux isotropic over Ω_0.

For the sphere, $G_0(\theta_0) = 2\pi^2 r^2 (1 - \cos\theta_0)$.

A cylindrical counter of length ℓ and radius a with axis in the vertical direction ($\theta = 0$) has a geometric factor,

$$G_o(\theta_o) = \int_0^{2\pi}\int_0^{\theta_o} A(\theta,\phi)\sin\theta d\theta d\phi$$

$$= 2\int_0^{\theta_o}(\pi a^2\cos\theta + 2\ell a\sin\theta)\sin\theta d\theta$$

$$= \pi^2 a^2\sin^2\theta_o + \pi a\ell(2\theta_o - \sin 2\theta_o) \qquad \ldots \text{A } 4.5$$

In a spherically or hemispherically isotropic field the counting rate is independent of orientation and is given by

$$\dot{n}(4\pi) = J_o G_o(\pi)$$

$$= 2\pi^2 a\ell(1 + a/\ell)J_o$$

$$\text{and } \dot{n}(2\pi) = J_o G_o(\pi/2)J_o \qquad \ldots \text{A } 4.6$$

$$= \pi^2 a\ell(1 + a/\ell)J_o$$

We note $G_o(\pi) = \pi S$ (Spherical Isotropy)

and $G_o(\pi/2) = (\pi/2)S$ (hemispherical Isotrophy) $\qquad \ldots$ A 4.7

for both spherical and cylindrical detectors where S is the area of the surface bounding the counting volume. For the omnidirectional detector,

(sphere) $\qquad G_o(\Omega_o) = \frac{\Omega}{4} \cdot S \qquad$ A 4.8

This is approximately true for the cylinder. We may define an effective projected area G_o for the cylinder such that

$$\dot{n} = J_o G_o$$

For a spherically isotropic flux,

$$\dot{n} = J_o G_o(\pi)$$

$$= J_\bullet G_\bullet$$

$$J_\bullet = 4\pi J_o$$

therefore $\qquad G_\bullet = \frac{1}{4\pi} G_o(\pi)$

$$= \frac{S}{4}$$

Mantes and Winckler (1960) erroneously take $G_\bullet = S$ (see Section 8.4)

For a hemispherically isotropic flux,

$$J_\bullet = 2\pi J_o$$

$$G_\bullet = S/_4 \quad \text{also.}$$

For the sphere,

$$G_\bullet = \frac{S}{4} \quad \text{for all} \quad J_\bullet = \Omega J_o \qquad \ldots \text{A } 4.9$$

but for the vertical cylinder,

$$G_\bullet(\theta_o) = \frac{G_o(\theta_o)}{\Omega} \quad \frac{\pi a^2 \sin^2\theta + \pi a \ell (2\theta_o - \sin 2\theta_o)}{2(1 - \cos\theta)}$$

The counting rates of a spherical and cylindrical detector are the same for a spherical or hemispherical isotropic flux if the radius of the sphere,

$$r = \left[\frac{a\ell}{2}\left(1 + \frac{a}{\ell}\right)\right]^{\frac{1}{2}} \qquad \ldots \text{A } 4.10$$

If the flux is not isotropic but depends only on θ, the counting rate is

$$\dot{n} = 2\pi \int_o^\pi A(\theta,\phi).J(\theta).\sin\theta d\theta \qquad \ldots \text{A } 4.11$$

BIBLIOGRAPHY

(arranged alphabetically)

ALFVEN H., "Cosmical Electrodynamics ", Oxford, 1950.

ANDERSON,K.A., Ph.D. Thesis, University of Minnesota,Minneapolis, 1955.

BAILEY, D.K., Proc.I.R.E., 47, 255, 1959.

BETHE, H. and J.ASHKIN, Experimental Nuclear Physics," 1 , 252, London,1953.

BIEHL,A.T., et al., Rev.Mod.Phys., 20. 1. 1948.

BHAVSAR, P.D., J.Geophys. Res., 67, 7, 2627, 1962.

BLAKE, J.R., Aust.J.Science, 24, 12,467, 1962.

BLACKMAN, M. and J.L. MICHIELS, Proc.Phys.Soc. 60, 6,549, 1948.

BROWN, W.L., J.D.GABBE, J. Geophys.Res., 68, 3,607, 1963.

BUECHNER, W.W., et al., Phys.Rev., 74, 10,1348, 1948.

CASAVERDE, M., et al., J.Geophys.Res., 68, 9, 2603, 1963.

CHAMBERLAIN, J.W., "Physics of the Aurora and Airglow",New York, 1961.

CHAPPELL, D.G., Nucleonics, 14, 1,40, 1956.

CHRISTOFFEL, D.A., N.Z.J. Geology and Geophysics, 5, 6,460, 1962.

COLGATE, S.A., "Phenomenology of the Mass Motion of a High Altitude Nuclear Explosion," University of California, Livermore, California, 1963.

COMPTON, A.H., and S.K.ALLISON, "X-rays in Theory and Experiment," London, 1936.

CURRAN, S.C.and J.D.CRAGGS, "Counting Tubes," London, 1949.

DANIELSON, R.E. and P.S.FREIER, "Phys,Rev., 109, 151, 1958.

DOMB, C. and M.H.L.PRICE, J.I.E.E., 94 (III), 325, 1947.

DRAGT, A.J., J.Geophys.Res., 66, 6, 1641, 1961.

DUNGEY, J.W., J.Fluid Mech., 15, 1,74, 1963.

DURNEY, A.C.,H.ELLIOTT, R.J.HYNDS and J.J.QUENBY, Preprint, 1963.

EDWARDS, P.J. B.Sc. (Hons) Thesis, University of Tasmania, Hobart. 1960.

EDWARDS, P.J., et al Nature, 196, 4852, 367, 1962.

ELLIS, R.A., et al., Phys.Rev. 95, 147, 1954.

EVANS, D., Proc.Moscow Cosmic Ray Conf. 3, 92, 1960.

FAN, C.Y., J.Geophys. Res., 66, 2607, 1961.

FANO, U., Nucleonics, 11, 9, 55, 1953.

FERMI, E., " Nuclear Physics", University of Chicago Press, 1949.

FERMI, E, and B.ROSSI, Redd.Della R.Accad. Maz.dei Lincei, Ser.6, 17, 346, 1933

FONGER, W.H., Phys.Rev. 91, 351, 1953.

FRANCEY, R., B.Sc.(Hons.) Thesis, University of Tasmania, Hobart, 1963.

FREIER, P.S., and W.R.WEBBER, J.Geophys.Res., 68, 6, 1605, 1963

GALL, R., J.Phys.Soc. (Japan) 17, A_II, 1962

GALL, R., J.Geophys.Res., 68, 12, 3565, 1963.

GLOVER, F.N., J.Geophys.Res., 68, 9, 2385, 1963.

GOLDSTEIN, H., "Attemuation of Gamma Rays and Neutrons in Reactor Shields," Nuclear Development Corporation of America, New York. 1957.

GREENHILL, J., B.Sc.(Hons.) Thesis, University of Tasmania, Hobart. 1960.

GREGORY, J.B., Nature, 196, 508, 1962

HAMLIN, D.A., et al J.Geophys.Res., 66, 1, 1 1961

HARRIS, R.W., J.Geophys.Res., 68, 18, 5125, 1963

HAYAKAWA, S., and H.OBAYASHI, J.Geophys.Res., 68, 10, 3311, 1963

HOFMANN, D.J., and J.R.WINCKLER, J.Geophys.Res., 68, 8, 2067, 1963

HESS, W.N., J.Geophys.Res., 68, 3, 667, 1963.

JACKLYN, R.M., Nuovo Cimento, 24, 1034, 1962.

JOHNSON, T.H., Rev.Mod.Phys., 10, 4, 193, 1938

JOHNSON, T.H. and J.G.BARRY, Phys.Rev., 56, 219, 1939

KANE, R.P., J.Geophys.Res., 67, 4, 1295, 1962

KENNEY J.F. and H.R.WILLARD, J.Geophys.Res., 68, 16 4645, 1963

KALPHOUSE, J.L., J.Geophys.Res., 68,19,5608, 1963

KOTHARI, D.S., 'Nuclear Explosions,' Delhi, 1956.

KRAUS, J.D., and H.KO, 'Celestial Radio Radiation,' Radio Observatory Report, 7, Ohio State University, Columbus, Ohio, 1957.

LABY, J.E., V.K.LIL and V.D.HOPPER, Nuovo Cimento (10) 5, 1, 249, 1957.

LATTER, R. and R.E.LeLEVIER, J.Geophys.Res., 68, 6, 1643, 1963.

LEES, C.F., et.al., Phil.Mag., 44, 304, 1953.

LEMAITRE, G. and I.S.VALLARTA, Phys.Rev., 43, 87, 1933

" " 49,719, 1936

" " 50,493, 1936.

LEW, J.S., J.Geophys.Res., 66, 9, 2681, 1961.

MACDONALD, G.J.F., J. Geophys.Res., 66, 11, 3639, 1961.

MANTIS, H.T.,and J.R.WINCKLER, J.Geophys.Res., 65, 11, 3515, 1960.

MATSUSHITA, S., J.Geophys.Res., 64, 9, 1149, 1959.

McCRACKEN, K.G., and A.FENTON, J.Phys.Soc. (Japan) 17,A-2,455, 1962

McCRACKEN, K.G., Phys.Rev. 117, 6, 1570, 1960.

McDIARMID, I.B., et al., Can.J.Phys., 41, 1332, 1963.

McDONALD, F.B.,and W.R.WEBBER, Phys.Rev., 115, 194, 1959.

McILWAIN, C.E., J.Geophys.Res., 66, 11, 3681, 1961

McILWAIN, C.E. and G.PIZZELLA, J.Geophys.Res., 68, 7,1811, 1963

McNISH, A.G., J.Geophys.Res., 64, 12, 2253, 1959.

MEREDITH, L.H., et al., Phys.Rev, 66, 198, 1955.

MILLBURN, S.P., et al., Phys.Rev., 95, 1268, 1954.

MONTGOMERY, D.J.X., 'Cosmic Ray Physics,' Princeton, 1949.

NEHER, H.V., Progress in Cosmic Ray Physics, Amsterdam, 1952.

NEHER, H.V.,et al., Phys. Rev., 50, 992, 1936.

NEHER, H.V. " " " " 53, 855, 1936.

NEHER, H.V., " " " " 61, 408,, 1942

NEHER, H.V. " " " " 90, 655, 1953.

NEHER, H.V., J.Geophys.Res., 66, 12, 4007, 1961

NEWELL, H.E., Rev.Sci.Instrum., 20, 568, 1949

NORTON, K.H., Proc. I.R.E., 40, 470, 1952

NORTHROP, T.G. and E.TELLER, Phys.Rev., 117, 215-225, 1960.

OBAYASHI, H., Prog.Theor. Phys., 25, 2, 297, 1961

OBAYASHI, T., Planet Space Sci., 10, 47, 1963.

ODENCRANTZ, F.K., J.Geophys.Res., 68, 7, 2157, 1963.

PARSON, N.R., Ph.D.Thesis, University of Tasmania, Hobart, 1959.

PERLIAN, S., et al., Trans. I.R.E., cs- 7, 3, 167, 1959.

PETRAUSKAS, A.A., et al., Phys.Rev. 63, 389, 1943.

PISHAROTY, P.R., Nature, 196, 822, 1962.

PHILLIPS, J., B.Sc.(Hons.) Thesis, University of Tasmania,Hobart, 1961.

POMERANTZ, M.A. and S.P.ARGARWAL, Phil.Mag., 7, 1503, 1962.

POMERANTZ M.A., et al Proc.Moscow Conf., 4, 344, 1960.

PRATT, H.J., Trans.I.R.E., cs-8, 4, 214, 1960.

PRICE, W.J., 'Nuclear Radiation Detection,' London, 1958.

QUENBY, J.J.,and G.WENK, Phil.Mag., 7, 1457, 1962.

QUENBY J.J. and W.R.WEBBER, Phil.Mag., 4, 90, 1959.

RATCLIFFE, J.A., 'Magneto-Ionic Theory and its applications to the Ionosphere,' Cambridge, 1959.

ROBERTS, J.A., Aust.J.Phys., 12, 327, 1959.

ROQUET J., et al., J.Geophys Res., 68, 3731, 1963.

ROSSI, B., 'High Energy Particles,' New York, 1952.

ROTHWELL P. and J.J.QUENBY, Proc. Varenna Conf., 1957.

SAUER, H.H., J.Geophys.Res., 68, 4, 957, 1963

SAUER, H.H. and E.C.RAY, Ann.Phys., 25, 2, 135, 1963

SCHLUTER, A., Nuovo Cimento, 8, Supp(II), 349, 1958

SCHREIP, E.J., Phys.Rev., 54, 158, 1938.

SCHWARTZ, M., Nuovo Cimento, II, 10(1), 27, 1959.

SHKLOVSKI, I.S.,'Cosmic Radio Waves,' Harvard University Press, 1960.

SIMPSON, J.A., Phys.Rev., 83, 1175, 1951

SINGER, F., Progress in Cosmic Ray Physics, 6, 1962.

SINGER, F., Nature, 196, 317, 1962.

SOBERMAN, R.K., Phys. Rev., 102, 5, 1399, 1956

SPENCER, L.V., 'Energy dissipation by fast electrons,' N B S Mono 1, Washington, 1959.

STOERMER, C., 'The Polar Aurora,' London, 1955.

STONE, E.C., J.Geophys.Res., 68, 14, 4157, 1963

SWANN, W.F.G., Phys.Rev. 44, 224, 1933.

THOMPSONA.R. and A.MAXWELL, Astrophys.J., 136, 2, 546, 1962

THOMPSON, A.R. and A.MAXWELL, Planet Space Sci., 2, 104, 1960

VAN ALLEN J.A. and C.E.McILWAIN, J.Geophys.Res., 61, 569, 1956

VAN ALLEN J.A.et al J.Geophys.Res., 64, 877, 1959.

VAN ALLEN, J.A. et al J.Geophys.Res., 68, 3, 619, 1963

WAIT, J.R., J.Res. N B S, 64D (Radio Prop), (2), 153, 1960.

WEBBER, W.R., J.Geophys. Res., 68, 10, 3065, 1963

WEBBER, W.R.,Progress in Cosmic Ray Physics, 6, Amsterdam, 1963.

WEBBER, W.R., Can.J.Phys., 40, 906, 1962.

WEBBER, W.R., J.Geophys.Res., 67, 13, 5091, 1962

WINCKLER, J.R., et al., Phys.Rev., 76, 1012, 1949

WINCKLER, J.R., Phys. Rev., 79, 660, 1950

WINCKLER, J.R., Phys.Rev., 85, 1054, 1952

WINCKLER J.R. and K.ANDERSON, Phys.Rev., 93, 596, 1954.

WINCKLER J.R. and L.E.PETERSON, J.Geophys.Res., 64, 697, 1959